

**SPECTROSCOPIC AND *AB INITIO* STUDIES ON THE
CONFORMATIONS AND VIBRATIONAL SPECTRA OF
SELECTED CYCLIC AND BICYCLIC MOLECULES**

A Dissertation

by

ABDULAZIZ A. H. AL-SAADI

Submitted to the Office of Graduate Studies of
Texas A&M University
in partial fulfillment of the requirements for the degree of

DOCTOR OF PHILOSOPHY

December 2006

Major Subject: Chemistry

**SPECTROSCOPIC AND *AB INITIO* STUDIES ON THE
CONFORMATIONS AND VIBRATIONAL SPECTRA OF
SELECTED CYCLIC AND BICYCLIC MOLECULES**

A Dissertation

by

ABDULAZIZ A. H. AL-SAADI

Submitted to the Office of Graduate Studies of
Texas A&M University
in partial fulfillment of the requirements for the degree of

DOCTOR OF PHILOSOPHY

Approved by:

Chair of Committee,	Jaan Laane
Committee Members,	John P. Fackler
	Rand L. Watson
	George Kattawar
Head of Department,	Emile A. Schweikert

December 2006

Major Subject: Chemistry

ABSTRACT

Spectroscopic and *ab initio* Studies on the Conformations and Vibrational Spectra of

Selected Cyclic and Bicyclic Molecules. (December 2006)

Abdulaziz A. H. Al-Saadi, B.S., King Fahd University for Petroleum and Minerals;

M.S., King Fahd University for Petroleum and Minerals

Chair of Advisory Committee: Dr. Jaan Laane

The structure, potential energy functions and vibrational spectra of several cyclic and bicyclic molecules have been investigated using several spectroscopic techniques and high-level *ab initio* and density functional theory (DFT) calculations. Laser induced fluorescence and Raman spectroscopies were used to study the conformation of 2-indanol in the electronic ground and excited states. These, along with detailed *ab initio* calculations, confirmed the existence of four different stable conformations with the one undergoing an intermolecular hydrogen bonding being the most stable. A theoretical two-dimensional surface in terms of the ring-puckering and the hydroxyl group internal rotation vibrations was constructed. This work was extended to obtain preliminary insights on the conformations and ring-puckering frequencies of 3-cyclopenten-1-ol using *ab initio* and DFT calculations.

Infrared and Raman spectra were also utilized to study the structures and vibrational spectra of γ -crotonolactone and 2,3-cyclopentenopyridine (pyrindan). *Ab*

initio results showed that γ -crotonolactone is rigidly planar in the electronic ground state and has a nearly harmonic ring-puckering potential function. The calculated vibrational levels were shown to be in very good agreement with the experimental ring-puckering frequency from vapor-phase Raman observations.

The structures, vibrational spectra, and potential energy functions of several cyclic molecules were reinvestigated using high-level *ab initio* computations, and detailed vibrational analyses based on DFT-B3LYP calculated frequencies were also carried out. A number of new insights were presented by re-evaluating the available experimental data for several cyclopentenes, silacyclobutanes and silacyclopentenes. It was found that the vibrational spectra of some deuterated cyclopentenes possess extensive coupling between several ring modes and other low-frequency modes. Reassignments of these spectra have been proposed. Frequencies from DFT-B3LYP calculations showed very good agreement with the experimental values for silacyclobutane and its derivatives. The presence of silicon and halogen atoms did not affect the accuracy of the DFT calculations. In addition, the ring-puckering potential energy function for silacyclopent-2-ene was studied and alternative assignments of the far-infrared results were proposed. The new assignments are in good agreement with computational results. Silacyclopent-2-ene and its -1,1- d_2 isotopomer were shown to be slightly puckered with barriers of less than 50 cm^{-1} .

DEDICATION

To my Lord, the most glorious, the most merciful.

Without His support, this would not have seen the light.

ACKNOWLEDGMENTS

First and foremost, I would like to express my sincere gratitude to my research advisor, Professor Jaan Laane, for his kindness, advice, support, and encouragement. He was more than just a research advisor. I am very proud to be his student and to have learned from him during the past few years. Also, my appreciation goes to Professors John Fackler, Rand Watson, and George Kattawar for serving on my Ph.D. committee.

All former and current group members deserve special thanks. Namely, I would like to thank Dr. Martin Wagner for collecting FES and SVLF spectra for 2-indanol, Dr. Daniel Autrey for familiarizing me with super computing facilities for running *ab initio* calculations, Dr. Juan Yang for teaching me how to operate the Raman spectrometer, Mohamed Rishard for his help in running the Bomem instrument, Kathleen McCann for her friendship and kindness, and Mrs. Linda Redd for helping me type some manuscripts and revise the English of my dissertation. Other former and current group members whom I did not mention by name also deserve my deep appreciation.

I will not forget the love, support and caring always shown by my small family, starting with my beloved wife, Nuha, and my dear little children: Asma, Arwa, and Ibrahim. Their sacrifice was a reason for this work to be completed. My heartfelt gratitude goes also to my beloved parents for their patience and words of support as well as their sincere prayers.

King Fahd University for Petroleum and Minerals is also highly appreciated for sponsoring me financially throughout the past five years in pursuing my Ph.D. degree.

TABLE OF CONTENTS

	Page
ABSTRACT.....	iii
DEDICATION.....	v
ACKNOWLEDGMENTS.....	vi
TABLE OF CONTENTS.....	vii
LIST OF TABLES.....	xi
LIST OF FIGURES.....	xv
 CHAPTER	
I INTRODUCTION.....	1
2-Indanol.....	4
3-Cyclopenten-1-ol.....	4
γ -Crotonolactone.....	5
2,3-Cyclopentenopyridine.....	6
Cyclopentene.....	7
Silacyclobutane.....	8
Silacyclopent-2-ene.....	8
II THEORETICAL AND COMPUTATIONAL METHODS.....	10
Introduction.....	10
<i>Ab initio</i> Calculations.....	11
1. Hartree-Fock Theory.....	12
2. Møller-Plesset Perturbation Theory.....	15
3. Coupled Cluster Theory.....	17
4. Density Functional Theory.....	18
5. Basis Sets.....	21
6. Calculation of Vibrational Frequencies.....	24
7. Calculation of Vibrational Infrared and Raman Spectra.....	26

CHAPTER		Page
	Vibrational Hamiltonian.....	27
	1. The Vibrational Kinetic Energy Operator.....	27
	2. The Vibrational Potential Energy Operator.....	30
III	EXPERIMENTAL METHODS.....	34
	Infrared Spectra.....	34
	Raman Spectra.....	35
	Electronic Absorption Spectra.....	35
	Laser-Induces Fluorescence (LIF) Spectra.....	36
IV	SPECTROSCOPIC AND COMPUTATIONAL STUDIES OF THE INTRAMOLECULAR HYDROGEN BONDING OF 2-INDANOL.....	37
	Introduction.....	37
	Experimental.....	39
	Computations.....	40
	Spectroscopic Results.....	47
	1. Raman and Infrared Spectra.....	47
	2. Laser-Induced Fluorescence (LIF) Spectra.....	57
	Conclusion.....	67
V	<i>AB INITIO</i> AND DFT STUDIES ON THE RING-PUCKERING VIBRATION AND INTRAMOLECULAR HYDROGEN BONDING OF 3-CYCLOPENTEN-1-OL.....	68
	Introduction.....	68
	<i>Ab initio</i> Computations.....	69
	Results and Discussion.....	70
	Conclusion.....	76
VI	VIBRATIONAL SPECTRA, <i>AB INITIO</i> CALCULATIONS AND RING-PUCKERING POTENTIAL ENERGY FUNCTION FOR γ -CROTONOLACTONE.....	83
	Introduction.....	83
	Experimental.....	85
	Computations.....	86
	Vibrational Spectra.....	87
	Kinetic and Potential Energy Functions.....	94
	Conclusion.....	100

CHAPTER		Page
VII	RAMAN AND INFRARED SPECTRA, <i>AB INITIO</i> AND DFT CALCULATIONS, AND VIBRATIONAL ASSIGNMENTS FOR 2,3-CYCLOPENTENOPYRIDINE.....	102
	Introduction.....	102
	Experimental.....	103
	<i>Ab initio</i> Calculations.....	104
	Results and Discussion.....	105
	1. Molecular Structure.....	105
	2. Raman and Infrared Spectra.....	110
	Conclusion.....	120
VIII	<i>AB INITIO</i> AND DFT CALCULATIONS FOR THE STRUCTURE AND VIBRATIONAL SPECTRA OF CYCLOPENTENE AND ITS ISOTOPOMERS.....	121
	Introduction.....	121
	1. <i>Ab initio</i> and DFT Calculations versus Experiments...	121
	2. Spectroscopic and Computational Studies on Cyclopentenes.....	123
	Experimental.....	125
	Computational Methods.....	125
	Molecular Structure.....	126
	Molecular Vibrations.....	126
	Vibrational Reassignments.....	139
	Conclusion.....	146
IX	MOLECULAR STRUCTURES, VIBRATIONAL SPECTRA, RING-PUCKERING POTENTIAL ENERGY FUNCTIONS, AND <i>AB INITIO</i> AND DFT STUDIES OF SILACYCLOBUTANES.....	148
	Introduction.....	148
	<i>Ab initio</i> and DFT Calculations.....	151
	Molecular Structures.....	151
	Vibrational Reassignments.....	159
	Conclusion.....	183
X	REINVESTIGATION OF THE STRUCTURE AND RING-PUCKERING POTENTIAL ENERGY FUNCTIONS FOR SILACYCLOPENT-2-ENE AND RELATED MOLECULES	187
	Introduction.....	187
	Computations.....	188

CHAPTER	Page
Results and Discussion.....	189
Reassignments of the Far-Infrared Spectra.....	191
Vibrational Frequencies.....	197
Silacyclopent-3-enes.....	200
Conclusion.....	205
XI CONCLUSION.....	208
REFERENCES.....	214
VITA.....	224

LIST OF TABLES

TABLE	Page
1. Calculated structural parameters, energies, puckering angles, OH internal rotation angles, and dipole moments for the conformations (A , B , C , and D) and planar structure (P) of 2-indanol in its electronic ground state.....	44
2. Comparison of energies and puckering and internal rotation angles from different basis sets for the four conformers and the planar structure.....	46
3. Energy barriers between the four conformers, puckering angles, and internal rotation angles of the transition structures in the energy map of 2-indanol.....	51
4. Total energies in Hartree and relative energies in cm^{-1} calculated from the MP2/6-31+G(d,p) level of theory for 2-indanol (for puckering angles from 0.0° to 58.0°).....	52
5. Total energies in Hartree and relative energies in cm^{-1} calculated from the MP2/6-31+G(d,p) level of theory for 2-indanol (for puckering angles from -8.0° to -58.0°).....	53
6. Vibrational assignments for the four conformers of 2-indanol based on experimental and calculated spectra.....	59
7. Spectroscopic transitions for the isomers of 2-indanol in its S_0 and $S_1(\pi, \pi^*)$ states.....	63
8. Populations (in %) of A , B , C , and D conformers of 2-indanol in the electronic ground state.....	66
9. Relative energies and puckering angles of the stable conformers and the planar structure for 3-cyclopenten-1-ol.....	75
10. Total energies in Hartree and relative energies in cm^{-1} calculated from the MP2/6-31+G(d,p) level of theory for 3-cyclopenten-1-ol (for puckering angles from 0.0° to 50.0°).....	77

TABLE	Page
11. Total energies in Hartree and relative energies in cm^{-1} calculated from the MP2/6-31+G(d,p) level of theory for 3-cyclopenten-1-ol (for puckering angles from -10.0° to -50.0°).....	78
12. Vibrational frequencies of the $-\text{OH}$ stretching and the lowest three large-amplitude motions for 3-cyclopenten-1-ol and 2-indanol calculated at the B3LYP/cc-pVTZ level.....	81
13. Vibrational assignments for γ -Crotonolactone.....	92
14. Total and relative energies for γ -crotonolactone from <i>ab initio</i> calculations.....	97
15. Ring-puckering vibrational levels for γ -crotonolactone as determined from <i>ab initio</i> results.....	99
16. Puckering barrier and puckering angle for pyrindan by different levels of theories.....	107
17. Vibrational assignments for pyrindan based on experimental and calculated spectra.....	115
18. Point groups, symmetry species, and structures for cyclopentene- d_0 and its isotopomers.....	122
19. Puckering angles, CH out-of-plane angles, and barriers to planarity in cyclopentene- d_0 from various experimental and theoretical methods.....	128
20. Reassignments of vibrational spectra of cyclopentene- d_0	131
21. Reassignments of vibrational spectra of cyclopentene- d_8	133
22. Reassignments of vibrational spectra of cyclopentene-1- d_1	135
23. Reassignments of vibrational spectra of cyclopentene-1,2,3,3- d_4	137
24. Experimental and calculated frequencies of the ring puckering and ring twisting vibrations for cyclopentene and its isotopomers.....	140
25. Frequencies shifts in ring fundamentals of cyclopentene and its isotopomers.....	141

TABLE	Page
26. Structural parameters of silacyclobutane from different experiments and from <i>ab initio</i> calculations.....	154
27. Structural parameters of 1,1-difluorosilacyclobutane.....	155
28. Structural parameters of 1,1-dichlorosilacyclobutane.....	156
29. Barriers to planarity and puckering angle for silacyclobutane from different experimental and <i>ab initio</i> methods.....	157
30. Barriers to planarity and puckering angles for 1,1-difluorosilacyclobutane and 1,1-dichlorosilacyclobutane from different methods of calculations.....	158
31. Puckering coordinates and theoretical potential energy function parameters based on <i>ab initio</i> calculations.....	162
32. Reassignments of vibrational spectra of silacyclobutane.....	171
33. Reassignments of vibrational spectra of silacyclobutane-1,1- d_2	173
34. Reassignments of vibrational spectra of 1,1-difluorosilacyclobutane.....	175
35. Reassignments of vibrational spectra of 1,1-dichlorosilacyclobutane.....	177
36. Calculated atomic charges for silacyclobutane, 1,1-difluorosilacyclobutane, and 1,1-dichlorosilacyclobutane from the DFT-B3LYP/cc-pVTZ level of theory.....	184
37. Calculated energies, barriers, and puckering frequencies for silacyclopent-2-ene and its 1,1- d_2 isotopomer using different levels of theories.....	190
38. Reassignments of the ring-puckering frequencies for silacyclopent-2-ene and silacyclopent-2-ene-1,1- d_2	193
39. Calculated barriers and puckering frequencies of 1,1-difluoro- and 1,1-dichlorosilacyclopent-2-ene.....	198
40. Assignments of some characteristic frequencies in the mid-infrared spectra of silacyclopent-2-ene and its 1,1-difluoro and 1,1-dichloro derivatives.....	199

TABLE	Page
41. Calculated energies, barriers, and puckering frequencies for silacyclopent-3-ene from different levels of theories.....	202
42. Vibrational frequencies for the CH ₂ ring bending motions as determined from the DFT-B3LYP/cc-pVTZ level of theory in different cyclic silanes and in cyclobutane and cyclopentene.....	204

LIST OF FIGURES

FIGURE	Page
1. Double-minimum potential energy function for the inversion vibration in ammonia.....	33
2. The four stable conformations of 2-indanol.....	42
3. Bond distances and angles of the most stable structure of 2-indanol for its S_0 and S_1 states calculated at the MP2/cc-pVTZ and UCIS/6-311++G(d,p) levels of theory, respectively.....	43
4. The four large-amplitude, low-frequency vibrations in 2-indanol.....	48
5. Calculated potential energy surface of 2-indanol in terms of its ring-puckering angle and the OH internal rotation angle.....	49
6. Topological map equivalent to Fig. 5.....	50
7. Comparison of the low-frequency liquid Raman spectrum of 2-indanol at 90° C to the computed spectra of its isomers.....	54
8. Comparison of the liquid Raman spectrum of 2-indanol at 90° C to the computed spectra of its isomers for the high-frequency region.....	55
9. Polarized spectra of the liquid 2-indanol.....	56
10. Solid-phase infrared and Raman spectra of 2-indanol.....	58
11. Laser-induced fluorescence excitation spectrum of 2-indanol.....	62
12. Dispersed fluorescence spectra from the 0_0^0 lines for conformers A , C and D compared with the calculated Raman spectra for each conformer.....	65
13. Structures and labels of the four stable conformers of 3-cyclopenten-1-ol.....	71
14. Structures for the four conformers of 3-cyclopenten-1-ol as determined from CCSD/6-311++G(d,p) calculations.....	73

FIGURE	Page
15. The ring-puckering potential energy function for 3-cyclopenten-1-ol calculated by MP2/cc-pVTZ and B3LYP/cc-pVTZ.....	74
16. Calculated potential energy surface of 3-cyclopenten-1-ol in terms of the ring-puckering angle and internal rotation angle of the -OH group.....	79
17. Contour of the energy map shown in Fig. 16.....	80
18. Ground-state structures of γ -crotonolactone and 2-cyclopenten-1-one from the CCSD/6-311++G(d,p) calculations.....	88
19. Vapor-phase, liquid-phase, and calculated Raman spectra for γ -crotonolactone.....	89
20. Polarized Raman spectra of the γ -crotonolactone liquid.....	90
21. Liquid-phase and calculated infrared spectra of γ -crotonolactone.....	91
22. Definitions of the puckering coordinate (x) and puckering angle (ϕ) for γ -crotonolactone.....	96
23. Ring-puckering potential energy function from different levels of calculations.....	98
24. Potential energy function for the ring-puckering vibration as determined from <i>ab initio</i> calculations using the MP2/cc-pVTZ level of theory.....	101
25. Structures of pyrindan and indan molecules as determined from the MP2/6-311++G(d,p) calculation.....	106
26. Definitions of the ring-puckering angle and the ring-puckering coordinate used to predict the ring-puckering potential energy function from <i>ab initio</i> calculations.....	108
27. Theoretical potential energy functions in terms of the ring-puckering coordinate for pyrindan as determined from MP2 and DFT-B3LYP calculations.....	109
28. Raman spectra of the vapor pyrindan compared to the theoretical spectra calculated at the B3LYP/6-311++G(d,p) level of theory.....	111

FIGURE	Page
29. Polarized spectra of pyrindan.....	113
30. Liquid-phase infrared spectra of pyrindan compared to the theoretical spectra calculated at the B3LYP/6-311++G(d,p) level of theory.....	114
31. Ring-twisting, ring-flapping, and skeletal-bending vibrations from the vapor-phase Raman experiment.....	118
32. UV spectra of pyrindan vapor taken at room temperature.....	119
33. Calculated planar and puckered structures of cyclopentene.....	127
34. Liquid and calculated mid-infrared spectra of cyclopentene- d_0	129
35. Liquid and calculated Raman spectra of cyclopentene- d_0	130
36. Correlation diagrams for the ring modes in cyclopentene and its isotopomers as determined from the original assignments and from DFT-B3LYP/cc-pVTZ calculations.....	142
37. Reassigned vibrational frequencies of the CH ₂ (CD ₂) bending motions for various isotopic structures of cyclopentene.....	144
38. Reassigned vibrational frequencies of the =C-H(=C-D) bending modes for cyclopentene and its isotopomers.....	145
39. Structure, puckering angle and atom labels for silacyclobutane and its derivatives.....	152
40. Puckering-angle potential energy functions for silacyclobutane from MP2/cc-pVTZ and B3LYP/cc-pVTZ levels of theory compared to far-infrared experimental values.....	160
41. Effect of basis sets in predicting the puckering barrier and puckering angle in silacyclobutane.....	161
42. Vapor-phase and calculated (DFT-B3LYP/cc-pVTZ) infrared spectra of silacyclobutane.....	163
43. Vapor-phase and calculated (DFT-B3LYP/cc-pVTZ) infrared spectra of silacyclobutane-1,1 d_2	164

FIGURE	Page
44. Vapor-phase and calculated (DFT-B3LYP/cc-pVTZ) infrared spectra of 1,1-difluorosilacyclobutane.....	165
45. Vapor-phase and calculated (DFT-B3LYP/cc-pVTZ) infrared spectra of 1,1-dichlorosilacyclobutane.....	166
46. Calculated (DFT-B3LYP/cc-pVTZ) Raman spectra for silacyclobutane compared with the line spectra of the frequencies and intensities of the vapor-phase Raman spectra reported in Refs. [39,121].....	167
47. Calculated (DFT-B3LYP/cc-pVTZ) Raman spectra for silacyclobutane-1,1- d_2 compared with the line spectra of the frequencies and intensities of the vapor-phase Raman spectra reported in Refs. [39,121].....	168
48. Calculated (DFT-B3LYP/cc-pVTZ) Raman spectra for 1,1-difluorosilacyclobutane compared with the line spectra of the frequencies and intensities of the vapor-phase Raman spectra reported in Refs. [39,121].....	169
49. Calculated (DFT-B3LYP/cc-pVTZ) Raman spectra for 1,1-dichlorosilacyclobutane compared with the line spectra of the frequencies and intensities of the vapor-phase Raman spectra reported in Refs. [39,121].....	170
50. Vector displacement representations of the in-phase α -CH ₂ wagging vibration (ν_6) in silacyclobutane.....	185
51. Structure of silacyclopent-2-ene optimized from the coupled cluster theory with single and double excitation calculations (CCSD) using the 6-311++G(d,p) basis set.....	192
52. Ring-puckering potential energy function of silacyclopent-2-ene from Calculation I.....	195
53. Ring-puckering potential energy function of silacyclopent-2-ene-1,1- d_2 from Calculation I.....	196
54. Structure of silacyclopent-3-ene calculated at CCSD/6-311++G(d,p) and MP2/cc-pVTZ levels of theory.....	203

FIGURE	Page
55. Calculated atomic charges for some cyclic molecules.....	206

CHAPTER I

INTRODUCTION

Many conformational processes undergone by cyclic molecules can be well represented by vibrational potential energy surfaces (PES). Such processes include isomerizations achieved by internal rotation, intramolecular hydrogen bonding, ring inversions and ring bendings [1]. Large-amplitude low-frequency motions, such as the ring-puckering and ring-twisting vibrations, in cyclic and bicyclic molecules are of special interest to spectroscopists since structural changes are often associated with these out-of-plane motions. In 1945 R. P. Bell postulated that unusual quartic oscillation potential energy functions would govern some of these vibrations [2] and the first spectroscopic observations of the ring puckering were achieved in 1960 at MIT (R. C. Lord laboratory) [3] and Berkeley (W. D. Gwinn laboratory) [4].

For the past few decades, high-resolution far infrared and low-frequency Raman spectroscopic techniques have been employed to characterize these large amplitude ring motions for a wide array of cyclic molecules and to determine the potential energy functions governing such motions [5-9]. The determination of the potential energy functions yields valuable information about the molecular conformations, energy

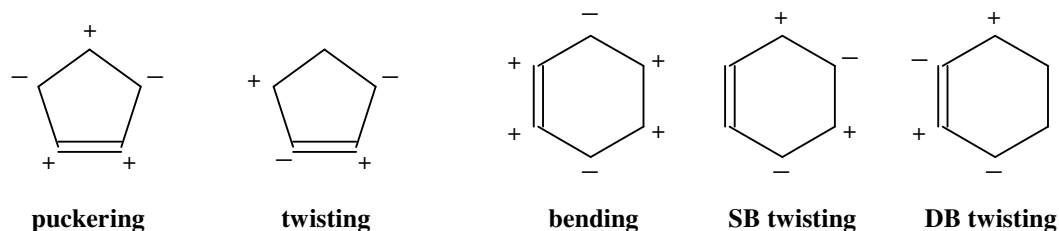
This dissertation follows the style of Journal of Molecular Structure.

barriers between different structures, as well as the forces responsible for the molecule configurations. *Ab initio* calculations have also become an integral part of this research. High-level quantum mechanical treatments of the cyclic and bicyclic molecules provide a great deal of information and guidance when such calculations are performed in the proper manner.

Since three points define a plane, three-membered rings possess no out-of-plane vibrations. However, four-, five-, and six-membered rings have one, two, and three out-of-plane motions, respectively. In most out-of-plane cases, the ring-puckering motion has the lowest frequency. In cyclobutane the only out-of-plane ring-bending motion is the ring-puckering vibration. In the case of cyclopentane and cyclohexane, however, there are two or three out-of-plane motions of comparable energies, and these have to be considered simultaneously.

When unsaturated ring molecules, such as cyclopentene and 1,4-cyclohexadiene, were studied, Laane and Lord [10,11] showed that such cyclic molecules can be regarded as pseudo-four-membered rings because they have ring puckering vibrations that are similar to that in cyclobutane. Because of the presence of the C=C bonds in the skeleton of the ring, the two olefinic carbon atoms move as a single unit during the puckering vibration. For cyclopentene [10] and 1,4-cyclohexadiene [11], the ring-twisting vibrations involving the double bonds are of higher energy than the puckering vibrations. The frequency for the twisting of the double bond in cyclopentene is 380 cm^{-1} whereas the sequence of ring-puckering frequencies lies below 160 cm^{-1} . Moreover, six-membered rings with one double bond, such as cyclohexene, can be envisioned as

pseudo-five-membered rings similar to cyclopentane, where no double bonds are present. In pseudo-five-membered rings, as with five-membered rings themselves, the ring-twisting and ring-bending (essentially ring-puckering) frequencies are relatively low and similar in frequency. The ring-bending motions of cyclopentene and cyclohexene are shown below.



In order to describe the out-of-plane motions with a mathematical model, R. P. Bell [2] proposed that the ring-puckering vibration of a four-membered ring molecule could be represented by a quartic potential energy function. Further far-infrared spectroscopic investigations [3,12,13] showed that the ring-puckering vibrations are best represented by mixed quartic-quadratic potential functions. In addition, Raman studies on cyclobutane found it to have a double-minimum energy function [14]. Double-minimum potential functions require both quartic and quadratic terms that can better describe the shape of the potential function. In this work, the conformations and vibrational frequencies of several cyclic molecules have been studied in the electronic ground and excited states using several spectroscopic techniques as well as *ab initio* calculations. The results of these investigations will be presented herein.

2-INDANOL

2-Indanol represents an interesting case for study since in its most stable form it is stabilized by internal hydrogen bonding that exists between the hydroxyl hydrogen atom and the π -electron cloud of the benzene ring. Infrared, Raman, and laser induced fluorescence spectroscopic investigations have been carried out on 2-indanol, and these results will be presented. Detailed *ab initio* calculations using the MP2/cc-pVTZ and DFT-B3LYP levels of theory have been also carried out to confirm our experimental results. A few spectroscopic investigations on 2-indanol have been previously reported [15-17]. These studies concluded that 2-indanol exists in four possible conformations, which can interchange through the ring-puckering vibration and the internal rotation of the OH group on the five-membered ring. A potential energy surface in terms of these two vibrational coordinates is essential in understanding how the molecule changes its conformations and which pathways it follows to interconvert from one structure to another. Density functional theory calculations will be used to predict the vibrational frequencies of each structure and to help in normal mode assignments of the fifty-four fundamentals associated with each structure. In addition, spectroscopic results of 2-indanol which confirm the presence of the four conformers in the electronic ground and electronic excited states will be presented.

3-CYCLOPENTEN-1-OL

3-Cyclopenten-1-ol is similar in structure to 2-indanol except that no benzene ring is attached to the five-membered ring. As in the case of 2-indanol, 3-cyclopenten-1-ol in

its global minimum structure is stabilized by the intramolecular bonding taking place between the hydroxyl hydrogen and the π -cloud of C=C bond. An ^1H NMR study has previously predicted the puckering angle in 3-cyclopenten-1-ol to be approximately 40° [18]. Liquid-phase infrared experiments showed that a splitting in the OH stretching region of approximately 24 cm^{-1} is present [18-20]. This indicated the presence of both a free -OH stretching and intramolecularly-bonded -OH stretching vibrations. *Ab initio* calculations have reproduced highly satisfactory results for the conformations and vibrational frequencies of 2-indanol. These findings provided incentive for investigating 3-cyclopenten-1-ol using *ab initio* and DFT calculations. Since 3-cyclopenten-1-ol has fewer atoms than 2-indanol, a higher level of calculation was possible on this molecule. The conformational behavior, calculated infrared and Raman vibrational spectra in the electronic ground state (S_0) for 3-cyclopenten-1-ol based on *ab initio* calculations will be presented.

γ -CROTONOLACTONE

The γ -crotonolactone molecule has been reported in microwave studies [21,22] to be planar in its electronic ground state, and its ring-puckering potential energy function was thought to be primarily governed by a quadratic term. An interesting feature of the molecule is the conjugation between the C=C and C=O groups. Several studies of unsaturated lactones in the spectral region below 1800 cm^{-1} have been reported [23-25]. These studies focused on the doublet bands associated with the C=O stretching vibration in various solvents. In the present work, the vapor-phase infrared and Raman spectra and

complete vibrational analysis based on experimental and calculated spectroscopic results will be presented. The potential energy function of the ring-puckering vibration in γ -crotonolactone was generated based on high-level *ab initio* results and kinetic energy expressions. The ring-puckering quantum transitions based on *ab initio* calculations will be presented. The structure and vibrational results obtained for γ -crotonolactone will be compared with 2-cyclopenten-1-one which has been previously characterized by different spectroscopic techniques.

2,3-CYCLPENTENOPYRIDINE

As a continuation of investigations on molecules of the indan family, the infrared and Raman spectra of 2,3-cyclopentenopyridine, which is also known as pyrindan, have been carried out. Pyrindan has C_1 symmetry in its puckered configuration, but due to its non-rigidity it can be analyzed as a planar molecule with C_s symmetry. Fantoni and Caminati reported a microwave study of the ring-puckering and ring-twisting vibrations of pyrindan and obtained a puckering barrier of 390 cm^{-1} [26]. The UV spectra of pyrindan in solvents have also been reported [27,28]. Apparently no other spectroscopic studies have been reported. In this work, a combined study of vibrational spectroscopy and *ab initio* calculations on pyrindan in its electronic ground and excited states will be presented. The conformational structure of pyrindan was compared to that of indan in its electronic ground state. Vibrational assignments of the forty-eight normal modes have been made on the basis of the observed and calculated infrared and Raman spectra. Preliminary UV spectroscopic results of the electronic excited state (S_1) showing the

region where the $n \rightarrow \pi^*$ transition is expected will also be presented. Detailed *ab initio* calculations using the MP2 and DFT-B3LYP theories for studying the puckering barrier and angle have been made. These computational results were used to construct theoretical potential energy functions in terms of the puckering coordinate.

CYCLOPENTENE

The structures and vibrational spectra of cyclopentene- d_0 and its 1- d_1 , 1,2,3,3- d_4 , and - d_8 isotopomers have been extensively studied by means of different spectroscopic techniques [10,29-37]. Cyclopentene is a pseudo-four-membered ring that can be thought of as a four-membered ring in terms of its out-of-plane ring motion. Far-infrared results fitted with a two-dimensional potential energy function in terms of the ring-puckering and ring-twisting coordinates showed that cyclopentene has a puckering barrier of 232 cm^{-1} and a dihedral angle of 26° [29]. The high level of accuracy with which *ab initio* and density functional theory calculations can reproduce the conformational energies and vibrational spectra for several cyclic and bicyclic hydrocarbons provides motivation to reinvestigate the structure and infrared and Raman spectra of cyclopentene. Revisions of the previously reported vibrational assignments for cyclopentene have been accomplished with the help of density functional theory (DFT) calculations. DFT calculations have also allowed the reassignments of several of the vibrational frequencies in the d_1 , d_4 , and d_8 isotopomers. These vibrational reassignments will be presented in detail. In addition, *ab initio* calculations using the MP2/cc-pVTZ basis set were used to predict the inversion barrier and dihedral angle of cyclopentene.

Comparison of the calculated barriers and angles when employing different basis sets to previously reported experimental values will be presented.

SILACYCLOBUTANE

The first preparation of silacyclobutane and some of its derivatives was reported by Laane in 1967 [38]. The structure of silacyclobutane was studied by several spectroscopic techniques and all these studies concluded that the molecule is puckered with a puckering angle of about 30° . Silacyclobutane-1,1- d_2 , 1,1-difluorosilacyclobutane and 1,1-dichlorosilacyclobutane have also been investigated. The vibrational infrared and Raman spectra and complete vibrational analyses on the basis of normal mode calculations were proposed for the four molecules [39]. The availability of high-level *ab initio* quantum mechanical calculations has now made it appropriate to reinvestigate the original assignments and revise them wherever necessary. Attention will be directed to the characteristic frequency always present near 1130 cm^{-1} which was recognized as the fingerprint of silacyclobutane rings. The detailed computational results and vibrational reassignment based on experiment and theory will be presented.

SILACYCLOPENT-2-ENE

Silacyclopent-2-ene and silacyclopent-3-ene were previously investigated and their ring-puckering vibrations were characterized by single-minima potential functions characteristic of planar structures [40,41]. The planar structure of the 2-ene was

explained in terms of an unusual interaction between the d orbital of the silicon atom and the π -electrons of the C=C double bond. High-level *ab initio* calculations on the structures of these two molecules have been carried out to evaluate the experimental conclusions. Revised potential energy functions for the silacyclopent-2-ene and silacyclopent-2-ene-1,1- d_2 will be proposed. The kinetic energy expressions for the molecules were also calculated based on the more accurate structure from the coupled cluster calculations. The structures and vibrational frequencies of 1,1-difluoro- and 1,1-dichlorosilacyclopent-2-ene were also investigated by *ab initio* and DFT calculations and the results will be presented. The CH₂ bending vibrations in cyclopentene, cyclobutane, silacyclopent-2-ene, silacyclopent-3-ene, and silacyclobutane, as well as some disilacyclic molecules will be discussed in some detail.

CHAPTER II

THEORETICAL AND COMPUTATIONAL METHODS

INTRODUCTION

In recent years, computational quantum chemistry has been very widely used not only by theoretical research groups but also by experimental chemists in various fields of chemistry, including molecular spectroscopy and structure. The rapid developments in molecular simulation software packages and the presence of powerful computing facilities have greatly aided many areas of both research and teaching and have helped solve many problems in science.

Limitations that computational tools had in the past which led to faulty conclusions have been overcome in recent years. Nowadays, new research problems in different areas of chemistry can be supported and properly guided by making use of available computational techniques. Moreover, quantum chemical techniques can help resolve issues that can not be practically achieved due to instrumentation limits. Computational chemistry, especially high-level theories and calculations, can also help refine, and perhaps change, some of the old concepts and understanding of chemical phenomena.

Quantum-mechanical calculations in chemistry started early in the last century with the use of empirical and semiempirical molecular orbital approaches, such as the

Hückel method. These methods applied a simplified Hamiltonian rather than the complete molecular Hamiltonian and used parameters whose values were adjusted to fit the experimental data or even the results from other *ab initio* calculations.

***AB INITIO* CALCULATIONS**

Ab initio is Latin for “from the beginning”. The name implies that the computations in *ab initio* quantum mechanical methods are based on theoretical principles and universal physical constants without involving experimental data. *Ab initio* calculations also utilize the correct Hamiltonian to investigate the properties of the molecule. Some useful approximations are needed in order for the calculations not to consume an intensive amount of time and to be more reliable with the computer facilities available for use. Examples of these types of approximations are the use of the time-independent Schrödinger equation, assuming the non-relativistic behavior of the wavefunctions describing the molecular system, and applying the Born-Oppenheimer approximation.

Since early in the last century, the developments in quantum mechanics evolved several theoretical approaches to find the approximate solutions of the Schrödinger equation and to calculate the chemical and physical properties for the molecules. In this chapter, brief highlights in simple mathematical formats will be presented to explain the Hartree-Fock (HF), second-order Møller-Plesset (MP2), and coupled cluster (CC) theories. The density-functional theory (DFT) will also be discussed briefly. These four

computational methods have been implemented in this research work. The following descriptions were mainly taken from Refs. [42-45].

1. Hartree-Fock Theory

The Hartree-Fock (HF) calculation is a very commonly used method of *ab initio* calculations. The Hartree-Fock method has not been used in this work except for a few cases. However, since it is the first step for the Møller-Plesset perturbation theory and other more sophisticated approaches, some discussion about the nature of HF calculations will be presented.

The molecular time-independent Schrödinger equation is given by

$$\left\{ -\frac{\hbar^2}{2} \sum_k \frac{1}{m_k} (\nabla_k^2) + \mathbf{V} \right\} \Psi(\bar{\mathbf{r}}, \bar{\mathbf{R}}) = E\Psi(\bar{\mathbf{r}}, \bar{\mathbf{R}}) \quad (1)$$

where \hbar is Planck's constant divided by 2π , m_k is the mass of the particle k , Ψ is the total wavefunction, $\bar{\mathbf{r}}$ and $\bar{\mathbf{R}}$ represent the positions of the electrons and nuclei, respectively, \mathbf{V} is the potential energy component of the Hamiltonian and is given by the Coulomb repulsion or interaction between the electrons and nuclei, E is the total energy of the system, and ∇_k^2 or "del squared" is the Laplacian operator and is defined by

$$\nabla_k^2 = \frac{\partial^2}{\partial x_k^2} + \frac{\partial^2}{\partial y_k^2} + \frac{\partial^2}{\partial z_k^2} . \quad (2)$$

The exact solution of the Schrödinger equation for many-electron systems is not possible. Some assumptions, however, can be made in order to approximate the solutions for the total molecular wavefunction, Ψ . Based on the molecular orbital theory the total

wavefunction can be represented by individual molecular orbitals ($\phi_1, \phi_2, \dots, \phi_n$) that are chosen to be normalized and orthogonal with respect to each other to fulfill some of the conditions for Ψ . The simplest wavefunction built from these molecular orbitals is a Hartree product:

$$\Psi(\vec{r}) = \phi_1(\vec{r}_1) \phi_2(\vec{r}_2) \dots \phi_n(\vec{r}_n). \quad (3)$$

One advantage of this method is that it breaks the many-electron systems into many simpler one-electron hydrogen-like problems each of which can be solved independently to give a single-electron wave function called an orbital and an energy called an orbital energy. This was the basis of the HF method which was introduced by Douglas Hartree in 1928 [46]. Later, more modifications were made to that approach to improve the outcome eigenvalues. For example, Slater- and Gaussian-type orbitals (STOs and GTOs) were used as mathematical functions to describe the wavefunctions in order to produce more reliable results.

An essential physical requirement of $\Psi(\vec{r})$ is that it must be antisymmetric with respect to exchange, meaning that it must change its sign when two identical particles are swapped within the system. The function shown in Eq. (3) does not fulfill the requirement of antisymmetry. The common way of having that requirement satisfied is by expressing the wavefunction in a form of a determinant. Switching any two electrons corresponds to swapping two rows of the determinant, which causes the sign to change.

The Hartree-Fock method is a variational calculation. Variational methods provide an upper bound to the ground-state energy for a specific system [47]. In other words, the exact wavefunction (Ψ_0) becomes a lower bound to the energy calculated by

another normalized, antisymmetric wavefunction (Ψ_ϕ). In mathematical form, the variational principle is given by

$$E_o(\Psi_o) \leq E_\phi(\Psi_\phi). \quad (4)$$

The closer the trial function (Ψ_ϕ) to the exact function (Ψ_o), the closer E_ϕ will be to E_o . This illustrates the importance of having a good approximation of the trial function at the start of the calculation.

In 1951 C. J. Roothaan [48] applied the variational principle to the solution from the Slater determinant to derive the following equation describing molecular orbital expansion coefficients, c_{vi} ,:

$$\sum_{\substack{\nu=1 \\ \mu=1}}^N (F_{\mu\nu} - \epsilon_i S_{\mu\nu}) c_{vi} = 0 . \quad (5)$$

Eq. (5) can be also written in matrix form as

$$\mathbf{FC} = \mathbf{SC}\boldsymbol{\epsilon} \quad (6)$$

where $\boldsymbol{\epsilon}$ is a diagonal matrix of orbital energies whose elements are the one-electron orbital energies, ϵ_i 's, \mathbf{F} is the Fock matrix, and \mathbf{S} is the overlap matrix indicating the overlap between the orbitals. The Fock matrix, \mathbf{F} , accounts for the Coulomb repulsion of each electron with the static field of all of the other electrons. Roothaan's approach was critical because he was the first to describe the matrix algebraic equations of the HF procedure using a basis set representation for the molecular orbitals as shown above in Eq. (5).

The steps in a Hartree-Fock calculation start with an initial guess of the orbital coefficients. This function is used to calculate an energy and a new set of orbital coefficients, which can then be used to obtain a smaller energy value with an improved set of coefficients. This optimization procedure continues until no more improvement can be obtained within the predefined convergence criteria. This iterative procedure is said to be the self-consistent field (SCF).

In the Hartree-Fock description, the molecular orbitals are the solutions of one-electron equations with each electron moving in the average field of all the other electrons. This accounts for the static interaction between the electrons but neglects the correlation between the motions of the electrons. The inadequate description of the electron correlation is the main deficiency of the HF theory. The methods that go beyond the Hartree-Fock theory in treating the electron-electron interaction more precisely are known as electron-correlation methods. These types of calculations begin with the HF calculation and then correct for correlation. Some of these methods are the Møller-Plesset perturbation theory (MP n , where n is the order of correction), configuration interaction (CI), and coupled cluster (CC) theory. In the next two sections, brief introductions to the Møller-Plesset and coupled cluster theories will be presented.

2. Møller-Plesset Perturbation Theory

The perturbation theory expresses the solution to one problem in terms of another problem which has been solved previously. Thus, the perturbation theory splits the Hamiltonian into two or more parts as follows:

$$\mathbf{H} = \mathbf{H}^{(0)} + \mathbf{H}^{(1)} + \mathbf{H}^{(2)} + \dots + \mathbf{H}^{(N)} . \quad (7)$$

The first term, $\mathbf{H}^{(0)}$, is the unperturbed term which can be solved exactly. The other terms ($\mathbf{H}^{(1)}$, $\mathbf{H}^{(2)}$, \dots , $\mathbf{H}^{(N)}$) are called the perturbation terms. In the Møller-Plesset method, the electron-correlation correction is added as a perturbation to the Hartree-Fock wavefunction. Specifically, for the MPn method, Eq. (7) can be rewritten as

$$\mathbf{H} = \mathbf{H}^{(0)} + \lambda \mathbf{V} \quad (8)$$

where \mathbf{V} is the perturbation operator and the $\lambda \mathbf{V}$ term is the perturbation applied to $\mathbf{H}^{(0)}$. The term $\lambda \mathbf{V}$ is assumed to be small in comparison with $\mathbf{H}^{(0)}$. The perturbed wave function, ψ , and energy, E , can be expanded in terms of the dimensionless parameter λ as

$$\psi = \psi^{(0)} + \lambda \psi^{(1)} + \lambda^2 \psi^{(2)} + \lambda^3 \psi^{(3)} + \dots \quad (9)$$

and

$$E = E^{(0)} + \lambda E^{(1)} + \lambda^2 E^{(2)} + \lambda^3 E^{(3)} + \dots . \quad (10)$$

Eqs. (9) and (10) are then substituted in the Schrödinger equation to derive the wavefunctions and orbital energies at different orders. The *ab initio* Møller-Plesset treatment considers $\mathbf{H}^{(0)}$ as the sum of the Fock operators and $E^{(0)}$ as the sum of orbital energies [49]. When the series is truncated after the first order of perturbation, the Hartree-Fock energy ($E^{(0)} + E^{(1)}$) from the full Hamiltonian is obtained. This is identical to the first order of the Møller-Plesset expansion (MP1). The third term on the right hand side of Eqs. (9) and (10) can be included in the Hamiltonian to obtain the first order

correction due to correlation. The second order energy, $E^{(2)}$, is the simplest correction that accounts for correlation and this method is called the second-order Møller-Plesset (MP2) theory.

The first perturbation to the Hartree-Fock energy, $E^{(2)}$, is always negative and thus lowers the energy of the system. Because the MPn theory is not variational, it may overcorrect for the correlation, but this is rare. The order of correction can be increased to the MP3, MP4, MP5 levels (to include $E^{(3)}$, $E^{(4)}$, $E^{(5)}$ terms, etc.) or even higher for more accurate results. Including correlation generally improves the accuracy of computed energies and geometry. High accuracy work which aims for quantitative results should use higher orders of the MP treatment. The MP3 and MP4 calculations are commonly seen in the literature.

3. Coupled Cluster Theory

The coupled cluster (CC) theory is another *ab initio* approach to account for the electron correlation. The coupled cluster theory expresses the wavefunction as linear combinations of multiple determinants

$$\Psi = c_0\Psi_{\text{HF}} + c_1\Psi_1 + c_2\Psi_2 + \dots \quad (11)$$

where the coefficients c_i reflect the weight of each determinant in each expansion term. The Hartree-Fock determinant is sometimes included as a leading term in Eq. (11) because of its reasonable efficiency. In general, the higher-order determinants are constructed by promoting electrons from the occupied to unoccupied orbitals. The order of coupled cluster theory is determined by the type of excitation. For example, S stands

for singly-excited and D for doubly-excited systems. While the MPn method corrects for all types of excitations (S, D, T, Q, etc.) to the n-th order, the CC method includes all types of corrections for the given type of excitations.

The main component in CC theory is the cluster operator, \mathbf{T} , which is defined as

$$\mathbf{T} = \mathbf{T}_1 + \mathbf{T}_2 + \mathbf{T}_3 + \dots + \mathbf{T}_n \quad (12)$$

where n is the total number of electrons and \mathbf{T}_i is the operator for the i excitations from the reference. The type of coupled cluster theory is determined by choosing the cluster operator. For example, consideration of $\mathbf{T} = \mathbf{T}_1$ yields the CCS level which is a coupled cluster treatment including only single excitations. Similarly, when $\mathbf{T} = \mathbf{T}_1 + \mathbf{T}_2$ is considered, this gives the CCSD (single and double excitations) method. Due to the number and complexity of the determinants used, *ab initio* calculations involving the coupled cluster method are very time-consuming. Generally, the CCSD method produces highly satisfactory results which are, in principle, more accurate than the results produced by the MP4 level of theory. Another commonly used approach of CC theory is the calculation of the triple excitation term as a perturbation to the CCSD terms. This gives rise to the CCSD(T) method which is commonly seen in the literatures.

4. Density Functional Theory

In recent years density functional theory (DFT) has become a popular choice for investigating the chemical properties of different types of molecules. The advantage of the DFT-based calculations is that they result in very satisfactory output and use less computational time than many other traditional quantum mechanical techniques. In 1964

Kohn and Hohenberg [50(a)] proposed that there exists a unique functional that determines the ground state energy and density exactly. However, the Kohn-Hohenberg theorem does not provide a specific form for this functional. This theorem was the basis of DFT which describes the energy of the molecule not from evaluating the total wavefunction but from solving for the electron density. Therefore, DFT can be classified as a method that is different from *ab initio* calculations.

In simple format, DFT methods split up the total electronic energy into smaller terms according to

$$E = E^T + E^V + E^J + E^{xc} \quad (13)$$

where E^T is the kinetic energy term associated with the electron motions, E^V is the potential energy term associated with the nucleus-electron attraction and nucleus-nucleus repulsion, E^J is the average electron-electron repulsion term, and E^{xc} is the exchange-correlation term which includes the rest of the electron-electron repulsion. All of the four energy terms in Eq. (13), except for the nucleus-nucleus repulsion, are functions of the electron density, $\rho(\mathbf{r})$. The DFT method determines one function in terms of another function, which is basically the meaning of the word *functional*. The density functional obtains the energy for the system from its electron density.

The non-classical term in Eq. (13) is the exchange-correlation term, E^{xc} . The E^{xc} term is approximated by integrals involving mainly the spin densities. The E^{xc} is divided into two parts:

$$E^{xc}(\rho) = E^x(\rho) + E^c(\rho) . \quad (14)$$

In Eq. (14) $E^X(\rho)$ is the exchange functional which corresponds to the same-spin electron-electron interaction, while $E^C(\rho)$ is the correlation functional which corresponds to the mixed-spin electron-electron interaction. There is no exact form for the functional. However, there are many forms of several functionals which have been developed and implemented to explore the chemical properties of different molecules. Some functionals were developed from fundamental quantum mechanics and some were developed by fitting them to experimental results. These different types of approaches are referred to as *ab initio* and semiempirical DFT methods, respectively.

Examples of developed and commonly used functionals are B3LYP, B3P86, and PW91. These functionals have advantages and disadvantages when they are incorporated in the calculations. The B3LYP method utilizes a three-term Becke functional [50(b)] combined with the Lee, Yang, Parr [50(c),(d)] exchange functional. The B3LYP functional is said to be hybrid, which means it includes Hartree-Fock and DFT exchange terms in addition to the DFT correlation terms. That is,

$$E_{\text{hybrid}}^{\text{XC}} = c_{\text{HF}} E_{\text{HF}}^{\text{X}} + c_{\text{DFT}} E_{\text{DFT}}^{\text{XC}}, \quad (15)$$

where the confinements c 's are constants. The B3LYP hybrid functional is currently the most widely used type of DFT calculation, especially for organic molecules.

More complicated types of density functionals are those incorporating the electron density and their gradients as well. Such methods are known as gradient-corrected methods. The gradient-corrected methods are usually hybrid. An example of gradient-corrected functionals is PW91 (Perdew and Wang 1991) [50(e),(f)].

The DFT method was found to predict the vibrational frequencies in very good agreement with experimental results, especially for hydrocarbons. DFT results are not as accurate for heavy elements, highly-charged systems, or systems sensitive to electron correlation. One technique for improving the efficiency of the density functionals is by minimizing the integration grid size of the electron density. Finer grids result in a greater number of integration points per unit volume of density, and thus more accurate results are obtained.

5. Basis Sets

A basis set is a set of linear combinations of mathematical functions that describe the shapes of the orbitals in a molecule. In order to be able to perform an *ab initio* calculation, basis sets must be used. The larger the basis set, the more accurate these descriptions are, and the fewer the restrictions imposed on the locations of the electrons will be. The basis sets use linear combinations of Gaussian-type functions to form the orbitals. Basis sets assign a group of basis functions to each atom within a molecule to describe its orbitals. There is a long list of existing basis sets that can be used to perform *ab initio* calculations. The choice of basis sets is a major factor in determining the amount of computation time and the degree of accuracy for a specific type of calculation.

A minimal basis set uses the minimum number of basis functions per atom. This has only three Gaussian primitives per basis function (3GTOs). The size of the basis set can be increased by incorporating a larger number of basis functions for each atom. For

example, instead of using one basis function to describe the 1s orbital for the hydrogen atom, two basis functions of different sizes are used. These types of basis sets are known as split-valence or sometimes as double-zeta (double- ζ) basis sets. Examples of split-valence basis sets are the 3-21G and 6-31G. When three different types of basis functions are used to describe each atomic orbital, it is known as triple-split-valence or triple-zeta (triple- ζ) basis sets. An example of a triple-split-valence basis set is the 6-311G. The basis sets 6-31G or 6-311G are known as the Pople basis sets. Split-valence and triple-split-valence basis sets allow the changes not only in the size of the orbitals but also in their shape.

When an angular momentum function is added to the basis function description, it gives the orbital the correct symmetry (s , p , d , etc.), and the basis set is said to be polarized. Polarization functions add more accuracy to *ab initio* results because they give the orbitals more flexibility to change their shape. Polarization functions are used to predict more accurate geometry and vibrational frequencies. Examples of polarized basis sets include the 6-31G(d) and 6-31(d,p). The notation 6-31G(d) implies that a set of d primitives has been added to each atom other than hydrogens, whereas the 6-31G(d,p) means that a set of d primitives has been added to each atom other than hydrogens and a set of p primitives has been added to the hydrogen atoms as well. Extra numbers of sets of polarization functions may also be added, depending on the need and the level of accuracy being sought. However, polarization functions are generally expensive in terms of the required computational time.

Other types of functions used with Pople basis sets are diffuse functions, and they are indicated with plus signs, such as 6-31+G(d) and 6-31++G(d) basis sets. Diffuse functions are primitives with small exponents and give a better description for the wavefunction far from the nucleus. They are helpful in several cases, such as for predicting the geometry for anions, for calculations involving molecules with lone pairs of electrons, for investigating the types of interactions that occur over long distances, and for calculations related to electronic excited states. Adding diffuse functions also changes the relative stabilities of different conformations within a molecule. The “plus” means a set of diffuse functions is added to nonhydrogen atoms. The additional plus implies that another set of diffuse functions is added to hydrogen atoms. In terms of computational time, diffuse functions are not as expensive as polarization functions.

Other commonly used basis sets are those developed by Dunning, Huzinaga, Duijneveldt and others. Two examples of widely used basis functions of the Dunning-type are VDZ and VTZ which stand for double-zeta valence and triple-zeta valence types, respectively. A very commonly used basis set of this type is the cc-pVTZ. The “cc” means it is a correlation-consistent basis set. In other words, the basis functions are optimized for the best performance with correlated calculations. The letter “p” implies the use of polarization functions of a large angular momentum. Dunning made a major contribution in developing different types of correlation-consistent basis functions. It has been noted that these large correlation-consistent basis sets with high angular-momentum polarization functions greatly improve the level of accuracy of the calculations.

6. Calculation of Vibrational Frequencies

Ab initio calculations use the harmonic oscillator approximation to compute the vibrational frequencies because the harmonic oscillator approach is more affordable as compared to other more accurate methods. Harmonic oscillator calculations are useful for predicting the frequencies for the fundamental vibrations.

For a diatomic molecule the potential energy, $U(r)$, from a Taylor series expansion truncated after the second order is given by

$$U(r_{AB}) = \frac{1}{2} k_{AB} (r_{AB} - r_{AB,eq})^2 \quad (16)$$

where r_{AB} is the distance between the atoms A and B, r_{eq} is the equilibrium distance at the energy minimum, and k_{AB} is the force constant which is defined as

$$k_{AB} = \left. \frac{d^2U}{dr^2} \right|_{r=r_{eq}} \quad (17)$$

To predict the rotational and vibrational frequencies for a molecule with N atoms, the Schrödinger equation in terms of nuclear motions:

$$\left[-\sum_i^N \frac{1}{2m_i} \nabla_i^2 + V(q) \right] \Psi^{nuc}(q) = E \Psi^{nuc}(q) \quad (18)$$

needs to be solved. Most of the parameters in Eq. (18) have been described above. The other terms are q , the nuclear coordinate (a total of $3N$ vibrational coordinates have to be considered), and Ψ^{nuc} , the nuclear wavefunction expressed in terms of the nuclear coordinate. Eq. (18) allows the rotational and vibrational frequencies to be calculated within the harmonic oscillator model. In the case of vibrational frequency calculations

for a polyatomic molecule of N atoms, Eqs. (16) and (18) lead to the multi-dimensional equation:

$$\left[-\sum_i^{3N} \frac{1}{2m_i} \nabla_i^2 + \frac{1}{2} (\mathbf{q} - \mathbf{q}_{\text{eq}}) \mathbf{H} (\mathbf{q} - \mathbf{q}_{\text{eq}}) \right] \Psi^{\text{nuc}}(\mathbf{q}) = E \Psi^{\text{nuc}}(\mathbf{q}) \quad (19)$$

where \mathbf{q} represents the mass-dependent spatial coordinate vector and \mathbf{H} is the Hessian matrix which is defined by

$$\mathbf{H} = \left. \frac{\partial^2 U}{\partial \mathbf{q}^2} \right|_{\mathbf{q}=\mathbf{q}_{\text{eq}}} \quad (20)$$

It can be seen that Eq. (19) is $3N$ -dimensional, but it can be divided into $3N$ one-dimensional Schrödinger equations. Each component of the vector \mathbf{q} corresponds to a molecular vibration which is called a normal mode. For each normal mode, a set of harmonic oscillator eigenfunctions and eigenvalues are expressed in terms of square roots of force constants in the Hessian matrix and in terms of atomic masses as well.

Eq. (19) can be applied to structures other than the minimum conformations. In this case, one or more imaginary frequencies will result from the calculations. These result from negative force constants of normal modes indicating that the displacements of specific molecular vibrations lead to lowering of the energy on the potential energy surface. Since the harmonic oscillator vibrational frequencies are computed from the square root of the force constants, this gives rise to imaginary, or sometimes called negative, frequencies. Thus, vibrational frequency calculations can be used to examine the optimized structure whether it is a minimum or a saddle point. In any case, the level

of theory and basis set used to compute the vibrational frequencies must not be changed from the one used to optimize the geometry for the molecule.

7. Calculation of Vibrational Infrared and Raman Spectra

Infrared and Raman intensities can be calculated from *ab initio* calculations. The IR intensities are proportional to the change in dipole moments as a function of vibrational displacements. *Ab initio* methods compute several properties using mixed derivatives originating from the energy expansion, and the infrared intensities can be predicted from

$$\text{IR intensity} \propto \left(\frac{\partial \boldsymbol{\mu}}{\partial \mathbf{q}} \right)^2 \propto \left(\frac{\partial^2 E}{\partial \mathbf{R} \partial \mathbf{F}} \right)^2 \quad (21)$$

where $\boldsymbol{\mu}$ is the electric dipole moment, \mathbf{q} is, as defined above, the vibrational normal coordinate, \mathbf{R} is the change in the nuclear geometry, and \mathbf{F} is the external electric field. The Raman intensities based on the harmonic oscillator approximation are proportional to the polarizability change ($\boldsymbol{\alpha}$) with respect to the vibrational coordinate and can be given by

$$\text{Raman intensity} \propto \left(\frac{\partial \boldsymbol{\alpha}}{\partial \mathbf{q}} \right)^2 \propto \left(\frac{\partial^3 E}{\partial \mathbf{R} \partial \mathbf{F}^2} \right)^2. \quad (22)$$

Eqs. (21) and (22) show that the infrared intensity is a second-order property while the Raman intensity is a third-order property that requires longer time to be computed. Computed infrared and Raman intensities are semi-quantitative. The level of accuracy

for intensities is not as good as for the vibrational frequencies. However, they are very helpful and are found to generally agree with experimental results.

VIBRATIONAL HAMILTONIAN

The potential energy surfaces governing the conformational changes in non-rigid molecules can be determined from spectroscopic data in conjunction with quantum mechanics. Consider the time-independent vibrational Schrödinger equation:

$$\hat{H}^{vib}\Psi^{vib} = E^{vib}\Psi^{vib} \quad (23)$$

where \hat{H}^{vib} is the vibrational Hamiltonian operator, Ψ^{vib} is the vibrational wavefunction, and E^{vib} represents the eigenvalues associated with the vibrational wavefunction. The vibrational Hamiltonian is defined by

$$\hat{H}^{vib} = \hat{T}^{vib} + \hat{V}^{vib} \quad (24)$$

where \hat{T}^{vib} and \hat{V}^{vib} are the kinetic and potential energy operators, respectively. In the following section, brief descriptions of the theory of determining these operators will be presented.

1. The Vibrational Kinetic Energy Operator

For a molecule having N atoms, the kinetic energy operator, \hat{T}^{vib} , can be expressed as [1]

$$\hat{T}^{vib} = \frac{1}{2}(\boldsymbol{\omega}^t \mathbf{q}^t) \mathbf{G} \begin{bmatrix} \boldsymbol{\omega} \\ \mathbf{q} \end{bmatrix} \quad (25)$$

where $\boldsymbol{\omega}$ is a three-dimensional angular momentum column vector, \mathbf{q} is the 3N-6 dimensional vector of momentum conjugate to the vibrational coordinate (q), \mathbf{G} is the Wilson G matrix [51], and the superscript t denotes the matrix transpose.

The Wilson G matrix depends only on the rotational and vibrational motions and is defined by

$$\mathbf{G} = \begin{bmatrix} \mathbf{I} & \mathbf{X} \\ \mathbf{X}^t & \mathbf{Y} \end{bmatrix}^{-1}. \quad (26)$$

The elements of \mathbf{I} , which is the 3×3 inertial moment tensor matrix, are given by

$$\mathbf{I} = \begin{bmatrix} I_{xx} & -I_{xy} & -I_{xz} \\ -I_{yx} & I_{yy} & -I_{yz} \\ -I_{zx} & -I_{zy} & I_{zz} \end{bmatrix} \quad (27)$$

where each element in \mathbf{I} is expressed in terms of atomic masses and coordinate vectors.

The matrix \mathbf{X} in Eq. (26) is the 3×(3N-6) rotational-vibrational interaction matrix defined by

$$\mathbf{X}_{ij} = \sum_{k=1}^N m_k \left(\mathbf{r}_k \times \left(\frac{\partial \mathbf{r}_k}{\partial q_j} \right) \right)_i \quad (28)$$

while \mathbf{Y} is the (3N-6)×(3N-6) matrix that describes the purely vibrational interactions and is given by

$$\mathbf{Y}_{ij} = \sum_{k=1}^N m_k \left(\frac{\partial \mathbf{r}_k}{\partial q_i} \right) \cdot \left(\frac{\partial \mathbf{r}_k}{\partial q_j} \right). \quad (29)$$

In Eqs. (28) and (29), m_k is the mass of the k 'th atom, \mathbf{r}_k is the coordinate vector from the k 'th atom to the center of mass of the molecule, and q is the vibrational coordinate.

In pseudo-four-membered ring molecules, such as γ -crotonolactone and silacyclopent-2-ene in this study, the ring-puckering vibration is assumed to be uncoupled with the other low-frequency vibrations. A complete vibrational analysis of a polyatomic molecule would require a multi-dimensional analysis which is difficult to achieve for molecules with a large number of atoms. However, the dimensionality of such a problem can be reduced by assuming that the vibration of the lowest frequency is separable from the rest of the vibrations and, as a result, can be analyzed independently. If the ring-puckering is treated as a vibration separable from the other low-frequency vibrations, the Wilson G matrix becomes

$$\mathbf{G} = \begin{bmatrix} I_{xx} & -I_{xy} & -I_{xz} & X_{11} \\ -I_{yx} & I_{yy} & -I_{yz} & X_{12} \\ -I_{zx} & -I_{zy} & I_{zz} & X_{13} \\ X_{11} & X_{12} & X_{13} & Y_{11} \end{bmatrix}^{-1} \quad (30)$$

After the matrix inversion, the \mathbf{G} matrix becomes

$$\mathbf{G} = \begin{bmatrix} g_{11} & g_{12} & g_{13} & g_{14} \\ g_{21} & g_{22} & g_{23} & g_{24} \\ g_{31} & g_{32} & g_{33} & g_{34} \\ g_{41} & g_{42} & g_{43} & g_{44} \end{bmatrix} \quad (31)$$

where g_{ij} is the reciprocal reduced mass. The g_{ij} in Eq. (31) with i and $j = 1, 2, \text{ or } 3$, represent by convention the pure rotational terms. The g_{i4} and g_{4j} terms with i and $j = 1, 2, \text{ or } 3$, represent the rotational-vibrational interactions. The purely vibrational term in Eq. (31) is g_{44} and this is the reciprocal of the reduced mass.

The reduced mass for small-amplitude motions is nearly constant. For a large-amplitude motion, where a substantial change of the molecular structure takes place, the reduced mass is dependent on the vibrational coordinate (x). The kinetic energy for one vibration can be written as a polynomial expansion in terms of the vibrational coordinate:

$$g_{44}(x) = \sum_{i=1}^n g_{44}^i x^i = \frac{1}{\mu(x)} \quad (32)$$

where g_{44}^i are the expansion coefficients and $\mu(x)$ is the coordinate-dependent reduced mass. Generally, Eq. (32) is truncated after the sixth-powered term. The odd-powered terms are zero for symmetric vibrations which pass through a planar conformation.

In order to obtain a proper kinetic energy expansion expression, it is necessary to express the position of each atom as a function of the vibrational coordinate in a center-of-mass system. Vector methods for calculating the kinetic energy expansion terms for different molecular types were previously reported by Laane's research group [52-54]. For molecules having significant interactions between the low-frequency, ring-bending vibrations that are not separable, two- or three- dimensional analyses are needed.

2. The Vibrational Potential Energy Operator

Describing the large-amplitude ring-puckering vibration by a harmonic potential function was shown to be inadequate. In 1945 R. P. Bell predicted that the ring-puckering vibration for a four-membered ring should be represented by a potential energy function with a quartic term [2]. Several years later, spectroscopic studies

[3,12,13] showed that the ring-puckering vibrations of four-membered ring molecules are more accurately described by a mixed quartic-quadratic potential energy function of the form:

$$\hat{V}^{vib} = ax^4 + bx^2 \quad (33)$$

where a is the force constant primarily related to the ring-angle strain, b is the force constant primarily related to the torsional strain, and x is the vibrational coordinate. The equilibrium conformation of four- and five-membered ring molecules is determined by a competition between these two types of forces. The sign of the parameter b determines whether the potential energy function is a single- or double-minimum. For a puckered molecule where the planar structure is a maximum point on the potential energy curve, the barrier to planarity, B , is given by

$$B = \frac{b^2}{4a} \quad (34)$$

and x_{\min} , which is the puckering coordinate at the energy minima, is given by

$$x_{\min} = \pm \sqrt{\frac{b}{2a}}. \quad (35)$$

Once the potential energy function and the kinetic energy terms have been determined, the vibrational energy levels for the ring-puckering vibration can be calculated. In addition, a prediction of the theoretical potential energy function can be made based on *ab initio* calculations. The optimized structures and total energies from *ab initio* calculations for the minimum structures and at the saddle points on the potential energy surface provide useful information to estimate the puckering potential function for the

molecule. For molecules having two large-amplitude vibrations that are strongly coupled, a two-dimensional vibrational potential energy analysis is essential.

A typical example that was studied very thoroughly using different spectroscopic techniques [55-57] is the inversion vibration in the ammonia molecule. Ammonia is pyramidal with an inversion coordinate of 0.38\AA . The inversion coordinate in ammonia is defined as the perpendicular distance between the nitrogen atom and the plane of the hydrogen atoms [57]. Since the inversion vibration of ammonia is almost uncoupled with the other vibrations, a one-dimensional potential energy function can be constructed in terms of the inversion coordinate and is, along with the associated vibrational level, shown in Fig. 1. The barrier height of the potential energy curve in Fig. 1 is 2076 cm^{-1} . The maximum corresponds to the planar structure of ammonia where the four atoms are coplanar. It can also be seen that the inversion vibrational levels below the barrier are doubly degenerate and begin spreading apart as they progress above the barrier. For phosphine and arsine analogues, the barrier heights were determined from infrared spectroscopy to be $6,085$ and $11,220\text{ cm}^{-1}$, respectively [56].

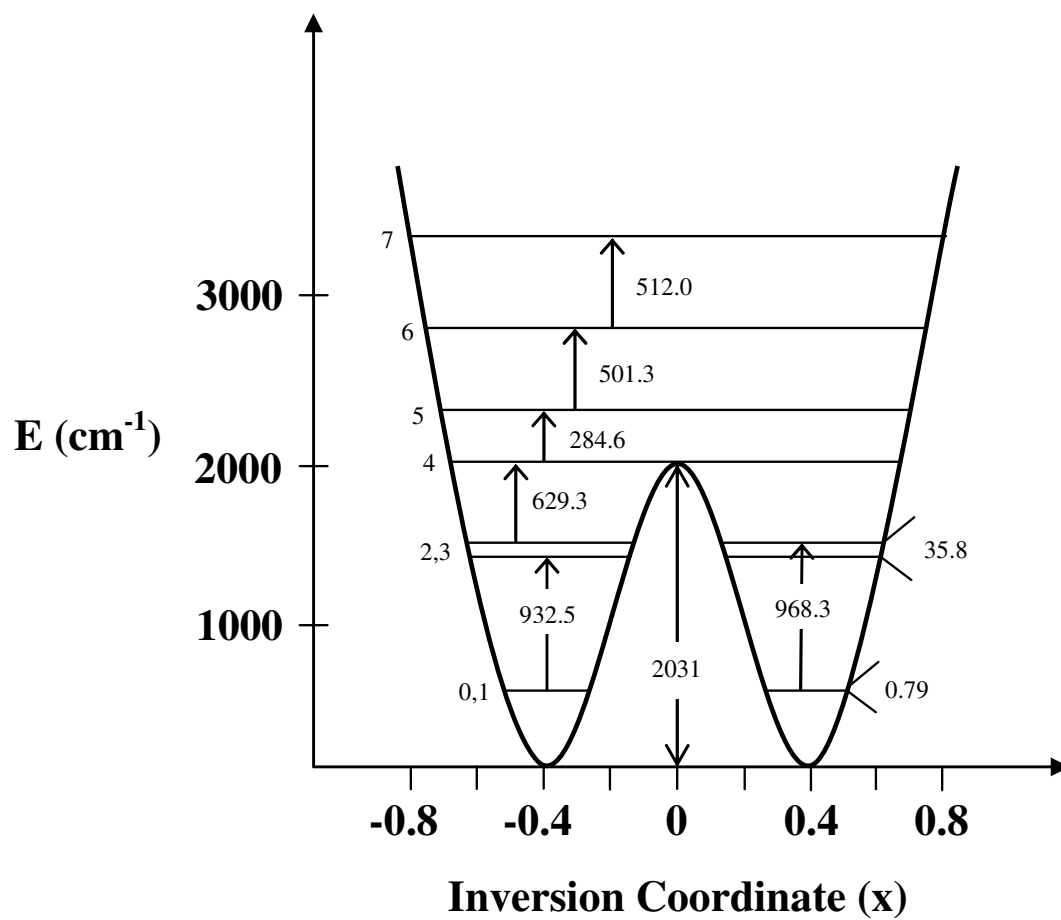


Fig. 1. Double-minimum potential energy function for the inversion vibration in ammonia.

CHAPTER III

EXPERIMENTAL METHODS

Several spectroscopic techniques were utilized in this work. In this chapter, these techniques will be described in general. The more specific procedures used for individual molecules will be discussed in the related chapters.

INFRARED SPECTRA

Mid-infrared spectra were recorded on a Biorad FTS-60 equipped with a globar source, a KBr beamsplitter, and a triglycerin sulfate detector. Typically, a total of 256 scans at 1 cm^{-1} resolution were averaged. The spectra of the sample and background were carried out under similar conditions. The spectrum of the sample was then subtracted from the spectrum of the background. The liquid-phase infrared spectra were taken by placing a drop of the sample between two polished KBr windows that are 25 mm in diameter by 4 mm in thickness. The solid-phase infrared spectra were obtained by dissolving the sample in an appropriate solvent and then applying one drop of the solution on a KBr window. The spectrum of the crystals formed on the KBr window was then obtained.

RAMAN SPECTRA

Raman spectra were recorded on a Jobin Yvon U-1000 spectrometer. (Instrument S. A., Edison, NJ) with a grating double monochromator using excitation at 5145 Å from an Innova I-100 argon-ion laser (Coherent, Santa Clara, Ca). A laser power of 4 to 5 W was used for the vapor-phase samples and of 0.15 to 0.5 W for the liquid- and solid-phase samples. For the vapor-phase experiments, the samples were contained in custom designed, heatable glass Raman cells (80 mm long by 15 mm in diameter). The vapor-phase spectra were carried out for samples heated to approximately 250° C. A liquid-nitrogen-cooled charge-coupled device (CCD) detector was used.

For the spectra of the liquid samples, the samples were contained in a glass tube which was 1 to 5 mm in thickness. The glass tube was then evacuated and sealed. To obtain the polarized spectra, a polarizing filter was put in front of the collection lens in order to deduce the ratio of the parallel to the perpendicular polarization Raman spectra. The Raman technique is sensitive to colored samples which absorb the excitation frequency. Thus, purification using vacuum transfer was normally carried out prior to the experiment.

ELECTRONIC ABSORPTION SPECTRA

The electronic absorption spectra of the vapor in the 25000 - 40000 cm⁻¹ spectral region were also recorded using a Bomem DA8.02 Fourier-transform spectrophotometer. A deuterium lamp source, a quartz beamsplitter, and a silicon detector were used. The vapor was contained in a pre-evacuated 25-cm glass cell fitted with quartz windows.

Heating the sample was necessary in some cases. Spectral acquisition was done either at room temperature or at ambient temperatures. Usually, the spectra were recorded at 0.5 cm^{-1} resolution and 10,000 to 15,000 scans were averaged.

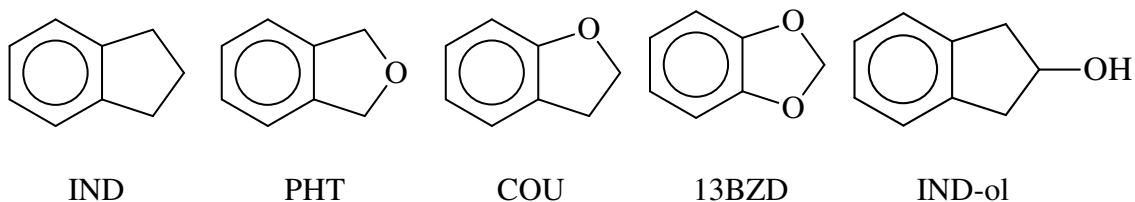
LASER-INDUCED FLUORESCENCE (LIF) SPECTRA

Two types of LIF techniques were implemented: the fluorescence excitation spectroscopy (FES) and single-vibronic level fluorescence (SVLF) spectroscopy. For FES spectra the sample that is originally solid was heated to its melting point and was then injected into a jet-cooled chamber. Excitation to the electronic excited state was accomplished using a tunable UV laser system which consists of a Continuum Powerlite 9020 Nd:YAG laser which pumps a Continuum Sunlite optical parametric oscillator (OPO). Visible output from the Sunlite OPO was frequency doubled using a Continuum FX-1 UV extension unit, which produced continuously tunable UV radiation from 355–225 nm with a resolution of 0.7 cm^{-1} . Dispersed fluorescence (SVLF) spectra were recorded on an ISA HR-640 monochromator equipped with a Spex Spectrum One CCD detector with a 2000×800 pixel chip. The FES spectral resolution was 1 cm^{-1} , whereas the SVLF spectra were taken at $\pm 2 \text{ cm}^{-1}$ resolution. Argon was used as a backing gas with stated purities of 99.99%. Backing gas pressures were selected to obtain the optimal spectra and were typically at pressures between 1 and 20 atmospheres.

CHAPTER IV
SPECTROSCOPIC AND COMPUTATIONAL STUDIES
OF THE INTRAMOLECULAR HYDROGEN BONDING
OF 2-INDANOL

INTRODUCTION

Over the past few years, several spectroscopic methods have been utilized to investigate the structures, conformations, and potential energy surfaces (PESs) [9] of indan (IND) [58] along with the related molecules phthalan (PHT) [59-61], coumaran (COU) [62,63], and 1,3-benzodioxole (13BZD) [64,65]. The structures of these molecules as well as 2-indanol (IND-ol) are shown below.



Laser-induced fluorescence (LIF) spectra of the jet-cooled molecules and ultraviolet absorption spectroscopy along with infrared and Raman spectroscopy and theoretical calculations (*ab initio*, DFT) have been used to investigate the PESs of these molecules in their ground (S_0) and first excited $S_1(\pi,\pi^*)$ electronic states [66]. The structural and

conformational changes in these two states have provided considerable insight into understanding the intramolecular forces and bonding of these molecules.

Here the attention has been directed to 2-indanol (IND-ol), which is of special interest due to its possibility of intramolecular hydrogen bonding between the OH group and the benzene ring. The Chakraborty laboratory in 2003 reported [15] a combined spectroscopic (two-photon ionization and dispersed fluorescence) and quantum chemistry calculation study of this molecule. They observed three isomers experimentally and their *ab initio* calculations estimated a hydrogen bond energy of 6.5 kJ/mole (540 cm^{-1}) for the most stable isomer. In the present work the infrared and Raman spectra of the IND-ol ground state and also the LIF spectra of the $S_1(\pi,\pi^*)$ state will be presented. In addition, high level *ab initio* optimizations for the molecule at different values of the ring-puckering and -OH internal rotation coordinates will be presented. From this information, a theoretical two-dimensional surface was constructed and this was then related to the experimental data.

Another study that has been reported very recently is the work by He and Kong [16] who examined the REMPI and ZEKE spectra of this molecule. These workers identified three conformers and assigned some vibronic levels to two of these. They also carried out *ab initio* and DFT calculations in order to obtain theoretical one-dimensional potential energy functions for the ground and excited states. Where appropriate, their results will be compared to the ones obtained by this work. Another very recent study has been published by Ottaviani, Velino, and Caminati [17]. They reported the rotational spectra of 2-indanol and its O-D isotopomer using free jet millimeter-wave absorption

spectroscopy. Only the main conformer possessing the intramolecular hydrogen bonding was observed.

EXPERIMENTAL

2-Indanol was obtained from Aldrich as a white powder with a stated purity of 99%. Its melting point is approximately 70°C. The sample was further purified by vacuum transfer and white crystals were obtained. For the liquid Raman experiment the sample was placed into a 1 mm tube, was evacuated, and then sealed. A metal wire was wrapped around the sample tube to heat the solid to 100°C and to melt the sample. A Jobin-Yvon U-1000 double monochromator equipped with a charged-coupled device (CCD) detector and an Innova I-100 argon ion laser operating at 5145Å with 0.5 watts of power were used. The polarization spectra of the liquid were also obtained under the same conditions. The Raman spectra of the solid were recorded using 150 mw of laser power. The infrared spectrum of the solid was obtained by dissolving it in CCl₄ and depositing it on a KBr window. After evaporation, white crystals were formed on the salt window. The mid-infrared spectrum was recorded using a Biorad FTS-60 equipped with a globar source, KBr beam splitter, and a triglycerin sulfate detector. A total of 256 scans at 1.0 cm⁻¹ were averaged.

Fluorescence excitation spectra (FES) were obtained with a spectral resolution of 1 cm⁻¹. The detailed experimental setup of the jet-cooled system is given in the previous chapter. The dispersed fluorescence (SVLF) spectra from the 0←0 bands for each conformer were recorded on an ISA HR-640 monochromator equipped with a Spex

Spectrum One CCD detector that is UV anti-reflection coated and back-thinned, making it sensitive in the UV. The SVLF spectra were taken at $\pm 2 \text{ cm}^{-1}$ resolution.

The electronic absorption spectra of the IND-ol vapor in the 25000 - 40000 cm^{-1} region was also recorded using a Bomem DA8.02 Fourier-transform spectrophotometer, as described in the previous chapter. Spectral acquisition was carried out at temperatures up to 250°C. Beyond that temperature the sample starts to decompose. 15000 scans were recorded at 0.5 cm^{-1} resolution and averaged. However, since solid 2-indanol has a very low vapor pressure, only several weak UV bands, mostly in the 0 \leftarrow 0 region, were observed and these were used to confirm some of the FES bands.

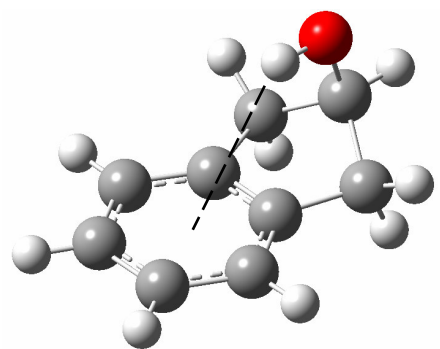
COMPUTATIONS

Ab initio calculations on the structure and vibrational frequencies of 2-indanol in the electronic ground and excited states have been previously reported [15-17]. The energies and structures of the lowest energy forms of the molecules in the S_0 electronic ground state were previously calculated using the MP2/6-311++G(d,p) level of theory [15] which is expected to give a good prediction of the geometry and the stability of the molecule. Density functional theory (DFT) has also been used to calculate the structure in the electronic ground state [16,17]. One-dimensional potential energy calculations of the S_0 state in terms of the ring-puckering and internal rotation of the OH group in 2-indanol were obtained using MP2/6-31G(d,p) [15] and DFT-B3LYP/6-311++G(d,p) [16] computations. The calculations of the S_1 excited state structures of 2-indanol and their relative stabilities were performed at the CIS/6-31+G(d) level of theory [16].

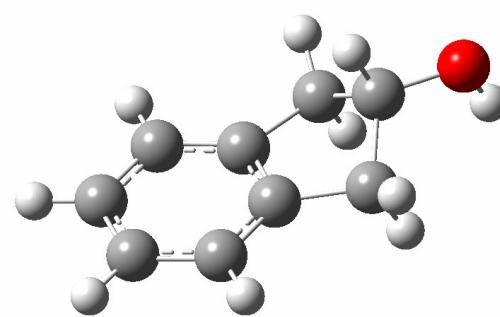
In the present study, additional high level *ab initio* and DFT computations including the triple zeta calculations have been carried out. Fig. 2 shows the four stable conformers which were studied. Conformer **A** with the intramolecular hydrogen bonding is the most stable. Fig. 3 shows the calculated structures for conformer **A** in its electronic ground (S_0) and electronic excited (S_1) states. During the calculations it was observed that when the diffuse functions in the basis sets were not used, the relative energies of the other three conformers (**B**, **C**, and **D**) were rearranged as compared to the 6-311++G(d,p) basis set [15]. Nonetheless, conformer **A** with the intramolecular hydrogen bonding was the most stable in all cases.

The cc-pVTZ basis set (triple- ζ) with the MP2 and DFT-B3LYP theories have been employed here to predict the molecular structures and relative energies of the four minimum structures shown in Fig. 2, and the planar structure as well, using the Gaussian 03 program [67]. The relative energies predicted by the MP2 theory with the triple- ζ basis set presented in Table 1 were found to be very similar to those predicted by the 6-311++G(d,p) basis set [15]. However, the effect of the triple- ζ basis set when used with the DFT-B3LYP theory (Table 1) gave more reliable predictions of the energies as well as the structures when compared to other basis sets [16,17].

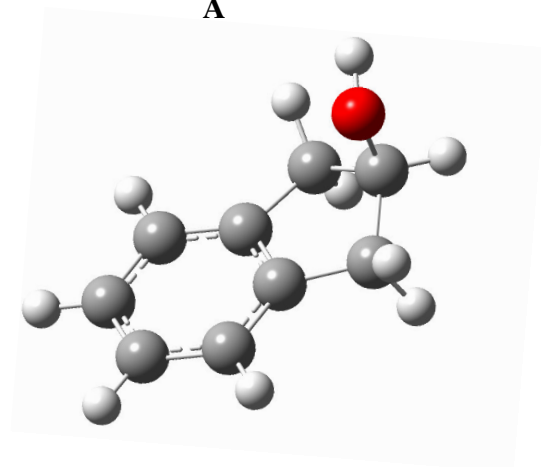
The structures shown in Fig. 3 indicate that the intramolecular hydrogen bonding becomes relatively weaker in the electronic excited state. This can be seen from the shorter O-H bond length and the larger \angle COH angle as compared to the electronic ground state values. The magnitude of the electron density of the benzene ring is predicted from the calculations to be less when the molecule is in the S_1 state.



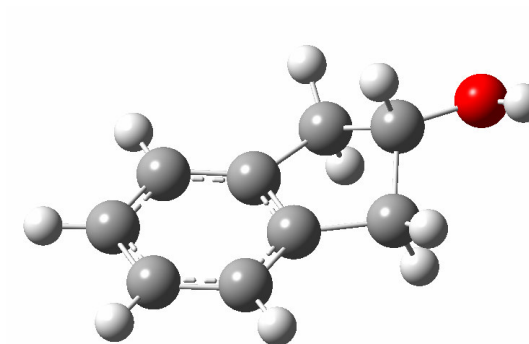
A



B



C



D

Fig. 2. The four stable conformations of 2-indanol. The intramolecular hydrogen bonding present in the most stable conformer (structure **A**) is represented by a dotted line.

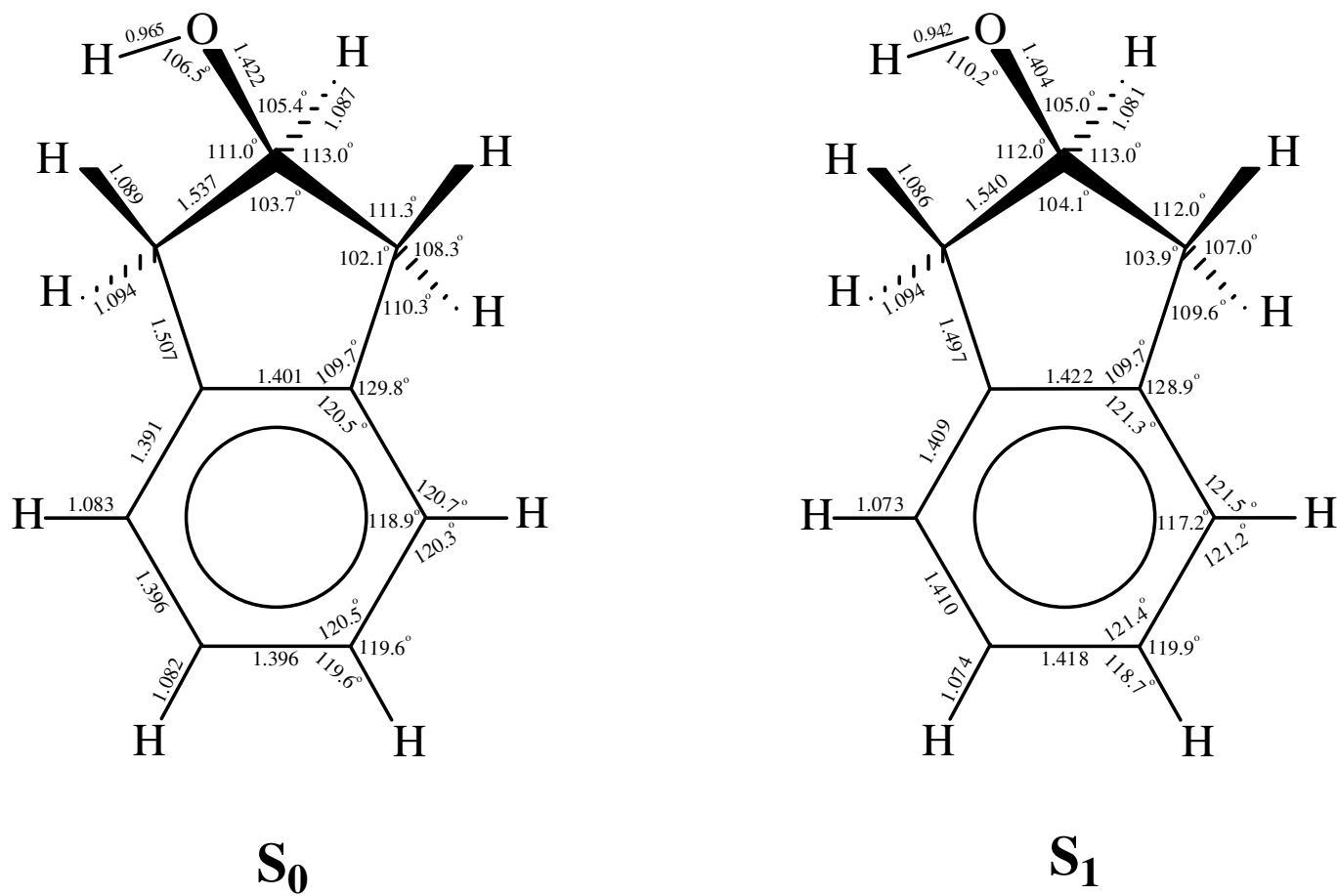
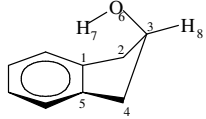
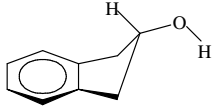
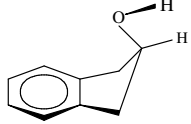
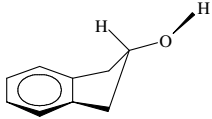
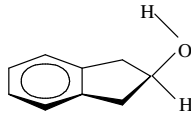


Fig. 3. Bond distances and angles of the most stable structure of 2-indanol for its S₀ and S₁ states calculated at the MP2/cc-pVTZ and UCIS/6-311++G(d,p) levels of theory, respectively.

Table 1

Calculated^a structural parameters, energies, puckering angles, OH internal rotation angles, and dipole moments for the conformations (**A**, **B**, **C**, and **D**) and planar structure (**P**) of 2-indanol in its electronic ground state

					
	A	B	C	D	P
Bond distances (Å)					
C ₃ -O ₆	1.422 (1.426)	1.413 (1.416)	1.424 (1.429)	1.417 (1.421)	1.423 (1.425)
O ₆ -H ₇	0.965 (0.964)	0.963 (0.963)	0.962 (0.962)	0.962 (0.961)	0.963 (0.963)
C ₃ -H ₈	1.087 (1.088)	1.091 (1.091)	1.093 (1.094)	1.096 (1.096)	1.087 (1.088)
Bond angles (deg)					
C ₃ O ₆ H ₇	106.5 (108.4)	107.2 (108.5)	107.6 (108.6)	107.8 (108.9)	107.0 (108.4)
C ₂ C ₃ C ₄	103.7 (104.1)	103.8 (104.3)	104.4 (104.9)	104.1 (104.7)	106.6 (106.3)
O ₆ C ₃ H ₈	105.4 (104.7)	105.2 (104.6)	110.4 (109.7)	110.7 (109.9)	104.0 (103.7)
Puckering angle (deg)	35.4 (29.7)	-35.1 (-30.4)	31.1 (25.5)	-35.0 (-29.7)	0.0 (0.0)
Internal rotation angle (deg)	180.0 (180.0)	180.0 (180.0)	66.9 (63.0)	54.5 (52.3)	180.0 (180.0)
Total energy (Hartrees)	-423.3316818 (-424.3550792)	-423.32948051 (-424.35422743)	-423.3296766 (-424.3537517)	-423.32954458 (-424.35415258)	-423.3257208 (-424.3520662)
Relative energy (cm ⁻¹)	0.0 (0.0)	483.1 (186.9)	440.1 (291.3)	469.1 (203.4)	1308.3 (661.3)
Total dipole moments (Debye)	1.59 (1.39)	1.45 (1.36)	1.80 (1.47)	1.46 (1.36)	1.33 (1.25)

^aMP2/cc-pVTZ theory was used. Results in parentheses are from the DFT-B3LYP/cc-pVTZ calculations.

An energy map has been constructed to enhance our understanding of the intramolecular forces governing the structure and interconversion of these four conformers. In order to get accurate results from *ab initio* calculations, the MP2 theory was used with a large basis set such as triple- ζ or 6-311++G(d,p), and this required a large amount of computational time. It was also noted that the MP2/6-31(d,p) calculation resulted in different relative energies of the less stable structures as compared to the 6-311++G(d,p) calculation [15]. A basis set which gives more reliable results in terms of energy and structure using a reasonable amount of computation time can be achieved by adding to the MP2/6-31(d,p) basis set a set of diffuse functions to the atoms other than the hydrogens. The role of the diffuse functions is primarily to give more flexibility for the description of the molecular orbitals, and they better describe the weak intramolecular forces [42-45]. It was found that the results from the MP2/6-31+G(d,p) with the diffuse functions reproduced in a satisfactory way the calculations from the triple- ζ basis set (Table 2). The calculated ring-puckering angles in the four conformers using the 6-31+G(d,p) basis set can be seen to be in excellent agreement with those obtained using the high level theory. The structure of 2-indanol was optimized at different puckering angles using the MP2/6-31+G(d,p) level of theory.

In order to construct the energy surface representing the effect of the internal rotation and the ring-puckering in 2-indanol, the OH group was allowed to rotate about the C-O bond from a dihedral angle of 0° to 180° at increments of 15° , with the puckering angle being fixed and all the carbon atoms, except the one bonded to the oxygen atom, lying in the plane of the molecule. The internal rotation angle was defined

Table 2

Comparison of energies and puckering and internal rotation angles from different basis sets for the four conformers and the planar structure

	MP2/cc-pVTZ				MP2/6-31+G(d,p)				DFT-B3LYP/cc-pVTZ			
	Total energy (Hartree)	Relative energy (cm ⁻¹)	Puckering angle (deg.)	Internal rotation angle (deg.)	Total energy (Hartree)	Relative energy (cm ⁻¹)	Puckering angle (deg.)	Internal rotation angle (deg.)	Total energy (Hartree)	Relative energy (cm ⁻¹)	Puckering angle (deg.)	Internal rotation angle (deg.)
A	-423.33168184	0	35.4	180.0	-422.9342967	0	35.4	180.0	-424.35507920	0	29.7	180.0
B	-423.32948051	483	-35.1	180.0	-422.9317951	549	-35.1	180.0	-424.35422743	187	-30.4	180.0
C	-423.32967663	440	31.1	66.9	-422.9325933	374	31.5	69.5	-424.35375170	291	25.5	63.0
D	-423.32954458	469	-35.0	54.5	-422.9322436	451	-34.5	56.2	-424.35415258	203	-29.7	52.3
P	-423.32572080	1308	0.0	180.0	-422.9279627	1390	0.0	180.0	-424.35206620	661	0.0	180.0

to be 180° for conformer **A** with the maximum amount of hydrogen bonding to the benzene ring. Fig. 4 provides descriptions of the ring-puckering and internal rotation modes along with those for two other lower frequency modes, the ring-flapping and ring-twisting. A computer program was utilized to interpolate the data points along the puckering angle axes and the OH internal rotation axes to produce the energy surface and contour shown in Figs. 5 and 6. To get even more accurate results at the saddle points, the energy and geometry of the transition structures were calculated using the triple-zeta basis set and the results are shown in Table 3. The detailed calculated structures for the energy map are given in Tables 4 and 5.

In addition, DFT with the triple-zeta basis set was used to calculate the vibrational frequencies for the four possible conformers of 2-indanol. Approximate normal mode assignments were made for each conformer by examining the atom vector displacements.

SPECTROSCOPIC RESULTS

1. Raman and Infrared Spectra

Figs. 7 and 8 compare the experimental liquid Raman spectra of IND-ol at 90° to the calculated spectrum of the four conformers. Under these conditions, a great deal of intermolecular hydrogen bonding between neighboring molecules is expected so the $-OH$ stretching region as well as other $-OH$ vibrations will reflect these interactions. Figs. 7 and 8 are primarily intended to demonstrate that on the whole the DFT calculations do a good job of reproducing the spectra. Fig. 9 shows the polarization

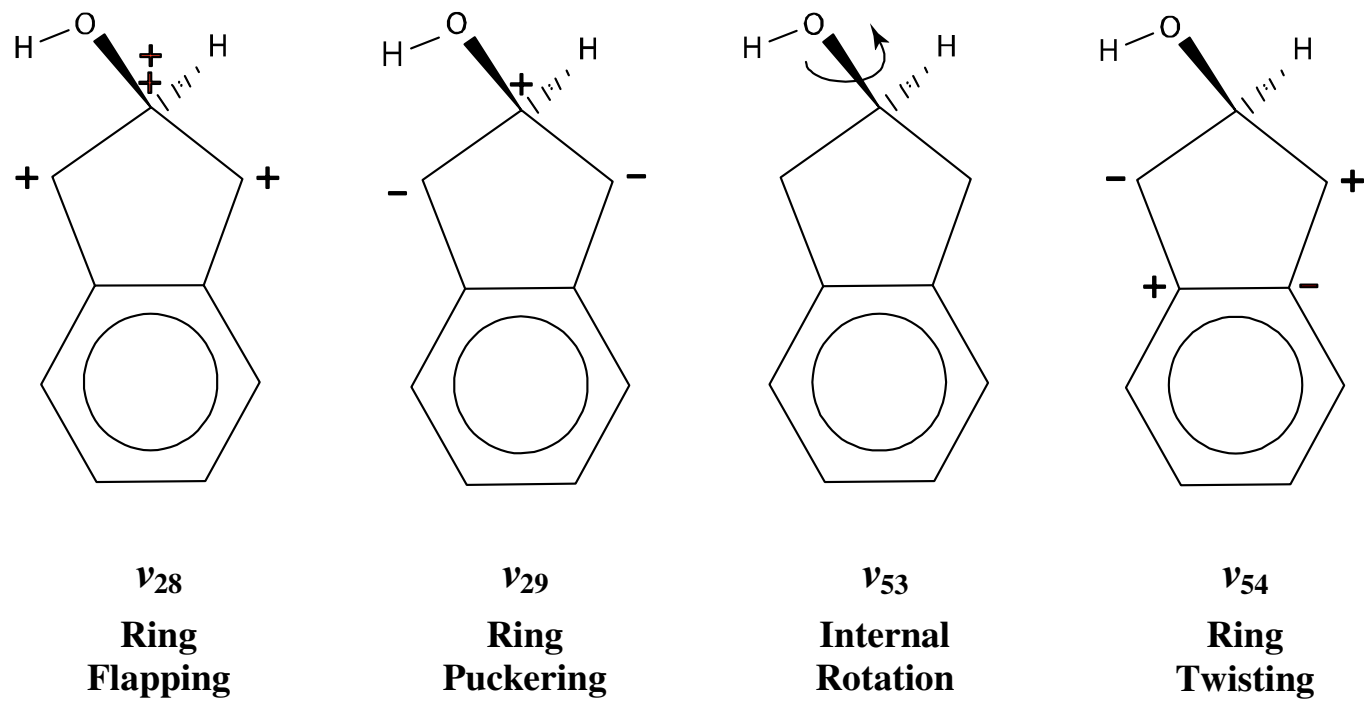


Fig. 4. The four large-amplitude, low-frequency vibrations in 2-indanol.

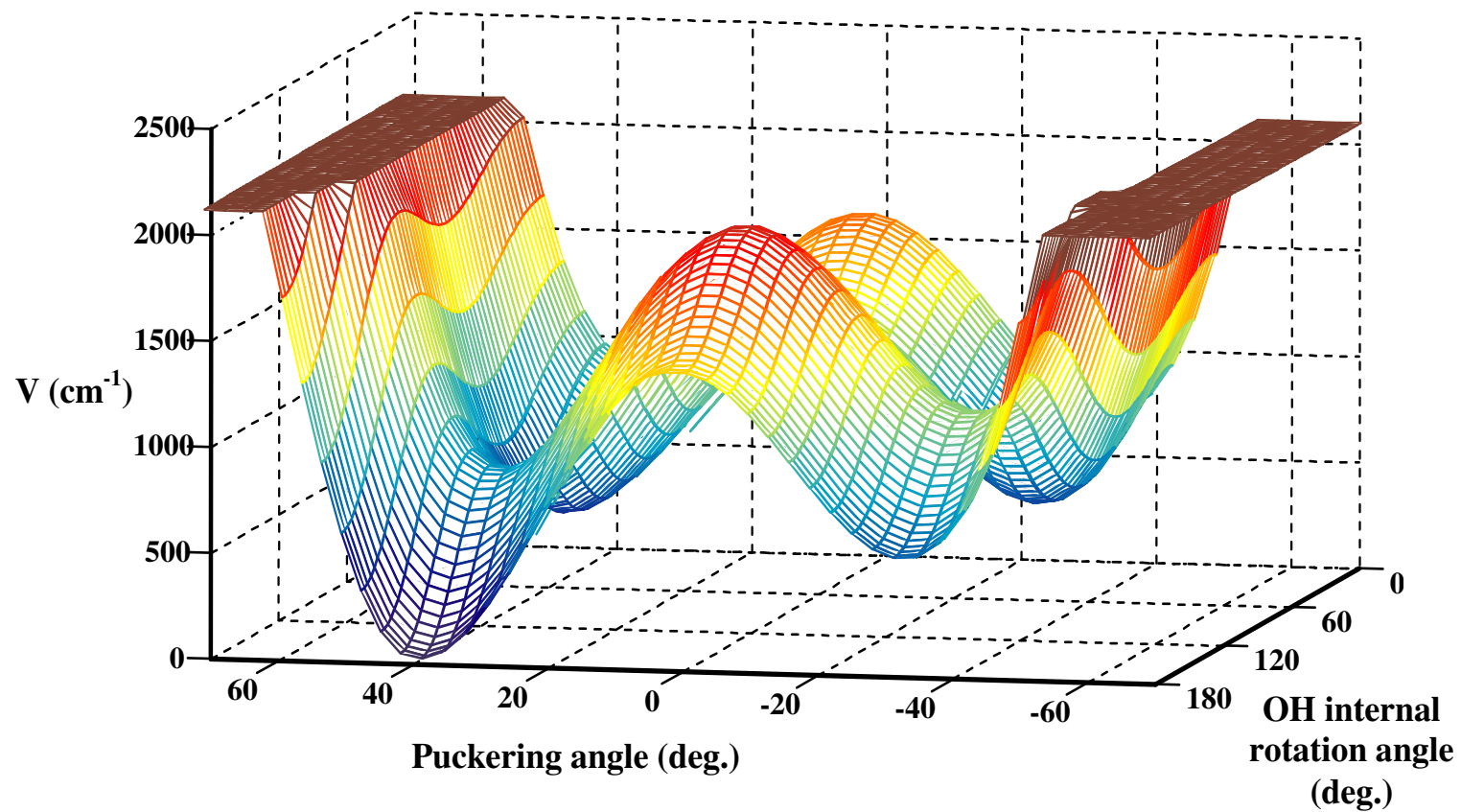


Fig. 5. Calculated potential energy surface of 2-indanol in terms of its ring-puckering angle (degrees) and the OH internal rotation angle (degrees relative to 180° at the A conformation).

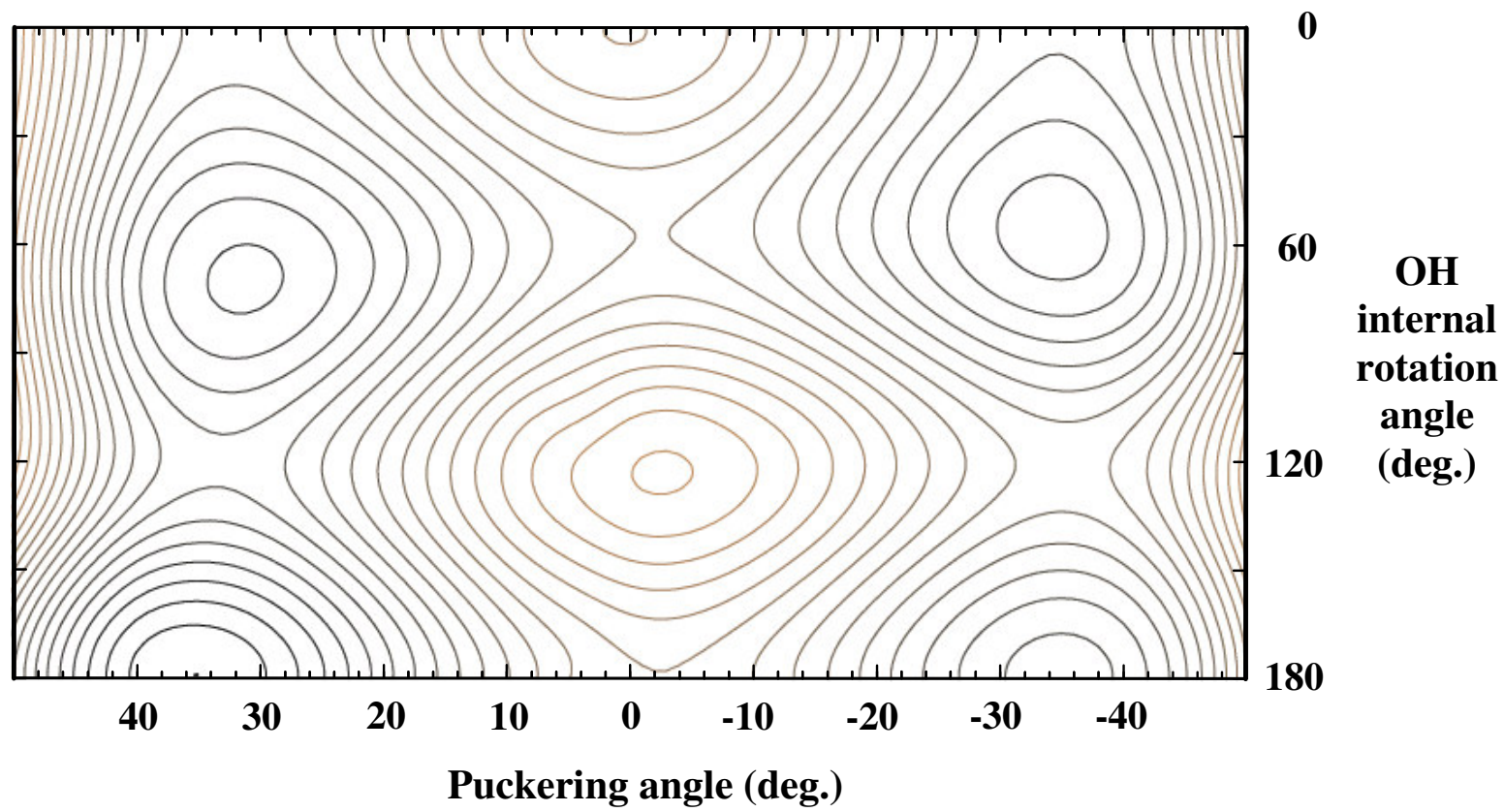


Fig. 6. Topological map equivalent to Fig. 5.

Table 3

Energy barriers between the four conformers, puckering angles, and internal rotation angles of the transition structures in the energy map of 2-indanol

Structure ^a	MP2/cc-pVTZ				DFT-B3LYP/cc-pVTZ			
	Total energy (Hartree)	Relative energy (cm ⁻¹)	Puckering angle (deg.)	Internal rotation angle (deg.)	Total energy (Hartree)	Relative energy (cm ⁻¹)	Puckering angle (deg.)	Internal rotation angle (deg.)
P	-423.32572080	1308	0.0	180.0	-424.35206620	661	0.0	180.0
S_{AB}	-423.32566750	1320	-2.5	180.0	-424.35203550	668	-2.5	180.0
S_{AC}	-423.32837524	726	33.1	116.1	-424.35223003	625	28.0	116.8
S_{BD}	-423.32713990	997	-35.4	118.8	-424.35178396	723	-30.3	117.7
S_{CD}	-423.32616328	1211	-1.8	57.9	-424.35237695	593	-1.0	55.6
S_{CC}	-423.32730904	960	32.0	0.0	-424.35181726	716	25.2	0.0
S_{DD}	-423.32827568	748	-34.8	0.0	-424.35308390	438	-29.8	0.0
b1	-423.32384930	1719	-0.8	119.6	-424.34979997	1159	-0.4	120.1
b2	-423.32435871	1607	0.1	0.0	-424.35095479	905	0.1	0.0

^a **P** = planar structure, **S_{xy}** = the structure at the saddle point between conformers **x** and **y**, **bn** = the transition structure at the barrier *n*.

Table 4

Total energies (upper) in Hartree and relative energies (lower) in cm^{-1} calculated from the MP2/6-31+G(d,p) level of theory for 2-indanol (for puckering angles from 0.0° to 58.0°)

OH Internal rotation angle (deg.)	Puckering angle (deg.)									
	0.0	3.0	8.0	15.0	25.0	31.5	35.4	40.0	48.0	58.0
0.0	-422.9269856 1605	-422.9270358 1594	-422.9273997 1514	-422.9283435 1307	-422.9298881 968	-422.9303966 856	-422.9302799 882	-422.9295622 1039	-422.9262654 1763	-422.9169482 3120
15.0	-422.9272735 1541	-422.9273326 1528	-422.9276991 1448	-422.9286405 1241	-422.9301521 910	-422.9306239 806	-422.9304843 837	-422.9297403 1000	-422.9264033 1732	-422.9170325 3101
30.0	-422.9279563 1392	-422.9280316 1375	-422.9284214 1289	-422.9293681 1082	-422.9308148 764	-422.9312071 678	-422.9310357 716	-422.9302072 898	-422.9267707 1652	-422.9172511 3053
45.0	-422.9286146 1247	-422.9287225 1223	-422.9291564 1128	-422.9301444 911	-422.9315799 596	-422.9319227 521	-422.9317184 566	-422.9308196 763	-422.9272583 1545	-422.9175079 2997
60.0	-422.9288314 1199	-422.9289869 1165	-422.9294841 1056	-422.9305676 818	-422.9321038 481	-422.9324759 400	-422.9322311 453	-422.9313383 649	-422.9276568 1457	-422.9176422 2967
75.0	-422.9283827 1298	-422.9285912 1252	-422.9291592 1127	-422.9303762 860	-422.9320976 483	-422.9325541 382	-422.9323369 430	-422.9314475 625	-422.9277007 1448	-422.9175125 2996
90.0	-422.9273774 1519	-422.9276291 1463	-422.9282555 1326	-422.9296029 1030	-422.9315233 609	-422.9320828 486	-422.9319133 523	-422.9310630 710	-422.9273521 1524	-422.9171875 3067
105.0	-422.9262756 1760	-422.9266470 1679	-422.9272004 1557	-422.928633 1243	-422.9307040 789	-422.9313617 644	-422.9312546 668	-422.9304799 838	-422.9269251 1618	-422.9170170 3104
120.0	-422.9256712 1893	-422.9259398 1834	-422.9265920 1691	-422.9280574 1369	-422.9302180 895	-422.9309649 731	-422.9309327 738	-422.9302687 884	-422.9269731 1607	-422.9174684 3005
135.0	-422.9258926 1844	-422.9261534 1787	-422.9268047 1644	-422.9282911 1318	-422.9305400 825	-422.9313974 636	-422.9314539 624	-422.9309186 741	-422.9278864 1407	-422.9187138 2732
150.0	-422.9267322 1660	-422.9269910 1603	-422.9276598 1457	-422.9291838 1122	-422.9315486 603	-422.9325327 387	-422.9326688 357	-422.9322374 452	-422.9293707 1081	-422.9203479 2373
165.0	-422.9276096 1468	-422.9278693 1411	-422.9285610 1259	-422.9301206 917	-422.9325760 378	-422.9336500 142	-422.9338329 102	-422.9334585 184	-422.9306635 797	-422.9216754 2082
180.0	-422.9279627 1390	-422.9281441 1350	-422.9289355 1177	-422.9305048 832	-422.9329954 286	-422.9341034 42	-422.9342967 0	-422.9339389 79	-422.9311619 688	-422.9221752 1972

Table 5

Total energies (upper) in Hartree and relative energies (lower) in cm^{-1} calculated from the MP2/6-31+G(d,p) level of theory for 2-indanol (for puckering angles from -8.0° to -58.0°)

OH Internal rotation angle (deg.)	Puckering angle (deg.)							
	-8.0	-15.0	-23.0	-30.0	-35.1	-40.0	-48.0	-58.0
0.0	-422.9274717 1498	-422.9284890 1275	-422.9298893 967	-422.9308385 759	-422.9310614 710	-422.9306686 796	-422.9281598 1347	-422.9202525 3082
15.0	-422.9277364 1440	-422.9287323 1221	-422.9301090 919	-422.9310412 714	-422.9312557 667	-422.9308587 755	-422.9283517 1305	-422.9204556 3038
30.0	-422.9283565 1304	-422.9292963 1097	-422.9306157 808	-422.9315077 612	-422.9317034 569	-422.9312980 658	-422.9287989 1207	-422.9209353 2932
45.0	-422.9289300 1178	-422.9298047 986	-422.9310673 709	-422.9319306 519	-422.9321174 478	-422.9317143 567	-422.9292403 1110	-422.9214274 2824
60.0	-422.9290583 1150	-422.9298845 968	-422.9311302 695	-422.9320107 502	-422.9322238 455	-422.9318534 536	-422.9294381 1066	-422.9216914 2767
75.0	-422.9285344 1265	-422.9293376 1088	-422.9306034 811	-422.9315360 606	-422.9317997 548	-422.9314827 618	-422.9291496 1130	-422.9214800 2813
90.0	-422.9274902 1494	-422.9282994 1316	-422.9296030 1030	-422.9305847 815	-422.9308907 748	-422.9306169 808	-422.9283493 1305	-422.9207420 2975
105.0	-422.9264036 1732	-422.9272520 1546	-422.9285983 1251	-422.9296037 1030	-422.9299213 960	-422.9296545 1019	-422.9273947 1515	-422.9197947 3183
120.0	-422.9258539 1853	-422.9267622 1654	-422.9281555 1348	-422.929165 1126	-422.9294624 1061	-422.9291646 1126	-422.9268432 1636	-422.9191731 3319
135.0	-422.9261176 1795	-422.9270745 1585	-422.9285084 1270	-422.9295219 1048	-422.9297999 987	-422.9294688 1060	-422.9270713 1586	-422.9193026 3291
150.0	-422.9269561 1611	-422.9279206 1399	-422.9293661 1082	-422.9303847 859	-422.9306601 798	-422.9303175 873	-422.9278866 1407	-422.9200672 3123
165.0	-422.9278080 1424	-422.9287526 1217	-422.9301817 903	-422.9311959 681	-422.9314720 620	-422.9311319 695	-422.9287001 1228	-422.9208745 2946
180.0	-422.9281593 1347	-422.9290917 1142	-422.9305087 831	-422.9315181 610	-422.9317951 549	-422.9314560 623	-422.9290273 1156	-422.9212046 2873

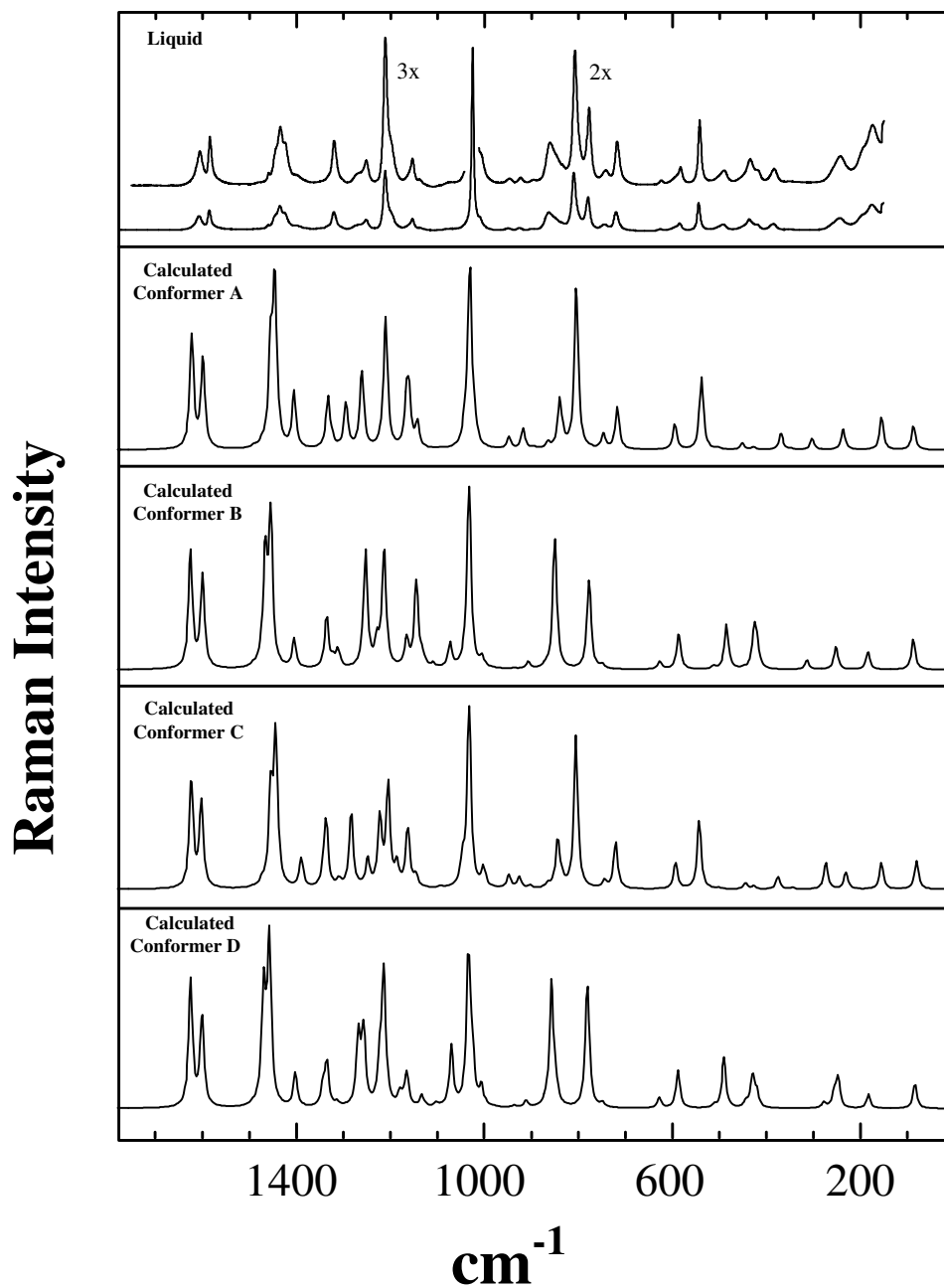


Fig. 7. Comparison of the low-frequency liquid Raman spectrum of 2-indanol at 90° C to the computed spectra of its isomers.

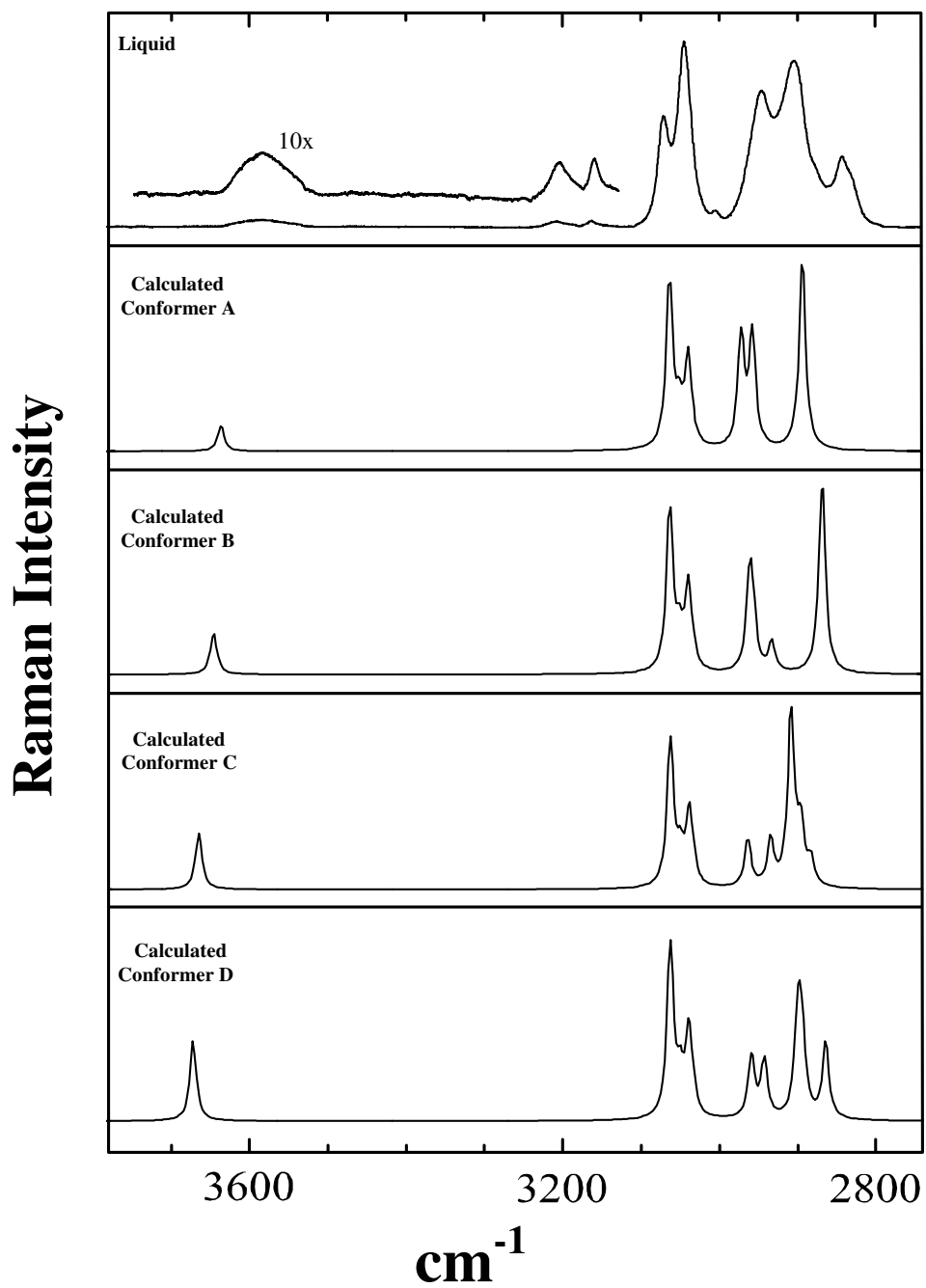


Fig. 8. Comparison of the liquid Raman spectrum of 2-indanol at 90° C to the computed spectra of its isomers for the high-frequency region.

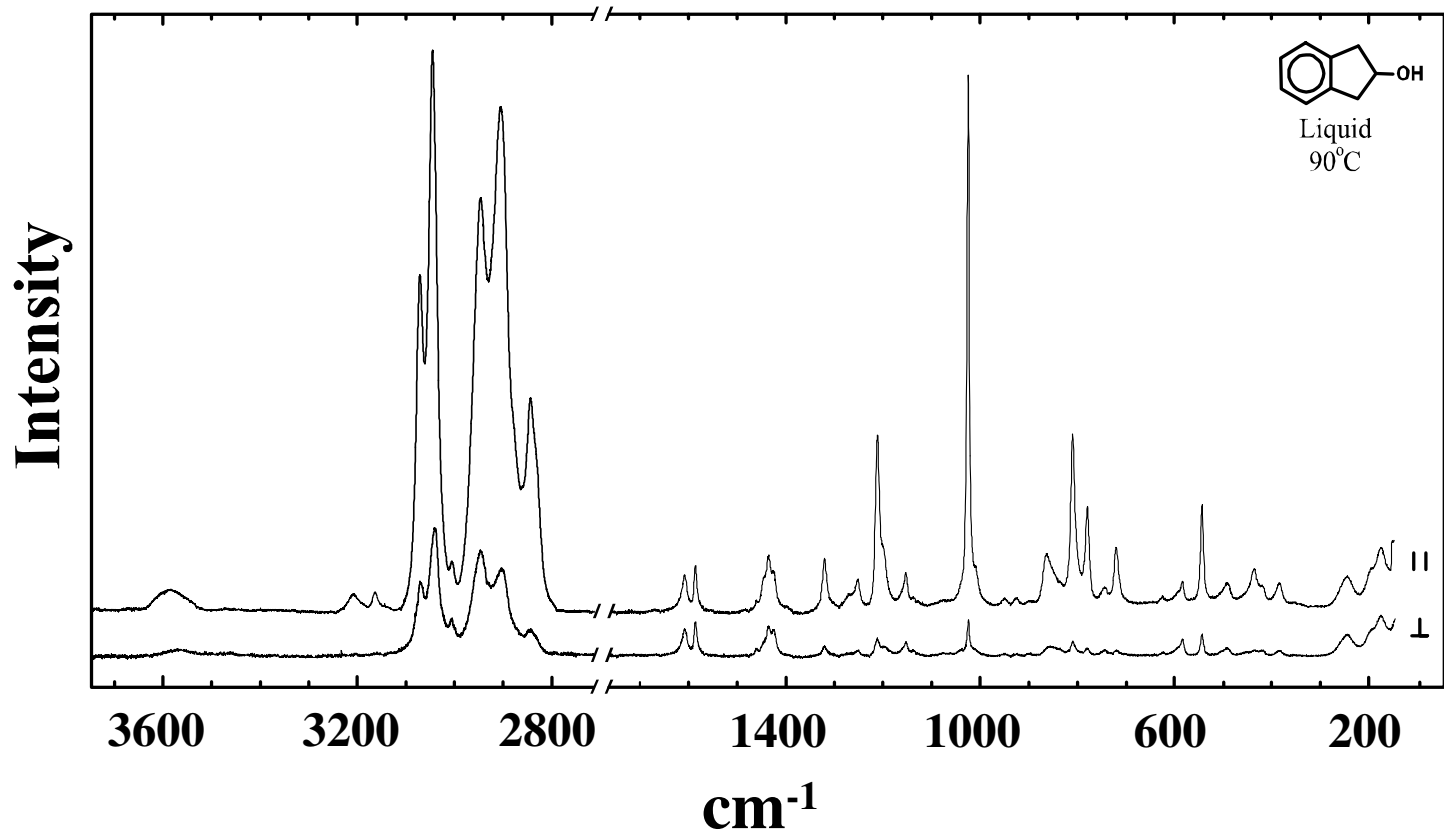


Fig. 9. Polarized spectra of the liquid 2-indanol.

spectra of the liquid taken under the same conditions.

These spectra provide great help in properly assigning the vibrational modes. Fig. 10 shows the infrared and Raman spectra of the solid-phase 2-indanol, where it can be seen that the –OH stretching vibration is shifted to a lower frequency as compared with the liquid-phase spectra. From the infrared and Raman spectra as well as the calculated spectra of 2-indanol, general vibrational assignments of the normal modes per conformer were carried out (Table 6). When examining the experimental and calculated spectra for the four conformers, it can be concluded that some vibrations of significant intensities in the infrared and Raman spectra have different frequencies. This information will greatly help identifying the four conformers, especially when the gas-phase spectra are obtained.

2. Laser-Induced Fluorescence (LIF) Spectra

Fig. 11 shows the fluorescence excitation spectra of IND-ol along with a number of the assignments. The presence of the four predicted conformers can be seen in the $S_1(\pi,\pi^*)$ excited state. Not only can the four 0_0^0 transitions be observed, but a number of the low-frequency vibrational assignments are shown in the figure. Table 7 lists the excitation frequencies (0_0^0) for the four conformers along with the assignments of several of these modes. The dispersed spectra from the 0_0^0 bands of conformers **A**, **C**, and **D** have also been recorded and these provide data for the S_0 state levels of these molecules. Table 7 summarizes some of these frequencies. It can be noted that the ring-puckering has values of 92, 86, and 90 cm^{-1} for the S_0 states of **A**, **C** and **D**, respectively.

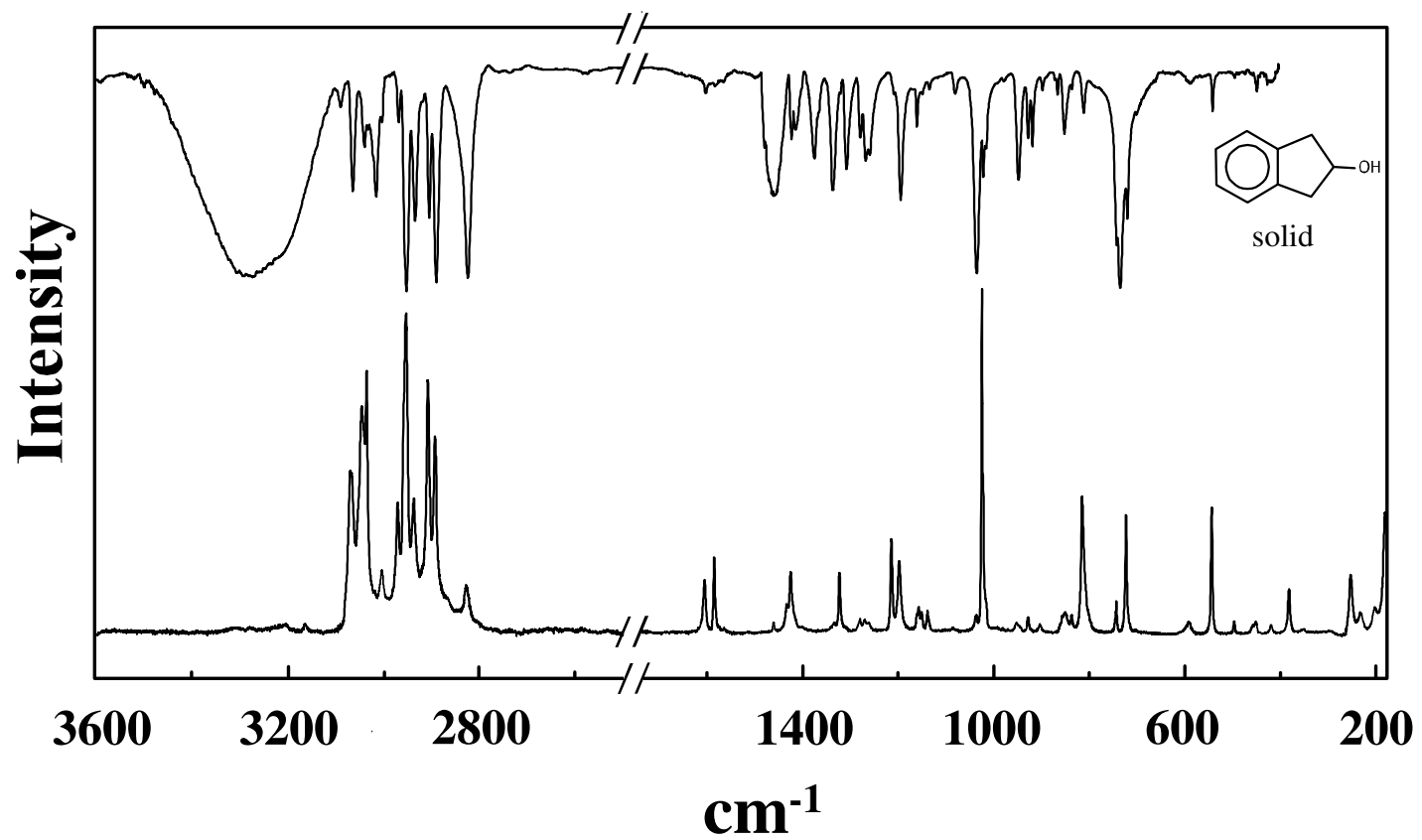


Fig. 10. Solid-phase infrared and Raman spectra of 2-indanol.

Table 6
Vibrational assignments for the four conformers of 2-indanol based on experimental and calculated spectra

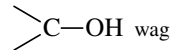
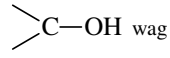
Description ^a	Experimental ^b				Calculated ^c							
	Liquid		Solid		A		B		C		D	
	IR	Raman	IR	Raman								
<i>A'</i> (A)												
v ₁ OH stretch	3396 ms	3586 (4) p	3270	3279	3637 (15,44) 0.1	3646 (17,75) 0.2	3665 (23,113) 0.3	3672 (31,137) 0.3				
v ₂ CH sym. stretch	3067 m	3071 (57) p	3065/3091	3070	3064 (22,288) 0.1	3064 (23,293) 0.1	3063 (24,290) 0.1	3063 (23,293) 0.1				
v ₃ CH sym. stretch	[3044] m	3045 (95) p	3041/3016	3047	3040 (2,146) 0.6	3040 (2,146) 0.6	3039 (2,146) 0.6	3039 (2,146) 0.6				
v ₄ CH str. (5-m)	2943 m	2946 (70) p	2953/2970	2953/2971	2972 (47,191) 0.2	2933 (17,53) 0.7	2883* (13,48) 0.2	2864 (32,131) 0.2				
v ₅ CH ₂ antisym. stretch	----	2904 (85) p	2905	2908	2958 (15,116) 0.2	2962 (28,161) 0.1	2964 (11,95) 0.4	2959 (25,108) 0.4				
v ₆ CH ₂ sym. stretch	2839 w	2844 (36) p	2890	2893	2894 (30,258) 0.1	2869 (52,293) 0.1	2909 (83,357) 0.1	2900 (26,184) 0.1				
v ₇ Ring stretch	1585 vw	1586 (11) d?	1583	1585	1600 (0,50) 0.7	1601 (0,52) 0.7	1603 (1,47) 0.7	1602 (1,62) 0.7				
v ₈ Ring stretch	1479 w	1482 (0) p	1479		1490 (15,1) 0.5	1492 (14,1) 0.7	1494 (17,0) 0.4	1494 (17,1) 0.4				
v ₉ CH ₂ deformation	----	1435 (19) d	---	1433	1455 (4,51) 0.3	1467 (3,63) 0.3	1455 (1,15) 0.3	1470 (3,78) 0.3				
v ₁₀ O-H (or C-H) in-plane wag*	1399 m	1400 (2) p	1414	1401/1406	1405 (59,31) 0.6	1405 (69,16) 0.6	1390 (4,16) 0.3	1403 (4,23) 0.4				
v ₁₁ Ring stretch	1320 vw	1320 (10) p	1321	1323	1333 (1,28) 0.2	1336 (3,29) 0.2	1337 (2,13) 0.2	1336 (2,28) 0.3				
v ₁₂ C-H (or O-H) in-plane wag*	----	1271 (3) p	1280/1308	1278/1280	1295 (8,21) 0.2	1311 (5,8) 0.4	1249 (44,15) 0.2	1258 (4,49) 0.4				
v ₁₃ CH ₂ wag	1251 w	1251 (6) p	1260/1268	1261/1270	1261 (1,43) 0.3	1253* (18,67) 0.2	1284 (1,42) 0.2	1268* (45,47) 0.3				
v ₁₄ Δ-CH wag (o.p)*	1213 mw	1211 (33) p	1209	1214	1211 (3,65) 0.1	1214 (2,68) 0.2	1205 (9,56) 0.2	1215 (0,90) 0.2				
v ₁₅ Δ-CH wag (i.p)	1157 m	1153 (7) d	1161	1160	1166 (11,20) 0.7	1165 (1,16) 0.5	1164 (0,16) 0.7	1165 (1,21) 0.5				
v ₁₆ CH ₂ twist	----	----		1157	1160* (60,24) 0.4	1145 (1,48) 0.6	1223 (6,38) 0.3	1180 (14,8) 0.7				
v ₁₇ C-O stretch	1037 ms	1038 (3) p	1036	1037	1041 (60,11) 0.2	1073 (167,41) 0.7	1047 (37,13) 0.6	1070 (116,41) 0.7				
v ₁₈ Benzene breath	1023 m	1024 (100) p	1022	1024	1031 (14,100) 0.1	1033 (13,100) 0.1	1033 (4,100) 0.1	1034 (5,100) 0.1				
v ₁₉ γ-CH wag (o.p.)	948 m	949 (2) d	948	952	948 (3,7) 0.7	937 (1,0) 0.7	948 (20,7) 0.4	937 (1,1) 0.6				
v ₂₀  wag	924 m	926 (2) p?	928/919	928	918 (4,11) 0.4	1005 (17,6) 0.6	926 (2,26) 0.2	1006 (27,13) 0.2				
v ₂₁ Ring stretch	----	863 (10) p 779 (19) p	866/872	861	840 (17,26) 0.3	778 (2,50) 0.1	844 (2,26) 0.5	781 (2,83) 0.1				
v ₂₂ Ring breath	----	809 (32) p ~857 (6) p	812/852	815/850	804 (1,91) 0.0	850 (1,73) 0.1	805 (2,85) 0.1	857 (1,86) 0.1				

Table 6
Continued

Description ^a	Experimental ^b					Calculated ^c							
	Liquid		Solid			A		B		C		D	
	IR	Raman	IR	Raman									
<i>A'(A)</i>													
v ₂₃ γ-CH wag (i.p.)	----	743 (4)	p?	735/742	743	747 (56,8)	0.1	749 (49,2)	0.1	744 (61,4)	0.1	749 (51,3)	0.1
v ₂₄ Δ-Ring bend	720 w 621 vw	720 (10) 625 (2)	p d	720/622	723	717 (0,23)	0.1	627 (2,4)	0.6	721 (3,26)	0.1	628 (5,7)	0.7
v ₂₅ γ-Ring bend	542 w	544 (16)	p	542	544	538 (2,40)	0.3	485* (6,25)	0.4	543 (4,38)	0.3	490* (6,34)	0.5
v ₂₆ CH ₂ rock*	415 w	419 (4) [436] (6)	p p	~420	419	427 (6,1)	0.5	419 (4,12)	0.3	427 (4,2)	0.5	429 (7,21)	0.2
v ₂₇ Δ-Ring bend*	----	385 (4)	p		382	369 (0,9)	0.3	426 (1,22)	0.2	375 (5,7)	0.3	420 (5,9)	0.3
v ₂₈ Ring flap	----	244 (7)	d?		231/253	236 (7,12)	~0.8	252 (6,9)	0.7	230 (10,9)	0.7	247 (2,20)	0.7
v ₂₉ Ring pucker	92 ^d	----				87 (1,14)	~0.8	87 (1,17)	~0.8	80 (1,16)	~0.8	84 (1,16)	~0.8
<i>A''(A)</i>													
v ₃₀ CH antisym. stretch	3044 mw	3041 (9)	d?	3034	3036	3051 (27,63)	0.8	3051 (28,63)	0.8	3050 (30,64)	~0.8	3050 (29,63)	0.8
v ₃₁ CH antisym. stretch	----	3005 (9)	d	3004	3004	3035 (5,19)	0.8	3035 (5,19)	0.8	3033 (6,21)	0.7	3034 (6,20)	0.7
v ₃₂ CH ₂ antisym. stretch	2944 mw	2932	d?	2935	2937	2957 (16,80)	0.8	2957 (28,83)	0.8	2935 (27,93)	0.5	2943 (32,97)	0.5
v ₃₃ CH ₂ sym. stretch	----	----		2824	2864/2827	2894 (20,74)	0.8	2869 (16,60)	0.8	2896 (45,115)	0.4	2894 (28,114)	0.2
v ₃₄ Ring stretch	----	1607 (8)	d	1603	1605	1624 (0,62)	0.8	1626 (0,67)	0.8	1625 (1,61)	~0.8	1626 (1,86)	0.8
v ₃₅ Ring stretch	1458 ms	1460 (3)	d	1459	1460	1473 (6,2)	0.8	1475 (6,2)	0.8	1473 (5,3)	0.7	1475 (6,2)	~0.8
v ₃₆ CH ₂ deformation	1422 mw	1424 (10)	d	1423	1425	1446 (7,90)	0.8	1455 (3,84)	0.8	1444 (7,84)	~0.8	1458 (3,111)	0.8
v ₃₇ Δ-CH wag (i.p.)	----	----		1337	1334	1325 (1,4)	0.8	1313 (1,3)	0.8	1310 (11,4)	0.7	1314 (1,3)	0.7
v ₃₈ CH wag (5-m)	1303 w	----		----	1294/1301	1293 (0,5)	0.8	1323 (0,4)	0.8	1341 (16,11)	0.7	1343 (20,31)	0.3
v ₃₉ CH ₂ wag	1197 m	1199	d?	1195	1197	1209 (8,8)	0.8	1229 (2,14)	0.8	1187 (16,12)	0.5	1223 (7,23)	0.6
v ₄₀ Ring stretch	----	[1153] (7)	d	1150	1151	1164 (2,6)	0.8	1174 (0,1)	0.8	1162 (6,18)	0.7	1171 (5,3)	0.7
v ₄₁ CH ₂ twist	----	1138 (2)	d	1135	1138	1143 (0,13)	0.8	1132 (0,6)	0.8	1146 (5,6)	0.7	1133 (0,8)	0.7

Table 6
Continued

Description ^a	Experimental ^b				Calculated ^d								
	Liquid		Solid		A		B		C		D		
	IR	Raman	IR	Raman									
<i>A''</i> (A)													
ν_{42} Δ -CH wag (o.p.)	1070 m	1074 (1) d	1081	1085	1090 (1,1)	0.8	1109 (6,2)	0.8	1093 (1,1)	0.7	1103 (3,2)	0.6	
ν_{43} Ring stretch	1005 mw	----	1016	----	1020 (3,9)	0.8	1039 (3,6)	0.8	1002 (7,11)	0.7	1026 (3,29)	0.2	
ν_{44} γ -CH wag (o.p.)	979 mw	----	979	981	985 (0,0)	0.8	983 (0,0)	0.8	981 (0,0)	-0.8	982 (0,0)	0.7	
ν_{45} CH ₂ rock	897 w	898 (1) d	898	904	895 (0,1)	0.8	907 (0,4)	0.8	903 (1,1)	0.7	911 (0,4)	0.7	
ν_{46} γ -CH wag (i.p.)	----	----	[866]	[861]	865 (0,4)	0.8	868 (0,1)	0.8	865 (0,2)	0.7	868 (0,2)	0.6	
ν_{47} Δ -Ring bend	----	837 (3) d	836	837	833 (1,3)	0.8	847 (0,0)	0.8	836 (0,5)	0.7	847 (0,8)	0.7	
ν_{48} γ -Ring bend	----	----	701	707	713 (0,1)	0.8	719 (0,0)	0.8	710 (0,0)	0.7	719 (0,0)	0.7	
ν_{49} Δ -Ring bend	591 vw	584 (4) d	590	591	595 (2,14)	0.8	587 (0,21)	0.8	593 (2,14)	-0.8	588 (1,26)	-0.8	
ν_{50} γ -Ring bend	----	491 (4) d	496	497	503 (0,1)	0.8	512 (0,2)	0.8	501 (0,1)	-0.8	511 (0,2)	0.7	
ν_{51}  C—OH wag	440 m	436 (6) p	450	451/457	451 (13,4)	0.8	448 (11,1)	0.8	444 (7,3)	0.6	443 (6,4)	0.4	
ν_{52} Δ -Ring bend	----	353 (0) d		350	348 (0,1)	0.8	313 (68,5) [*]	0.8	344 (2,1)	0.7	277 (42,4)	0.7	
ν_{53} OH torsion	----	----		296	302 (72,6)	0.8	251 (18,4) [*]	0.8	273 (113,15)	0.7	255 (71,10)	0.7	
ν_{54} Skeletal twist	----	156 (14) d ~192 (9) d		177 194	155 (0,18)	0.8	184 (1,10)	0.8	155 (1,15)	-0.8	183 (2,9)	0.8	

^a Δ = In-plane with respect to the plane of the benzene ring, γ = out-of-plane with respect to the plane of the benzene ring, i.p. = in-phase, o.p. = out-of-phase.

^b Frequencies in brackets are assigned for more than one vibration.

^c Scaled frequencies from the B3LYP/cc-pVTZ calculations. Numbers in parentheses are infrared and Raman intensities, respectively. The last number for each vibrational mode is the depolarization ratio.

^d From the vapor-phase SVLF experiment.

^{*} Heavily mixed vibrations.

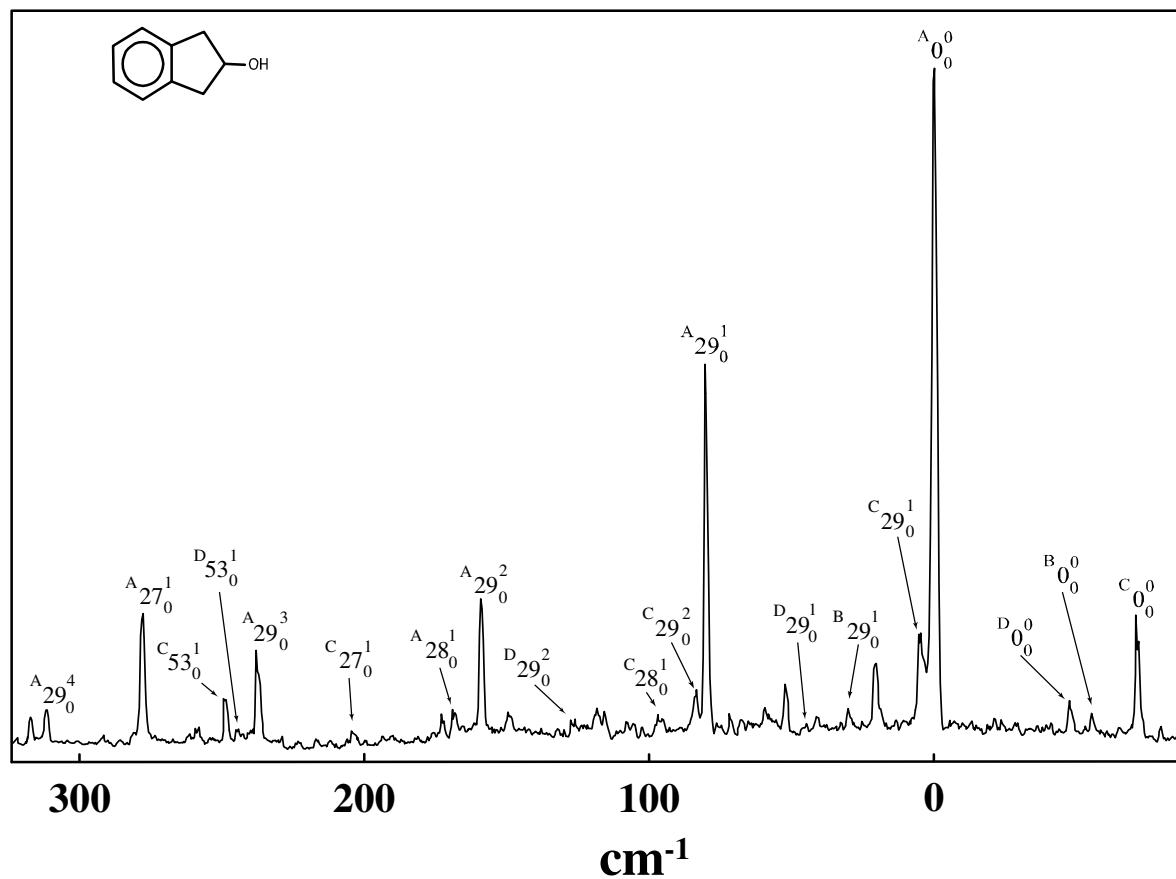


Fig. 11. Laser-induced fluorescence excitation spectrum of 2-indanol.

Table 7

Spectroscopic transitions (cm^{-1}) for the isomers of 2-indanol in its S_0 and $S_1(\pi,\pi^*)$ states^{a,b}

	A		B		C		D	
	S_0	S_1	S_0	S_1	S_0	S_1	S_0	S_1
ν_0 (cm^{-1})		37008.4		36953.7		36936.9		36961.2
$\nu_{29}(0-1)$	92 (87)	79.7 (81)	(87)	84.5 (81)	86 (87)	77.0 (76)	90 (84)	88.1 (76)
$\nu_{29}(0-2)$	182	157.9			171	154.1	178	174.1
$\nu_{29}(0-3)$		235.7						
$\nu_{29}(0-4)$		314.9						
ν_{28}	243 (236)	167.7 (136)	(252)	(152)	(230)	166.8 (138)	(247)	(138)
ν_{27}	354 (396)	275.8 (264)	(485)	(256)	366 (338)	273.7 (261)	(490)	(260)
$\nu_{54}(0-1)$	<i>157</i> (155)	(117)	(184)	(133)	(155)	(116)	(183)	(115)
$\nu_{54}(0-2)$	313	309.2						
ν_{53}	(302)	(305)	(251)	(250)	281 (273)	318.5 (271)	(255)	274.2 (271)

^aNumbers in parentheses are calculated frequencies. S_1 calculated frequencies were obtained from CIS/6-311++G(d,p) level of theory.^b S_0 values in *italics* are from the liquid-phase Raman experiment.

The calculated value for **B** is 87 cm^{-1} . In the S_1 states the values are 80 (**A**), 77 (**C**), 88 (**D**), and 85 (**B**).

Table 7 also shows some of the higher quantum states for the ring-puckering and lists values for the flapping (ν_{28}), ring angle bending (ν_{27}), ring twisting (ν_{54}) and the OH internal rotation (ν_{53}). He and Kang [16] also reported a few of the values that are shown in Table 7 for the **A** and **C** isomers in their S_1 states. For **A** they reported the 0_0^0 band at 37017 cm^{-1} with a puckering frequency of 80 cm^{-1} (82 cm^{-1} calculated). In this work the 0_0^0 is at 37008 cm^{-1} and the puckering at 79.7 cm^{-1} . For **C** their 0_0^0 origin is reported to be at 36948 and the puckering levels at 75 cm^{-1} (81 cm^{-1} calculated) and 146 cm^{-1} for the 0-1 and 0-2 transitions. In this work the 0_0^0 band is at 36937 cm^{-1} and the puckering levels at 77.0 and 154.1 cm^{-1} . Fig. 12 shows the single vibronic laser dispersed spectra from the 0_0^0 bands of conformers **A**, **C** and **D** compared with the calculated Raman spectra. The agreement can be seen to be very well.

Based on the intensities of the 0_0^0 bands, which are all expected to have very similar transition moments, the distribution of conformers in the S_0 state can be calculated. The distribution can also be calculated based on the theoretical calculations of the energies of the four conformers and based on the assumption that the molecules have not had a chance to equilibrate upon jet-cooling. Table 8 presents these results. The sample before jet-cooling was heated to 90° C , and at this temperature the MP2/6-311++G(d,p) computation leads to a distribution of 70% (**A**), 8% (**B**), 13% (**C**), and 9% (**D**) versus experimental values of 82, 3, 11, and 5%, respectively. Although the relative

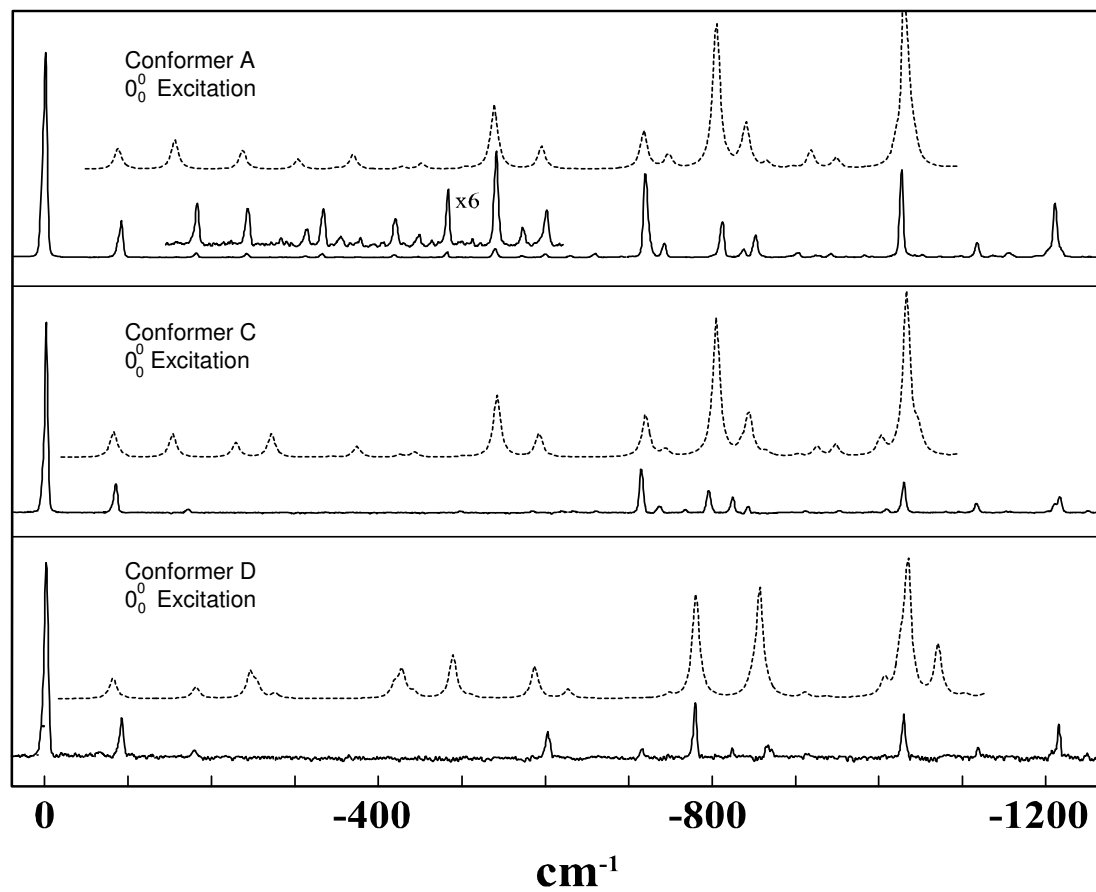


Fig. 12. Dispersed fluorescence spectra from the 0₀⁰ lines for conformers A, C and D compared with the calculated Raman spectra for each conformer.

Table 8
Populations (in %) of **A**, **B**, **C**, and **D** conformers of 2-indanol in the electronic ground state

	Exp.	Calc. MP2/cc-pVTZ		Calc. MP2/6-311++G(d,p)	
		25°C	90°C	25°C	90°C
		A	81	76	67
B	3.1	7.4	10	5.3	7.7
C	11	9.0	12	11	13
D	4.5	7.9	11	6.3	8.9

energies from the calculations can only be approximate, they do suggest that there has been some sample equilibration upon cooling since experimentally more molecules are observed for the lowest energy conformer **A**. More importantly, the agreement between the experimental and computational results is highly satisfactory.

CONCLUSION

Detailed computations have been carried out in order to produce a two-dimensional energy map of 2-indanol in terms of its ring-puckering and –OH internal rotation coordinates. The isomer with intramolecular hydrogen bonding to the benzene ring is calculated to be about 1.1 to 1.5 kcal/mol lower in energy than the three other conformers, which have similar conformational energies. The LIF spectra support these calculations and show evidence of all four isomers. Several of the vibronic bands, including those for the ring-puckering and –OH torsion, have been observed for the different isomers. The distribution of isomers calculated from the FES spectra and the *ab initio* calculations are in satisfactory agreement.

CHAPTER V

***AB INITIO* AND DFT STUDIES ON THE RING-PUCKERING
VIBRATION AND INTRAMOLECULAR HYDROGEN BONDING
OF 3-CYCLOPENTEN-1-OL**

INTRODUCTION

Intramolecular hydrogen bonding plays an important role in determining the stability and structures for many chemical and biochemical molecules. Examples of chemical groups undergoing weak intramolecular bonding with hydrogen atoms include amine groups, carboxylic acids, aromatic rings and C=C double bonds. In the previous chapter, detailed computational and spectroscopic studies of 2-indanol in its electronic ground and excited states were presented. These studies showed that 2-indanol has four possible conformations, with the conformer undergoing the intramolecular hydrogen bonding being the most stable.

The weak intramolecular hydrogen bonding in 3-buten-1-ol has been the subject of several previous infrared spectroscopic investigations [18,68-70]. The –OH stretching region in 3-buten-1-ol shows that there are two bands present and they are approximately 40 cm⁻¹ apart, corresponding to structures with and without a weak -O-H··· π -electron interaction. Other infrared investigations were also carried out for similar cyclic

molecules, including 2-cyclopenten-1-ol [19] and 3-cyclopenten-1-ol [18,20]. As was the case for 2-indanol, 3-cyclopenten-1-ol exists in four possible conformations. In its infrared spectra the splitting in the OH stretching region has a smaller frequency difference ($\sim 25\text{ cm}^{-1}$) than the noncyclic 3-buten-1-ol ($\sim 40\text{ cm}^{-1}$). The presence of more than one isomer for 3-cyclopenten-1-ol was also confirmed in a ^1H NMR experiment [18]. The puckering angle of the conformer with the bonding between the alcoholic hydrogen and the π -electrons of the C=C double bond was estimated from the ^1H NMR experiment to be 40° . In each of these studies, only two conformations of 3-cyclopenten-1-ol were observed.

This chapter presents results from high-level *ab initio* and DFT calculations. The work performed concentrates on determining the geometries of the four different conformations of 3-cyclopenten-1-ol and their energy differences. The calculated frequencies of several of the low-frequency vibrations will also be presented.

AB INITIO COMPUTATIONS

The structure and conformations of 3-cyclopenten-1-ol were studied at high levels of theories using the Gaussian 03 program [67]. For 2-indanol discussed in the previous chapter, very good agreement between the experimental and calculated results was found for both the structures and vibrational frequencies. This provided motivation for studying 3-cyclopenten-1-ol in its electronic ground state (S_0). The 3-cyclopenten-1-ol molecule has fewer atoms than 2-indanol and, as a result, higher levels of calculations were more readily carried out. The cc-pVTZ (triple- ζ) basis set was used with Hartree-

Fock (HF), second-order Møller-Plesset (MP2) and density functional theory (DFT) methods to calculate the energies and to compute the geometries for each of the four conformers. The coupled cluster theory with single and double excitations (CCSD) using the 6-311++G(d,p) basis set was used to obtain more accurate results for the geometry and conformations of the molecule.

The vibrational frequencies for the four conformations were computed using the DFT method by utilizing the B3LYP hybrid functional. These frequencies were scaled using a scaling factor of 0.961 for the spectral region above 1800 cm^{-1} , and 0.985 for the region below 1800 cm^{-1} . These theoretical results were compared with the previously reported experimental results of 3-cyclopenten-1-ol and 2-indanol where appropriate.

The conformational changes associated with the ring-puckering vibration and the -OH group internal rotation were analyzed by constructing a two-dimensional potential energy scan in terms of these two low-frequency motions. For this purpose, the MP2/6-31+G(d,p) level of computation was used. The procedure utilized here is similar to the one used for 2-indanol [71].

RESULTS AND DISCUSSION

The four conformations calculated for 3-cyclopenten-1-ol are shown in Fig. 13. Conformer **A** is the only conformer that can undergo the intramolecular hydrogen bonding which is represented with a dotted line. Both conformers **A** and **B** have C_s symmetry with the plane of symmetry bisecting the molecule through the C-O-H bond. The calculated structures from the CCSD/6-311++G(d,p) level of theory for **A** and **B** are

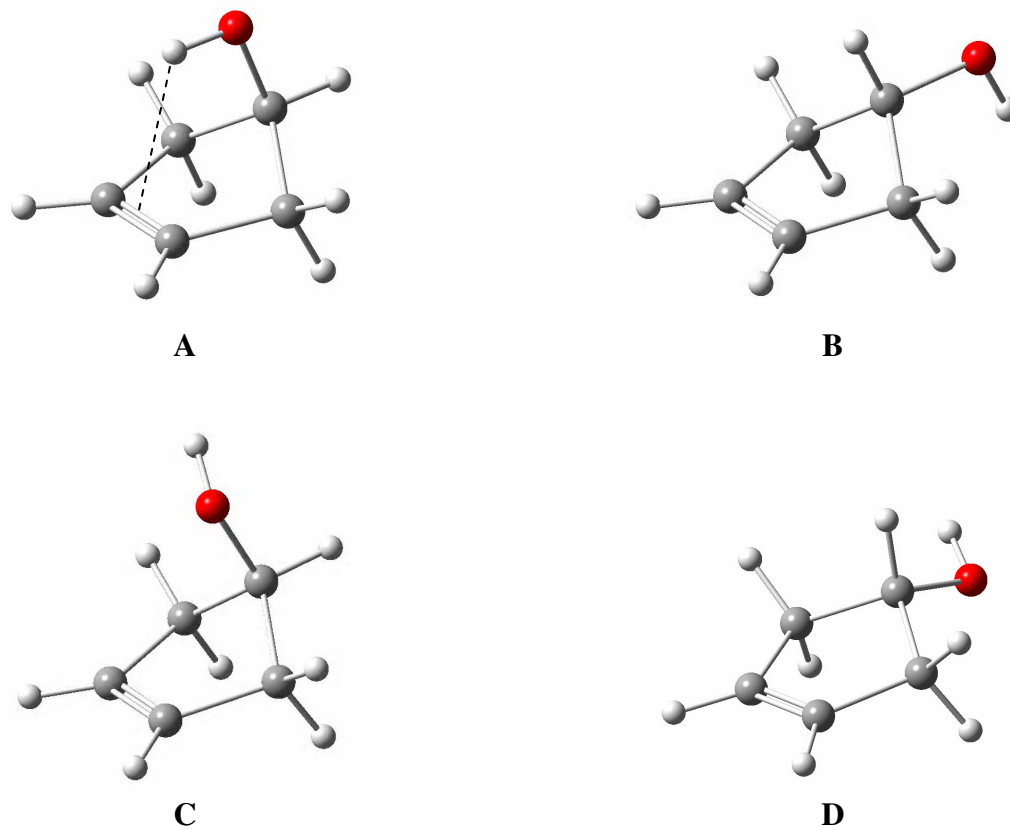


Fig. 13. Structures and labels of the four stable conformers of 3-cyclopenten-1-ol. The dotted line in A represents the intramolecular hydrogen bonding.

given in Fig. 14. The bond distances and angles of the molecule do not vary much with or without the presence of the hydrogen bonding. The potential energy function in terms of the ring-puckering angle was calculated and is shown in Fig. 15 for the MP2 and B3LYP calculations using the triple- ζ basis set. This function characterizes the interchange between conformers **A** (right side) and **B** (left).

The relative stabilities and puckering angles of the four conformers were also computed at different levels of theories and the results are given in Table 9. These calculations confirm that there exist four stable isomers for 3-cyclopenten-1-ol, and they show that the conformer with the intramolecular hydrogen bonding is the most stable. Fig. 15 also shows that the transition structure located at the ring-puckering pathway between conformers **A** and **B** is not completely planar (approximately 60 cm^{-1} higher in energy than the planar structure), but is slightly puckered towards the direction of the **B** isomer. This suggests that the molecule retains some magnitude of the weak interaction between the hydroxyl hydrogen and the C=C double bond at the planar geometry. Another interesting result is that for conformer **A** the puckering angle was calculated to be about 5° greater than that for conformer **C**. This indicates that the contribution of the intramolecular hydrogen bonding in **A** causes a slight increase in the puckering angle so that the -OH group can move closer to the C=C double bond. The high-level computational results of the puckering angle of **A** listed in Table 9 are significantly lower than the previously reported experimental value of 40° from the proton NMR experiment [18]. Moreover, the computed energies predicted that conformers **A** and **C** with the alcoholic group in the axial position are predominant over the other two

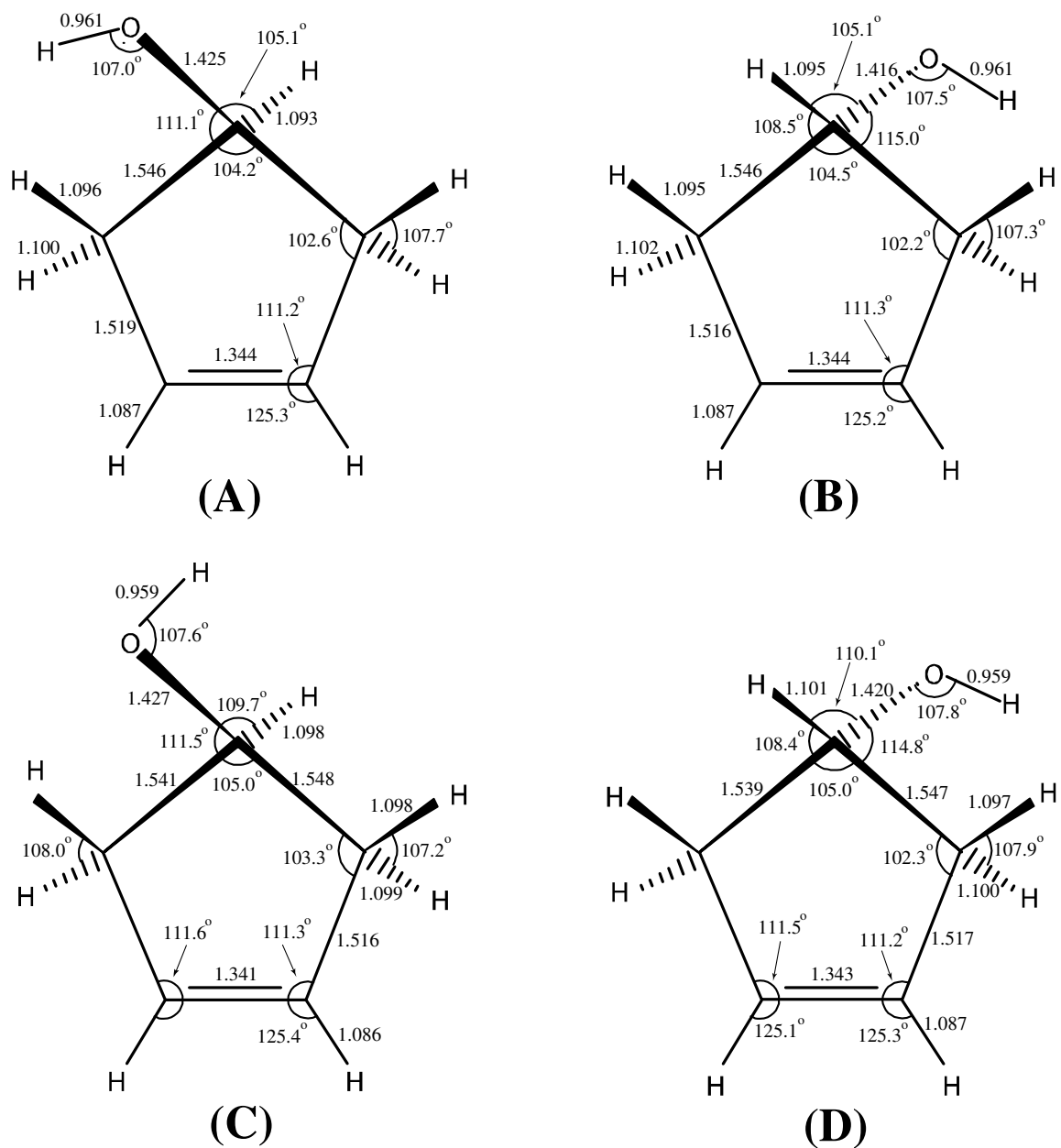


Fig. 14. Structures for the four conformers of 3-cyclopenten-1-ol as determined from CCSD/6-311++G(d,p) calculations.

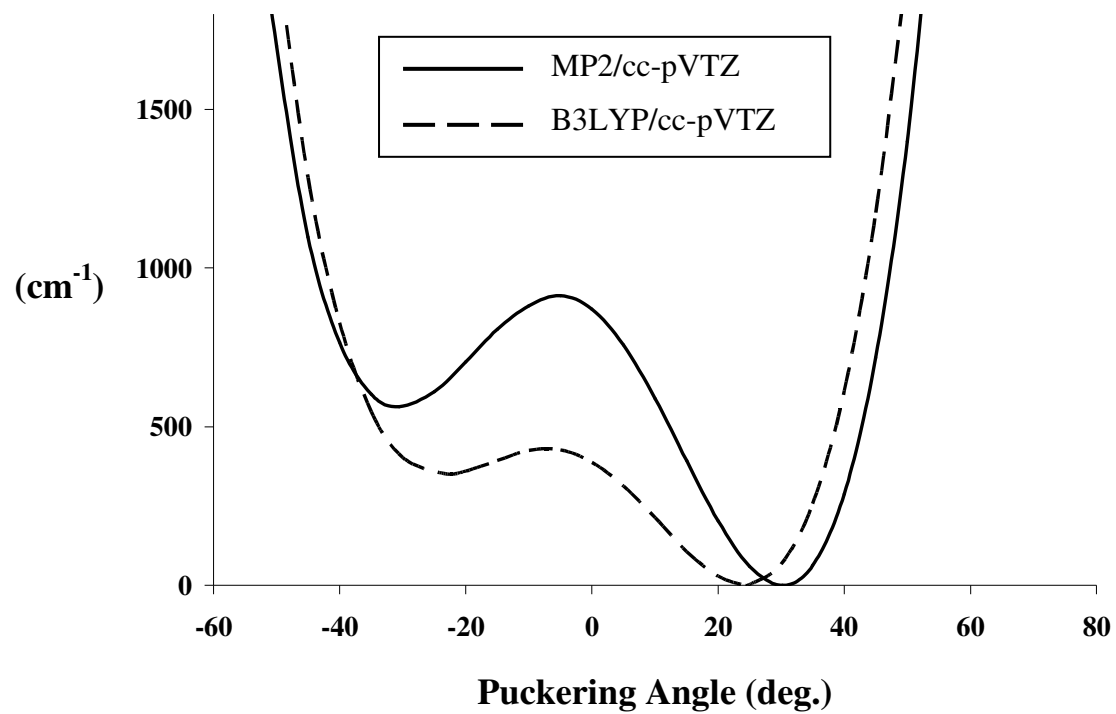
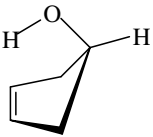
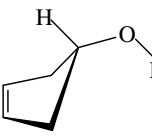
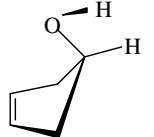
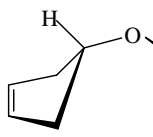
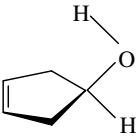


Fig. 15. The ring-puckering potential energy function for 3-cyclopenten-1-ol calculated by MP2/cc-pVTZ and B3LYP/cc-pVTZ.

Table 9

Relative energies^a (ΔE) and puckering angles (ϕ) of the stable conformers and the planar structure (**P**) for 3-cyclopenten-1-ol

									
	ΔE (cm ⁻¹)	ϕ (deg.)	ΔE (cm ⁻¹)	ϕ (deg.)	ΔE (cm ⁻¹)	ϕ (deg.)	ΔE (cm ⁻¹)	ϕ (deg.)	ΔE (cm ⁻¹)
HF/cc-pVTZ	0	24.9	200	-25.1	180	19.0	147	-24.4	401
B3LYP/cc-pVTZ	0	24.3	353	-23.5	226	17.2	325	-20.6	388
B3LYP/6-311++G(2d,2pd)	0	23.8	337	-22.8	146	17.0	284	-19.7	348
MP2/6-31+G(d,p)	0	30.1	530	-31.0	294	24.5	443	-29.8	896
MP2/cc-pVTZ	0	30.2	564	-30.6	401	24.3	560	-29.5	871
CCSD/6-311++G(d,p)	0	28.5	420	-29.0	274	23.5	409	-27.9	693

^aRelative energies were calculated with respect to the total energy of **A**.^bPlanar structure was optimized at a 0° puckering angle.

conformers. The MP2/6-31+G(d,p) theory was used to produce a set of optimized energies for 3-cyclopenten-1-ol by changing the ring-puckering angle from -50° to 50° and the hydroxyl group internal rotation angle from 0° to 180° . These energies were subtracted from the energy of the most stable conformer (Tables 10 and 11). A program was then used to construct two-dimensional energy maps (Figs. 16 and 17) in terms of the puckering angle and $-OH$ internal rotation.

The vibrational frequencies for the four conformers in the S_0 electronic ground state have been calculated using the B3LYP/cc-pVTZ and B3LYP/6-311++G(2d,2pd) levels of theories. Only the frequencies of the lowest three large-amplitude motions and the $-OH$ stretching vibration are shown in Table 12. These values are also compared to the ones observed and calculated for 2-indanol [71]. The $-OH$ stretching frequency for **A** was calculated to be 25 cm^{-1} lower than those for **C** and **D**, in excellent agreement with experimental values [18,20]. *Ab initio* and DFT results (Tables 9 and 12) suggested that the two $-OH$ stretching bands observed in the infrared experiments are due to the most stable conformers (**A** and **C**) with minor contributions from the other two conformers. Unlike 2-indanol, the ring-puckering frequencies in 3-cyclopenten-1-ol were predicted from DFT calculations to spread over a wider spectral region (from 60 to 120 cm^{-1}). This indicates that the puckering vibrations could be experimentally resolved from one conformer to another and be analyzed independently.

CONCLUSION

The conformations and vibrational frequencies of 3-cyclopenten-1-ol were

Table 10

Total energies (upper) in Hartree and relative energies (lower) in cm^{-1} calculated from the MP2/6-31+G(d,p) level of theory for 3-cyclopenten-1-ol (for puckering angles from 0.0° to 50.0°)

OH internal rotation angle (deg.)	Puckering angle (deg.)								
	0.0	5.0	10.0	17.0	24.5	30.1	35.0	43.0	50.0
0.0	-269.7284151 1124	-269.7286169 1079	-269.7290019 995	-269.729655 852	-269.7300949 755	-269.7299054 797	-269.7291348 966	-269.7261289 1625	-269.7210546 2739
15.0	-269.7286940 1062	-269.7289015 1017	-269.7292867 932	-269.7299288 791	-269.7303412 701	-269.7301225 749	-269.7293227 924	-269.7262652 1596	-269.7211412 2720
30.0	-269.7293580 917	-269.7295845 867	-269.7299764 781	-269.7305997 644	-269.7309525 567	-269.7306671 629	-269.7297984 820	-269.7266148 1519	-269.7213623 2672
45.0	-269.7300116 773	-269.7302767 715	-269.7306966 623	-269.7313312 484	-269.7316507 414	-269.7313103 488	-269.7303735 694	-269.7270434 1425	-269.7216181 2615
60.0	-269.730264 718	-269.7305897 646	-269.7310701 541	-269.7317747 386	-269.7321309 308	-269.7317817 385	-269.7308077 599	-269.7273532 1357	-269.7217511 2586
75.0	-269.7298815 802	-269.7302770 715	-269.7308378 592	-269.7316568 412	-269.7321108 313	-269.7318017 380	-269.7308332 593	-269.727323 1363	-269.7216092 2617
90.0	-269.7289367 1009	-269.7293867 910	-269.730021 771	-269.7309605 565	-269.7315404 438	-269.7313081 489	-269.7303906 690	-269.7269269 1450	-269.721222 2702
105.0	-269.7278596 1246	-269.7283292 1143	-269.7290057 994	-269.7300343 768	-269.7307325 615	-269.7305961 645	-269.7297662 827	-269.7264535 1554	-269.7208916 2775
120.0	-269.7272353 1383	-269.7276930 1282	-269.7283791 1132	-269.7294568 895	-269.7302533 720	-269.7302226 727	-269.7295091 884	-269.7264319 1559	-269.721112 2727
135.0	-269.7274166 1343	-269.7278639 1245	-269.7285574 1092	-269.7296827 845	-269.7305878 647	-269.7306804 627	-269.7301032 753	-269.7272903 1371	-269.7222203 2483
150.0	-269.7282286 1165	-269.7286891 1064	-269.7294111 905	-269.7306092 642	-269.7316416 416	-269.7318606 367	-269.7314106 466	-269.7288188 1035	-269.7239382 2106
165.0	-269.7290915 975	-269.7295777 869	-269.7303344 702	-269.7316016 424	-269.7327367 175	-269.7330481 107	-269.7326853 186	-269.7302373 724	-269.7254759 1769
180.0	-269.7294513 896	-269.7299500 787	-269.7307218 617	-269.7320166 333	-269.7331902 76	-269.733535 0	-269.7332032 73	-269.7308055 599	-269.7260859 1635

Table 11

Total energies (upper) in Hartree and relative energies (lower) in cm^{-1} calculated from the MP2/6-31+G(d,p) level of theory for 3-cyclopenten-1-ol (for puckering angles from -10.0° to -50.0°)

OH internal rotation angle (deg)	Puckering angle (deg)							
	-10.0	-15.0	-23.0	-29.7	-31.0	-35.0	-43.0	-50.0
0.0	-269.7287032 1060	-269.7291289 967	-269.7298935 799	-269.7302401 723	-269.7302368 724	-269.7300216 771	-269.7282616 1157	-269.724582 1965
15.0	-269.7289611 1004	-269.7293742 913	-269.7301184 750	-269.7304496 677	-269.7304441 678	-269.7302223 727	-269.7284546 1115	-269.7247741 1923
30.0	-269.7295661 871	-269.7299458 788	-269.7306407 635	-269.7309361 570	-269.7309254 573	-269.7306888 625	-269.7289042 1016	-269.7252231 1824
45.0	-269.7301335 747	-269.7304741 672	-269.7311186 530	-269.7313872 471	-269.7313733 474	-269.7311287 528	-269.7293417 920	-269.7256716 1726
60.0	-269.7302866 713	-269.7305958 645	-269.7312198 508	-269.7314976 447	-269.7314872 449	-269.7312589 500	-269.7295156 882	-269.725888 1678
75.0	-269.729815 816	-269.7301073 752	-269.7307414 613	-269.7310584 544	-269.731057 544	-269.7308615 587	-269.7291959 952	-269.7256334 1734
90.0	-269.7288247 1034	-269.7291213 969	-269.7297864 823	-269.7301455 744	-269.7301525 742	-269.7299882 778	-269.7283848 1130	-269.7248746 1901
105.0	-269.7277702 1265	-269.7280945 1194	-269.728805 1038	-269.7291934 953	-269.729204 951	-269.7290489 985	-269.7274577 1334	-269.7239541 2103
120.0	-269.727221 1386	-269.7275919 1304	-269.7283581 1136	-269.7287605 1048	-269.7287701 1046	-269.7286048 1082	-269.7269701 1441	-269.7234179 2220
135.0	-269.7274669 1332	-269.727879 1241	-269.7286976 1062	-269.7291151 970	-269.729124 968	-269.728949 1007	-269.7272664 1376	-269.7236541 2169
150.0	-269.7282808 1153	-269.7287041 1060	-269.7295451 876	-269.7299769 781	-269.7299872 779	-269.7298144 817	-269.7281224 1188	-269.7244901 1985
165.0	-269.7291081 972	-269.7295197 881	-269.7303521 699	-269.7307862 603	-269.7307976 601	-269.7306294 638	-269.7289486 1007	-269.7253247 1802
180.0	-269.7294482 897	-269.7298517 808	-269.7306751 628	-269.7311069 533	-269.7311185 530	-269.7309518 567	-269.7292771 935	-269.7256598 1728

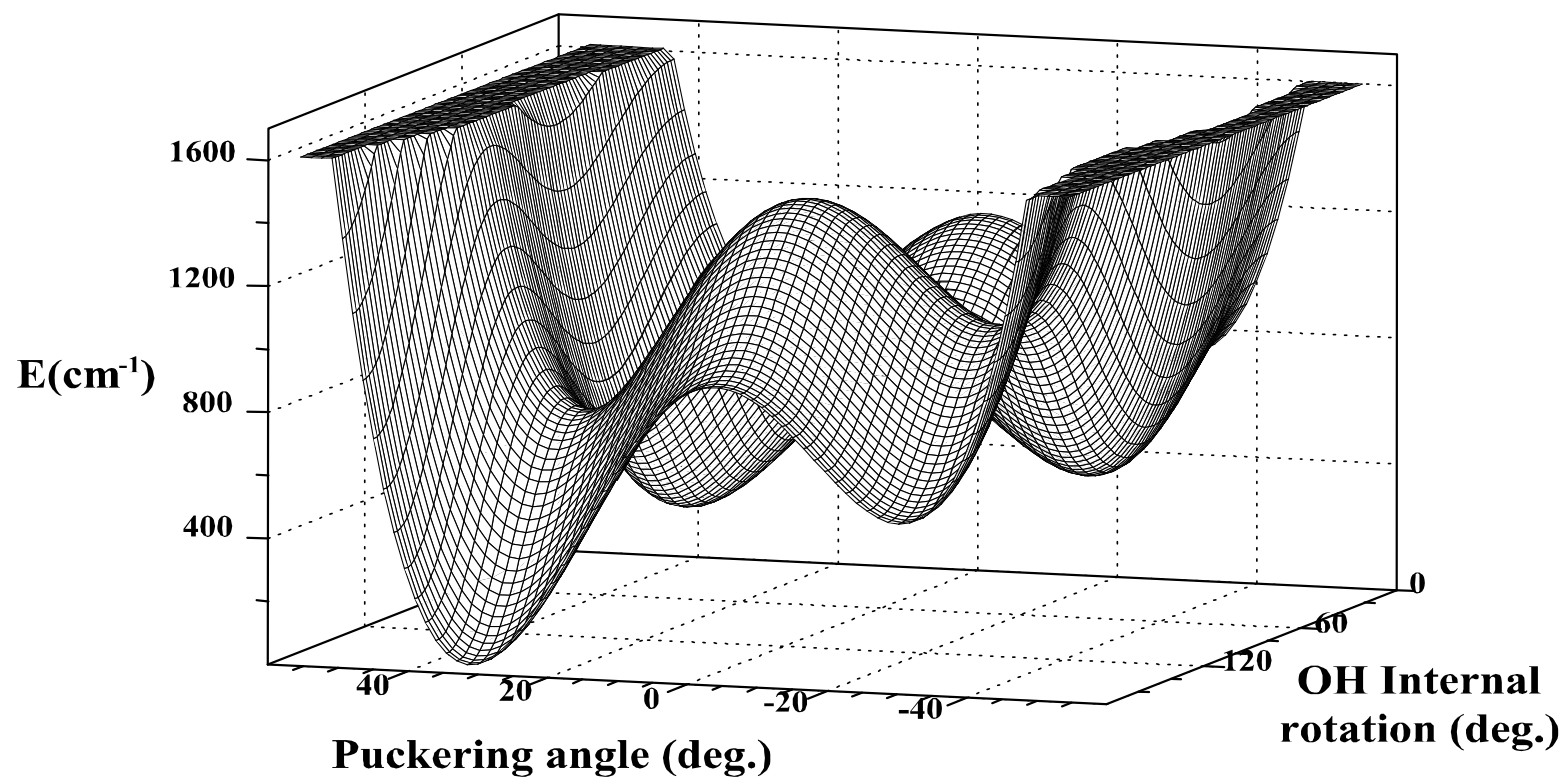


Fig. 16. Calculated potential energy surface of 3-cyclopenten-1-ol in terms of the ring-puckering angle and internal rotation angle of the -OH group.

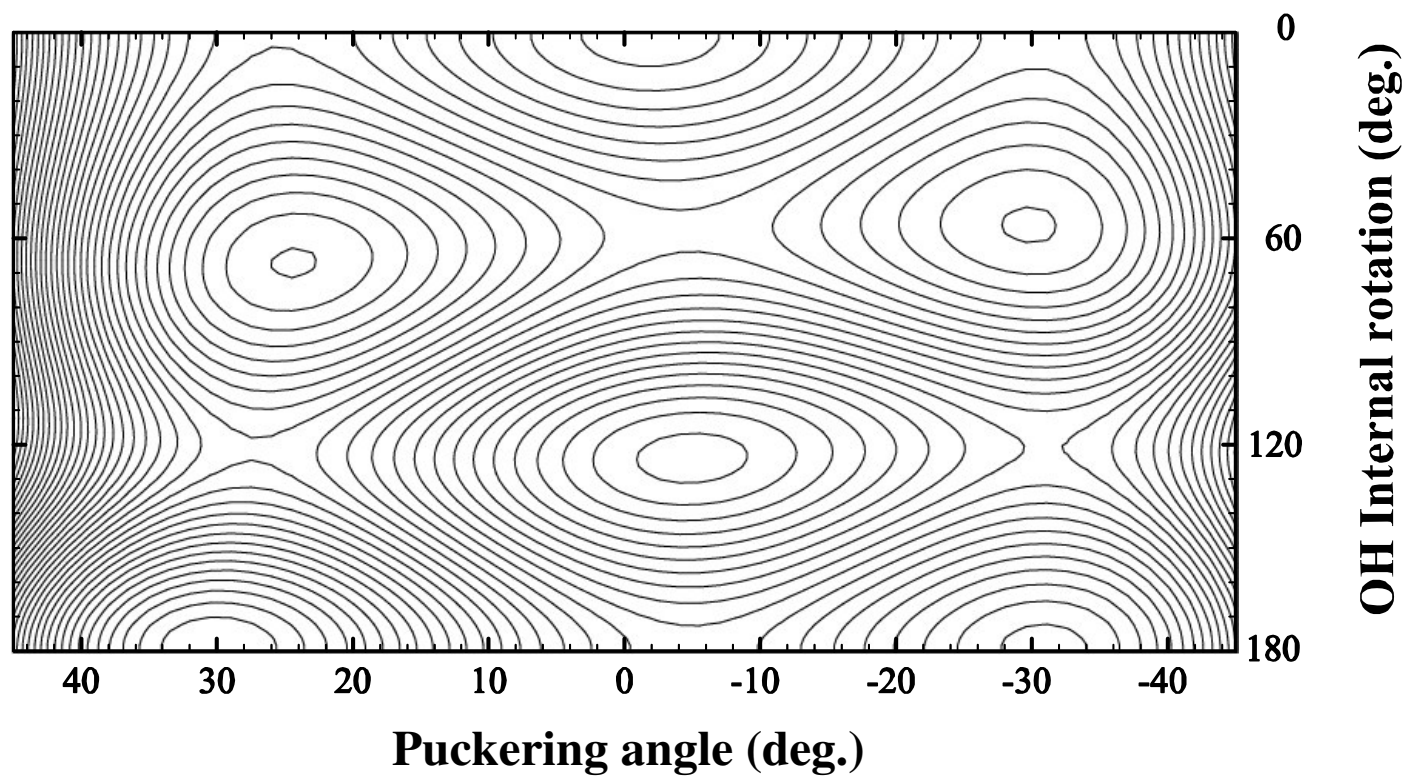


Fig. 17. Contour of the energy map shown in Fig. 16.

Table 12

Vibrational frequencies^a of the –OH stretching and the lowest three large-amplitude motions for 3-cyclopenten-1-ol and 2-indanol calculated at the B3LYP/cc-pVTZ level

	3-Cyclopenten-1-ol ^b				2-Indanol ^c			
	A	B	C	D	A	B	C	D
–OH stretching	3640	3646	3665	3670	3637	3646	3665	3672
	<i>3661</i>	<i>3666</i>	<i>3682</i>	<i>3688</i>	(3586) ^R			
–OH torsion	322	255	277	275	302	251	273	255
	<i>307</i>	<i>250</i>	<i>273</i>	<i>271</i>	(296) ^{DF}			
Ring twisting	376	395	363	391	155	184	155	183
	<i>371</i>	<i>392</i>	<i>359</i>	<i>388</i>	(156) ^R	(192) ^R		
Ring puckering	119	93	104	72	87	87	80	84
	<i>115</i>	<i>87</i>	<i>99</i>	<i>66</i>	(92) ^{DF}		(86) ^{DF}	(90) ^{DF}

^aScaled.

^bFrequencies in *italics* are calculated using the 6-311++G(2d,2pd) basis set.

^cRef. [71]. Frequencies in parentheses are from liquid-phase Raman (R) and dispersed fluorescence (DF) experiments.

studied by different levels of *ab initio* and DFT calculations. Agreements between the calculations presented in this study and available experimental results are very good.

Conformer **A** with the intramolecular hydrogen bonding between the hydroxyl hydrogen and the π -electron density of the C=C double bond is the most stable one. CCSD/6-311++G(d,p) and MP2/cc-pVTZ levels of calculations predicted the stabilities of the four conformers in the order **A** > **C** > **D** > **B**, with the planar structure being 700 cm^{-1} higher in energy than **A** with its hydrogen bonding. One important result from the high-level DFT-B3LYP calculations is that the frequencies of the ring-puckering vibrations of the four isomers in 3-cyclopenten-1-ol are spread apart in the far-infrared region, which indicates that this vibration can be characterized independently for each conformer.

CHAPTER VI
VIBRATIONAL SPECTRA, *AB INITIO* CALCULATIONS, AND
RING-PUCKERING POTENTIAL ENERGY FUNCTION
FOR γ -CROTONOLACTONE

INTRODUCTION

γ -Crotonolactone is similar in structure to 2-cyclopenten-1-one which has been investigated in its ground and excited states using several spectroscopic and computational techniques. The infrared and Raman vibrational spectra [72-75] as well as density functional theory (DFT) [76] have shown 2-cyclopenten-1-one to be strictly planar in its S_0 electronic ground state and to be governed by a stiff single-minima potential energy function [75,76]. This is the result of conjugation involving both the C=C and C=O double bonds.

The studies on the structure of 2-cyclopenten-1-one have been carried out for its singlet (S_1) and triplet (T_1 and T_2) electronic excited states [77-80]. Cheatham and Laane used fluorescence excitation spectroscopy (FES) to investigate the $S_1(n,\pi^*)$ state and showed that the molecule retains its planar structure in the $S_1(n,\pi^*)$ excited state but becomes much less rigid as compared to the ground state [77]. DFT calculations agreed very well with the FES results and confirmed the planar conformation of 2-cyclopenten-

1-one in its $S_1(n,\pi^*)$ excited state [76]. The $T_1(n,\pi^*)$ triplet state for 2-cyclopenten-1-one was later studied using cavity ringdown (CRD) absorption spectroscopy [78] along with several theoretical calculations [76,79,80]. It was concluded from CRD that the molecule is slightly puckered in the $T_1(n,\pi^*)$ state with a barrier to planarity of 43 cm^{-1} [78]. The calculated barrier for the $T_2(\pi,\pi^*)$ triplet state was calculated using DFT-B3LYP/6-311+G(d,p) to be 999 cm^{-1} [76].

γ -Crotonolactone differs from 2-cyclopenten-1-one in that it has an oxygen atom instead of a carbon atom across the ring from the C=C double bond. However, as in the case of 2-cyclopenten-1-one, γ -crotonolactone has also been shown from microwave studies [21,22] to be planar and to possess the C_s symmetry in the electronic ground state. It was also suggested [22] that the ring-puckering vibration can be described by an essentially quadratic potential energy function.

As with 2-cyclopenten-1-one, an interesting feature of γ -crotonolactone is the conjugation between the C=C and C=O groups. This feature has been of particular interest in several infrared and Raman studies of some unsaturated monocyclic lactones in various solvents [23-25]. Considerable attention in these studies was directed to the spectral region just below 1800 cm^{-1} which includes the C=O stretching vibration. In general, lactones in the liquid phase show two significant peaks related to the C=O stretching motion. The interpretation of such a phenomenon has been ascribed to the Fermi resonance between the carbonyl stretching vibration and the overtones or combinations of other low-frequency vibrations [23-25]. Nyquist *et al.* presented a mathematical model for calculating the approximate unperturbed C=O stretching

vibration for several cyclic five- and six-membered ring lactones in CCl_4 and CHCl_3 solvents [25]. A different study on the integrated intensities of the carbonyl stretching bands of several unsaturated five-membered cyclic γ -lactones in acetonitrile solution concluded that the presence of the conjugation between the $-\text{O}-\text{C}=\text{C}$ group and the $\text{C}=\text{C}$ bond moderately enhances the intensity of the carbonyl stretching band as compared to the no conjugation case [81]. No detailed vibrational assignments or gas-phase vibrational studies, however, have been carried out on γ -crotonolactone. For its excited state structure, the partially overlapping $\pi-\pi^*$ and $n-\pi^*$ transitions in the UV spectra of the liquid have been reported [82].

EXPERIMENTAL

γ -Crotonolactone was obtained from Aldrich with a stated purity of 98%. It is a colorless liquid with a very slightly pinkish color in the commercial sample that disappeared with further purification under vacuum. Its melting point and boiling point are 3°C and 214°C , respectively.

The vapor and liquid Raman spectra of γ -crotonolactone were recorded using a JobinYvon U-1000 double monochromator equipped with a CCD detector and an Innova I-100 argon ion laser operating at 5145 \AA . For the vapor-phase Raman spectra, the sample was transferred under vacuum into a custom designed, thermally controlled glass Raman cell previously described [83,84]. The sample was heated to approximately 240°C . The Raman spectra of the liquid γ -crotonolactone were recorded for a sample in an evacuated 1mm glass tube at room temperature. The polarization spectra of the liquid

were also recorded to help in the assignments. Laser powers of 0.2 W for the liquid-phase spectra and 4.5 W for the vapor-phase spectra were used.

The infrared spectrum of a drop of γ -crotonolactone liquid between two KBr windows was recorded using a Biorad FTS-60 spectrometer equipped with a globar source, KBr beamsplitter, and a triglycerin sulfate detector. A total of 256 scans at 1.0 cm^{-1} resolution were averaged. The background spectrum taken under same conditions was subtracted from the γ -crotonolactone spectrum in order to obtain the transmittance spectrum.

COMPUTATIONS

Density functional theory (DFT) with the B3LYP hybrid functional, *ab initio* second-order Moller-Plesset (MP2) and Hartree-Fock (HF) calculations using the Gaussian 03 program [67] were carried out for γ -crotonolactone in its electronic ground state. In this work the coupled-cluster treatment was used to predict the geometry of the most stable structure as well as the structure of 2-cyclopenten-1-one, and the DFT-B3LYP with the cc-pVTZ (triple- ζ) basis set was used to calculate the vibrational frequencies, infrared and Raman intensities, and depolarization ratios.

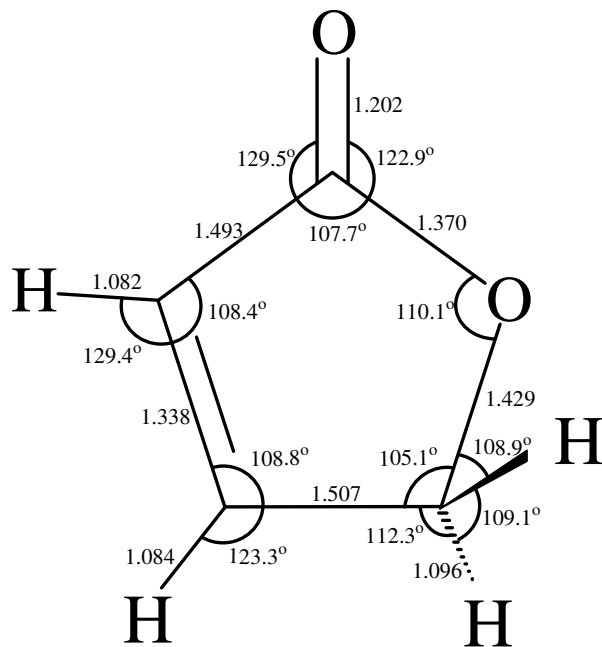
The one dimensional single-minimum puckering potential function for γ -crotonolactone was calculated by varying the puckering angle from -30° to 30° by increments of 5° at the MP2, DFT-B3LYP, and HF theories using the triple- ζ basis set. The optimized structure from the CCSD/6-311++G(d,p) calculation was used to determine the kinetic energy expansion terms for γ -crotonolactone using a program

previously described [53]. These kinetic energy terms and the potential function from *ab initio* computations were used to calculate the puckering quantum transitions.

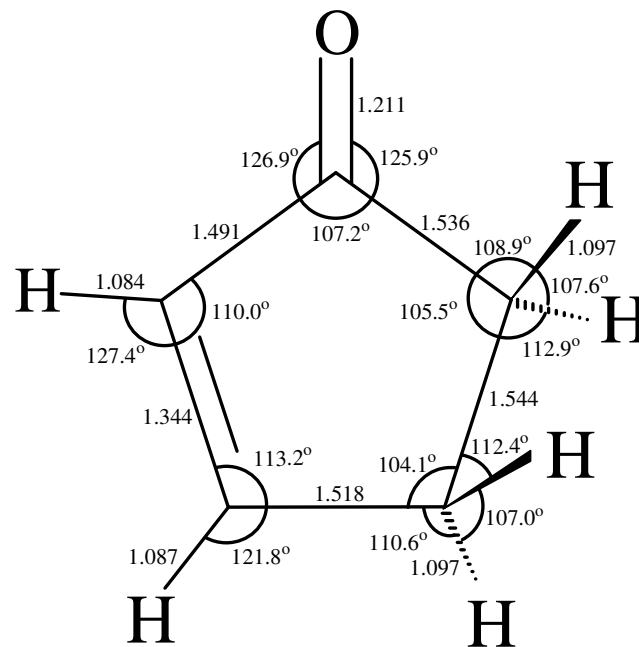
VIBRATIONAL SPECTRA

The high-level *ab initio* calculations predicted γ -crotonolactone to be planar in its minimum energy structure, in agreement with previous experimental results from microwave studies [21,22]. Fig. 18 shows the calculated C_s planar structure of γ -crotonolactone from the CCSD/6-311++G(d,p) calculation and compares it to the structure of 2-cyclopenten-1-one. From Fig. 18 it can be seen for both molecules that as a result of conjugation the C-C single bond connecting the carbonyl carbon atom to the C=C group is shorter in length than the other C-C single bonds. For γ -crotonolactone this is 1.493Å vs. 1.507Å while for 2-cyclopenten-1-one it is 1.491Å vs. values in the 1.518 to 1.544Å range.

γ -Crotonolactone, as previously discussed, is planar with the ring atoms and the carbonyl oxygen lying in the symmetry plane. Its vibrational spectra are expected to be governed by C_s symmetry. γ -Crotonolactone possesses 24 vibrations with symmetry species $16A' + 8A''$. These vibrations were studied by recording the spectra for both the vapor and liquid phases. Fig. 19 shows the Raman spectra (vapor, liquid, and calculated), while Fig. 20 presents the polarized Raman spectra of the liquid. The liquid and calculated mid-infrared spectra are given in Fig. 21. Based on the vibrational spectra in Figs. 19-21, complete assignments of the vibrational modes were made, and they are shown in Table 13. The computed frequencies and depolarization ratios from the DFT



γ -Crotonolactone



2-Cyclopenten-1-one

Fig. 18. Ground-state structures of γ -crotonolactone and 2-cyclopenten-1-one from the CCSD/6-311++G(d,p) calculations.

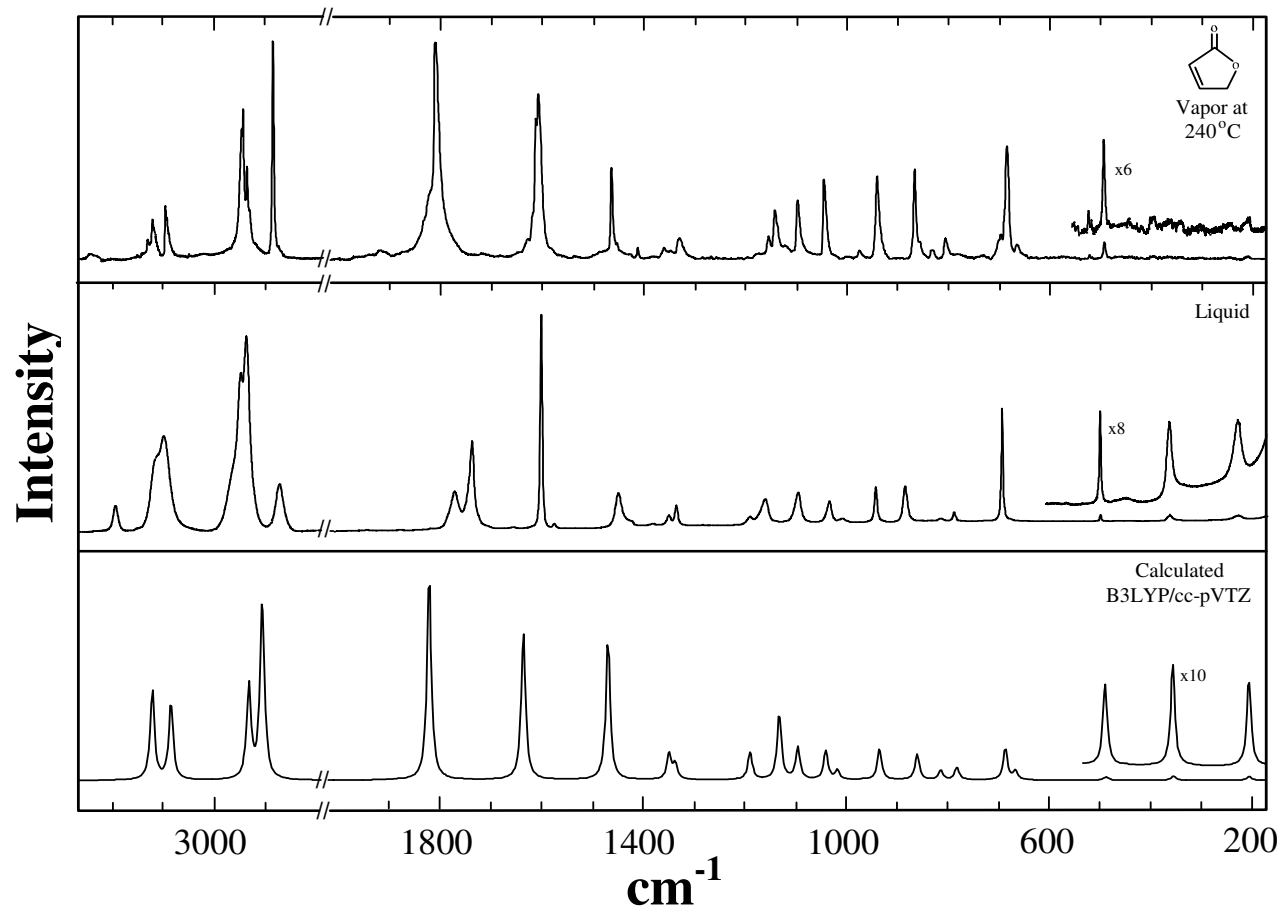


Fig. 19. Vapor-phase, liquid-phase, and calculated Raman spectra for γ -crotonolactone.

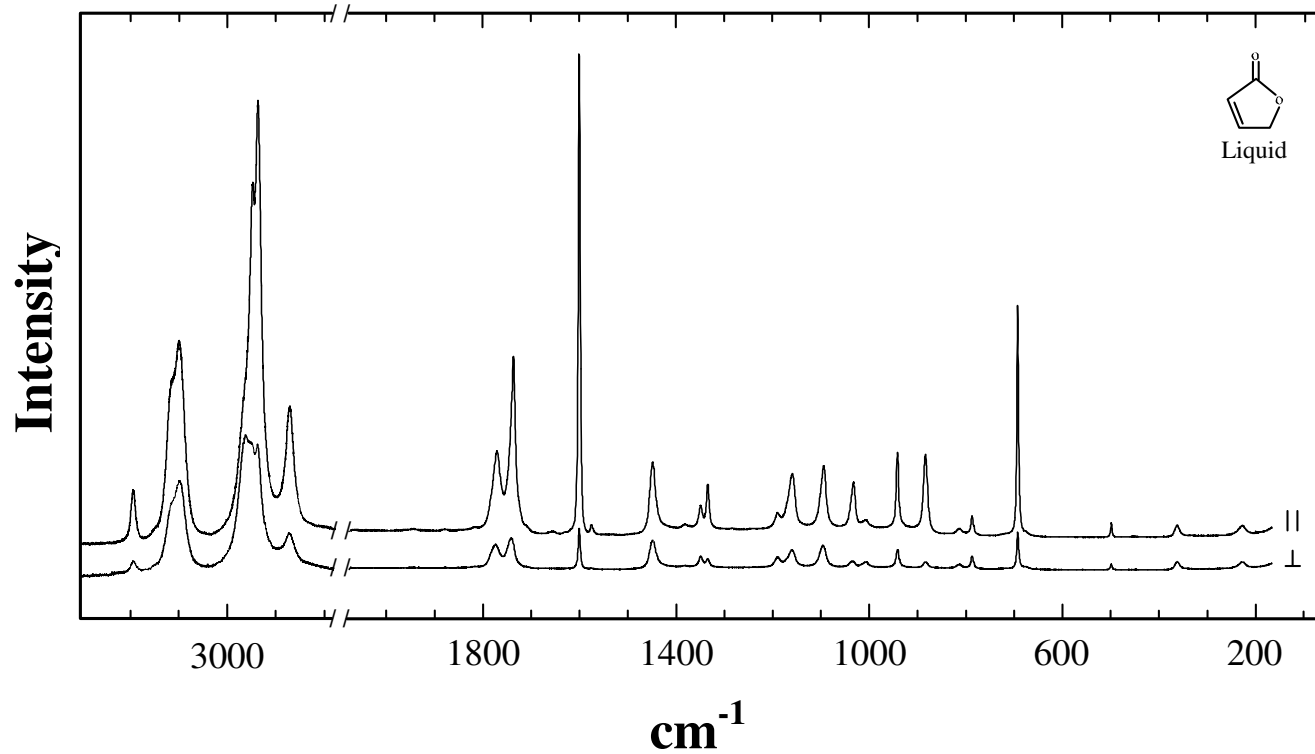


Fig. 20. Polarized Raman spectra of the γ -crotonolactone liquid.

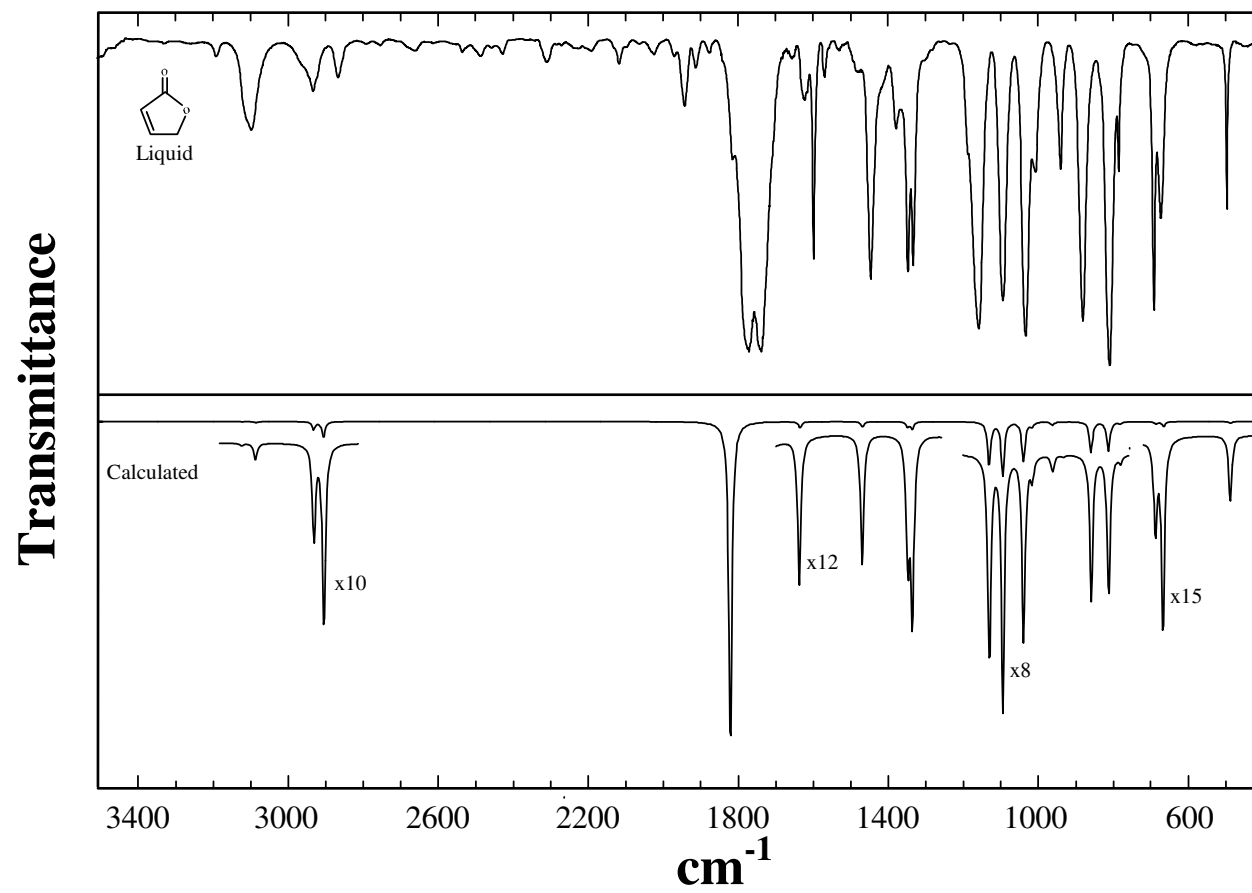


Fig. 21. Liquid-phase and calculated infrared spectra of γ -crotonolactone.

Table 13
Vibrational assignments for γ -Crotonolactone

		Experimental			Calculated ^b		
		Vapor	Liquid		B3LYP/cc-pVTZ		
	Description	Raman	IR ^a	Raman	Scaled	Intensities ^c	ρ^d
<i>A'</i>	ν_1 CH str.	3123 (47)	~3113 m	3116 p	3123	(1,286)	0.2
	ν_2 CH str.	3097 (80)	3098 ms	3100 p	3086	(5,247)	0.4
	ν_3 CH ₂ sym. str.	2885 (233)	2868 m	2872 p	2907	(50,577)	0.1
	ν_4 C=O str.	1809 (100)	1739/1773 vs	1737/1772 p	1822	(1000,100)	0.4
	ν_5 C=C str.	1609 (77)	1599 ms	1600 p	1636	(18,72)	0.1
	ν_6 CH ₂ def.	1462 (46)	1447 ms	1448 p	1469	(16,67)	0.5
	ν_7 CH ₂ wag	1358 (5)	1347 ms	1349 p?	1349	(15,13)	0.7
	ν_8 CH in-plane bend	1328 (8)	1333 ms	1334 p	1337	(22,8)	0.2
	ν_9 Ring str.	1140 (19)	1158 s	1159 p	1132	(135,32)	0.4
	ν_{10} CH in-plane bend	1095 (25)	1094 s	1094 p	1095	(162,16)	0.6
	ν_{11} Ring str. (C-O str.)	1043 (37)	1034 s	1032 p	1040	(118,14)	0.2
	ν_{12} Ring breath	939 (40)	940 m	941 p	934	(1,15)	0.2
	ν_{13} Ring def.	865 (45)	881 ms	883 p	860	(93,12)	0.1
	ν_{14} Ring def.	804 (9)	786 m	787 d	782	(5,6)	0.7
	ν_{15} Ring mode	683 (55)	692 ms	693 p	686	(7,15)	0.3
	ν_{16} C=O in-plane bend	490 (8)	497 m	498 p	488	(5,2)	0.7

Table 13
Continued

Description		Experimental			Calculated ^b		
		Vapor	Liquid		B3LYP/cc-pVTZ		
		Raman	IR ^a	Raman	Scaled	Intensities ^c	ρ^d
A''	ν_{17} CH ₂ antisym. str.	2947 (134)	~2961 w	2963 d?	2933	(25,299)	0.8
	ν_{18} CH ₂ twist	1153 (8)	~1187 m	1189 d	1189	(0,14)	0.8
	ν_{19} CH ₂ rock	998 (1)	1008 m	1006 d	1017	(14,5)	0.8
	ν_{20} CH out-of-plane bend	973 (4)	977 vw	----	963	(11,0)	0.8
	ν_{21} C=O out-of-plane bend	830 (4)	810 s	813 d	814	(91,5)	0.8
	ν_{22} CH out-of-plane bend	663 (5)	673 m	677 ?	666	(14,4)	0.8
	ν_{23} C=C twist	~366 (0)	----	362 d	356	(13,2)	0.8
	ν_{24} Ring puckering	208 (1)	----	226 d	206	(1,2)	0.8

^aIR intensities: v=very, s=strong, m=medium, w=weak.

^bScaled.

^cInfrared and Raman intensities, respectively.

^dDepolarization ratio.

calculations are also listed in Table 13 and these are in good agreement with the experimental results. Several combination bands and overtones were also observed in the infrared and Raman spectra of the vapor, but these are not present in the calculated spectra. In several cases there are significant frequency shifts between the liquid and vapor spectra indicating that there are fairly strong intermolecular interactions in the liquid state. In addition, extra bands of some intensity indicate the presence of Fermi resonance.

The puckering frequency was found from the vapor-phase Raman spectra to be 208 cm^{-1} with no observable side bands indicating that γ -crotonolactone is rigidly planar with a nearly harmonic potential function. The more intense bands in the Raman vapor of γ -crotonolactone were for the most part assigned with the help of the polarization measurement and the calculated frequencies to the A' modes. The C=O stretching vibration can be readily assigned to the most intense peaks in the infrared and Raman spectra. In the liquid-phase experiment these peaks are doublets in agreement with the previous studies on other unsaturated lactones [23-25]. In the vapor phase the C=O vibration is only a singlet of a higher frequency (1809 cm^{-1}), which is in good agreement with the calculated value of 1822 cm^{-1} (Table 13).

KINETIC AND POTENTIAL ENERGY FUNCTIONS

In order to predict the quantum states associated with the ring-puckering vibration, the potential energy function was generated by calculating the energy as a function of coordinates using MP2/cc-pVTZ calculations. The CCSD/6-311++G(d,p)

level of theory was used to determine the kinetic energy expansion terms [53] to the sixth power. Fig. 22 shows the definitions for the puckering angle (ϕ) and puckering coordinate (x). Table 14 lists the relative energies for γ -crotonolactone obtained from varying ϕ from -30° to 30° in steps of 5° and fixing the four carbon atoms in the plane of the molecule. Fig. 23 shows the potential functions of the puckering motion in terms of the dihedral angle (ϕ) from different levels of theory. As can be seen from the figure, all four calculations predict a planar structure for the molecule and a stiff potential function, in good correlation with the experimental.

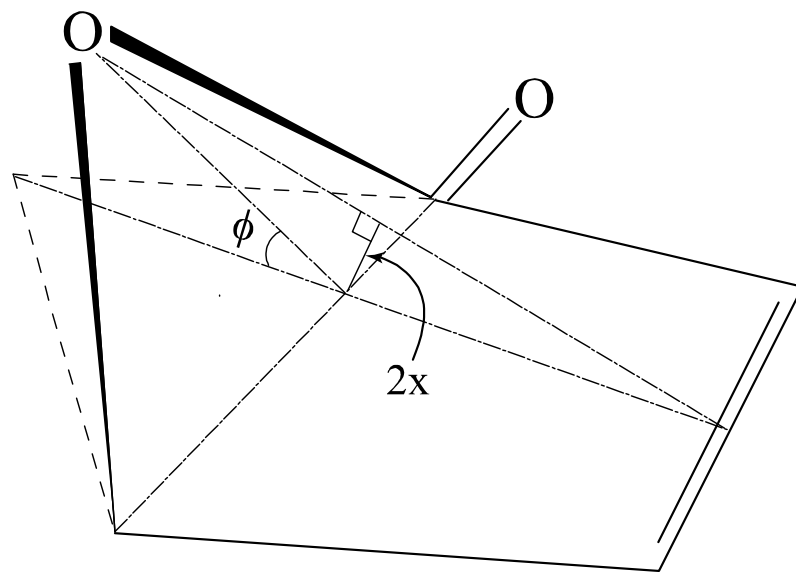
When the MP2/cc-pVTZ results are used to calculate the potential function curve, this can be fitted with

$$V(\text{cm}^{-1}) = 10.08 \times 10^4 x^2 + 45.90 \times 10^4 x^4 \quad (36)$$

where x is the puckering coordinate in \AA . The calculated kinetic energy expression is

$$g_{44}(x) = 0.00473872 - 0.0394847 x^2 + 0.114150 x^4 - 0.198735 x^6. \quad (37)$$

When these functions are utilized to calculate the quantum levels, the spacings shown in Table 15 result. As is evident, the vibration is almost totally harmonic with a calculated frequency of 181 cm^{-1} , in excellent agreement with the experimentally observed value of 208 cm^{-1} . It should be noted that although the quartic term in Eq. (36) appears significant, it only makes a minor contribution as the value of x only ranges from -0.1\AA to $+0.1 \text{\AA}$, while the dihedral angle goes from -30° to $+30^\circ$. Here, the x^4 contribution for x values in this range is more than 100 times less than the x^2 contribution. The *ab initio* potential function in terms of the puckering coordinate is



----- Planar structure

Fig. 22. Definitions of the pucker coordinate (x) and pucker angle (ϕ) for γ -crotonolactone.

Table 14

Total (Hartree) and relative (cm^{-1}) energies for γ -crotonolactone from *ab initio* calculations

Puckering angle, ϕ (deg.)	HF/cc-pVTZ		MP2				B3LYP/cc-pVTZ	
	Total energy	Rel. energy	cc-pVTZ		6-311+G(d,p)		Total energy	Rel. energy
			Total energy	Rel. energy	Total energy	Rel. energy		
0	-303.6319823	0	-304.7161657	0	-304.5352194	0	-305.3814126	0
3	-303.6318828	22	-304.7160743	20	-304.5351428	17	-305.3813142	22
5	-303.6317046	61	-304.7159109	56	-304.5350068	47	-305.3811374	60
7	-303.6314368	120	-304.7156648	110	-304.5348016	92	-305.3808707	119
10	-303.6308647	245	-304.7151384	226	-304.5343588	189	-305.3803019	244
15	-303.6294418	558	-304.7138318	512	-304.5332407	434	-305.3788918	553
20	-303.6274027	885	-304.7119630	812	-304.5316023	794	-305.3768764	996
25	-303.6247001	1479	-304.7094896	1355	-304.5293804	1282	-305.3742084	1581
30	-303.6212686	2232	-304.7063587	2042	-304.5264995	1914	-305.3708277	2323

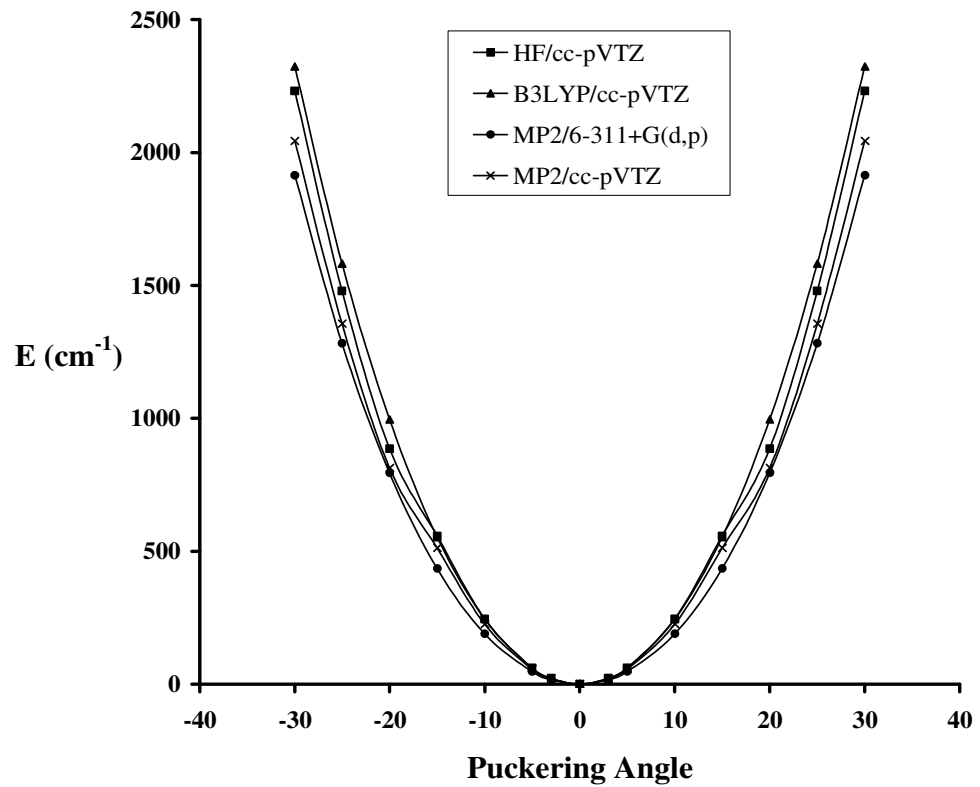


Fig. 23. Ring-puckering potential energy function from different levels of calculations.

Table 15
Ring-puckering vibrational levels for γ -crotonolactone as determined from *ab initio* results

Levels	Frequency (cm ⁻¹)	Relative intensity
0-1	180.6	1.0
1-2	181.6	0.8
2-3	182.7	0.5
3-4	183.7	0.3
4-5	184.7	0.2
5-6	185.7	0.07
6-7	186.7	0.04
7-8	187.7	0.02

shown in Fig. 24. The figure also shows the quantum transitions determined from *ab initio* calculations and compares this potential function of γ -crotonolactone with the one previously reported for 2-cyclopenten-1-one [75]. The greater ring rigidity in γ -crotonolactone as compared to 2-cyclopenten-1-one can be explained in terms of the higher angle strain in the case of γ -crotonolactone. The bending force constant for the C-O-C angle is greater than that for a C-C-C angle, and the former also prefers to have a smaller value than the latter.

CONCLUSION

γ -Crotonolactone was confirmed to be planar in its ground state from its vibrational spectra and theoretical calculations. Unlike 2-cyclopenten-1-one, the ring-puckering vibration in γ -crotonolactone is governed by a stiff potential energy function whose quadratic term is predominant. *Ab initio* calculations predicted the vibrational spectra and energies for γ -crotonolactone to be in very good agreement with the experiment. The vibrational analysis was carried out on the basis of infrared, Raman, and calculated spectra.

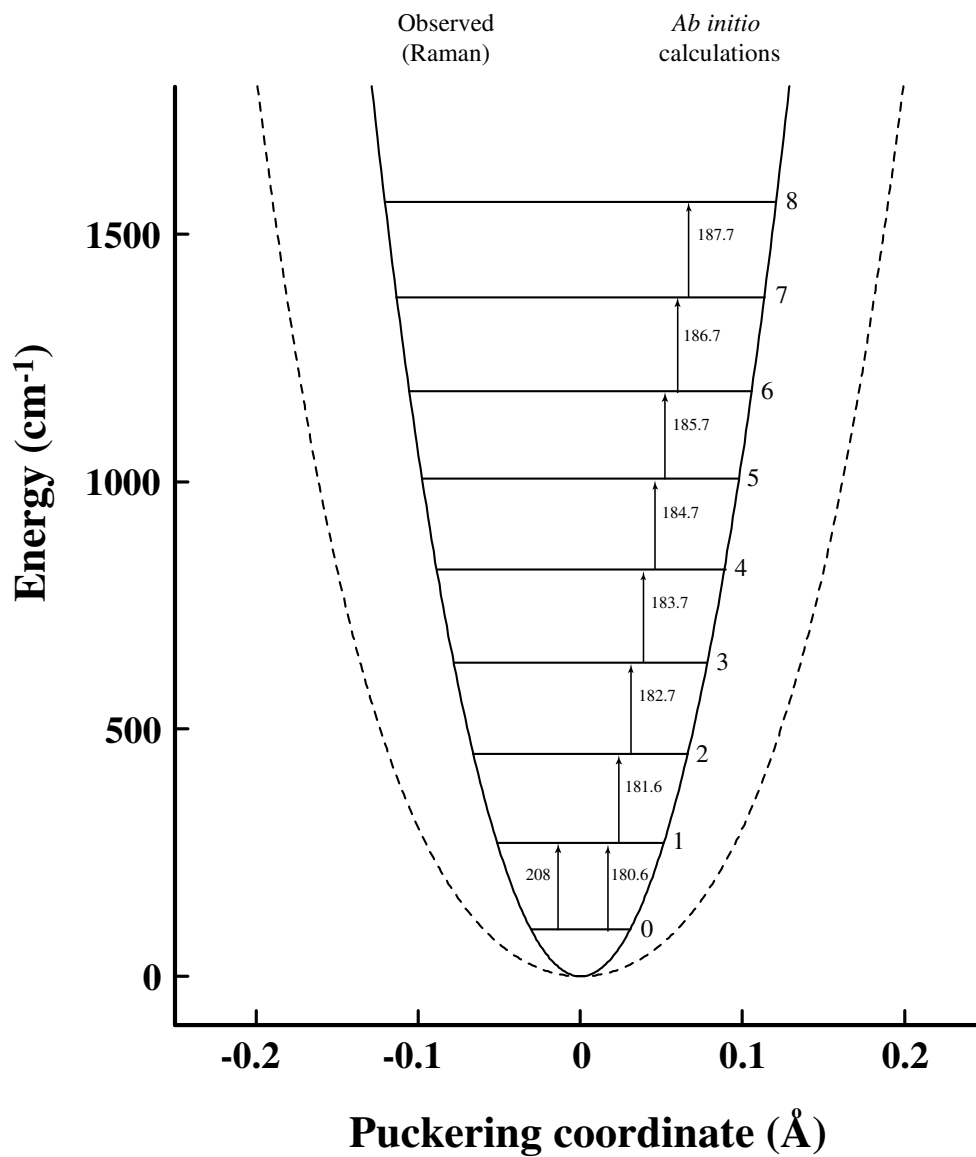


Fig. 24. Potential energy function for the ring-puckering vibration as determined from *ab initio* calculations using the MP2/cc-pVTZ level of theory. The ring-puckering potential function for 2-cyclopenten-1-one is shown with dotted lines.

CHAPTER VII
RAMAN AND INFRARED SPECTRA, *AB INITIO* AND DFT
CALCULATIONS, AND VIBRATIONAL ASSIGNMENTS FOR
2,3-CYCLOPENTENOPYRIDINE

INTRODUCTION

2,3-Cyclopentenopyridine (also known as pyrindan) is identical in structure to indan except that its five-membered ring is attached to a pyridine ring instead of a benzene ring. Several spectroscopic techniques have been previously utilized to investigate the potential energy surfaces which govern the conformational changes for the indan family in electronic ground and excited states [9,58-66,71]. For pyrindan the nitrogen atom in the aromatic ring lowers the symmetry of the molecule to C_s for the planar structure and to C_1 for its puckered structure. Indan itself has C_{2v} symmetry for its planar form.

A microwave investigation of pyrindan was reported by Fantoni and Caminati [26], and the rotational spectra of the ground state and some of the lower energy vibrational excited states were assigned. The barrier to planarity was reported to be 390 cm^{-1} [26]. The ultraviolet spectra of pyrindan in 95% ethanol have also been reported [27,28]. Absorption bands were observed at 35,971, 36,496, 37,037, and $37,736\text{ cm}^{-1}$. In

the present study, infrared, Raman, and UV absorption spectroscopy have been used to investigate the conformational properties of pyrindan and to carry out the vibrational analysis. High-level *ab initio* calculations have also been used to confirm these results.

EXPERIMENTAL

Pyrindan was obtained from Aldrich with a stated purity of 98%. It was purified using vacuum transfer. The original sample was a light, yellow-brownish liquid but became clear and colorless after purification. Pyrindan has a molecular weight of 119.16 g/mol, density of 1.081 g/ml, and a boiling point of 212°C.

The Raman spectra of the vapor and liquid were recorded using a Jobin Yvon U-1000 double monochromator equipped with a charge-coupled device (CCD) detector. The pyrindan sample was observed to absorb laser radiation of the 5145Å wavelength and to reemit it as fluorescence, causing the spectra to be obscured by a broad fluorescence band. This problem is fairly common in Raman spectroscopy and can be caused by impurities in the sample or by the sample itself [85,86]. In order to decrease the magnitude of the fluorescent effect, the excitation laser beam was tuned to a different wavelength. In this experiment an Innova I-100 argon ion laser operating at 4889Å was used to excite the sample. The vapor sample of pyrindan was transferred under vacuum into a custom designed, thermally controlled glass Raman cell of a cylindrical shape that is 80 mm long and 15 mm in diameter [83,84]. The sample was heated to slightly above 260°C. The Raman spectra of the liquid were recorded for a pyrindan sample in an evacuated 10-mm glass tube at room temperature. The polarized spectra were also

recorded. Laser powers of 4.5W and 0.2W were used for the vapor-phase and liquid-phase experiments, respectively.

The infrared spectrum was recorded by placing a drop of the pyridan sample between KBr windows. A Biorad FTS-60 spectrometer equipped with a globar source, KBr beamsplitter, and a triglycerin sulfate detector was used. A total of 256 scans at 1.0 cm^{-1} resolution were averaged and subtracted from a background spectrum taken under same conditions.

The electronic absorption spectra of the vapor using a Bomem DA8.02 Fourier-transform spectrophotometer have also been recorded in the $25000 - 40000\text{ cm}^{-1}$ region. A deuterium lamp source, a quartz beamsplitter, and a silicon detector were used. The vapor was contained in a 25 cm glass cell with quartz windows. Spectral acquisition was done at room temperature. Pyridan, however, showed only very weak absorptions which could not conclusively be used to determine the vibronic levels of the first electronic excited state.

***AB INITIO* CALCULATIONS**

The Gaussian 03 program [67] was used to carry out the quantum-chemical second-order Møller-Plesset (MP2) and density functional theory (DFT) calculations using several basis sets. The geometry of the stable structure and the conformational energies for pyridan were predicted using the MP2 theory. The vibrational frequencies, infrared and Raman intensities, and the polarization ratios for the planar (C_s) and puckered (C_7) structures of the molecule were calculated from the DFT with the B3LYP

hybrid functional. The double-minima potential energy functions in terms of the puckering coordinate were also calculated based on *ab initio* structures and energies.

RESULTS AND DISCUSSION

1. Molecular Structure

Pyrindan was previously shown from a microwave study [26] to be puckered with an inversion barrier of 390 cm^{-1} . In its puckered structure the molecule has C_1 symmetry. But because it is a non-rigid molecule, its vibrations can be assigned on the basis of a planar structure of C_s symmetry, where all of the ring atoms are lying in the plane of symmetry. Its forty-eight vibrational modes are then represented by symmetry species $30A' + 18A''$.

The calculated structure of pyrindan from *ab initio* calculation is shown in Fig. 25. The figure also shows the calculated structure of the indan molecule. The energies of the planar transition structure and the most stable puckered structure of pyrindan were optimized using the MP2 and DFT-B3LYP theories to determine the barrier of inversion and dihedral angle for the molecule. These *ab initio* values are listed in Table 16 and were used to obtain the potential energy function in terms of the puckering coordinate (x). Fig. 26 shows the definition of the puckering coordinate (x) and the puckering angle (ϕ). Fig. 27 shows the ring-puckering potential energy function determined from the MP2 and DFT-B3LYP with the 6-31G and cc-pVTZ basis sets. Table 16 and Fig. 27 show clearly the improvement of the calculated energy barriers when the polarization and diffusion functions are included in the basis sets. It should also be noted that the

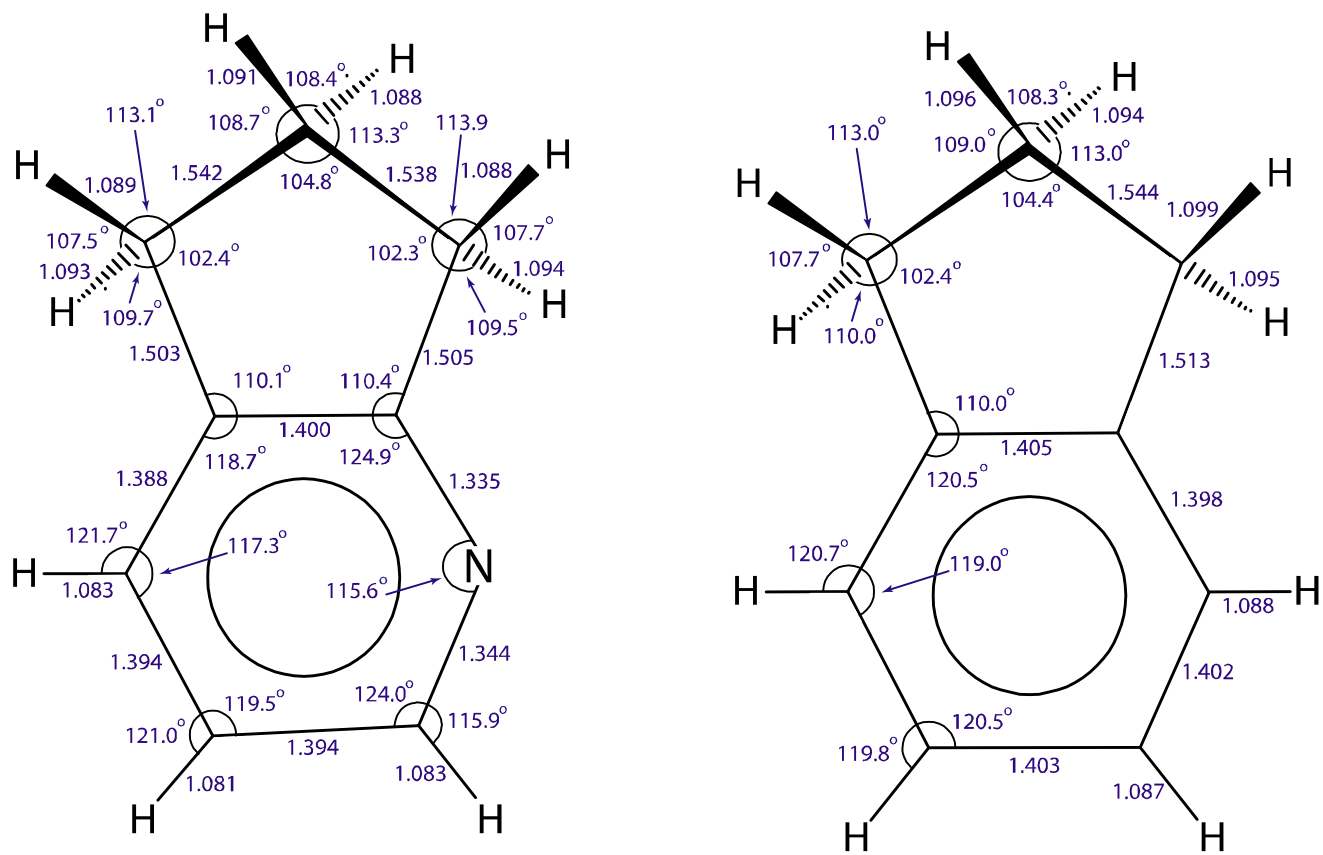


Fig. 25. Structures of pyridan and indan molecules as determined from the MP2/6-311++G(d,p) calculation.

Table 16
Puckering barrier (cm^{-1}) and puckering angle (deg.) for
pyrindan by different levels of theory

Theory	Puckering angle (ϕ)	Puckering barrier
DFT-B3LYP/3-21G	27	319
DFT-B3LYP/6-31G	24	186
DFT-B3LYP/6-31+G(d)	27	298
DFT-B3LYP/6-311++G(d,p)	26	286
DFT-B3LYP/cc-pVDZ	28	369
DFT-B3LYP/cc-pVTZ	26	276
MP2/3-21G	28	283
MP2/6-31G	24	179
MP2/6-31+G(d)	31	595
MP2/6-311++G(d,p)	32	631
MP2/cc-pVDZ	33	717
MP2/cc-pVTZ	32	587

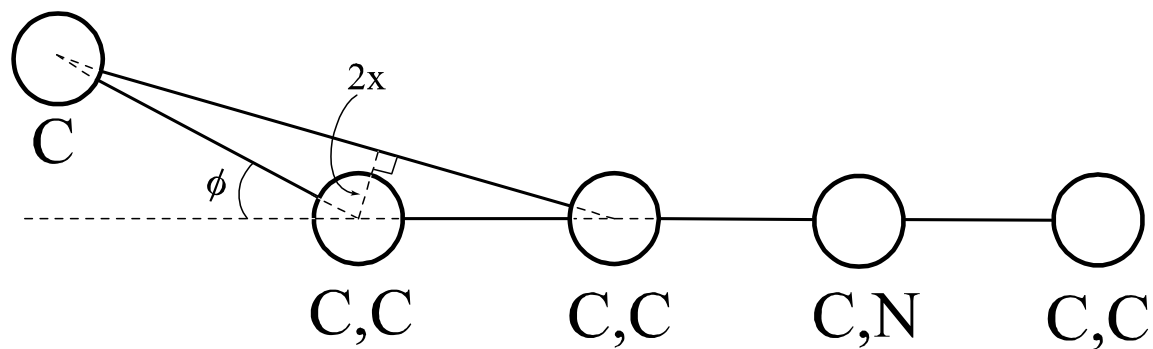


Fig. 26. Definitions of the ring-puckering angle (ϕ) and the ring-puckering coordinate (x) utilized to predict the ring-puckering potential energy function from *ab initio* calculations.

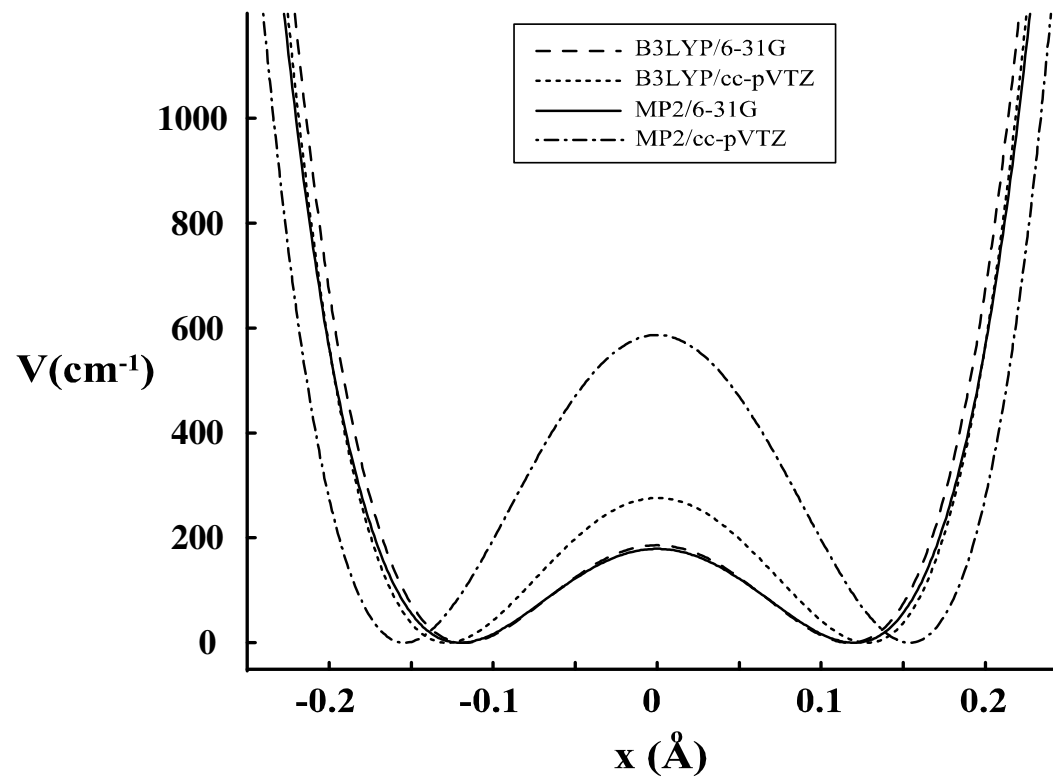


Fig. 27. Theoretical potential energy functions in terms of the ring-puckering coordinate for pyridan as determined from MP2 and DFT-B3LYP calculations.

barriers predicted by DFT are smaller as compared with those computed using the MP2 theory.

It can also be seen from Fig. 25 that the presence of the nitrogen atom in the six-membered ring has almost no effect on the bond lengths and angles of the five-membered ring as compared to the indan molecule. This suggests that the ring-puckering barrier and angle in pyrindan should not differ much from those previously determined for indan [58]. Even though the experimental values for the ring-puckering angle and barrier from one side of the five-membered ring to the other are not available, the *ab initio* values of pyrindan are very close to the experimental values obtained for indan. The two-dimensional potential energy function determined for indan gave a puckering barrier of 488 cm^{-1} and a puckering angle of 30° [58] as compared to the calculated values of 587 cm^{-1} and 31° for pyrindan.

2. Raman and Infrared Spectra

Fig. 28 shows the Raman spectra of pyrindan vapor compared to the calculated spectra of the C_s planar and C_1 puckered structures of pyrindan. The agreement is quite good between the experimental and theoretical spectra. The experimental vapor-phase Raman spectrum can be seen to be well-represented by the calculated spectrum of the puckered molecule. Nonetheless, in most cases, the calculated Raman spectrum of the planar structure also shows reasonably good agreement with the experimental spectrum. Long acquisition and integration times were used to collect the vapor-phase Raman spectra because the vapor Raman bands are quite weak.

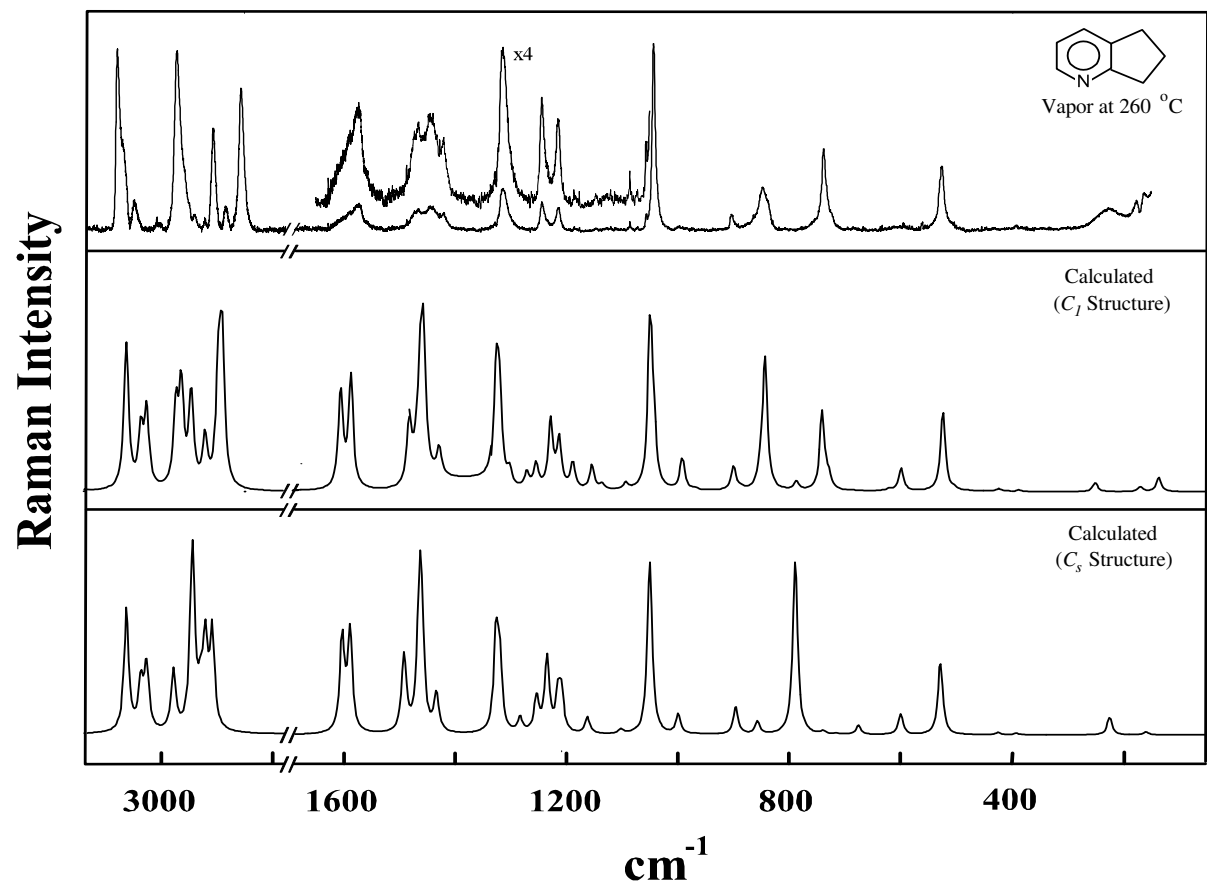


Fig. 28. Raman spectra of the vapor pyridan compared to the theoretical spectra calculated at the B3LYP/6-311++G(d,p) level of theory.

The polarized spectra of pyrindan were also recorded and the spectral region below 1800 cm^{-1} is shown in Fig. 29. Theoretically, none of the Raman bands are depolarized since the molecule holds the lowest symmetry species C_1 in its ground state. However, some Raman bands, especially those of A'' symmetry for the C_s conformation are expected to be nearly depolarized and thus can be more accurately assigned to the appropriate vibrational modes when the depolarization ratios are utilized. Fig. 29 shows also that DFT calculations can predict the depolarization ratios of the vibrational modes in very good agreement with the experimental ones. This provides a great help in assigning the vibrational spectra of such molecules which do not possess much symmetry.

The infrared spectra of the liquid sample were also recorded and are shown in Fig. 30 compared to the calculated infrared spectra of the puckered and planar molecules. The agreement in terms of calculated frequencies is very good, but the agreement between the experimental and calculated intensities, as is typical, is not as good. Based on the vapor- and liquid-phase Raman, polarized Raman, and liquid-phase infrared spectra, the complete vibrational assignments were carried out and are presented in Table 17 based on the higher symmetry structure, the planar C_s . The calculated frequencies of the fundamentals, infrared and Raman intensities, and depolarization ratios for the C_1 and C_s conformations were also used to confirm these assignments and are listed in Table 17. For the purpose of comparison, the vibrational frequencies previously reported for indan [58] are listed in Table 17 to show that for most of the

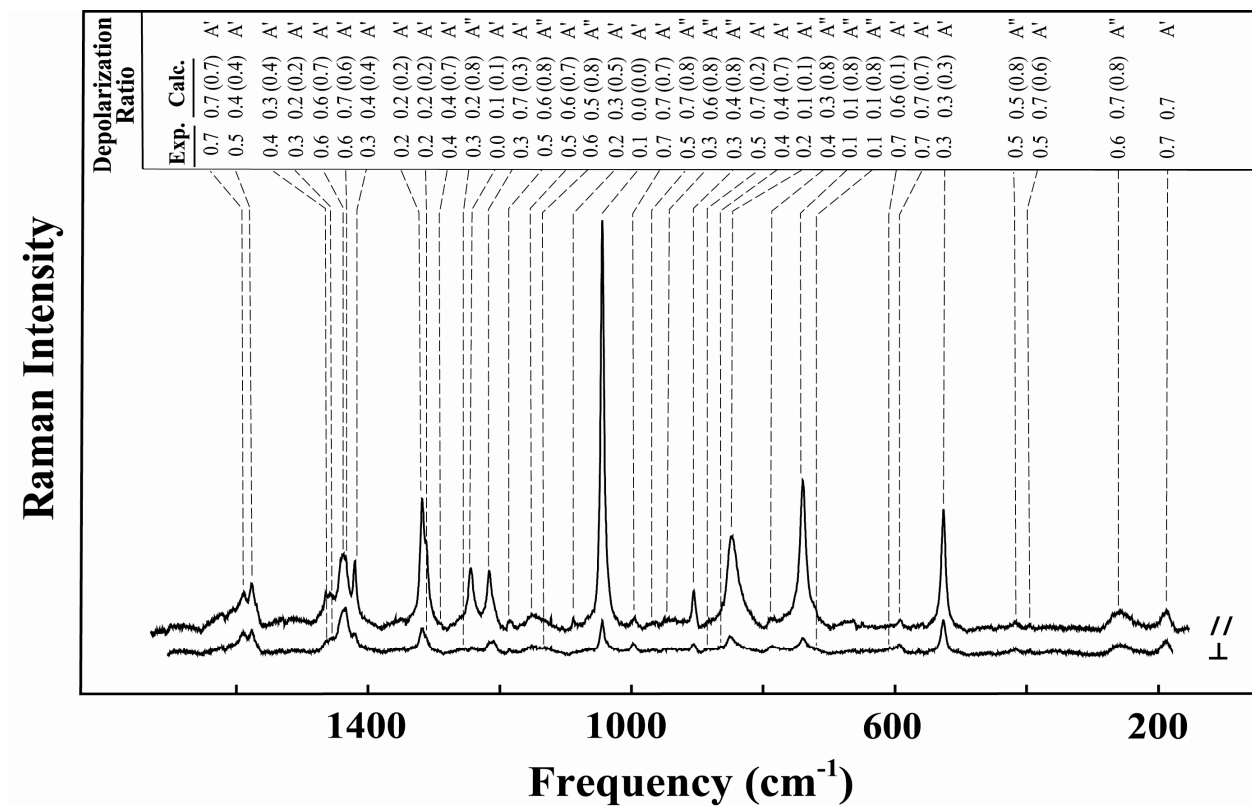


Fig. 29. Polarized spectra of pyrindan. Depolarization ratios were calculated using the B3LYP/6-311++G(d,p) level of theory. Calculated depolarization ratios in parentheses are for the planar C_s structure.

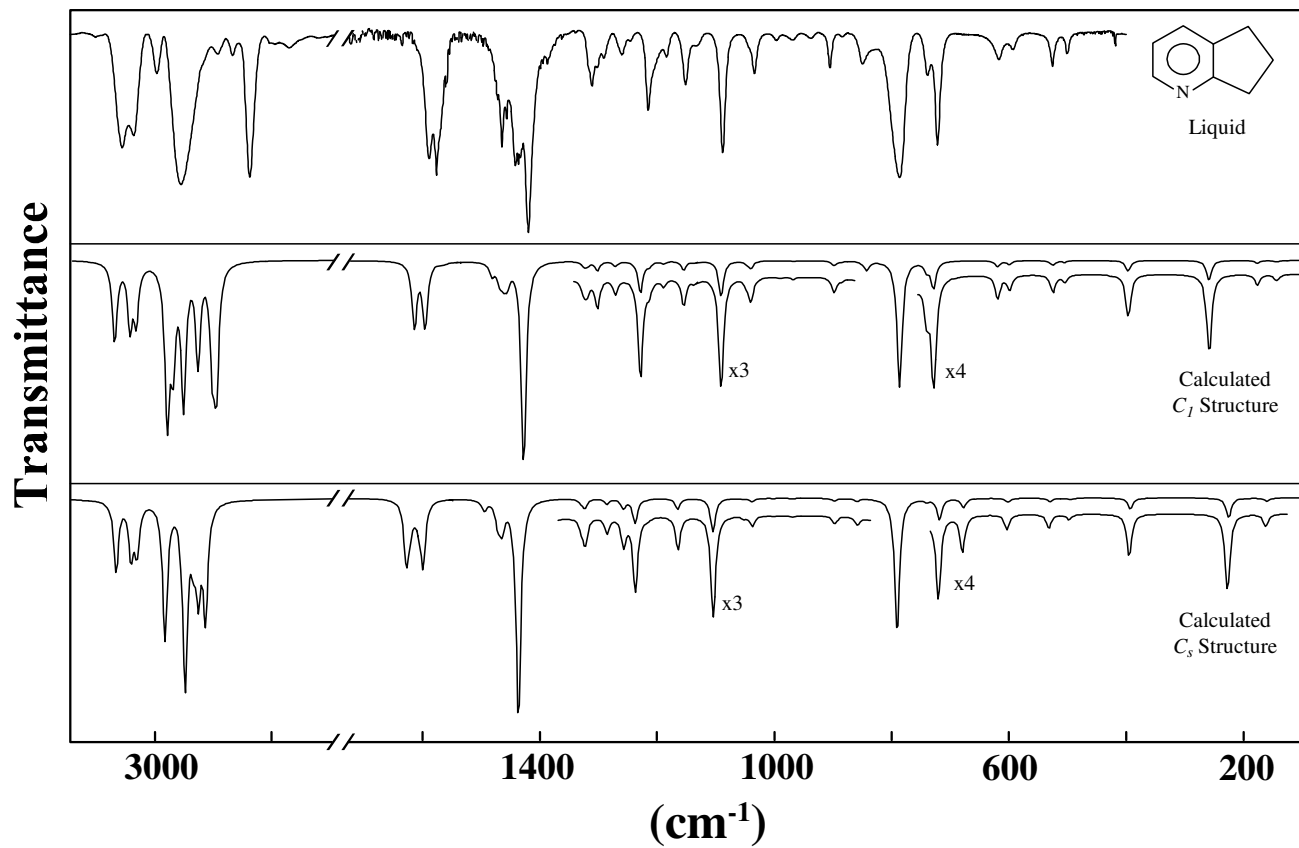


Fig. 30. Liquid-phase infrared spectra of pyridan compared to the theoretical spectra calculated at the B3LYP/6-311++G(d,p) level of theory.

Table 17

Vibrational assignments for pyridinane based on experimental and calculated spectra

Vibrational assignments			Raman		IR	Calculated ^a DFT-B3LYP/6-311++G(d,p)				Indan ^b
			Vapor	Liquid	Liquid	C_I		C_s		(vapor)
A'	v ₁	CH str.	3076 (216)	3063	3060 m	3063	(20,221) 0.2	3063	(20,202) 0.2	3075
	v ₂	CH str.	3046 (37)	3040	3041 m	3037	(15,85) 0.6	3037	(15,84) 0.6	3042
	v ₃	CH str.	3002 (11)	2997	3000 m	3026	(14,118) 0.4	3025	(15,118) 0.4	3035
	v ₄	CH ₂ sym. str.	2905 (123)	2895	2897 w	2946	(35,142) 0.2	2943	(50,244) 0.0	2902
	v ₅	CH ₂ sym. str.	2884 (31)	2872	2870 m	2897	(22,167) 0.2	2920	(23,149) 0.2	2885
	v ₆	CH ₂ sym. str.	2857 (170)	2843	2841 s	2890	(29,214) 0.1	2906	(32,175) 0.1	-----
	v ₇	Pyridine-ring str.	1589 (12)	1587	1588 m	1607	(18,60) 0.7	1628	(19,54) 0.7	1610
	v ₈	Pyridine-ring str.	1575 (16)	1576	1576 s	1589	(18,64) 0.4	1590	(19,58) 0.4	1589
	v ₉	CH ₂ def.	1487 (7)	1483	1468 vvw	1483	(3,37) 0.3	1492	(3,45) 0.4	1474
	v ₁₀	CH in-plane-bend	1473 (12)	1471	1472 vw	1471	(5,9) 0.2	1470	(5,7) 0.2	1467
	v ₁₁	CH ₂ def.	1466 (13)	1465	1465 m	1464	(4,55) 0.6	1465	(3,60) 0.7	1460
	v ₁₂	CH ₂ def.	1444 (14)	1457	1456 w	1457	(5,83) 0.7	1461	(6,49) 0.6	1445
	v ₁₃	Pyridine-ring str.	1421 (11)	1420	1419 vs	1429	(57,17) 0.4	1434	(64,23) 0.4	1431
	v ₁₄	CH ₂ wag	1329 (4)	1317	-----	1327	(1,64) 0.2	1327	(1,53) 0.2	1318
	v ₁₅	CH ₂ wag	1314 (24)	1312	1311 w	1321	(1,50) 0.2	1322	(2,32) 0.2	1316
	v ₁₆	CH ₂ wag	-----	-----	1302 sh	1302	(3,9) 0.3	1284	(2,7) 0.1	1302 ^c
	v ₁₇	Pyridine-ring str.	1293 (4)	1292	1291 w	1272	(1,9) 0.4	1256	(3,5) 0.7	1271
	v ₁₈	Pyridine-ring str.	1243 (17)	1244	1246 m	1228	(9,41) 0.1	1236	(7,40) 0.1	1213
	v ₁₉	CH in-plane-bend	1214 (14)	1216	1215 vw	1214	(1,28) 0.7	1215	(0,18) 0.3	1205
	v ₂₀	Ring mode	1147 (2)	1151	1151 w	1154	(3,15) 0.6	1163	(3,8) 0.7	1158
	v ₂₁	CH in-plane-bend	1085 (6)	1088	1088 s	1093	(10,4) 0.3	1103	(10,2) 0.5	1069
	v ₂₂	Pyridine-ring breath	1043 (100)	1044	-----	1050	(1,100) 0.0	1051	(0,100) 0.0	1025
	v ₂₃	5-mem.-ring C-C str.	997 (1)	996	996 vw	992	(0,21) 0.7	1001	(0,11) 0.7	971
	v ₂₄	5-mem.-ring C-C str.	890 (2)	-----	884 vw	887	(0,1) 0.7	896	(1,14) 0.2	856
	v ₂₅	Ring def.	847 (24)	847	849	850	(0,60) 0.4	858	(1,8) 0.7	831
	v ₂₆	5-Mem.-ring breath	838 (18)	-----	-----	843	(2,78) 0.1	790	(1,94) 0.1	787
	v ₂₇	Ring def.	611 (1)	607	617 m	619	(2,1) 0.6	676	(3,2) 0.1	610
	v ₂₈	Ring bend	594 (5)	594	593 w	598	(1,13) 0.7	600	(1,11) 0.7	570
	v ₂₉	Pyridine-ring bend	525 (35)	526	526 w	523	(1,46) 0.3	529	(1,41) 0.3	515
	v ₃₀	Skeletal bend	393 (1)	396	-----	394	(3,1) 0.7	392	(3,1) 0.6	372

Table 17
Continued

Vibrational assignments	Raman		IR	Calculated ^a DFT-B3LYP/6-311++G(d,p)			Indan ^b (vapor)
	Vapor	Liquid	Liquid	C_l	C_s		
A'' V ₃₁ CH ₂ antisym. str.	2970 (215)	2957	2959 s	2974 (38,121) 0.7	2977 (39,106) 0.8	2971	
V ₃₂ CH ₂ antisym. str.	2939 (29)	-----	-----	2964 (32,150) 0.2	2945 (2,89) 0.8	2949	
V ₃₃ CH ₂ antisym. str.	2920 (26)	-----	~2921 w	2921 (24,75) 0.3	2927 (11,59) 0.8	-----	
V ₃₄ CH ₂ twist	1263 (2)	1259	1260 w	1255 (0,14) 0.2	1254 (0,12) 0.8	1264	
V ₃₅ CH ₂ twist	1186 (2)	1185	1184 w	1189 (1,16) 0.6	1210 (0,19) 0.8	1151 ^c	
V ₃₆ CH ₂ twist	-----	1133	1134 w	1137 (0,3) 0.5	1150 (0,1) 0.8	1128 ^c	
V ₃₇ CH ₂ rock	1056 (9)	-----	1034 m	1042 (2,23) 0.1	1036 (1,2) 0.8	1041	
V ₃₈ CH out-of-plane bend	973 (1)	973	969 vw	969 (0,1) 0.7	968 (0,1) 0.8	-----	
V ₃₉ CH out-of-plane bend	937 (1)	----	938 vw	943 (0,0) 0.6	844 (0,0) 0.8	947	
V ₄₀ CH ₂ rock	903 (10)	905	905 m	899 (1,14) 0.4	899 (0,2) 0.8	908	
V ₄₁ CH out-of-plane bend	----	789	786 s	787 (35,5) 0.3	789 (38,3) 0.8	-----	
V ₄₂ CH ₂ rock	737 (45)	739	739 m	741 (2,46) 0.1	739 (1,3) 0.8	750	
V ₄₃ Pyridine-ring bend	725 (12)	726	722 s	728 (8,8) 0.1	717 (6,1) 0.8	737	
V ₄₄ Pyridine-ring bend	503 (6)	----	501 w	503 (1,1) 0.7	494 (0,1) 0.8	499 ^c	
V ₄₅ Pyridine-ring bend	~410 (0)	416	419 w	423 (0,1) 0.5	425 (0,0) 0.8	412	
V ₄₆ Ring flap	227 (2)	261	----	255 (6,6) 0.7	225 (0,15) 0.8	248	
V ₄₇ Skeletal twist	172 (3)	188	----	172 (1,3) 0.7	160 (0,3) 0.8	178	
V ₄₈ Ring puckering	----	----	----	139 (0,10) 0.7	i^d -----	143	

^a Scaled frequencies. Numbers in parentheses are infrared and Raman intensities. Numbers in *italics* are depolarization ratios.

^b From Ref. [58].

^c Frequencies from liquid-phase experiments.

^d Imaginary frequency associated to the higher energy structure.

vibrations, including the low-lying large-amplitude motions, the frequencies are shown to be almost identical.

Fig. 31 shows the vapor-phase Raman spectrum for the 150 – 450 cm^{-1} region that was taken at an elevated temperature using a higher concentration of the sample and employing a greater number of acquisitions and longer integration times. The B-type Raman band at 172 cm^{-1} resembling a B-type infrared band was assigned to the skeletal-twisting vibration (ν_{47}). The ring-flapping vibration (ν_{46}) was observed to be lower in frequency than expected from both the calculated value and the observed frequency for indan (Table 17). However, its observed frequency (227 cm^{-1}) agrees very well with the calculated value for the planar C_s structure (226 cm^{-1}). No side bands other than the fundamentals were observed in the vapor-Raman spectrum for pyrindan.

The investigation of the electronic excited state (S_1) for pyrindan has been also attempted. The UV absorption spectra for pyrindan were recorded at room temperature and are shown in Fig. 32. The molecule showed very weak UV transitions that can not be fully interpreted. The UV spectrum is presented and shows that the ν_0^0 is located in the region near 36,300 cm^{-1} . Running the UV spectra at higher temperatures and higher vapor pressure could possibly improve these results. The molecule also had very weak fluorescence in the jet-cooled chamber in a trial investigation for collecting the laser induced fluorescence (LIF) spectra. The UV and LIF spectra did not provide the usual complementary information that is helpful for studying the structure and vibronic levels in the electronic excited state.

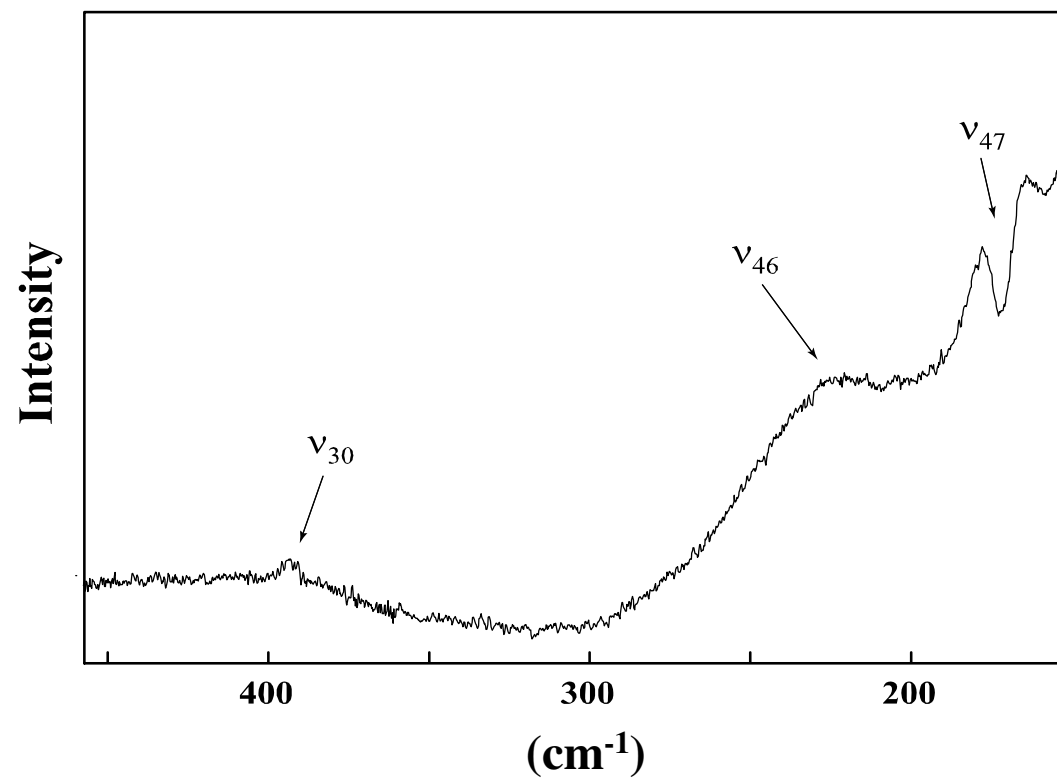


Fig. 31. Ring-twisting (ν_{47}), ring-flapping(ν_{46}), and skeletal-bending vibrations(ν_{30}) from the vapor-phase Raman experiment.

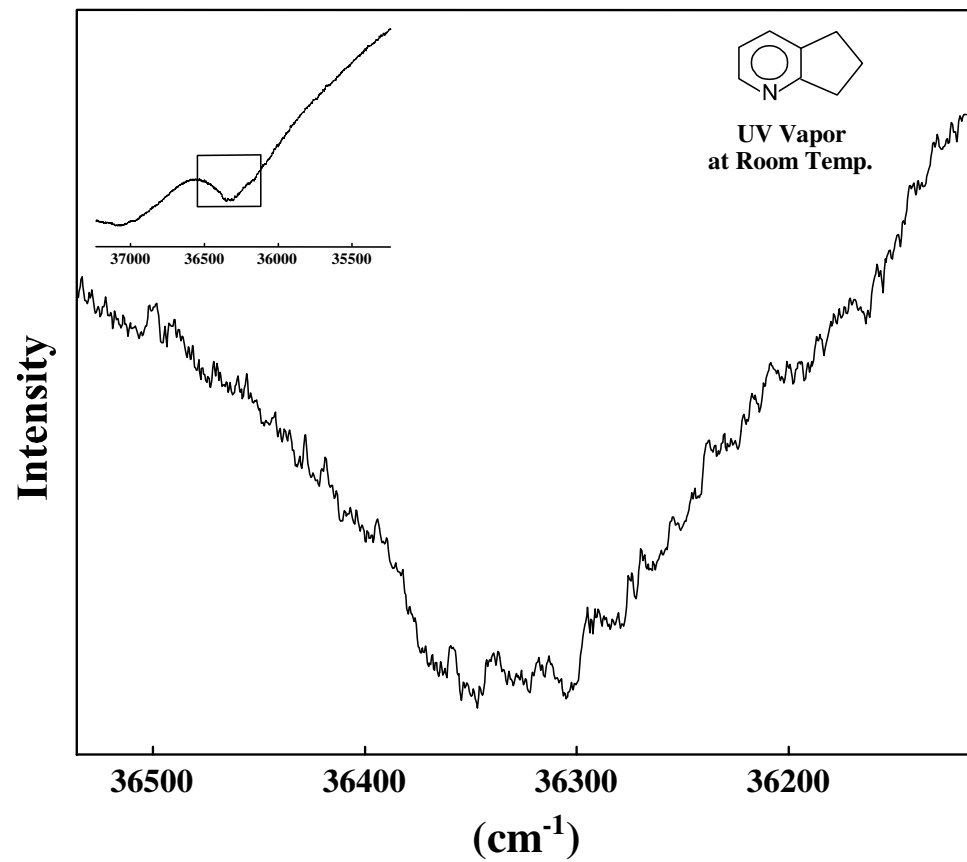


Fig. 32. UV spectra of pyrindan vapor taken at room temperature.

CONCLUSION

2,3-Cyclopentenopyridine (pyrindan) was investigated by means of several vibrational spectroscopic techniques. Substituting the carbon atom adjacent to the cyclopentene ring with a nitrogen atom seems to have a very small effect on the vibrational frequencies and inversion barrier in comparison to indan. An inversion barrier of 587 cm^{-1} , a puckering angle of 31° , and a puckering frequency of 139 cm^{-1} were predicted from *ab initio* calculations. The agreement between experiment and calculation for the vibrational spectra and energy barrier of the ring inversion is quite satisfactory.

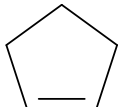
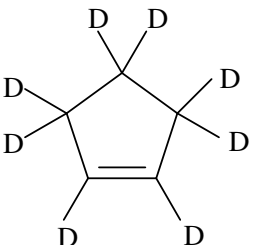
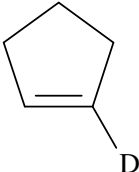
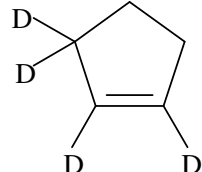
CHAPTER VIII
***AB INITIO* AND DFT CALCULATIONS FOR THE STRUCTURE**
AND VIBRATIONAL SPECTRA OF CYCLOPENTENE AND ITS
ISOTOPOMERS

INTRODUCTION

1. *Ab initio* and DFT Calculations versus Experiments

Ab initio and density functional theory (DFT) calculations are used to predict the structures and vibrational spectra of organic molecules. Three decades ago, when these types of computations were not possible, vibrational assignments were assisted by force constant calculations. A considerable number of comprehensive assignments and normal coordinate calculations for a variety of molecules has been previously reported. In some recent studies [87-91], where the experimental infrared and Raman data were compared with calculated results, spectroscopists have been very impressed how well the DFT computations do in calculating the frequencies and how well *ab initio* calculations do in predicting structures. In this study the structure and vibrational spectra of cyclopentene and its 1- d_1 , 1,2,3,4- d_4 , and d_8 isotopomers have been reinvestigated. The structures of the four molecules and their symmetry species are shown in Table 18.

Table 18
 Point groups, symmetry species, and structures for cyclopentene- d_0 and its isotopomers

				
Isotopomer	d_0	d_8	d_1	d_4
Point group:				
planar		C_{2v}		C_s
puckered		C_s		C_1
Symmetry species		$11A_1 + 6A_2 + 9B_1 + 7B_2$		$20A' + 13A''$

2. Spectroscopic and Computational Studies on Cyclopentenenes

The ring-puckering potential energy function of cyclopentene- d_0 was reported by Laane and Lord [10] in 1967. They determined the one-dimensional ring-puckering potential in its reduced form to be $V(\text{cm}^{-1}) = 24.3(z^4 - 6.18z^2)$. An inversion barrier of 232 cm^{-1} (0.66 kcal/mol) and a puckering angle of $23^\circ \pm 1^\circ$ were proposed from the one-dimensional ring-puckering potential energy function [10]. The two-dimensional potential energy surface associated with the ring-puckering and ring-twisting vibrations was later determined [29]. It reflected the fact that the ring-twisting tends to hinder the puckering process. The two-dimensional analysis showed that the puckering angle for cyclopentene is 26° (compared to 23° for the one-dimensional analysis).

In 1972 the vapor-phase Raman spectra were reported by Chao and Laane [30]. These spectra were used to confirm the assignments. In that study a series of lines between 109 and 256 cm^{-1} corresponding to $\Delta\nu = 2$ transitions of the ring-puckering were observed. This was one of the pioneer studies that implemented low-frequency vapor-phase Raman spectroscopy to confirm the form of the ring-puckering potential energy function previously determined from the far-infrared experiment [6,29]. Also, in the work reported by Chao and Laane [30], a set of difference and combination bands corresponding to the ring-puckering vibration, with the 3070 cm^{-1} line as a reference, were observed in the C-H spectral region of cyclopentene- d_0 .

The structure of cyclopentene- d_0 was also investigated by other spectroscopic techniques. The puckering angle determined from the two-dimensional far-infrared analysis (26°) [29] was somewhat higher than the microwave value [31,32]. A study of

the near-infrared band progressions, which only indirectly provide the energies of the puckering levels, obtained a barrier to planarity of 244 cm^{-1} for cyclopentene- d_0 [33]. Gas-phase electron diffraction work [34], which is generally not as accurate for these floppy molecules, reported a value of 28.8° .

The studied of the ring-puckering potential energy functions and the vibrational frequencies were later extended to the $1-d_1$, $1,2,3,4-d_4$, and d_8 isotopomers of cyclopentene [29,35-37]. The barrier to planarity in cyclopentene- d_8 was found to be 17 cm^{-1} less than the barrier in the undeuterated cyclopentene. The lowering in the barrier for the d_8 molecule is attributed to the mixing between the ring-puckering vibration and the other low-frequency vibrations. One-dimensional potential energy functions were found for cyclopentene- $1-d_1$ and cyclopentene- $1,2,3,3-d_4$, and a regular decrease in the barrier heights in going from the d_0 molecule (233 cm^{-1}) to the d_1 molecule (231 cm^{-1}) to the d_4 molecule (224 cm^{-1}) to the d_8 molecule (215 cm^{-1}) occurs. Full vibrational assignments of the four molecules were also reported [37].

In 1992, Allen, Csaszar, and Haner [92] carried out some comprehensive *ab initio* calculations on cyclopentene and its isotopomers and computed a puckering angle of 23.4° and a barrier to planarity of $235 \pm 20\text{ cm}^{-1}$. In our view this paper represented a major breakthrough in computations as it did an excellent job in matching the experimental data for each of the isotopic species. In addition to Allen's work [92], several other *ab initio* investigations of the structure of cyclopentene- d_0 are found in the literature [93-96]. In the work presented in this chapter, a basic target is to evaluate how well standard basis sets from the Gaussian 03 package [67] do in computing the structure

and vibrational spectra of this molecule using methodology applicable by experimental research groups. The accuracy of previous vibrational assignments and correcting these where necessary will also be assessed.

EXPERIMENTAL

The high quality infrared and Raman spectra of cyclopentene and its deuterated isotopomers have been previously published by Villarreal *et al.* [37]. For the present work only the infrared and Raman spectra of the liquid phase were recorded so a direct comparison between observed and calculated spectra could be shown.

Cyclopentene (Aldrich-99%) was used without further purification. The liquid infrared spectrum of a drop of sample between two KBr windows was recorded using a Biorad FTS-60 equipped with a globar source, KBr beamsplitter, and a triglycerin sulfate detector. A total of 256 scans at 1.0 cm^{-1} resolution were averaged. The Raman spectra of the liquid cyclopentene were recorded for a sample in a 1mm glass tube. A JobinYvon U-1000 double monochromator equipped with a CCD detector and an Innova I-100 argon ion laser operating at 5145 \AA with 1 watt of power were used.

COMPUTATIONAL METHODS

Density functional theory (DFT) with the B3LYP hybrid functional and *ab initio* second-order Moller-Plesset (MP2) calculations using the Gaussian 03 program [67] were carried out for the four isotopomers of cyclopentene. Four basis sets, 6-31+G(d), 6-311++G(d,p), cc-pVDZ (double- ζ) and cc-pVTZ (triple- ζ) were all used. The

vibrational frequencies of the four molecules were calculated for the puckered and planar forms. The total energies were also calculated.

MOLECULAR STRUCTURE

Fig. 33 shows the calculated C_s and C_{2v} structures for cyclopentene- d_0 using the MP2/cc-pVTZ and MP2/6-311++G(d,p) levels of theory, compared to the structure from the gas-phase electron diffraction experiment [34]. Fig. 33 shows that calculations using the triple- ζ and 6-311++G(d,p) basis sets predicted the bond lengths and angles to be very nearly the same. Table 19 compares several geometric parameters from our calculations to previous experimental and theoretical work. As can be seen, when the triple- ζ basis set was utilized in the MP2 calculations, it agrees very well with the experimental puckering angle (26°), and the calculated barrier of 247 cm^{-1} differs only slightly from the experimental value of 232 cm^{-1} . From the results shown in Table 19, the importance of electron correlation and its affect on the accuracy of the predicted structure and energy can be seen. The calculated DFT structure can be seen to slightly underestimate the puckering angle (19° vs. 26° experimental) but greatly underestimates the inversion barrier (42 vs. 232 cm^{-1}) in cyclopentene.

MOLECULAR VIBRATIONS

Fig. 34 compares the computed infrared spectrum (both for the puckered C_s and planar C_{2v} structures) of cyclopentene to the experimental liquid-phase spectrum. Fig. 35 similarly compares the computed and experimental liquid Raman spectra. Tables 20-23

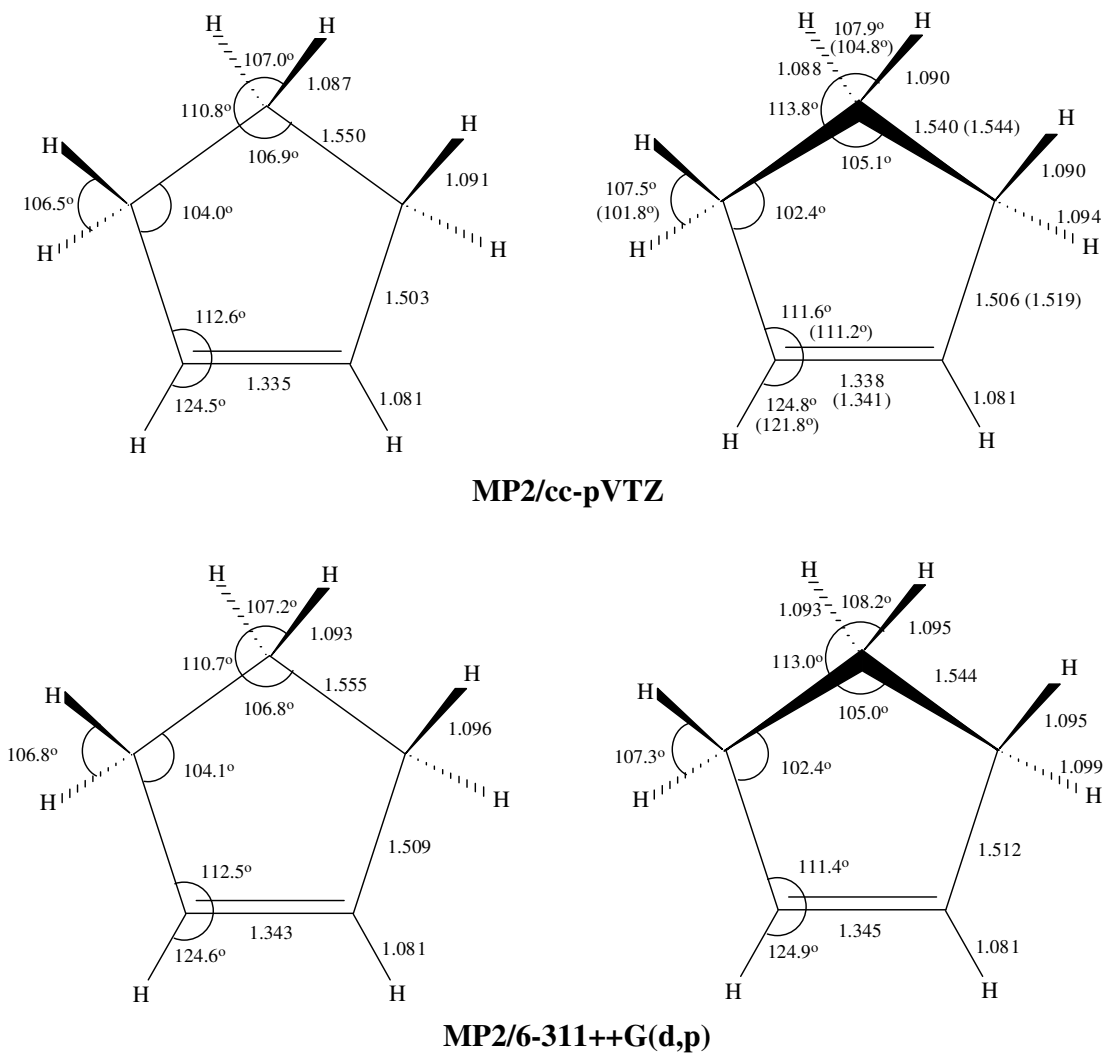
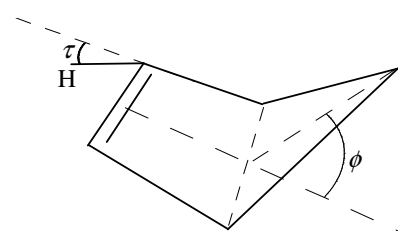


Fig. 33. Calculated planar (on the left) and puckered (on the right) structures of cyclopentene. Values in parentheses are from the gas-phase electron diffraction experiment in Ref. [34].

Table 19
Puckering angles (deg.), CH out-of-plane angles (deg.), and barriers to planarity (cm^{-1}) in cyclopentene- d_0 from various experimental and theoretical methods

		Puckering angle ^a (ϕ)	CH out-of-plane angle ^a (τ)	Barrier to planarity	Ref. ^b
Expt.	Gas-phase diffraction	28.8°			34
	Microwave	22.2°		230	32
	Far-IR one-dimensional study	23.3°		233	10
	Far-IR two-dimensional study	26°		232	29
	Near-IR	22.1°		244	33
Calc.	MM2 method	23°			97
	HF/DZ	13.6°			94
	HF/6-31+G(d)	20.0°	2.1°	90	
	HF/6-311++G(d,p)	20.2°	2.2°	94	
	MP2/DZ	23.4°	2.3°	177	92
	MP2(full)/6-31G(d)	26.3°		289	96
	MP2/6-31+G(d)	25.4°	2.8°	284	
	MP2/6-311++G(d,p)	27.1°	3.0°	298	
	MP2/cc-pVDZ	24.7°	2.6°	323	
	MP2/cc-pVTZ	26.1°	3.1°	247	
	DFT-B3LYP/6-31+G(d)	19.7°	2.4°	73	
	DFT-B3LYP/6-311++G(d,p)	20.0°	2.3°	60	
	DFT-B3LYP/cc-pVDZ	19.0°	2.1°	78	
	DFT-B3LYP/cc-pVTZ	19.3°	2.1°	42	

^aThese are defined below



^bResults not referenced indicate this work.

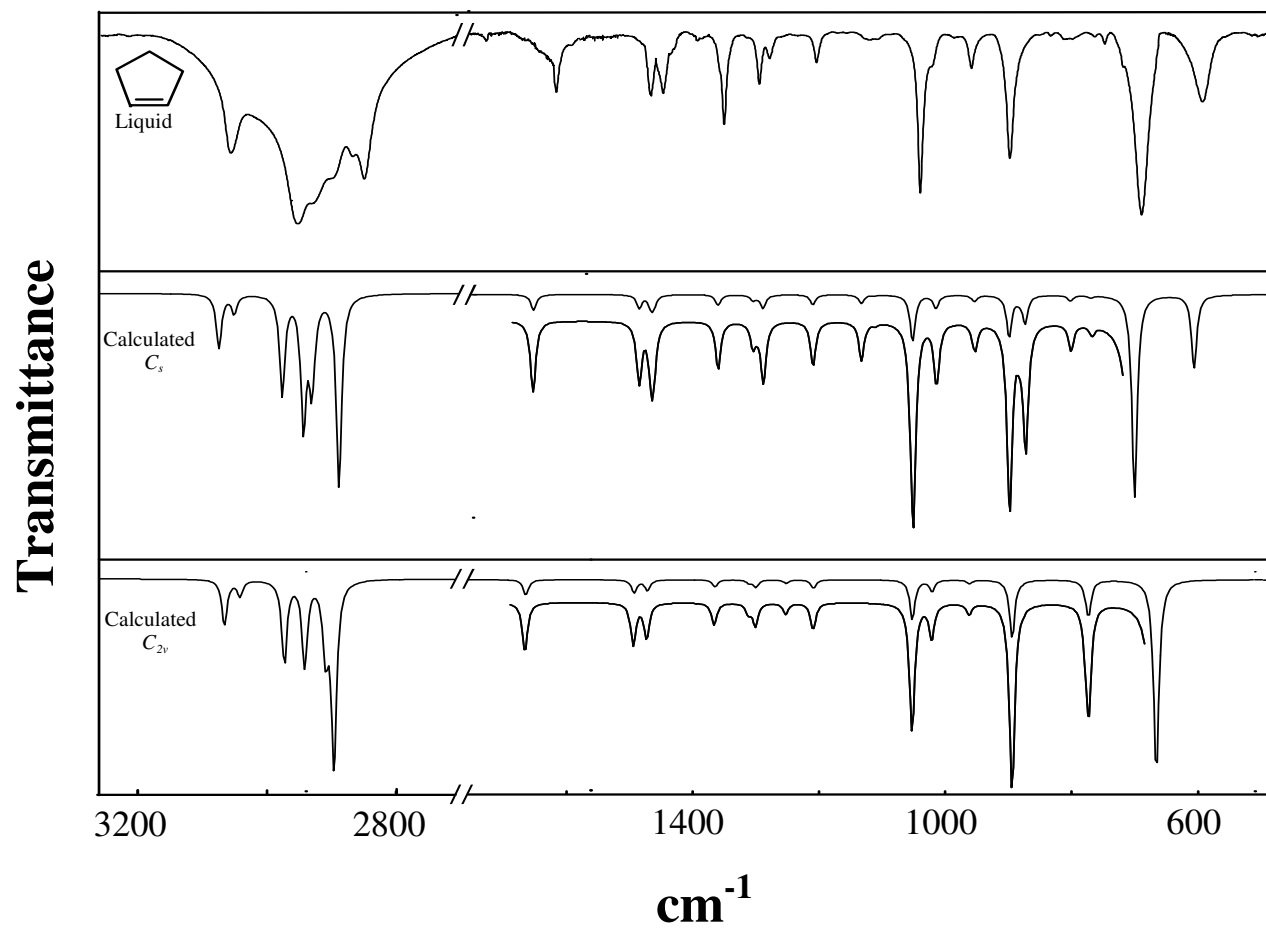


Fig. 34. Liquid and calculated (using the DFT-B3LYP/cc-pVTZ level of theory) mid-infrared spectra of cyclopentene- d_0 .

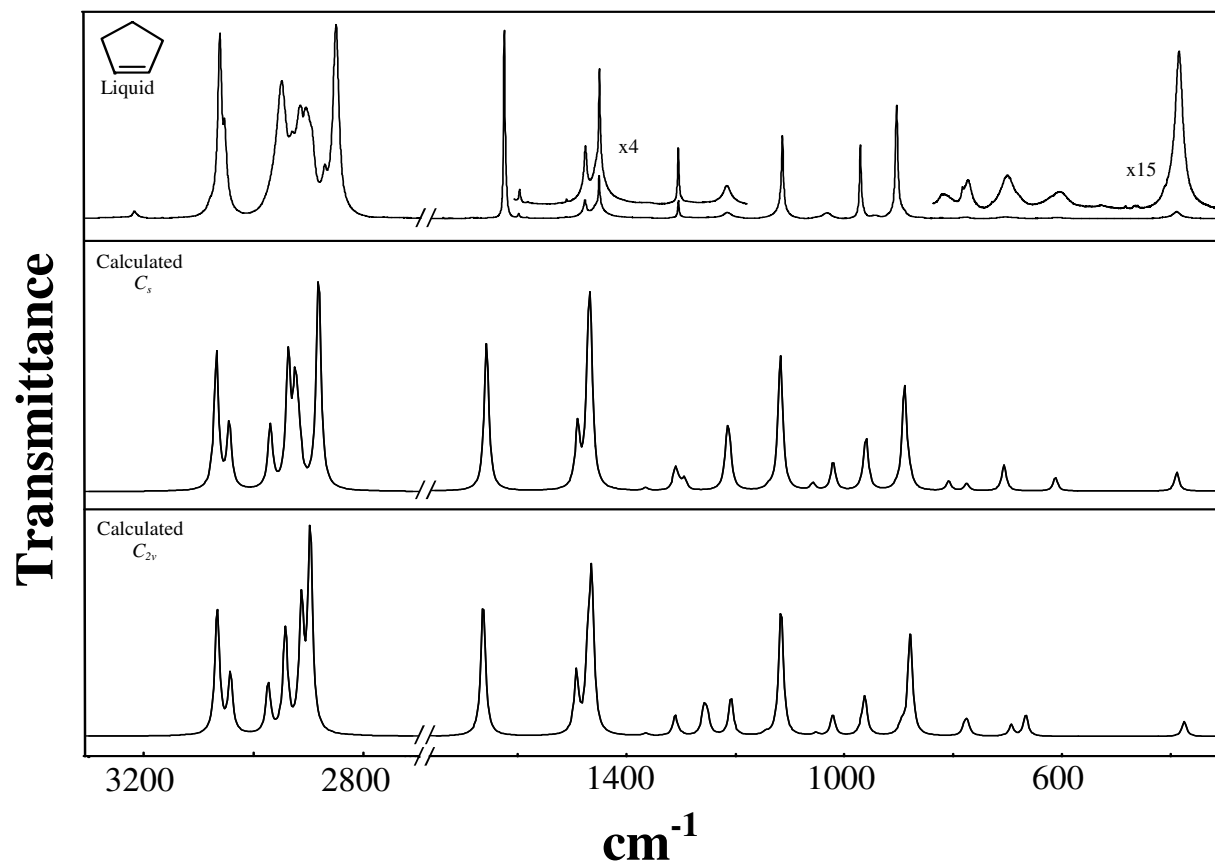


Fig. 35. Liquid and calculated (using the DFT-B3LYP/cc-pVTZ level of theory) Raman spectra of cyclopentene- d_0 .

Table 20[†]
 Reassignments of vibrational spectra of cyclopentene-*d*₀

Description	Reassignments ^{a,b}				Calculated ^c (DFT-B3LYP/cc-pVTZ)				This work (liquid)	
	IR		Raman		<i>C</i> _s		<i>C</i> _{2v}		IR	Raman
<i>A</i> ₁ , <i>A</i> '	ν_1	CH sym. str.	3078	s	3070 (140)	p	3068 (23,186)	3066 (24,187)		3062
	ν_2	β -CH ₂ sym. str.	2903	s	2900 (7)	p	2937 (56,173)	2942 (44,154)	2897 m	2903
	ν_3	α -CH ₂ sym. str. (i.p.)	2860	s	2857 (153)	p	2881 (31,218)	2896 (2,267)	2848 vs	2849
	ν_4	C=C str.	1623	m	1617 (91)	p	1649 (2,143)	1657 (3,125)	1610 m	1614
	ν_5	β -CH ₂ def.	1471	vw	1473 (16)	p	1481 (2,57)	1486 (3,56)	1463 m	1467
	ν_6	α -CH ₂ def. (i.p.)	1445	m	1448 (23)	p	1459 (1,143)	1459 (0,138)	1444 m	1442
	ν_7	α -CH ₂ wag (i.p.)	1290	m	1302 (10)	p	1303 (1,21)	1306 (1,19)	1295 m	1297
	ν_8	CH in-plane bend (i.p.)	1101	m	1109 (66)	p	1111 (0,129)	1112 (0,119)	1108 vw	1107
	ν_9	Ring str.	962	w	962 (55)	p	955 (1,50)	958 (1,31)	963 m	965
	ν_{10}	Ring breathing	900	m	896 (100)	p	885 (0,100)	875 (0,100)	903 s	898
	ν_{11}	Ring def.	593*	m	600 (1)	p?	608 (12,7)	691 (0,11)	603 m	605
<i>A</i> ₂ , <i>A</i> ''	ν_{12}	α -CH ₂ antisym. str. (o.p.)	2955*	s	2938 (54)		2924 (37,120)	2913 (0,184)		2949
	ν_{13}	α -CH ₂ twist (o.p.)	1268*	m	1279* (1)	[sol]	1287 (2,7)	1253 (0,25)	1279 w	1290
	ν_{14}	β -CH ₂ twist	1140*	w	1134 (1)	[sol]	1132 (1,0)	1140 (0,3)		
	ν_{15}	CH out-of-plane bend (o.p.)	933*	w [sol]	933* (2)	d	961 (0,7)	965 (0,5)		938
	ν_{16}	α -CH ₂ rock (o.p.)	878*	m [sol]	879 (1)		875 (4,7)	893 (0,3)		875
	ν_{17}	Ring twist			390 (2)	d	387 (0,21)	374 (0,11)		385

Table 20[†]
Continued

Description	Reassignments ^{a,b}		Calculated ^c (DFT-B3LYP/cc-pVTZ)		This work (liquid)		
	IR	Raman	C_s	C_{2v}	IR	Raman	
B_1, A'	ν_{18} CH antisym. str.	3068 s	3062 (18)	3044 (8,87)	3043 (8,87)	3055 s	3053
	ν_{19} α -CH ₂ sym. str. (o.p.)	2873 s	2882 (57) p	2883 (54,75)	2896 (95,33)	2866 s	2870
	ν_{20} α -CH ₂ def. (o.p.)	1438 vw		1463 (2,71)	1466 (2,56)		1451
	ν_{21} CH in-plane bend (o.p.)	1353 m	1354 (1) [sol]	1358 (2,0)	1360 (1,3)	1350 vw	1352
	ν_{22} α -CH ₂ wag (o.p.)		1297 (1) [sol]	1296 (0,7)	1295 (1,0)		
	ν_{23} β -CH ₂ wag	1207* m		1205 (0,29)	1247 (1,19)	1167 vw	
	ν_{24} Ring str.	1037 w	1030 (1)	1015 (2,29)	1071 (2,18)	1025 w	1026
	ν_{25} Ring str.	906* m		900 (7,0)	891 (11,5)		
	ν_{26} Ring def.	796* vw	800* (1)	771 (0,7)	776 (1,4)	770 vw	771
B_2, A''	ν_{27} α -CH ₂ antisym. str. (i.p.)	2933* s	2929* [sol]	2918 (4,61)	2910 (35,2)	2925 s	2915
	ν_{28} β -CH ₂ antisym. str.	2963* s	2973* (39)	2970 (43,84)	2973 (43,74)	2949 s	2929
	ν_{29} α -CH ₂ twist (i.p.)	1211* m (c-type)	1209* (2) d	1209 (2,43)	1204 (2,38)	1205 m	1207
	ν_{30} α -CH ₂ rock (i.p.)	1047 s (c-type)	1047 (1)	1052 (7,7)	1048 (8,3)	1043 s	1044
	ν_{31} CH out-of-plane bend (i.p.)	695 s (c-type)	690* (1) d	702 (31,21)	663 (37,16)	696 s	700
	ν_{32} β -CH ₂ rock	793* w	783* (1) d	803 (1,7)	770 (7,11)	803 vw	817
	ν_{33} Ring puckering	127.1	128.5	130 (0,7)	i^d		

^a Vapor-phase vibrational spectra from Ref. [37], unless otherwise indicated. Frequencies given in *italics* are from Ref. [98].

^b [sol]=solid state, d=depolarized, p=polarized, reassigned frequencies are marked with (*).

^c Scaled frequencies, values in parentheses are infrared and Raman intensities.

^d Imaginary frequency calculated for higher energy structure.

[†] The footnotes above also apply for the Tables 21-23 that follow.

Table 21[†]
 Reassignments of vibrational spectra of cyclopentene-*d*₈

Description	Reassignments ^{a,b}				Calculated ^c (DFT-B3LYP/cc-pVTZ)			
	IR		Raman		<i>C_s</i>		<i>C_{2v}</i>	
<i>A₁, A'</i>	ν_1	CD sym. str.	2310	s	2305 (68)	p	2315 (9,78)	2314 (10,78)
	ν_2	β -CD ₂ sym. str.	2153	w	2145 (100)	p	2160 (18,67)	2168 (22,77)
	ν_3	α -CD ₂ sym. str. (i.p.)			2100 (136)	p	2128 (10,132)	2135 (1,134)
	ν_4	C=C str.	1580	m	1577 (50)	p	1600 (4,143)	1609 (5,123)
	ν_5	β -CD ₂ def.	1070*	m	1072* (2)	p	1071 (1,19)	1072 (0,18)
	ν_6	α -CD ₂ def. (i.p.)	1110*	w	1113* (7)	p	1110 (1,14)	1110 (1,11)
	ν_7	α -CD ₂ wag (i.p.)	750*	w	750* (7)	p	744 (1,13)	750 (0,14)
	ν_8	CD in-plane bend (i.p.)	792*	vw	790* (7)	p?	785 (0,38)	781 (0,33)
	ν_9	Ring str.	1150*	vw [sol]	1158* (2)	d	1149 (1,4)	1148 (0,6)
	ν_{10}	Ring breathing	878	m	878* (100)	p	871 (2,100)	865 (0,100)
	ν_{11}	Ring def.	696*	w	693* (1)	d	681 (0,3)	645 (0,6)
<i>A₂, A''</i>	ν_{12}	α -CD ₂ antisym. str. (o.p.)	2180*	w	2202 (15)	d	2190 (7,79)	2186 (0,96)
	ν_{13}	α -CD ₂ twist (o.p.)	882*	w [sol]	887* (1)		890 (1,19)	891 (0,16)
	ν_{14}	β -CD ₂ twist	926*	w [sol]	930* (1)	p	929 (0,4)	930 (0,2)
	ν_{15}	CD out-of-plane bend (o.p.)	716*	w	720* (1)	d [liq]	728 (1,3)	733 (0,4)
	ν_{16}	α -CD ₂ rock (o.p.)	660*	w [sol]	667 (1)	[sol]	661 (0,0)	673 (0,0)
	ν_{17}	Ring twist			317 (2)	d	320 (2,9)	308 (0,7)

Table 21[†]
Continued

Description	Reassignments ^{a,b}				Calculated ^c (DFT-B3LYP/cc-pVTZ)		
	IR		Raman		C_s	C_{2v}	
B_1, A'	ν_{18} CD antisym. str.	2276	m	2268 (15)	d	2270 (3,44)	2268 (3,44)
	ν_{19} α -CD ₂ sym. str. (o.p.)	2138	m	2132 (20)	p	2128 (38,24)	2133 (46,19)
	ν_{20} α -CD ₂ def. (o.p.)	1062	m			1062 (2,14)	1059 (1,9)
	ν_{21} CD in-plane bend (o.p.)	1024*	vw			1027 (1,0)	1029 (1,0)
	ν_{22} α -CD ₂ wag (o.p.)	724*	m	725* (1)	[sol]	707 (6,2)	706 (8,2)
	ν_{23} β -CD ₂ wag			790* (7)	p?	788 (0,20)	804 (0,14)
	ν_{24} Ring str.	1128*	vw [sol]	1130* (1)	p? [liq]	1122 (1,3)	1113 (1,6)
	ν_{25} Ring str.			1190* (1)	d	1195 (0,10)	1198 (1,9)
	ν_{26} Ring def.	750*	w [sol]			757 (1,0)	760 (1,3)
	B_2, A''	ν_{27} α -CH ₂ antisym. str. (i.p.)	2200*	s (c-type)	2235* (30)	p	2192 (23,31)
ν_{28} β -CH ₂ antisym. str.		2230*	s (c-type)	2202* (15)		2230 (22,40)	2233 (20,37)
ν_{29} α -CH ₂ twist (i.p.)		849*	s (c-type)	850* (7)	d?	852 (5,29)	857 (8,9)
ν_{30} α -CH ₂ rock (i.p.)		954*	w [sol]	950* (1)	d	954 (0,8)	943 (0,5)
ν_{31} CH out-of-plane bend (i.p.)		465*	s (c-type)	460* (1)	d	464 (13,3)	483 (19,6)
ν_{32} β -CH ₂ rock		543*	s	550* (1)	d	549 (10,8)	574 (4,4)
ν_{33} Ring puckering		108.2				103 (0,1)	i^d

[†] See footnotes for Table 20.

Table 22[†]Reassignments of vibrational spectra of cyclopentene-1-*d*₁

Description	Reassignments ^{a,b}					Calculated ^c (DFT-B3LYP/cc-pVTZ)			
	IR		Raman			<i>C</i> _I		<i>C</i> _s	
	Wavenumber	Intensity	Wavenumber	Intensity	Polarization	Wavenumber	Intensity	Wavenumber	Intensity
<i>A'</i> , <i>A</i>	<i>v</i> ₁ CH str.	3065 m	3066 (188)	p	3056 (16,138)	3054 (16,139)			
	<i>v</i> ₂ β-CH ₂ sym. str.	2903 s	2904 (122)	p	2937 (54,178)	2943 (43,157)			
	<i>v</i> ₃ α-CH ₂ sym. str.	2865 s	2879 (105)	p	2882 (53,74)	2897 (12,246)			
	<i>v</i> ₄ α-CH ₂ sym. str.	2859 s	2859 (224)	p	2881 (31,220)	2896 (85,57)			
	<i>v</i> ₅ =C-D str.	2294 m	2290 (37)	p	2293 (7,55)	2291 (7,56)			
	<i>v</i> ₆ C=C str.	1600 m	1597 (79)	p	1628 (3,23)	1637 (4,153)			
	<i>v</i> ₇ β-CH ₂ def.	1470 m	1472 (22)	p	1481 (2,8)	1486 (3,66)			
	<i>v</i> ₈ α-CH ₂ def.	1446 m	1448 (32)	p	1464 (2,10)	1466 (2,60)			
	<i>v</i> ₉ α-CH ₂ def.	1435 w			1458 (1,20)	1459 (0,153)			
	<i>v</i> ₁₀ CH in-plane bend	1261* m [liq]	1257* (3)	p	1263 (1,2)	1266 (1,14)			
	<i>v</i> ₁₁ α-CH ₂ wag	1300* w	1298* (10)	p	1303 (1,2)	1305 (1,13)			
	<i>v</i> ₁₂ α-CH ₂ wag	1322* m [liq]	1327* (5)	p	1329 (2,1)	1330 (2,9)			
	<i>v</i> ₁₃ β-CH ₂ wag	1284* m [sol]			1288 (2,2)	1242 (0,21)			
	<i>v</i> ₁₄ Ring str.	1033 m	1029 (8)	p	1020 (3,5)	1023 (3,31)			
	<i>v</i> ₁₅ CD in-plane bend	988 w	978 (65)	p	971 (2,11)	967 (2,64)			
	<i>v</i> ₁₆ Ring str.	966 w	952 (33)	p	946 (2,5)	950 (1,33)			
	<i>v</i> ₁₇ Ring breathing	900* w	899 (100)	p	886 (2,13)	877 (1,100)			
	<i>v</i> ₁₈ Ring str.	750 w	750 (1)	d	747 (3,2)	751 (3,13)			
	<i>v</i> ₁₉ Ring def.	770* m [sol]	779* (1)	p	774 (1,1)	800 (3,10)			
	<i>v</i> ₂₀ Ring def.	634* s	630* (1)	d	642 (4,1)	683 (0,6)			

Table 22[†]
Continued

Description	Reassignments ^{a,b}				Calculated ^c (DFT-B3LYP/cc-pVTZ)			
	IR		Raman		C_I		C_S	
A'' , A	ν_{21}	α -CH ₂ antisym. str.	2939	s	2939 (126)		2925 (38,117)	2913 (0,184)
	ν_{22}	α -CH ₂ antisym. str.	2939	s	2924 (126)		2918 (4,61)	2910 (35,2)
	ν_{23}	β -CH ₂ antisym. str.	2962	s	2969 (60)		2969 (43,84)	2973 (43,74)
	ν_{24}	α -CH ₂ twist	1211	s	1209 (2)	d	1208 (2,43)	1203 (1,41)
	ν_{25}	α -CH ₂ twist	1116 [*]	w	1121 [*] (1)	d	1133 (1,2)	1140 (0,3)
	ν_{26}	β -CH ₂ twist	1207 [*]	w			1199 (0,38)	1253 (0,27)
	ν_{27}	α -CH ₂ rock	1044	s (c-type)	1045 m	[sol]	1048 (6,5)	1044 (6,5)
	ν_{28}	CH out-of-plane bend	893 [*]	w			902 (2,17)	915 (1,13)
	ν_{29}	α -CH ₂ rock	855	s (c-type)	855 (1)	d	864 (3,18)	866 (4,10)
	ν_{30}	β -CH ₂ rock	807 [*]	s [liq]	802 [*] (1)	d	813 (3,6)	747 (0,4)
	ν_{31}	CD out-of-plane bend	565	s (c-type)	565 (1)	d	567 (25,15)	579 (30,12)
	ν_{32}	Ring twist	369	w	369 (3)	d	372 (0,10)	359 (0,12)
	ν_{33}	Ring puckering	126.0				129 (0,4)	i^d

[†]See footnotes for Table 20.

Table 23[†]
 Reassignments of vibrational spectra of cyclopentene-1,2,3,3-*d*₄

Description		Reassignments ^{a,b}				Calculated ^c (DFT-B3LYP/cc-pVTZ)			
		IR		Raman		<i>C_l</i>		<i>C_s</i>	
<i>A'</i> , <i>A</i>	ν_1 CD sym. str.	2310	m	2313 (13)	p	2315 (11,71)	2314 (11,72)		
	ν_2 β -CH ₂ sym. str.	2904	s	2905 (20)	p	2934 (52,156)	2941 (41,134)		
	ν_3 α -CD ₂ sym. str.	2110	s	2100 (51)	p	2128 (24,87)	2135 (24,89)		
	ν_4 α -CH ₂ sym. str.	2854	s	2861 (46)	p	2882 (41,152)	2897 (48,156)		
	ν_5 CD antisym. str.	2277	m	2265 (5)	d	2270 (3,44)	2268 (3,44)		
	ν_6 C=C str.	1560	m	1580 (51)	p	1604 (4,141)	1613 (5,132)		
	ν_7 β -CH ₂ def.	1460	m	1467 (4)	p	1477 (1,27)	1483 (2,30)		
	ν_8 α -CH ₂ def.	1449	m	1452 (7)	p	1459 (1,82)	1461 (1,77)		
	ν_9 α -CD ₂ def.	1081	vw	1085 (4)	p	1084 (0,20)	1085 (0,22)		
	ν_{10} CD in-plane bend	800*	w	802* (3)	d	798 (0,28)	793 (0,32)		
	ν_{11} α -CH ₂ wag	1286	w	1290 (1)	p?	1286 (1,10)	1272 (1,18)		
	ν_{12} α -CD ₂ wag	821*	m	825* (7)	p	815 (1,22)	823 (1,27)		
	ν_{13} β -CH ₂ wag	1308*	w	1310* (1)	?	1314 (1,8)	1315 (1,2)		
	ν_{14} Ring str.	1107*	m (c-type)	1100* (1)	d	1104 (2,6)	1102 (2,8)		
	ν_{15} CD in-plane bend	715*	vw	719*	[sol]	715 (2,4)	719 (7,4)		
	ν_{16} Ring str.	1143*	w	1156*	[sol]	1153 (0,7)	1167 (1,9)		
	ν_{17} Ring breathing	910	m	910 (100)	p	903 (1,100)	897 (1,100)		
	ν_{18} Ring str.	985*	vw	985* (2)		974 (0,20)	978 (0,14)		
	ν_{19} Ring def.	771*	w	774* (1)	d [liq]	769 (1,9)	771 (2,3)		
	ν_{20} Ring def.	604	m	604 (1)	d	607 (4,5)	664 (0,4)		

Table 23[†]
Continued

Description		Reassignments ^{a,b}				Calculated ^c (DFT-B3LYP/cc-pVTZ)			
		IR		Raman		C_I		C_S	
A'', A	ν_{21} α -CH ₂ antisym. str.	2941	s	2941 (20)	[sol]	2920	(17,74)	2913	(18,90)
	ν_{22} α -CD ₂ antisym. str.	2200	s	2194 (10)	d	2191	(16,53)	2187	(15,51)
	ν_{23} β -CH ₂ antisym. str.	2964	s	2969 (30)		2969	(36,84)	2971	(33,72)
	ν_{24} α -CH ₂ twist	1163*	vw	1160* (1)	d	1166	(1,15)	1162	(0,14)
	ν_{25} α -CD ₂ twist	872*	s (c-type)	875* (4)	d	875	(3,24)	878	(3,11)
	ν_{26} β -CH ₂ twist	1226*	m [sol]	1211* (1)	d	1229	(0,15)	1240	(0,19)
	ν_{27} α -CH ₂ rock	1035*	w (c-type)	1045* (1)	d	1042	(2,4)	1037	(1,3)
	ν_{28} CH out-of-plane bend	735*	w	726* (1)	?	736	(3,4)	729	(1,3)
	ν_{29} α -CD ₂ rock	700*	m			706	(2,2)	669	(0,1)
	ν_{30} β -CH ₂ rock	858*	m	860* (3)	?	849	(1,8)	844	(0,2)
	ν_{31} CD out-of-plane bend	502*	s (c-type)	500* (1)	d	506	(23,8)	514	(26,12)
	ν_{32} Ring twist	337*	w	338* (2)	d	338	(0,6)	327	(0,7)
	ν_{33} Ring puckering	120.0				120	(0,2)	t^d	

[†] See footnotes for Table 20.

list the calculated (scaled) vibrational frequencies and infrared and Raman intensities and compare these to previously reported experimental results [37]. Table 24 compares the experimental and calculated ring-puckering (ν_{33}) and ring-twisting (ν_{17}) frequencies for the d_0 , d_1 , d_4 , and d_8 isotopes utilizing three different basis sets. The scaling factors used are 0.961, 0.973, and 0.985 for the regions where $\nu > 2800 \text{ cm}^{-1}$, $2800 > \nu > 1800 \text{ cm}^{-1}$, and $\nu < 1800 \text{ cm}^{-1}$, respectively. Although these vibrations are slightly anharmonic, the agreement is very good. Tables 20 to 23 show that most of the previous assignments in Ref. [37] were made correctly. However, the DFT calculations do allow several of the less clear assignments to be reassigned. It is highly satisfactory to see how well the computations do in predicting the experimental values. In order to provide a bit more insight into the cyclopentene isotopomer vibrations, Table 25 shows the experimental and calculated frequencies of the nine ring vibrations of these molecules. Fig. 36 shows how frequencies of these specific modes change for the different isotopomers.

VIBRATIONAL REASSIGNMENTS

Several vibrational reassignments in cyclopentene and its isotopomers were made based on the calculated frequencies and the original data from the dissertation of J. R. Villarreal [98], and the reassigned values are shown in Tables 20 to 23. The original definitions of the vibrational modes used by Villarreal *et al.* [37] were retained in this work for easier comparison. Scaled vibrational frequencies, infrared and Raman intensities, and depolarization ratios from the triple- ζ calculations were all used to attain better reassignments for the four molecules.

Table 24

Experimental and calculated frequencies of the ring-puckering and ring-twisting vibrations for cyclopentene and its isotopomers



	Experimental				Calculated (DFT-B3LYP)					
	ν_{33}		ν_{17}^e		6-31+G(d)		6-311++G(d,p)		cc-pVTZ	
	IR	Raman	IR	Raman	ν_{33}	ν_{17}	ν_{33}	ν_{17}	ν_{33}	ν_{17}
d_0	127 ^a	128.5 ^d		390	140	384	135	385	130	387
d_1	126 ^b		369	369	142	370	134	370	129	372
d_4	120 ^c		337	338	132	338	128	337	120	338
d_8	108 ^c			317	111	319	109	318	103	320

^aRef. [10].




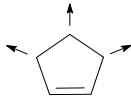
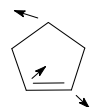
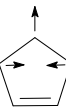
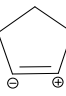
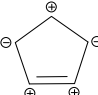
^bRef. [35].

^cRef. [36].

^dRef. [30].

^eRef. [37].

Table 25
Frequencies shifts (cm^{-1}) in ring fundamentals of cyclopentene and its isotopomers

Ring mode ^a			Experimental IR ^b				Calculated ^c B3LYP/6-311++G(d,p)			
			d_0	d_1	d_4	d_8	d_0	d_1	d_4	d_8
$A_1(A')$	$\nu_4 (\nu_6)$	C=C str.	1623	1600	1560	1580	1672 (1682)	1650 (1660)	1626 (1636)	1622 (1633)
$B_1(A')$	$\nu_{24} (\nu_{14})$		1037	1033	1027	1024	1034 (1038)	988 (984)	1122 (1187)	1146 (1136)
$A_1(A')$	$\nu_9 (\nu_{18})$		962	750	800	750	972 (976)	963 (968)	992 (998)	1170 (1171)
$B_1(A')$	$\nu_{25} (\nu_{16})$		933	966	872	724	916 (908)	1039 (1043)	1173 (1120)	1214 (1218)
$A_1(A')$	$\nu_{10} (\nu_{17})$		900	893	910	878	902 (892)	903 (893)	918 (911)	886 (880)
$B_1(A')$	$\nu_{26} (\nu_{19})$		695	698	715	709	783 (788)	759 (762)	782 (784)	769 (773)
$A_1(A')$	$\nu_{11} (\nu_{20})$		608	600	604	574	616 (702)	650 (693)	615 (674)	695 (655)
$A_2(A'')$	$\nu_{17} (\nu_{32})$		390	369	337	317	392 (377)	377 (362)	344 (329)	324 (311)
$B_2(A'')$	$\nu_{33} (\nu_{33})$		127.1	126.0	120.0	108.2	133	131	122	105

^aWavenumbers in parentheses refer to descriptions of the d_1 and d_4 isotopes.

^bAs assigned in Ref. [37]

^cFrequencies in parentheses are for the planar structure. Ring puckering frequencies are those calculated with the cc-pVTZ basis set.

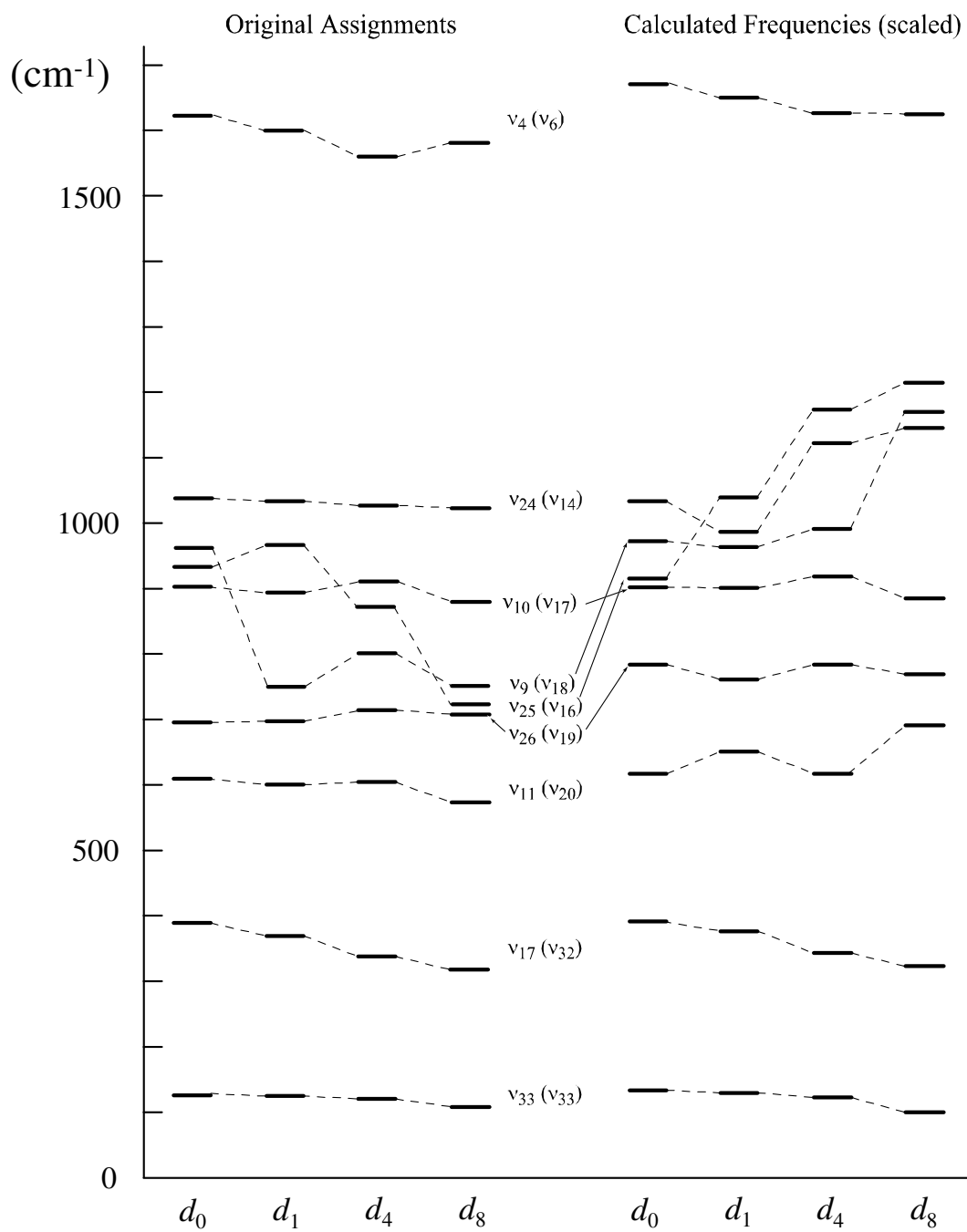


Fig. 36. Correlation diagrams for the ring modes in cyclopentene and its isotopomers as determined from the original assignments and from DFT-B3LYP/cc-pVTZ calculations.

In the case of cyclopentene- d_0 most of the original assignments were shown to be reliable but a few were reassigned. For example, the medium-intensity band at 593 cm^{-1} in the IR spectrum was reassigned to ν_{11} (ring deformation). Calculations showed such a vibration considerably changes its intensity as the molecule changes from the planar to the puckered structure (Table 20). The ν_{11} vibration was also observed to be partially depolarized, and this was confirmed by the depolarization ratio value (0.7) from the DFT calculation. One interesting result from the calculations is that the vapor-phase c-type bands originally observed in the cyclopentene infrared spectrum [37,98] were confirmed to be of B_2 (A'') symmetry, and several were reassigned based on the frequencies and infrared band intensities calculated in this work as shown in Table 20. It was shown from the calculation that when the molecule changes its conformation from the planar C_{2v} structure to the puckered C_s structure, some of the A_2 vibrations, such as ν_{12} and ν_{16} , would become infrared active. Therefore, some weak and medium-intensity IR bands were reassigned to some of the A_2 -symmetry vibrations.

As can be seen from Table 21, more reassignments were made in the case of cyclopentene- d_8 as compared to the d_0 molecule. DFT frequency calculations predicted strong coupling in the vibrational spectra of cyclopentene- d_8 which led to unexpected frequency changes due to isotope shifts. Fig. 36 shows the correlation diagram of the ring modes in the d_8 molecule. The diagram shows the changes of frequencies of the ring modes as a result of the coupling with other CH_2 and CD_2 modes, such as the case for ν_9 and ν_{25} . For more clarification, Figs. 37 and 38 were also done based on the reassignments made in this work to compare the changes in frequencies for the CH_2

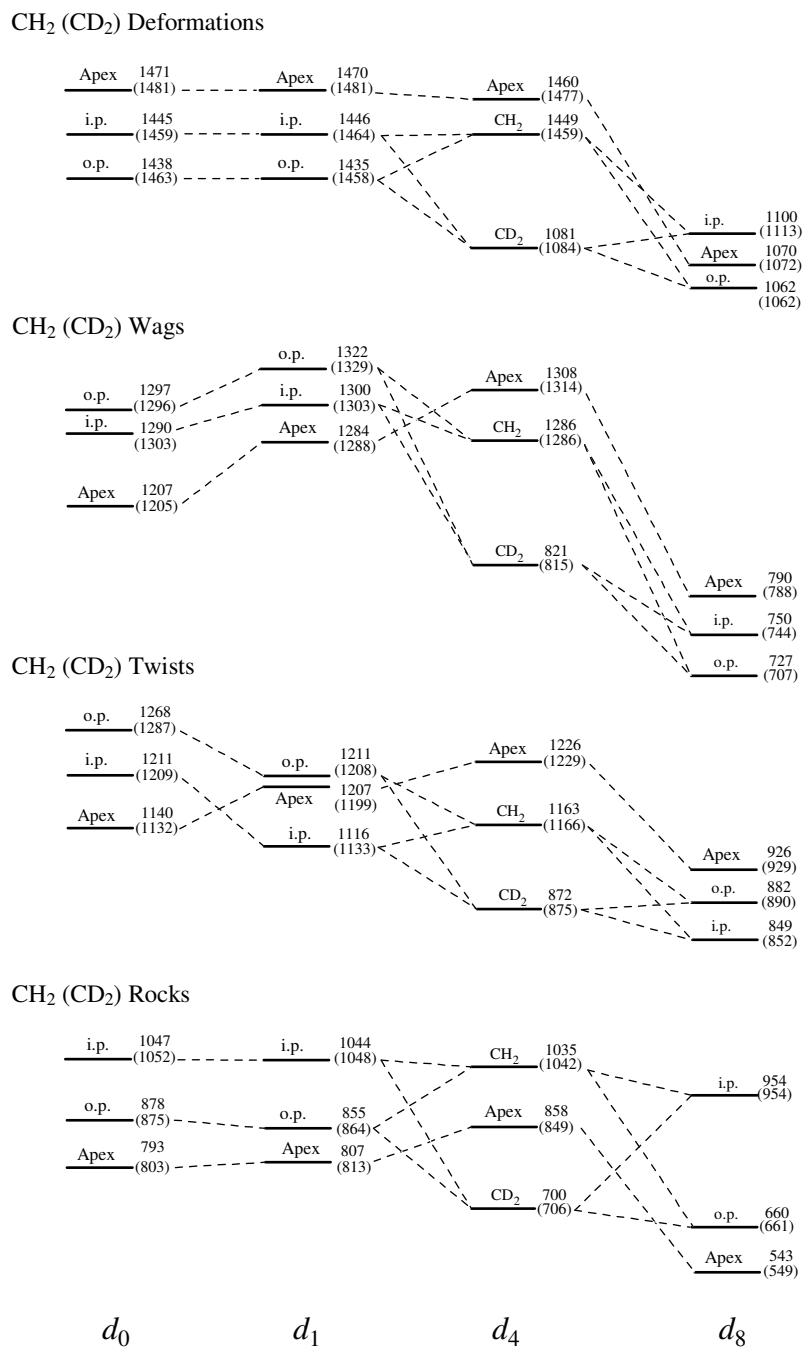
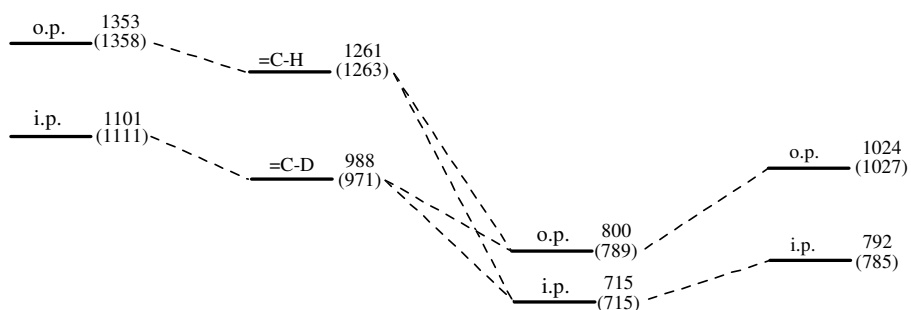


Fig. 37. Reassigned vibrational frequencies of the CH₂ (CD₂) bending motions for various isotopic structures of cyclopentene. Frequencies from DFT-B3LYP/cc-pVTZ calculations are given in parentheses.

=C-H (=C-D) In-plane bends



=C-H (=C-D) Out-of-plane bends

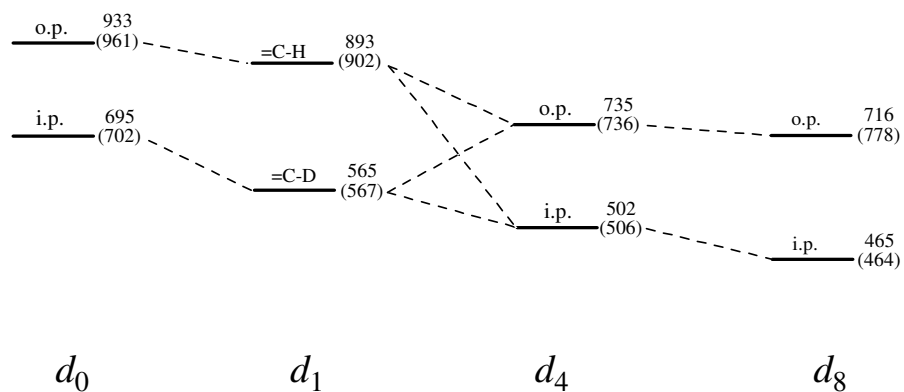


Fig. 38. Reassigned vibrational frequencies of the =C-H (=C-D) bending modes for cyclopentene and its isotopomers. Frequencies from DFT-B3LYP/cc-pVTZ calculations are given in parentheses.

(CD₂) and =C-H (=C-D) motions. While the out-of-plane =C-H (or =C-D) bending vibrations do not show any evidence of coupling with other vibrations in cyclopentene and its isotopomers, the in-plane =C-D bending for *d*₄ is expected to couple with other vibrations causing their frequencies to shift to lower wavenumbers.

Tables 22 and 23 show the reassignments for the other two less symmetric isotopomers, cyclopentene-1-*d*₁ and cyclopentene-1,2,3,3-*d*₄. Most of the reassignments made were related to the CH₂ bending vibrations below 1300 cm⁻¹. Calculated frequencies of the in-plane and out-of-plane CD bendings agree very well with the experiment, and this gave us confidence in the DFT calculated frequencies in predicting frequency changes due to isotopic shifts. In the case of the *d*₄ molecule, quite a large number of reassignments had to be made from the original work of Villarreal [37] as shown in Table 23.

CONCLUSION

The calculations carried out here demonstrated how well density functional theory calculations can reproduce vibrational frequencies of organic molecules such as cyclopentene. The DFT calculations also predict the shifts in frequency due to isotopic substitutions in very good agreement with the experiment. DFT calculations have also allowed a more definitive set of assignments to be made for cyclopentene and its isotopomers. The triple zeta *ab initio* calculation, when a minimal amount of electron correlation is included by using the second order Møller-Plesset perturbation theory, was

also shown to do an excellent job of predicting the barrier to inversion and the dihedral angles.

CHAPTER IX
**MOLECULAR STRUCTURES, VIBRATIONAL SPECTRA, RING-
PUCKERING POTENTIAL ENERGY FUNCTIONS, AND *AB*
INITIO AND DFT STUDIES OF SILACYCLOBUTANES**

INTRODUCTION

In 1967 J. Laane reported the first preparation of silacyclobutane and some of its derivatives [38]. Later, the far-infrared studies of silacyclobutane and silacyclobutane-1,1- d_2 were reported [13]. Full vibrational assignments of the infrared and Raman spectra and normal coordinate analyses for silacyclobutane and its 1,1- d_2 as well as 1,1-difluorosilacyclobutane and 1,1-dichlorosilacyclobutane were reported [39]. These spectroscopic studies concluded that the ring is puckered due to the $\text{CH}_2\text{-CH}_2$ and $\text{CH}_2\text{-SiH}_2$ torsional interactions, and a dihedral angle of approximately 36° with a barrier height of $440 \pm 3 \text{ cm}^{-1}$ was determined from a one-dimensional analysis [13].

The structures of silacyclobutane and its 1,1-difluoro and 1,1-dichloro derivatives have also been investigated by means of other experimental techniques [99-106]. A microwave study on silacyclobutane using several assumed geometrical parameters was carried out, from which a puckering angle of 28° and a barrier of 441 cm^{-1} were determined [101]. Electron diffraction (ED) analyses of silacyclobutane [102,106] gave

slightly smaller puckering angles as compared to the far-IR results [13]. The first electron-diffraction study in 1975 reported a puckering angle of 33.6° [102]. A second gas-phase ED study combined with detailed *ab initio* calculations of the structure and puckering potential function of silacyclobutane was recently published [106]. The puckering angle (33.5°) reported is also close to the far-IR value (36°), but gave a considerably lower barrier (286 cm^{-1}) as compared to the far-IR value (440 cm^{-1}) [13]. Since ED studies average over many vibrational states, they do not typically yield reliable barrier values.

1,1-Difluorosilacyclobutane and 1,1-dichlorosilacyclobutane have also been studied by gas-phase electron diffraction experiments [103-105]. A dihedral angle of 25° and a barrier height of 418 cm^{-1} , with a large uncertainty, were determined for 1,1-difluorosilacyclobutane [104]. Other gas-phase ED studies showed that the puckering angle and the inversion barrier in 1,1-dichlorosilacyclobutane are slightly higher than the values for the difluoro compound but are lower as compared to silacyclobutane [103,105].

In addition, several *ab initio* investigations of the structures, energetic behavior, and vibrational frequencies of silacyclobutane and its derivatives can be found in the literature [104-115]. A few molecular mechanics MM2 [97,116] and MM3 [117] force field studies on the structure of silacyclobutane have also been carried out. The MM2 method predicted the barrier to inversion between the two planar forms to be 462 cm^{-1} [116] with a puckering angle of 32° [97], while the extended MM3 method predicted a barrier of 395 cm^{-1} [117].

The vibrational frequencies of silacyclobutane were computed using the restricted Hartree-Fock self-consistent field (HF-SCF) calculations [108] and density functional theory (DFT-B3LYP) utilizing the 6-311G(d,p) basis set [113]. In these two studies [108,113], the vibrational assignments were made based on the unscaled frequencies and the infrared intensities with comparison to the previously reported vibrational spectral data [39]. In the theoretical work on 1,3-disilacyclobutane, E. T. Seidl *et al.* [108] made a few vibrational reassignments on the basis of the HF calculated frequencies and the observed vibrational spectra [118]. In another recent work, the calculated frequencies from DFT-B3LYP treatment have been more thoroughly used to reassign the infrared and Raman spectra of 1,3-disilacyclobutane and its d_4 isotopomer [119].

While the results of the present study were being completed, a combined study of a gas-phase ED experiment and *ab initio* calculations on the structure of silacyclobutane has been very recently published by Navikov, Dakkouri and Vilkov [106] (abbreviated as NDV herein). In the NDV work, Hartree-Fock, second-order Møller-Plesset and DFT-B3LYP theories were implemented using different basis sets. It can clearly be seen from that work that the effect of including electron correlations yields better predictions of structures and barriers. Comparisons between the present work and NDV paper [106] are presented later in this chapter.

AB INITIO AND DFT CALCULATIONS

Silacyclobutane has C_s symmetry for its puckered structure but closely follows C_{2v} planar structure selection rules since it is a non-rigid molecule. The structures, the inversion barriers, and the vibrational frequencies of silacyclobutane, 1,1-difluorosilacyclobutane, and 1,1-dichlorosilacyclobutane were studied in this work using high-level density functional theory (DFT) with the B3LYP hybrid functional and second-order Møller-Plesset (MP2) calculations using the Gaussian 03 program [67]. The vibrational frequencies of silacyclobutane-1,1- d_2 were also calculated. Different basis sets including the cc-pVTZ (triple- ζ) were used to compute the geometry of the planar and puckered structures of silacyclobutane. The triple- ζ basis set was used to calculate the structures of the dihalo derivatives. Barriers to interconversion in silacyclobutane and the difluoro and dichloro derivatives were calculated and were zero-point corrected. The vibrational frequencies, infrared and Raman peak intensities, and depolarization ratios for the four molecules were calculated using the DFT-B3LYP/cc-pVTZ level of theory and by implementing the appropriate scaling factors.

MOLECULAR STRUCTURES

Fig. 39 shows the structure, atom labeling, and the puckering angle definition for these molecules, where X can be H, F, or Cl for silacyclobutane, 1,1-difluorosilacyclobutane and 1,1-dichlorosilacyclobutane, respectively. The bond lengths, bond angles, and puckering angles for the puckered C_s and planar C_{2v} structures of

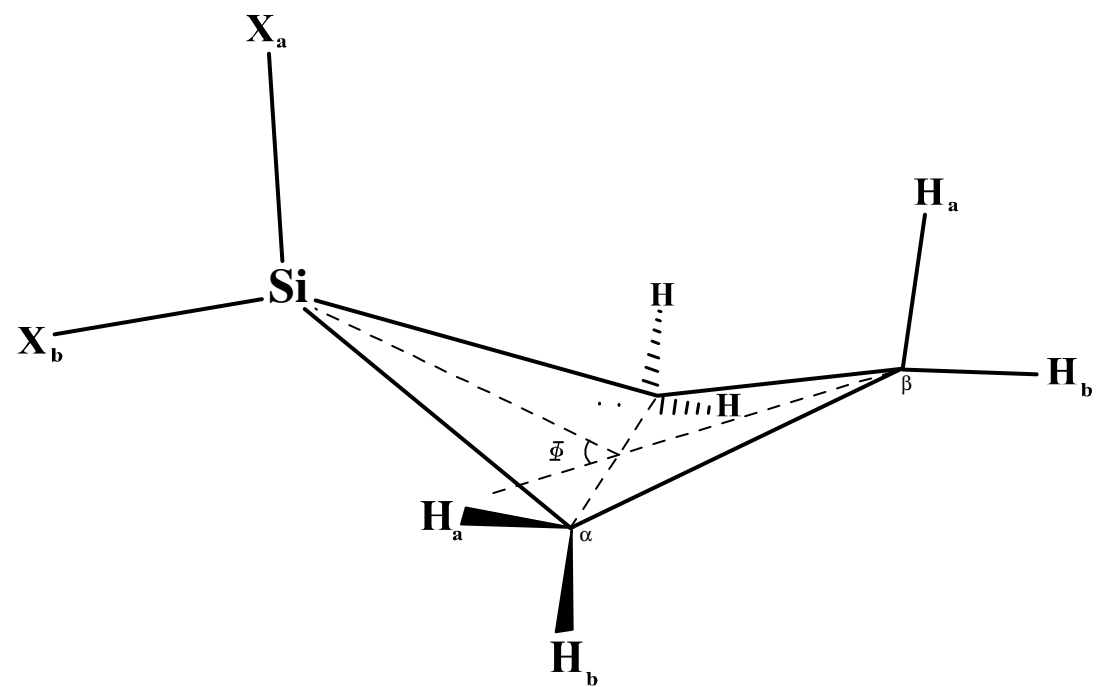


Fig. 39. Structure, puckering angle and atom labels for silacyclobutane and its derivatives. (X could be H, D, F, or Cl).

silacyclobutane and its difluoro and dichloro derivatives are given in Tables 26-28 and are compared to observed structures from different experimental techniques. The calculated C-H bond distances for the dihalo derivatives were predicted to be shorter as compared to silacyclobutane, which indicates stronger C-H bonds in the case of the difluoro and dichloro molecules. This result is consistent with the observed vibrational frequencies for these molecules in the C-H stretching region [39].

In the case of silacyclobutane, different basis sets at the MP2 and DFT theories were used. Table 29 shows the calculated inversion barrier and puckering angle in silacyclobutane. It can be noted that a relatively small basis set such as the 6-31G gave a better prediction of the barrier to planarity (489 cm^{-1}) as compared to larger basis sets. Implementing smaller basis sets means there are more restrictions in describing the molecular orbitals of the system because of the lower number of basis functions employed in the calculations. In addition, the 6-31G includes neither diffuse functions nor polarization functions which are responsible for giving more flexibility to the description of the orbitals involved [42-45]. However, the calculated puckering angle from the triple- ζ basis set (34.5°) was the closest to the experimental value (Table 29). The barriers and puckering angles calculated by the Hartree-Fock and DFT methods were found to be considerably lower than the experimental values for the silacyclobutane molecule and its difluoro and dichloro derivatives (Tables 29 and 30). The underestimation of the inversion barriers and dihedral angles by the DFT method for different cyclic molecules as compared to experimental values, including the ones being studied in this work, has been noted in several cases [88-90,120].

Table 26

Structural parameters of silacyclobutane from different experiments and from *ab initio* calculations

	MP2 ^a		DFT-B3LYP ^a		Experimental		
	6-311++G(2d,p)	cc-pVTZ	6-311++G(2d,p)	cc-pVTZ	Far-IR ^b	MW ^c	ED (NVD work) ^d
Bond lengths (Å)							
Si—C	1.892 (1.894)	1.893 (1.895)	1.860 (1.897)	1.900 (1.895)	1.870	1.91	1.895(2)
C—C	1.561 (1.569)	1.558 (1.565)	1.565 (1.571)	1.563 (1.565)	1.550		1.571(3)
C _α —H _a	1.089 (1.090)	1.086 (1.088)	1.089 (1.090)	1.087 (1.088)			
C _α —H _b	1.093 (1.090)	1.090 (1.088)	1.093 (1.090)	1.091 (1.088)			
C _β —H _a	1.094 (1.091)	1.091 (1.088)	1.092 (1.091)	1.091 (1.088)	1.090		1.100(3)
C _β —H _b	1.092 (1.091)	1.089 (1.088)	1.093 (1.091)	1.091 (1.088)			
Si—H _a	1.478 (1.479)	1.483 (1.483)	1.485 (1.486)	1.488 (1.483)			1.467(96)
Si—H _b	1.479 (1.479)	1.483 (1.483)	1.486 (1.486)	1.489 (1.483)	1.480		1.468(96)
Bond angles (°)							
∠CSiC	78.3 (80.5)	78.2 (80.5)	79.0 (80.5)	78.8 (80.5)	80.2		77.2(9)
∠SiCC	86.0 (88.4)	85.9 (88.3)	86.9 (88.5)	86.9 (88.3)	88.9		87.9(12)
∠CCC	99.8 (102.6)	100.0 (102.9)	100.8 (102.6)	100.9 (102.9)	102		97.0(15)
∠HSiH	109.0 (108.0)	108.6 (107.6)	108.2 (107.5)	108.0 (107.6)			108.3
∠HC _α H	109.1 (108.1)	109.1 (108.0)	108.4 (107.8)	108.4 (108.0)	114		
∠HC _β H	107.7 (107.3)	107.8 (107.3)	107.3 (107.1)	107.3 (107.3)	111		107.7
∠C _β C _α H _a	116.5 (113.5)	116.6 (113.6)	116.0 (113.7)	116.0 (113.6)	112.9		118.4(24)
∠C _β C _α H _b	110.1 (113.5)	110.1 (113.6)	111.2 (113.7)	111.3 (113.6)			112.3(24)
∠C _α C _β H _a	109.5 (111.8)	109.5 (111.7)	109.4 (111.8)	109.8 (111.7)	110.9		
∠C _α C _β H _b	115.1 (111.8)	114.9 (111.7)	114.5 (111.8)	114.4 (111.7)			
∠SiCH _a	122.7 (116.2)	122.6 (116.2)	121.3 (116.2)	121.3 (116.2)			123.5(16)
∠SiCH _b	110.5 (116.2)	110.5 (116.2)	111.6 (116.2)	111.6 (116.2)	112.9		111.9(16)
∠CSiH _a	112.2 (116.6)	112.3 (116.8)	113.7 (116.8)	113.8 (116.8)	114.3		
∠CSiH _b	121.1 (116.6)	121.4 (116.8)	120.0 (116.8)	120.1 (116.8)			
Φ (°)	34.3 (0.0)	34.5 (0.0)	27.4 (0.0)	27.6 (0.0)	35.9 ± 2	28	33.5 ± 2.7

^a Calculated values in parentheses are for the planar structure.^b Ref. [13].^c Ref. [101].^d Ref. [106].

Table 27
Structural parameters of 1,1-difluorosilacyclobutane

	MP2/cc-pVTZ ^a	DFT-B3LYP/ cc-pVTZ ^a	ED ^b
Bond lengths (Å)			
Si—C	1.859 (1.860)	1.865 (1.865)	1.836(3)
C—C	1.567 (1.572)	1.574 (1.577)	1.574(8)
C _α —H _a	1.085 (1.087)	1.087 (1.088)	
C _α —H _b	1.089 (1.087)	1.090 (1.088)	1.099(6)
C _β —H _a	1.088 (1.086)	1.089 (1.088)	
C _β —H _b	1.087 (1.086)	1.088 (1.088)	
Si—F _a	1.601 (1.600)	1.607 (1.606)	
Si—F _b	1.597 (1.600)	1.605 (1.606)	1.574(3)
Bond angles (°)			
∠CSiC	81.7 (83.2)	82.3 (83.1)	82.7(6)
∠SiCC	84.9 (86.6)	86.0 (86.8)	86.8(8)
∠CCC	101.7 (103.6)	102.5 (103.3)	100.6(8)
∠FSiF	105.6 (105.5)	105.2 (105.2)	106.9(5)
∠HC _α H	109.3 (108.6)	108.5 (108.3)	111.3(34)
∠HC _β H	108.4 (108.1)	108.0 (107.8)	111.3(34)
∠C _β C _α H _a	116.0 (113.5)	115.3 (113.7)	
∠C _β C _α H _b	110.6 (113.5)	112.0 (113.7)	
∠C _α C _β H _a	109.7 (111.3)	110.2 (111.4)	
∠C _α C _β H _b	113.6 (111.3)	113.0 (111.4)	
∠SiCH _a	122.1 (116.6)	120.4 (116.6)	
∠SiCH _b	111.8 (116.6)	113.2 (116.6)	
∠CSiF _a	113.6 (116.9)	115.1 (117.0)	
∠CSiF _b	120.7 (116.9)	119.3 (117.0)	
Φ (°)	28.7 (0.0)	19.4 (0.0)	25(2)

^a Calculated values in parentheses are for the planar structure.

^b Ref. [104].

Table 28
Structural parameters of 1,1-dichlorosilacyclobutane

	MP2/cc-pVTZ ^a	DFT-B3LYP/ cc-pVTZ ^a	ED		
			Vilkov ^b	Cyvin ^c	Novikov ^d
Bond lengths (Å)					
Si—C	1.868 (1.870)	1.877 (1.878)	1.88(2)	1.886(4)	1.860(3)
C—C	1.564 (1.570)	1.569 (1.573)	1.59(3)	1.544(6)	1.557(4)
C _α —H _a	1.085 (1.087)	1.087 (1.088)			
C _α —H _b	1.090 (1.087)	1.090 (1.088)		1.091(7)	1.091(8)
C _β —H _a	1.089 (1.087)	1.089 (1.088)			
C _β —H _b	1.088 (1.087)	1.089 (1.088)			
Si—Cl _a	2.058 (2.057)	2.080 (2.078)			2.043(2)
Si—Cl _b	2.053 (2.057)	2.074 (2.078)	2.05(1)	2.032(2)	2.038(2)
Bond angles (°)					
∠CSiC	80.6 (82.5)	81.1 (82.2)	80(2)	84.0(6)	81.1(10)
∠SiCC	85.1 (87.0)	86.3 (87.2)		79.0(6)	85.7(12)
∠CCC	101.2 (103.5)	102.2 (103.3)		110.7(9)	102.0(15)
∠ClSiCl	107.9 (107.7)	107.5 (107.4)	105(1)	105.1(3)	105.2(8)
∠HC _α H	109.7 (109.0)	108.9 (108.5)			125.7(91)
∠HC _β H	108.4 (108.0)	107.9 (107.8)		111.1(1)	108.0
∠C _β C _α H _a	116.6 (113.9)	116.0 (114.0)			105.3(63)
∠C _β C _α H _b	110.7 (113.9)	112.0 (114.0)			100.9(63)
∠C _α C _β H _a	109.8 (111.3)	110.1 (111.4)			110.0
∠C _α C _β H _b	113.7 (111.3)	113.2 (111.4)			113.4
∠SiCH _a	121.7 (116.0)	120.4 (116.0)			118.9(54)
∠SiCH _b	110.9 (116.0)	111.9 (116.0)			109.7(54)
∠CSiCl _a	112.4 (116.3)	114.2 (116.5)			114.7(4)
∠CSiCl _b	120.8 (116.3)	119.2 (116.5)			120.2(4)
Φ (°)	31.1 (0.0)	22.6 (0.0)	30(5)	31.7(10)	25.9(26)

^a Calculated values in parentheses are for the planar structure.

^b Ref. [99].

^c Ref. [103].

^d Ref. [105].

Table 29

Barriers to planarity and puckering angle for silacyclobutane from different experimental and *ab initio* methods

Method	Puckered (C_s)		Planar (C_{2v})		Barrier (cm^{-1})	Zero-point corrected barrier (cm^{-1})	Puckering angle (deg.)
	E_{tot} (Hart.)	Zero-point correction (Hart.)	E_{tot} (Hart.)	Zero-point correction (Hart.)			
MP2/6-31G	-407.3854310	0.100865	-407.3832035	0.100199	489	343	30.2
MP2/6-31+G(d)	-407.6282517	0.101581	-407.6252320	0.100904	663	514	32.9
MP2/6-311++G(d,p)	-407.7591071	0.100600	-407.7556352	0.099677	762	559	34.2
MP2/6-311++G(2d,p)	-407.7875089	0.100237	-407.7842642	0.099324	712	512	34.3
MP2/6-311+G(df,pd) ^a					786		35.0
MP2/cc-pVTZ	-407.8671832	0.100217	-407.8642028	0.099618	654	523	34.5
B3LYP/6-31G	-408.5441521	0.099544	-408.5436369	0.099252	113	49	22.9
B3LYP/6-31+G(d)	-408.6105168	0.099214	-408.6094226	0.098835	240	157	27.0
B3LYP/6-311++G(d,p)	-408.6663936	0.098595	-408.6652839	0.098213	243	160	27.2
B3LYP/6-311++G(2d,p)	-408.6718241	0.098663	-408.6706503	0.098257	257	169	27.4
B3LYP/6-311++G(df,pd) ^a					276		27.9
B3LYP/cc-pVTZ	-408.6818994	0.098616	-408.6803682	0.098213	336	248	27.7
Far-infrared ^b					440		35.9
Microwave ^c					441		28
Early ED ^d							33.6(21)
Recent ED (NVD work) ^a					286		33.5(18)

^aRef. [106].^bRef. [13].^cRef. [101].^dRef. [102].

Table 30

Barriers to planarity and puckering angles for 1,1-difluorosilacyclobutane and 1,1-dichlorosilacyclobutane from different methods of calculations

Method	Puckered (C_s)		Planar (C_{2v})		Barrier (cm^{-1})	Zero-point corrected barrier (cm^{-1})	Puckering angle (deg.)
	E_{tot} (Hart.)	Zero-point correction (Hart.)	E_{tot} (Hart.)	Zero-point correction (Hart.)			
1,1-Difluoro-1-silacyclobutane							
MP2/6-31G	-605.4296905	0.090779	-605.4284190	-0.090123	279	135	25.2
MP2/6-311++G(d,p)	-606.0734321	0.089729	-606.0718945	0.089014	338	181	28.1
MP2/cc-pVTZ	-606.2981788	0.089689	-606.2968243	0.089182	297	186	28.7
B3LYP/cc-pVTZ	-607.3909500	0.088362	-607.3906877	0.088048	58	-11	19.4
ED ^a					418		25
1,1-Dichloro-1-silacyclobutane							
MP2/6-31G	-1325.3370857	0.088343	-1325.3353188	0.087698	388	246	27.8
MP2/6-311++G(d,p)	-1325.9898424	0.087814	-1325.9867646	0.086892	676	473	30.6
MP2/cc-pVTZ	-1326.2281801	0.087359	-1326.2261154	0.086860	453	344	31.1
B3LYP/cc-pVTZ	-1328.0675080	0.086144	-1328.0670690	0.085832	96	28	22.6
ED (Vilkov) ^b							30(5)
ED (Cyvin) ^c							31.7(10)
ED (Novikov) ^d					199		25.9(26)

^aRef. [104].

^bRef. [99].

^cRef. [103].

^dRef. [105].

The theoretical puckering vibration potential energy functions of the type $V = ax^4 - bx^2$ from the optimized structures and calculated barrier heights of silacyclobutane using different quantum chemical theories were determined and are shown in Figs. 40 and 41 and Table 31. Fig. 40 compares the barriers calculated from the MP2 and DFT theories, and how these barriers compare to the experimental one for such a strained molecule. Fig. 41 shows the effect of different basis sets using MP2 calculations. As has been mentioned above and as can be seen from Fig. 41 and Table 29, the larger the basis set, the better is the predicted puckering angle and the higher is the barrier to planarity as compared to the experimental one.

VIBRATIONAL REASSIGNMENTS

Figs. 42-45 show the experimental vapor-phase infrared spectra reproduced from Refs. [39,121] and the calculated IR spectra for the four molecules. Similarly, Figs. 46-49 compare the experimental frequencies and intensities of the Raman spectra with those computed from the DFT-B3LYP level of theory. Vibrational spectra from the DFT-B3LYP/cc-pVTZ calculations for silacyclobutane, its 1,1- d_2 , the 1,1-difluoro and the 1,1-dichloro derivatives show very good agreement with the experimental ones as can be seen from these figures. Tables 32 to 35 give the detail of the reassigned frequencies carried out in this work for the four molecules. The descriptions of the vibrational fundamentals from the original study [39] were followed here for easier comparison. The vibrational frequencies of both the C_s and C_{2v} structures were calculated. Except for a few cases the frequencies calculated for the two structures in the four molecules are

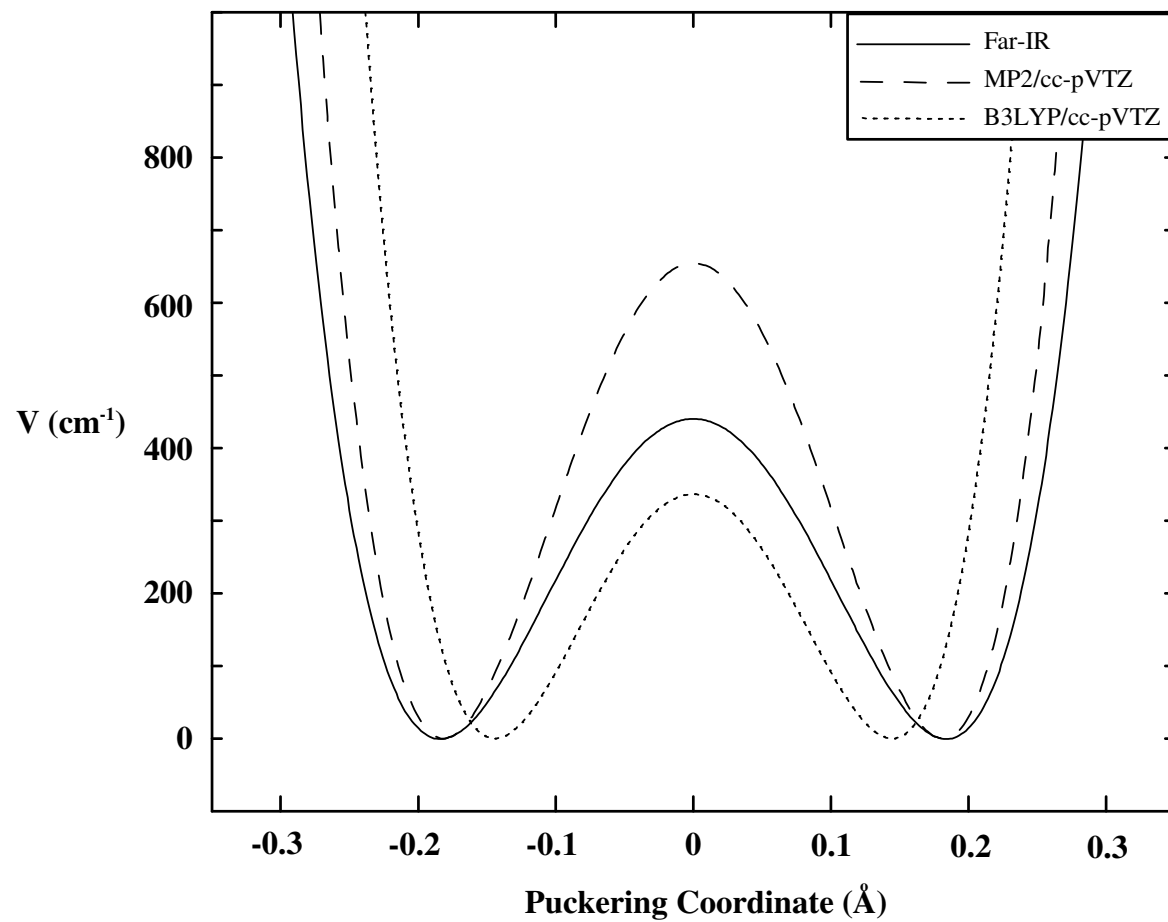


Fig. 40. Puckering-angle potential energy functions for silacyclobutane from MP2/cc-pVTZ and B3LYP/cc-pVTZ levels of theory compared to far-infrared experimental values.

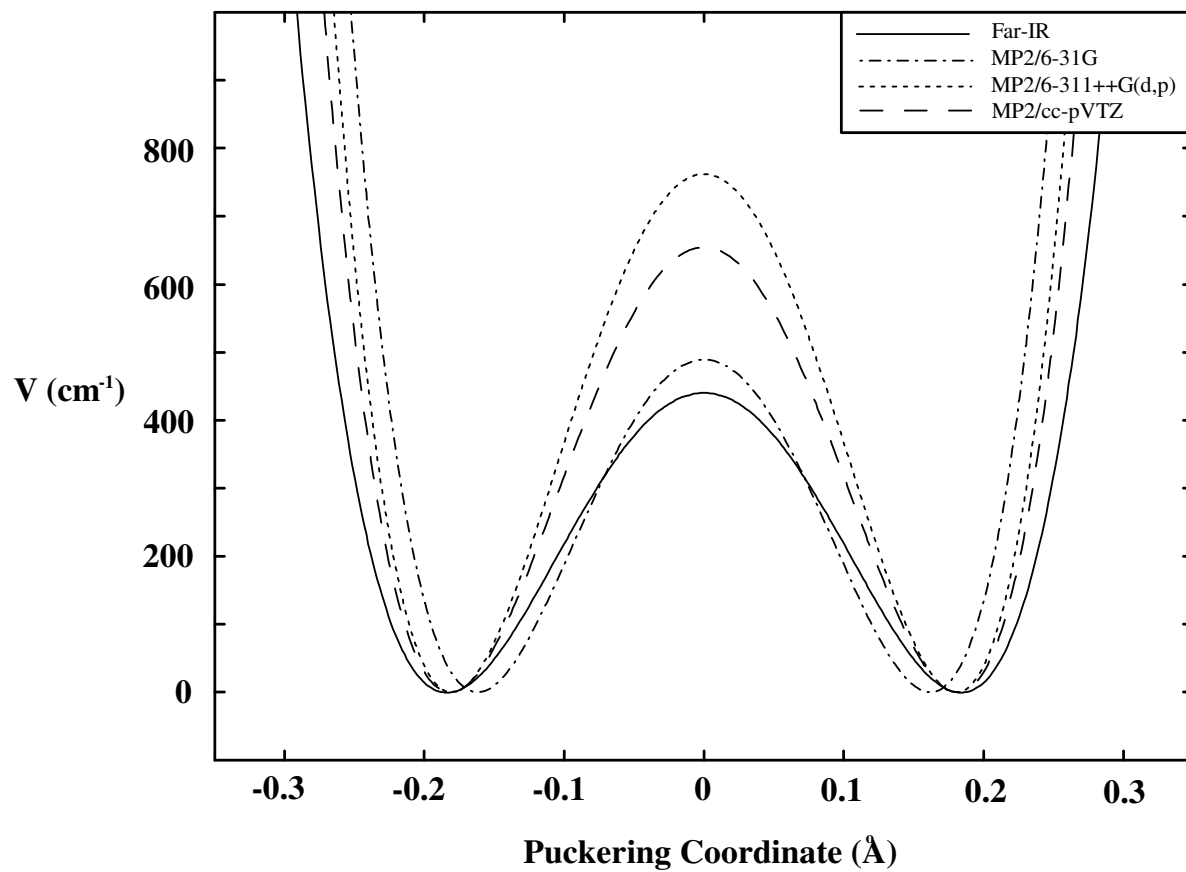


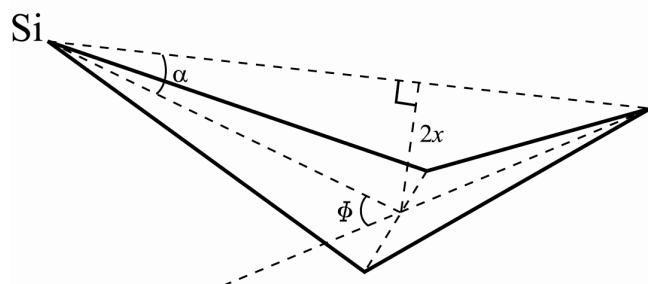
Fig. 41. Effect of basis sets in predicting the puckering barrier and puckering angle in silacyclobutane.

Table 31
Puckering coordinates and theoretical potential energy function parameters based on *ab initio* calculations

Method	Puckering angle		x (Å)	$V(\text{cm}^{-1}) = ax^4 - bx^2$	
	$\angle \Phi$ (deg.)	$\angle \alpha$ (deg.)		a (Å ⁻⁴)	b (Å ⁻²)
MP2/6-31G	30.24	13.89	0.182	3.008×10^5	19.84×10^5
MP2/6-31+G(d)	32.91	11.92	0.162	3.548×10^5	18.63×10^5
MP2/6-311++G(d,p)	34.21	13.23	0.173	3.689×10^5	22.11×10^5
MP2/cc-pVTZ	34.50	13.82	0.181	3.572×10^5	23.32×10^5
B3LYP/cc-pVTZ	27.67	11.13	0.144	3.867×10^5	16.12×10^5
Experimental ^a	36		0.184	3.852×10^5	26.06×10^3

^a Ref [13,97].

^b Definitions of the parameters Φ , α and x are shown below



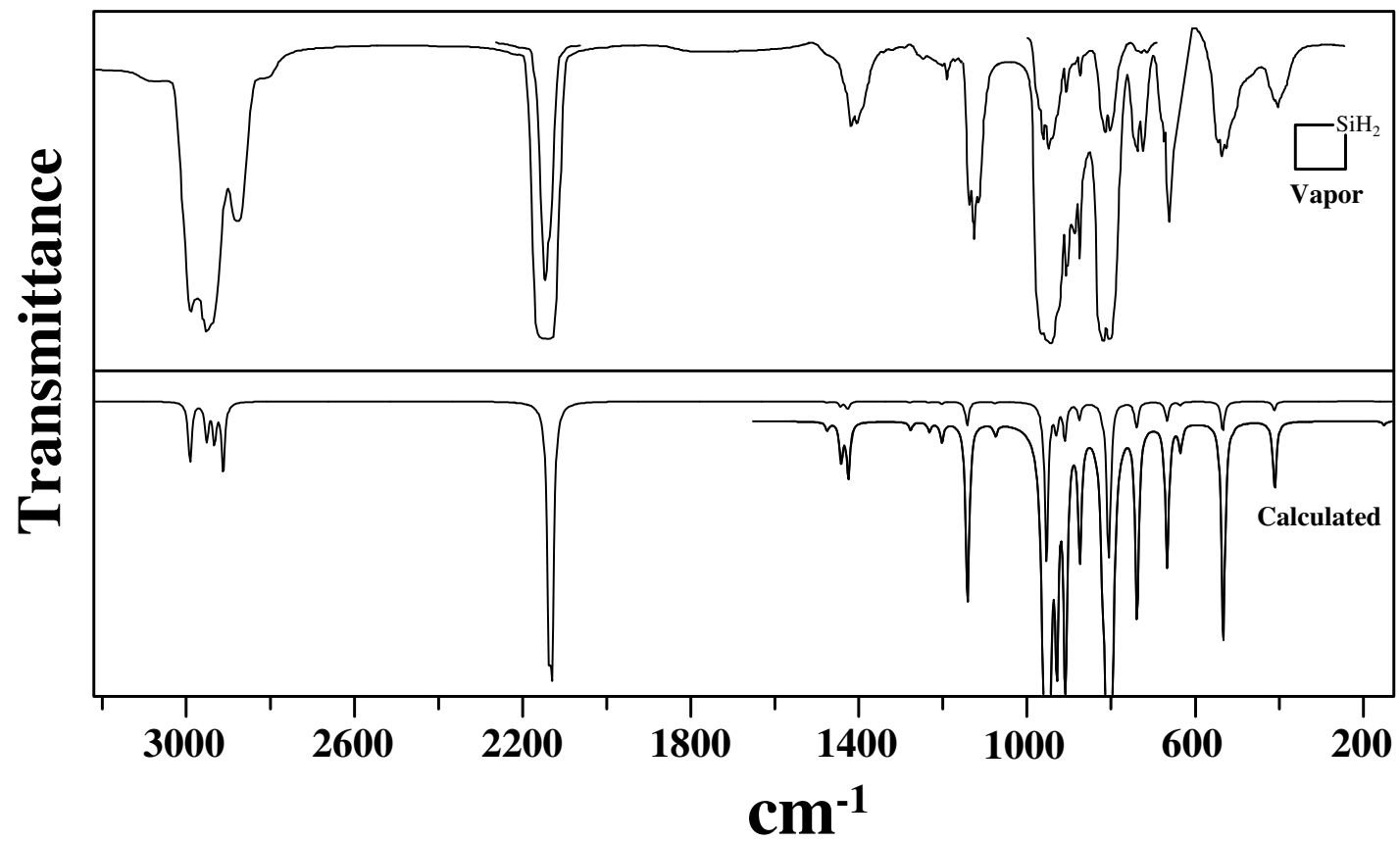


Fig. 42. Vapor-phase (Ref. [121]) and calculated (DFT-B3LYP/cc-pVTZ) infrared spectra of silacyclobutane.

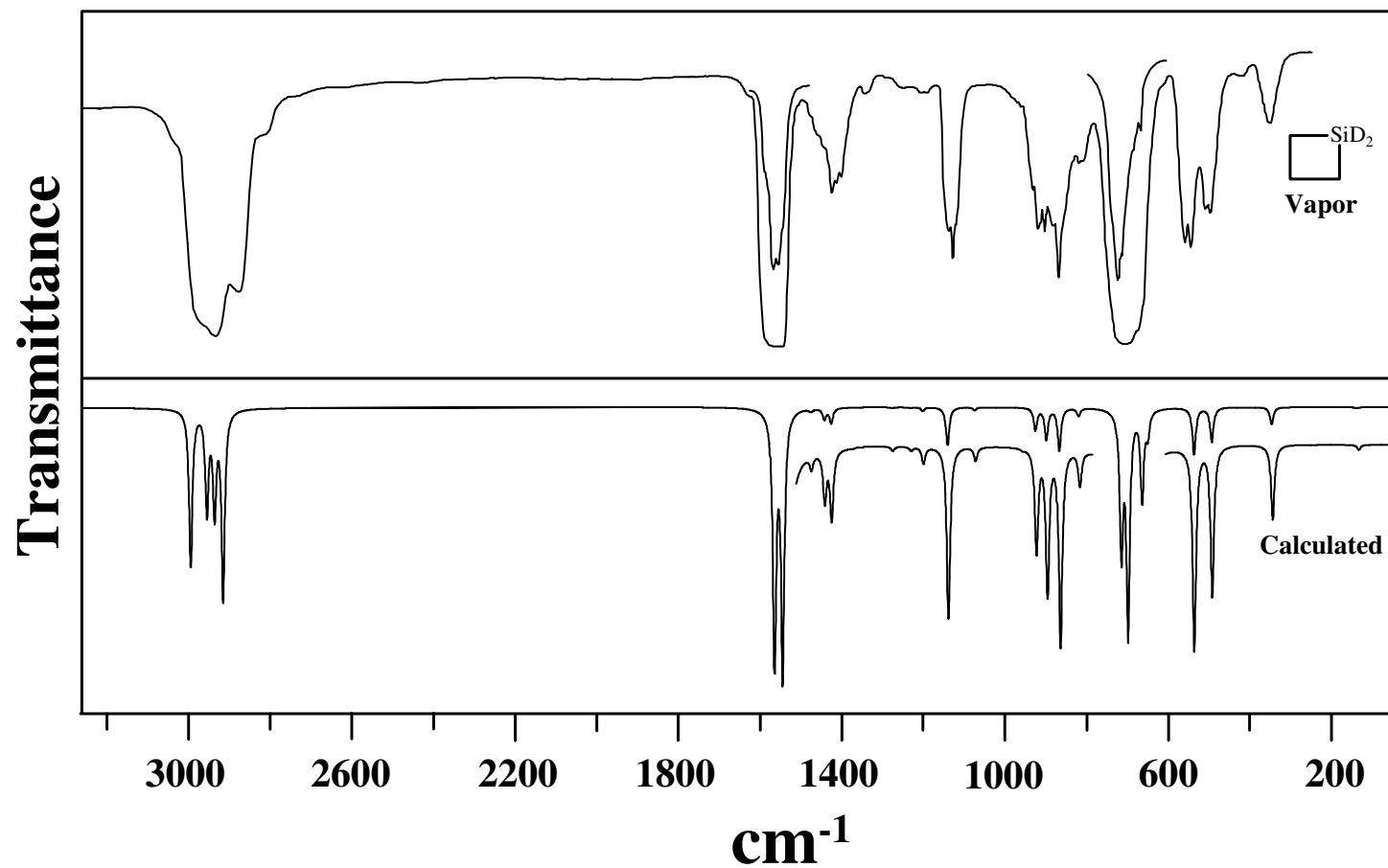


Fig. 43. Vapor-phase (Ref. [121]) and calculated (DFT-B3LYP/cc-pVTZ) infrared spectra of silacyclobutane-1,1-*d*₂.

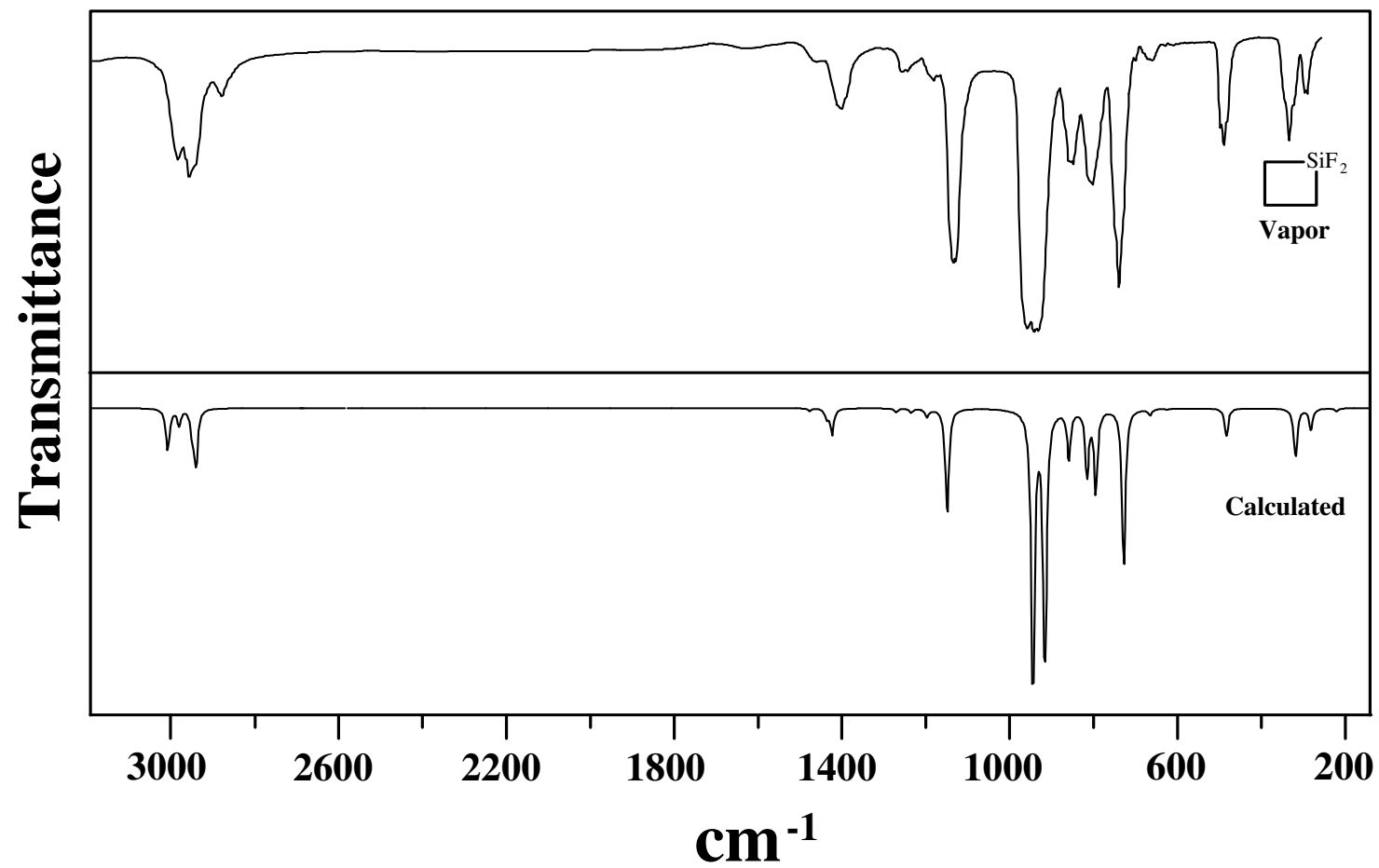


Fig. 44. Vapor-phase (Ref. [121]) and calculated (DFT-B3LYP/cc-pVTZ) infrared spectra of 1,1-difluorosilacyclobutane.

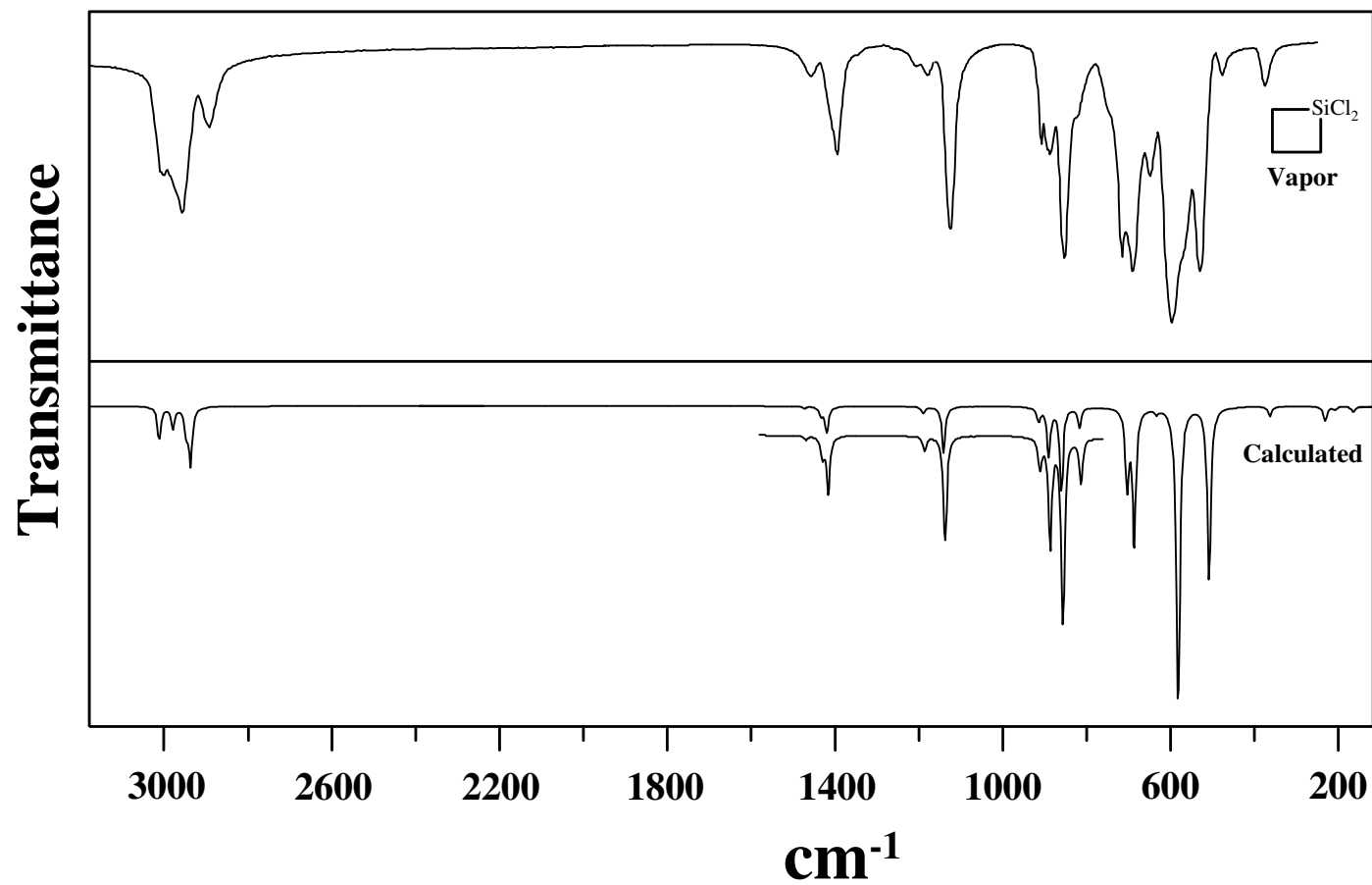


Fig. 45. Vapor-phase (Ref. [121]) and calculated (DFT-B3LYP/cc-pVTZ) infrared spectra of 1,1-dichlorosilacyclobutane.

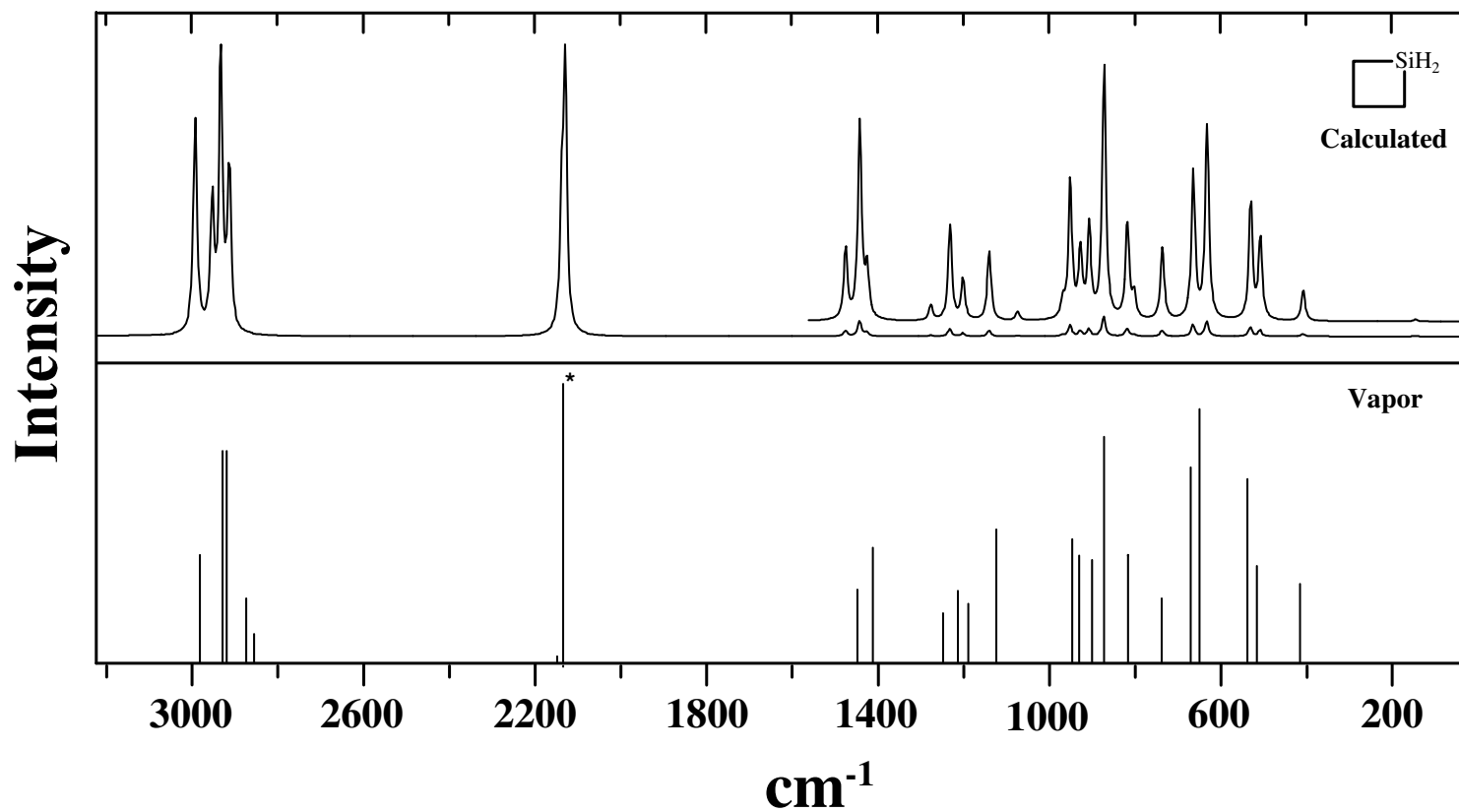


Fig. 46. Calculated (DFT-B3LYP/cc-pVTZ) Raman spectra for silacyclobutane compared with the line spectra of the frequencies and intensities of the vapor-phase Raman spectra reported in Refs. [39,121]. Line marked with (*) indicates a peak with reduced intensity.

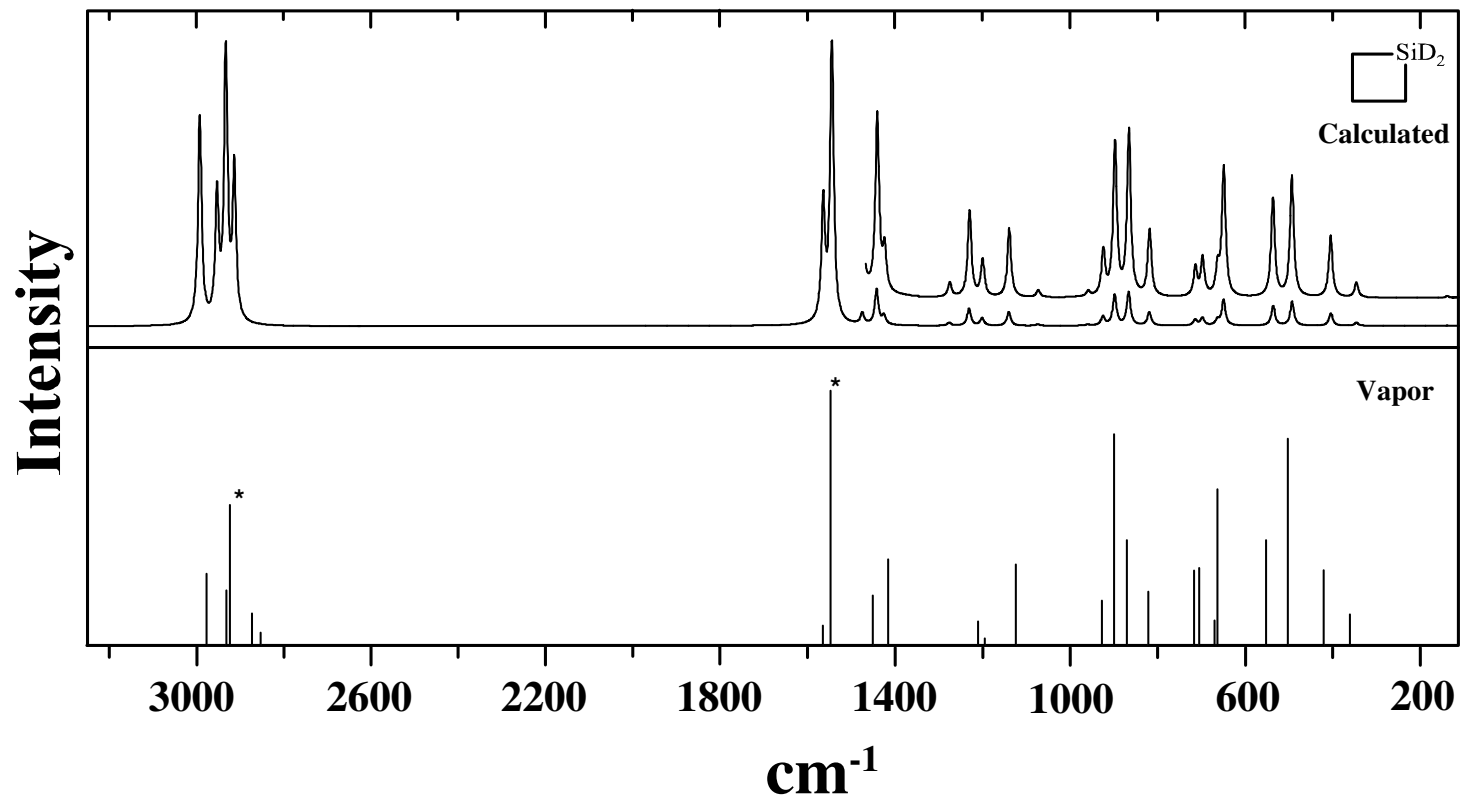


Fig. 47. Calculated (DFT-B3LYP/cc-pVTZ) Raman spectra for silacyclobutane-1,1- d_2 compared with the line spectra of the frequencies and intensities of the vapor-phase Raman spectra reported in Refs. [39,121]. Lines marked with (*) indicate peaks with reduced intensities.

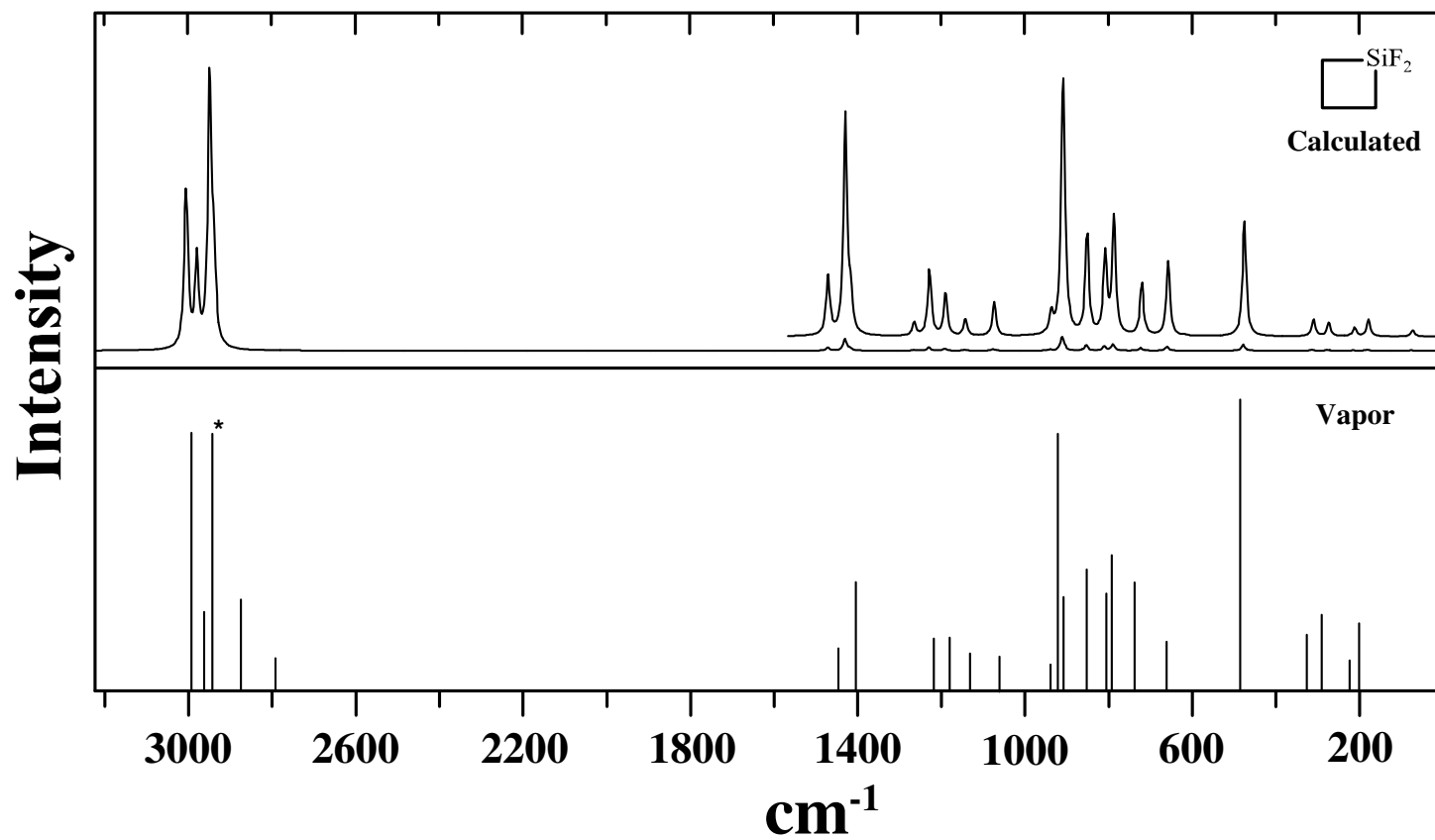


Fig. 48. Calculated (DFT-B3LYP/cc-pVTZ) Raman spectra for 1,1-difluorosilacyclobutane compared with the line spectra of the frequencies and intensities of the vapor-phase Raman spectra reported in Refs. [39,121]. Line marked with (*) indicates a peak with reduced intensity.

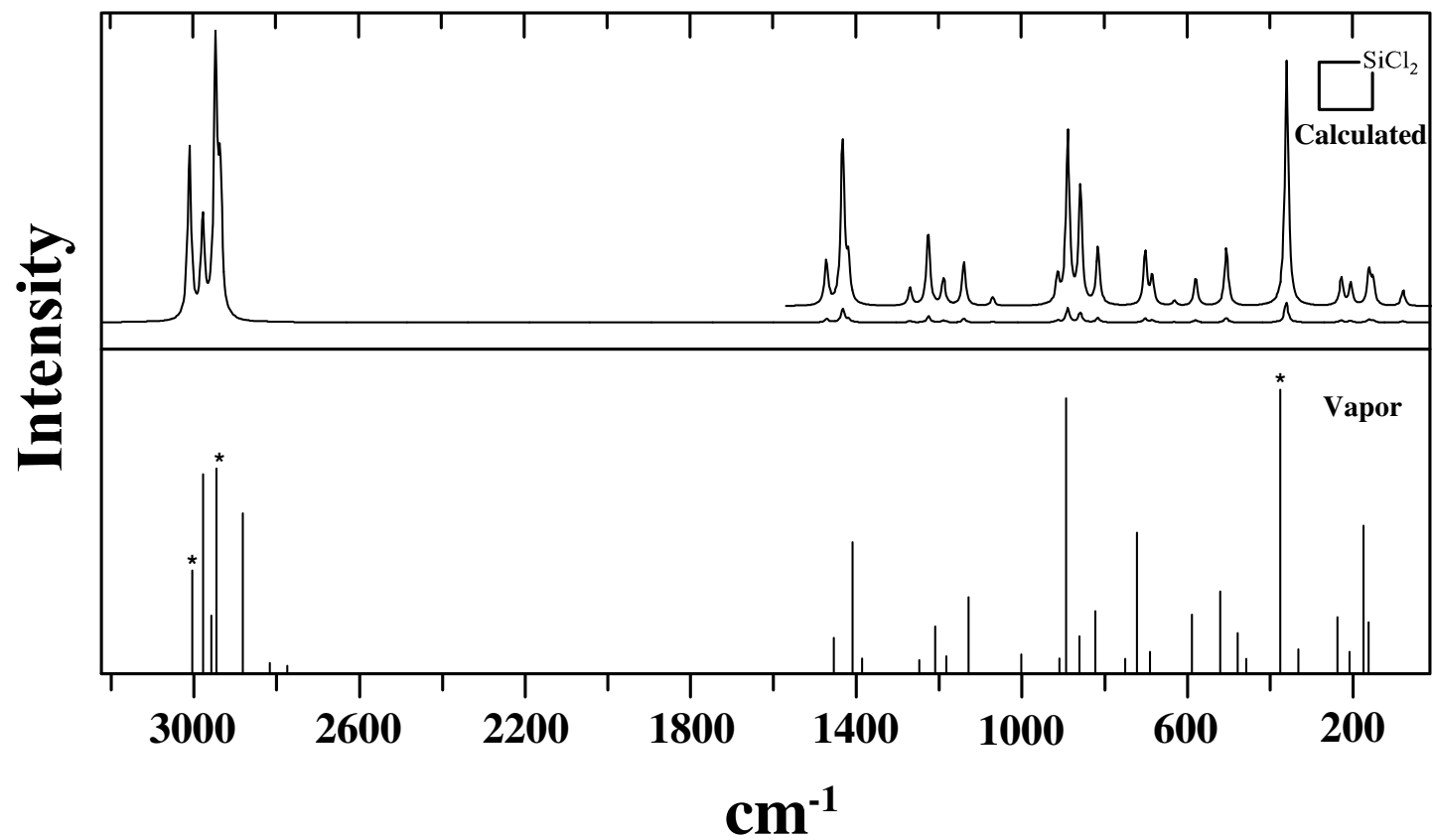


Fig. 49. Calculated (DFT-B3LYP/cc-pVTZ) Raman spectra for 1,1-dichlorosilacyclobutane compared with the line spectra of the frequencies and intensities of the vapor-phase Raman spectra reported in Refs. [39,121]. Lines marked with (*) indicate peaks with reduced intensities.

Table 32
Reassignments of vibrational spectra of silacyclobutane

Description		Reassignments ^a		Calculated DFT-B3LYP						
				C_s			C_{2v}			
				IR ^b	Raman ^b	Scaled	Intensity	Dep. ratio	Scaled	Intensity
A_1, A'	ν_1 β -CH ₂ sym. str.	2935 m	2927 (756) p	2914	(32,602)	0.2	2925	(275,410)	0.3	
	ν_2 α -CH ₂ sym. str. (i.p.)	2873 m	2858 (90) p	2933	(1,989)	0.2	2948	(37,1284)	0.3	
	ν_3 SiH ₂ sym. str.	2145 vvvs	2137 (1000) p	2130	(100,1000)	0.1	2127	(1000,1000)	0.1	
	ν_4 α -CH ₂ deform. (i.p.)	1422* m	1414* (67) d	1443	(2,56)	0.7	1435	(3,66)	0.7	
	ν_5 β -CH ₂ deform.	1458* vvw	1450* (29) d	1476	(1,20)	0.7	1471	(4,15)	0.7	
	ν_6 α -CH ₂ wag. (i.p.)	1127 s	1123 (84) p	1141	(11,20)	0.2	1137	(113,18)	0.1	
	ν_7 SiH ₂ deform.	962 vvs	948 (75) d	952	(73,40)	0.7	954	(760,39)	0.7	
	ν_8 C-C sym. str.	877* s	876* (169) p	873	(7,73)	0.1	874	(1,87)	0.1	
	ν_9 Si-C sym. str.		817* (60) p	819	(4,28)	0.1	763	(0,70)	0.1	
	ν_{10} Ring deform.	532 m	539 (130) p	531	(13,34)	0.2	507	(86,46)	0.2	
A_2, A''	ν_{11} α -CH ₂ antisym. str. (o.p.)	2992* vs	2980* (378) d	2992	(11,410)	0.8	2987	(0,633)	0.8	
	ν_{12} α -CH ₂ twist. (o.p.)			969	(0,5)	0.8	976	(0,3)	0.8	
	ν_{13} β -CH ₂ twist.	1211* vw	1214* (28) d	1232	(1,27)	0.8	1238	(0,18)	0.8	
	ν_{14} α -CH ₂ rock. (o.p.)	736 m	740 (21) d	737	(11,21)	0.8	751	(0,25)	0.8	
	ν_{15} SiH ₂ twist	514 w	517 (50) d	508	(1,23)	0.8	484	(0,22)	0.8	

Table 32
Continued

Description		Reassignments ^a		Calculated DFT-B3LYP					
				<i>C_s</i>			<i>C_{2v}</i>		
				IR ^b	Raman ^b	Scaled	Intensity	Dep. ratio	Scaled
<i>B₁, A'</i>	ν_{16} α -CH ₂ sym. str. (o.p.)	2888 m	2876 (220) p	2935	(16,71)	0.8	2945	(260,32)	0.8
	ν_{17} α -CH ₂ deform. (o.p.)	1401 m		1426	(3,14)	0.8	1426	(48,1)	0.8
	ν_{18} α -CH ₂ wag (o.p.)			1074	(1,3)	0.8	1102	(1,0)	0.8
	ν_{19} β -CH ₂ wag	1255* vw [sol.]	1250* (7) d	1277	(1,4)	0.8	1271	(16,9)	0.8
	ν_{20} C–C antisym. str.	927 s	932 (60) d	928	(11,19)	0.8	937	(110,18)	0.8
	ν_{21} Si–C antisym. str.	653 m [sol.]	652 (194) d	633	(2,56)	0.8	640	(20,55)	0.8
	ν_{22} SiH ₂ wag	814 vs		803	(71,7)	0.8	799	(886,5)	0.8
	<i>B₂, A''</i>	ν_{23} β -CH ₂ antisym. str.	2953* vs		2954	(17,491)	0.4	2957	(33,198)
ν_{24} α -CH ₂ antisym. str. (i.p.)		2992* vs	2980* (378) d	2994	(16,418)	0.2	2993	(255,163)	0.8
ν_{25} SiH ₂ antisym. str.		2145 vvvs	2150 w d	2138	(92,424)	0.7	2132	(984,421)	0.8
ν_{26} α -CH ₂ twist. (i.p.)		1191 mw	1191 (16) d	1202	(1,12)	0.4	1191	(22,9)	0.8
ν_{27} α -CH ₂ rock. (i.p.)		906* ms	903 (58) p	908	(16,26)	0.2	879	(248,5)	0.8
ν_{28} β -CH ₂ rock		673 ms	671 (141) p	665	(9,42)	0.1	712	(75,0)	0.8
ν_{29} SiH ₂ rock		409 mw	418 (34) d	409	(4,9)	0.3	427	(81,3)	0.8
ν_{30} Ring puckering		158 ^c		147	(0,1)	0.4	<i>i</i> ^d		

^aReassigned frequencies are labeled with (*).

^bVapor-phase experiments from Ref. [39], [sol.] = solid state.

^cRef. [13].

^dImaginary frequencies for the higher energy structure. This also applies for the notation *i* that appears in Tables 33-35.

Table 33
Reassignments of vibrational spectra of silacyclobutane-1,1- d_2

Description	Reassignments ^a		Calculated DFT-B3LYP					
			C_s			C_{2v}		
			IR ^b	Raman ^b	Scaled	Intensity	Dep. ratio	Scaled
A_1, A' ν_1 β -CH ₂ sym. str.	2935	m	2925 (570)	p	2914 (55,1269)	0.2	2925 (45,874)	0.3
ν_2 α -CH ₂ sym. str. (i.p.)	2873	m	2857 (70)	p	2933 (75,2087)	0.2	2948 (6,2732)	0.1
ν_3 SiD ₂ sym. str.	1554	vvvs	1548 (1000)	p	1545 (100,1000)	0.1	1542 (100,1000)	0.1
ν_4 α -CH ₂ deform. (i.p.)	1422*	m	1416 (89)	d	1442 (4,127)	0.8	1435 (0,145)	0.7
ν_5 β -CH ₂ deform.	1458*	vw	1450 (53)	d	1475 (1,40)	0.7	1470 (0,35)	0.7
ν_6 α -CH ₂ wag. (i.p.)	1128	ms	1123 (84)	p	1140 (14,50)	0.2	1136 (14,46)	0.1
ν_7 SiD ₂ deform.	712	vvs	700 (80)	p	698 (84,27)	0.2	686 (68,43)	0.6
ν_8 C-C sym. str.	867*	m	867* (107)	p	867 (16,119)	0.1	875 (1,191)	0.1
ν_9 Si-C sym. str.	821*	w	819* (58)	p	819 (3,48)	0.0	768 (9,129)	0.0
ν_{10} Ring deform.	496	mw	499 (204)	p	494 (13,86)	0.3	489 (8,109)	0.2
A_2, A'' ν_{11} α -CH ₂ antisym. str. (o.p.)	2992*	vs	2980* (260)	d	2992 (20,866)	0.8	2987 (0,1352)	0.8
ν_{12} α -CH ₂ twist. (o.p.)					960 (0,4)	0.8	968 (0,1)	0.8
ν_{13} β -CH ₂ twist.	1216*	vw	1210* (29)	d	1231 (0,62)	0.8	1238 (0,39)	0.8
ν_{14} α -CH ₂ rock. (o.p.)	669*	ms	669* (30)	d	664 (34,19)	0.8	677 (0,14)	0.8
ν_{15} SiD ₂ twist	410	vvw	417 (78)	d	405 (0,44)	0.8	393 (0,45)	0.8

Table 33
Continued

Description		Reassignments ^a		Calculated DFT-B3LYP						
				C_s			C_{2v}			
				IR ^b	Raman ^b	Scaled	Intensity	Dep. ratio	Scaled	Intensity
B_1, A'	ν_{16} α -CH ₂ sym. str. (o.p.)	2885 ms	2874 (152) p	2935	(28,150)	0.8	2945	(43,68)	0.8	
	ν_{17} α -CH ₂ deform. (o.p.)	1404 m		1426	(6,31)	0.8	1426	(8,3)	0.8	
	ν_{18} α -CH ₂ wag (o.p.)			1074	(1,5)	0.8	1102	(0,0)	0.8	
	ν_{19} β -CH ₂ wag	<i>1271</i> [*] vvw			1277	(0,10)	0.8	1270	(1,22)	0.8
	ν_{20} C–C antisym. str.	925 m	927 (49) d	925	(9,32)	0.8	934	(8,28)	0.8	
	ν_{21} Si–C antisym. str.	720 [*] m	716 (78) d	715	(53,21)	0.8	696	(91,27)	0.8	
	ν_{22} SiD ₂ wag	550 [*] m	550 [*] (107) d	537	(18,71)	0.8	544	(18,71)	0.8	
	B_2, A''	ν_{23} β -CH ₂ antisym. str.	2935 [*] m	2934 [*] (230) p	2954	(30,1037)	0.2	2957	(6,419)	0.8
ν_{24} α -CH ₂ antisym. str. (i.p.)		2953 vs		2994	(27,885)	0.4	2993	(41,353)	0.8	
ν_{25} SiD ₂ antisym. str.		1566 vvvvs	1564 (100) d	1564	(95,428)	0.7	1561	(95,440)	0.8	
ν_{26} α -CH ₂ twist. (i.p.)		1193 w	1193 (13) d	1201	(1,27)	0.4	1190	(3,20)	0.8	
ν_{27} α -CH ₂ rock. (i.p.)		902 [*] ms	898 [*] (209) p	899	(12,109)	0.1	857	(27,10)	0.8	
ν_{28} β -CH ₂ rock		656 ms	660 (156) p	650	(9,92)	0.2	698	(11,1)	0.8	
ν_{29} SiD ₂ rock		352 mw	358 (36) d	347	(6,10)	0.5	338	(9,8)	0.8	
ν_{30} Ring puckering		150 ^c		139	(0,1)	0.4	<i>i</i>			

^aReassigned frequencies are labeled with (*). Frequencies given in *italics* are from Ref. [121].

^bVapor-phase experiments from Ref. [39].

^cRef. [13].

Table 34
Reassignments of vibrational spectra of 1,1-difluorosilacyclobutane

Description		Reassignments ^a		Calculated DFT-B3LYP					
				<i>C_s</i>			<i>C_{2v}</i>		
				IR ^b	Raman ^b	Scaled	Intensity	Dep. ratio	Scaled
<i>A₁, A'</i>	<i>v</i> ₁ β-CH ₂ sym. str.	2885* ms	2883* (92) p	2939	(20,329)	0.3	2943	(18,232)	0.4
	<i>v</i> ₂ α-CH ₂ sym. str. (i.p.)	2955* s	2950* (1000) p	2949	(1,1000)	0.1	2958	(1,1000)	0.0
	<i>v</i> ₃ SiF ₂ sym. str.	934* vs	925* (277) p	912	(83,46)	0.1	908	(80,41)	0.1
	<i>v</i> ₄ α-CH ₂ deform. (i.p.)	1400* ms	1409* (111) d	1430	(3,46)	0.7	1425	(2,44)	0.7
	<i>v</i> ₅ β-CH ₂ deform.	1460* ms	1452* (32) d	1471	(1,13)	0.7	1468	(1,9)	0.7
	<i>v</i> ₆ α-CH ₂ wag. (i.p.)	1135 vs	1135 (25) p	1144	(38,4)	0.2	1141	(38,2)	0.0
	<i>v</i> ₇ SiF ₂ deform.	293* m	291* (65) p	277	(8,3)	0.5	273	(7,2)	0.5
	<i>v</i> ₈ C–C sym. str.	862* s	855* (123) p	854	(17,22)	0.1	843	(25,24)	0.0
	<i>v</i> ₉ Si–C sym. str.	796* ms	797* (138) p	790	(29,25)	0.1	753	(25,34)	0.0
	<i>v</i> ₁₀ Ring deform.	489* s	488* (315) p	478	(10,24)	0.1	484	(10,22)	0.1
<i>A₂, A''</i>	<i>v</i> ₁₁ α-CH ₂ antisym. str. (o.p.)			3004	(4,411)	0.8	3000	(0,442)	0.8
	<i>v</i> ₁₂ α-CH ₂ twist. (o.p.)			945	(0,0)	0.8	949	(0,0)	0.8
	<i>v</i> ₁₃ β-CH ₂ twist.	1222* w [sol.]	1222* (42) d	1230	(1,14)	0.8	1232	(0,14)	0.8
	<i>v</i> ₁₄ α-CH ₂ rock. (o.p.)			620	(0,0)	0.8	607	(0,0)	0.8
	<i>v</i> ₁₅ SiF ₂ twist		203 (54) d	182	(0,4)	0.8	181	(0,3)	0.8

Table 34
Continued

Description		Reassignments ^a		Calculated DFT-B3LYP					
				C_s			C_{2v}		
				IR ^b	Raman ^b	Scaled	Intensity	Dep. ratio	Scaled
B_1, A'	ν_{16} α -CH ₂ sym. str. (o.p.)	2850* m [sol.]		2948	(8,46)	0.8	2955	(10,12)	0.8
	ν_{17} α -CH ₂ deform. (o.p.)			1418	(9,8)	0.8	1416	(10,1)	0.8
	ν_{18} α -CH ₂ wag (o.p.)		<i>1064*</i> (19) d	1075	(0,7)	0.8	1092	(0,4)	0.8
	ν_{19} β -CH ₂ wag	1242* w		1266	(1,3)	0.8	1260	(3,1)	0.8
	ν_{20} C–C antisym. str.	913 m	912 (92) d	908	(11,13)	0.8	908	(10,10)	0.8
	ν_{21} Si–C antisym. str.	742 vs	743 (111) d	724	(55,11)	0.8	725	(54,9)	0.8
	ν_{22} SiF ₂ wag	328 s	331 (42) d	314	(17,4)	0.8	314	(17,3)	0.8
	B_2, A''	ν_{23} β -CH ₂ antisym. str.	2995 s	2998 (385) d	2980	(6,339)	0.3	2979	(1,122)
ν_{24} α -CH ₂ antisym. str. (i.p.)		2970 mw [liq.]	2970 (77) ?	3008	(12,242)	0.5	3007	(15,117)	0.8
ν_{25} SiF ₂ antisym. str.		962 vs	945 vw ?	940	(100,4)	0.1	935	(100,0)	0.8
ν_{26} α -CH ₂ twist. (i.p.)		1185	1184 (42) d	1192	(3,9)	0.6	1184	(4,8)	0.8
ν_{27} α -CH ₂ rock. (i.p.)		805	809 (100) ?	810	(23,17)	0.2	807	(7,8)	0.8
ν_{28} β -CH ₂ rock		665	666 (38) p	660	(2,16)	0.1	690	(1,1)	0.8
ν_{29} SiF ₂ rock		228*	229* (12) d	215	(1,2)	0.7	188	(1,2)	0.8
ν_{30} Ring puckering		63 ^c		77	(0,1)		<i>i</i>		

^aReassigned frequencies are labeled with (*). Frequencies given in *italics* are from Ref. [121].

^bVapor-phase experiments from Ref. [39]. [sol.] = solid state, [liq.] = liquid phase.

^cRef. [13].

Table 35
Reassignments of vibrational spectra of 1,1-dichlorosilacyclobutane

Description		Reassignments ^a					Calculated DFT-B3LYP						
		IR ^b		Raman ^b			C _s			C _{2v}			
							Scaled	Intensity	Dep. ratio	Scaled	Intensity	Dep. ratio	
A ₁ , A'	v ₁	β-CH ₂ sym. str.	2952	ms	2941	(748)	p	2936	(20,690)	0.1	2942	(21,536)	0.0
	v ₂	α-CH ₂ sym. str. (i.p.)	2887	mw	2878	(141)	p	2948	(1,1282)	0.3	2960	(2,1512)	0.3
	v ₃	SiCl ₂ sym. str.	376	m	379	(1000)	p	364	(3,100)	0.1	365	(4,100)	0.1
	v ₄	α-CH ₂ deform. (i.p.)	1414*	mw	1410*	(115)	d	1433	(3,67)	0.7	1427	(2,79)	0.7
	v ₅	β-CH ₂ deform.	1463*	w	1452*	(31)	d	1472	(1,18)	0.7	1469	(0,13)	0.7
	v ₆	α-CH ₂ wag. (i.p.)	1130	ms	1127	(66)	p	1141	(16,18)	0.2	1139	(18,15)	0.1
	v ₇	SiCl ₂ deform.	168	w	167	(44)	d	165	(2,14)	0.8	164	(2,15)	0.7
	v ₈	C–C sym. str.	893	m	893	(243)	p	890	(16,70)	0.1	873	(5,104)	0.1
	v ₉	Si–C sym. str.	824*	w	826*	(54)	p	817	(7,23)	0.1	783	(10,46)	0.1
	v ₁₀	Ring deform.	601	vs	592	(51)	p	583	(100,12)	0.2	585	(100,7)	0.0
A ₂ , A''	v ₁₁	α-CH ₂ antisym. str. (o.p.)	2952	ms	2952	(50)	?	3010	(4,492)	0.8	3004	(0,677)	0.8
	v ₁₂	α-CH ₂ twist. (o.p.)						946	(0,0)	0.8	953	(0,0)	0.8
	v ₁₃	β-CH ₂ twist.	1212*	w	1211*	(41)	d	1226	(0,30)	0.8	1233	(0,21)	0.8
	v ₁₄	α-CH ₂ rock. (o.p.)	653*	m				633	(2,0)	0.8	623	(0,0)	0.8
	v ₁₅	SiCl ₂ twist	174	mw	177	(130)	d	154	(0,10)	0.8	153	(0,11)	0.8

Table 35
Continued

Description		Reassignments ^a		Calculated DFT-B3LYP					
				<i>C_s</i>			<i>C_{2v}</i>		
				IR ^b	Raman ^b	Scaled	Intensity	Dep. ratio	Scaled
<i>B₁, A'</i>	ν_{16} α -CH ₂ sym. str. (o.p.)	2891 mw		2947	(7,117)	0.8	2957	(10,64)	0.8
	ν_{17} α -CH ₂ deform. (o.p.)	1395 m	1385 (12) d	1419	(9,16)	0.8	1418	(12,4)	0.8
	ν_{18} α -CH ₂ wag (o.p.)			1071	(0,4)	0.8	1093	(0,0)	0.8
	ν_{19} β -CH ₂ wag	1260* vw	1248* (11) ?	1271	(0,7)	0.8	1261	(0,14)	0.8
	ν_{20} C–C antisym. str.	914 m	914 (12) d	915	(4,11)	0.8	916	(4,10)	0.8
	ν_{21} Si–C antisym. str.	723 s	725 (123) d	704	(25,22)	0.8	702	(31,23)	0.8
	ν_{22} SiCl ₂ wag	240* mw	241* (49) d	231	(5,1)	0.8	231	(5,11)	0.8
	<i>B₂, A''</i>	ν_{23} β -CH ₂ antisym. str.	2972* m	2972* (175) p?	2979	(7,516)	0.4	2980	(3,197)
ν_{24} α -CH ₂ antisym. str. (i.p.)		3002* m	2999* (379) p	3011	(7,431)	0.5	3010	(12,277)	0.8
ν_{25} SiCl ₂ antisym. str.		533 s	523 (71) p	509	(56,24)	0.5	517	(80,23)	0.8
ν_{26} α -CH ₂ twist. (i.p.)		1183 w	1181 (13) p	1190	(2,11)	0.4	1181	(3,8)	0.8
ν_{27} α -CH ₂ rock. (i.p.)		857* s	863* (32) p	860	(27,47)	0.1	854	(48,1)	0.8
ν_{28} β -CH ₂ rock		696* s	693* (18) d	687	(46,11)	0.2	705	(28,1)	0.8
ν_{29} SiCl ₂ rock			212* (18) d	208	(1,9)	0.7	168	(1,14)	0.8
ν_{30} Ring puckering				81	(0,7)	0.7	<i>i</i>		

^aReassigned frequencies are labeled with (*).

^bVapor-phase experiments from Ref. [39].

within 10 cm^{-1} of each other. This greatly helps in the reassignment of some of the vibrational modes which are coupled with other modes, especially for the less symmetric C_s structure. In addition, since the predicted frequencies do not vary much between the puckered and planar structures, the vibrational analysis can be carried out on the basis of the higher symmetry (C_{2v}) for an easier comparison.

The calculated frequencies in the C-H stretching region for silacyclobutane and its dihalo derivatives were not found to have the same trend that was originally proposed [39]. Previously, the C-H vibrational frequencies appeared to be slightly lower for the difluoro and dichloro derivatives, which indicates stiffer C-H bonds and hence shorter C-H bond distances as compared to silacyclobutane. However, it can be seen from the calculated Raman spectra in Figs. 46-49 that the calculated frequencies of the C-H vibrations are lower for silacyclobutane than for the dihalo derivatives.

The strongest band in the Raman spectra for the four molecules, except for the difluoro derivative, was the SiX_2 symmetric stretching (ν_{12}) as determined from the experiment and calculations. That peak intensity was set to be the maximum in the scale of the relative intensities, and the rest of the calculated peak intensities were readjusted accordingly. The depolarization ratios were also recorded and these agree very well with the previously determined Raman polarization spectra, which provides confidence in the reassignments.

From the calculations it can be seen that most of the original assignments were made correctly, especially frequencies located in the region above 1000 cm^{-1} and those related to the SiX_2 stretching and bending motions. However, some of the original

assignments needed to be revised. Most of the reassigned frequencies are those of the CH₂ twisting and wagging vibrations, which generally have very weak intensities in the infrared and Raman spectra and, as a result, had previously been hard to assign.

The DFT calculations predicted the frequencies of the two CH₂ deformation motions of the *A₁* symmetry to be switched as compared with the original assignments that were based on the normal coordinate analysis for the four molecules (Tables 32-35). Their predicted depolarization ratios are 0.7 which agrees with the fact that these two vibrations are nearly depolarized in the Raman spectra even though they belong to the most symmetric species.

Calculated frequencies of the symmetric ring stretching vibrations (ν_8 and ν_9) were predicted to be lower than the originally assigned experimental values. These two vibrations were also shown to have some contribution from the in-phase CH₂ rocking vibration of the *B₂*-type. In silacyclobutane, for instance, the change in frequency in the case of the Si-C symmetry stretching motion from 819 cm⁻¹ for the puckered form (where mixing with in-phase CH₂ rocking is present) to 763 cm⁻¹ for the planar form demonstrates the fact that some contribution comes from the *B₂* species vibration (Table 32). That observation suggested some reassignments were to be made. On the other hand, the antisymmetric ring stretching modes (ν_{20} and ν_{21}) are less difficult to assign, since they are among the few strongly depolarized Raman in the region between 700 cm⁻¹ to 950 cm⁻¹ for the four molecules.

The SiX₂ stretching and bending vibrations and the shift in their vibrational frequencies calculated for the four molecules agree very well with the experiment, and

only a few reassignments were needed for such types of motions, mostly in the case of the dihalo derivatives as shown in Tables 34 and 35. In the case for 1,1-dichlorosilacyclobutane, a strong coupling between the A_1 symmetric SiCl_2 stretch (ν_3) and the A_1 ring deformation (ν_{10}) were observed and confirmed by normal coordinate analysis [39]. DFT calculations very interestingly reproduced that strong coupling in the vibrational spectra of the dichloro derivative as shown in Table 35.

Tables 32-35 also show that several frequencies were reassigned to different vibrational modes of the A_2 symmetry. Being infrared active for such modes is evidence for the puckered structure that the four molecules have in their ground states. However, in the case of the 1,1-difluoro-1-silacyclobutane, it was noted from the reassignments that the A_2 type motions are almost inactive (Table 34) as compared to the hydride, deuteride and dichloro derivatives. This could be evidence that the 1,1-difluorosilacyclobutane ring is less puckered in the minimum structure of the molecule than silacyclobutane and 1,1-dichlorosilacyclobutane. The MP2/cc-pVTZ optimized-structure puckering angles listed in Tables 28-30 show that the puckering angle for the difluoro molecule is 28.7° as compared to 34.5° and 31.1° for silacyclobutane and the dichloro derivative, respectively.

One unusual result noticed while the reassignments have been carried out was that the frequencies of the out-of-phase CH_2 twisting (ν_{12}) and the out-of-phase CH_2 wagging (ν_{18}) from the DFT calculations are much lower as compared to the original assignments [39] and are much lower than where these would be normally expected [122]. The difficult part in experimentally determining these two A_2 -type vibrations is

that they are of the weakest intensities among the fundamentals for the four molecules. Several studies [123-126] have employed DFT calculations to predict the vibrational frequencies and to compare them with previous experimental results for some non-cyclic silicon-containing molecules [127,128], such as dimethylsilane [125,127], trimethylsilane [124,127], disilylmethane [126,128], and ethylsilane [123]. These studies used the calculated frequencies as supporting tools to restudy some of the unclear aspects in the vibrational spectra obtained years ago, but none of these studies pointed out specifically why such a discrepancy between the experimental and calculated frequencies for these CH₂ out-of-plane modes would happen. Nevertheless, one conclusion drawn from these studies is that the effect of having silicon atoms in the structure of the molecule does not affect the accuracy of the vibrational frequencies reproduced by the DFT method. Moreover, in the case of disilylmethane (CH₃SiH₂CH₃), the CH₂ twisting vibration was predicted using the B3LYP/6-311G(d,p) level of theory [126] to be at 1043 cm⁻¹, which is somewhat lower than what it had been assigned to before (1101 cm⁻¹) [128].

A recent *ab initio* study on 1,3-disilacyclobutane [119] suggested that there is an electrostatic interaction between the electronegative silicon atoms and the electropositive hydrogen atoms of the CH₂ groups. The hydrogen atoms were calculated to have a somewhat larger partial positive charge than normal, causing the CH₂ out-of-phase frequencies to be shifted to lower frequencies below 1000 cm⁻¹. This trend was noticed also in the case of the deuterated isotopomers [119]. In silacyclobutane, as shown in Table 32, the out-of-phase CH₂ twisting (ν_{12}) and the out-of-phase CH₂ wagging (ν_{18})

frequencies were calculated to be 969 cm^{-1} and 1074 cm^{-1} , respectively. In the case of the difluoro and dichloro derivatives (Tables 34 and 35), the frequency of the ν_{12} mode was calculated to be even lower (946 cm^{-1}). This result also supported the explanation [119] that the electrostatic interaction between the hydrogen atoms of the SiH_2 and CH_2 groups caused that unusual shift in the CH_2 bending frequencies to take place. For the dichloro and difluoro derivatives, the silicon atom becomes more electropositive as can be seen in Table 36. The reassignments for the ν_{18} mode were made based on the observed Raman bands as well, since that mode is normally of a noticeable intensity in the Raman spectra.

One additional feature of the spectra of all these molecules is that they have a characteristic frequency near 1130 cm^{-1} . This was recognized long ago [39] as being a valid identifier for the silacyclobutane ring. All the molecules in this present study possess this type of fingerprint band. It is confirmed from DFT results in Tables 32-35 that it is primarily the in-phase $\alpha\text{-CH}_2$ wagging motion coupled to symmetric stretchings of the C-C and Si-C bonds. Fig. 50 shows this vibration which is very similar for each of these molecules.

CONCLUSION

In this chapter detailed reassignments of silacyclobutane and three of its derivatives were presented. Detailed *ab initio* and DFT calculations of the structures, inversion barriers, and infrared and Raman spectra were presented. Calculated spectra of silacyclobutane agree very well with the experiment. The DFT method gives highly

Table 36
 Calculated atomic charges for silacyclobutane, 1,1-difluorosilacyclobutane, and 1,1-dichlorosilacyclobutane from the DFT-B3LYP/cc-pVTZ level of theory^a

	Silacyclobutane (X=H)	1,1-Difluoro- silacyclobutane (X=F)	1,1-Dichloro- silacyclobutane (X=Cl)
Si	0.27	0.77	0.59
X _a	- 0.05	- 0.29	- 0.24
X _b	- 0.05	- 0.29	- 0.24
C _α	- 0.29	- 0.32	- 0.29
H _a ^(C_α)	0.10	0.11	0.11
H _b ^(C_α)	0.10	0.10	0.10
C _β	-0.16	-0.17	-0.17
H _a ^(C_β)	0.09	0.10	0.11
H _b ^(C_β)	0.09	0.10	0.11

^aSee Fig. 39 for atom labels.

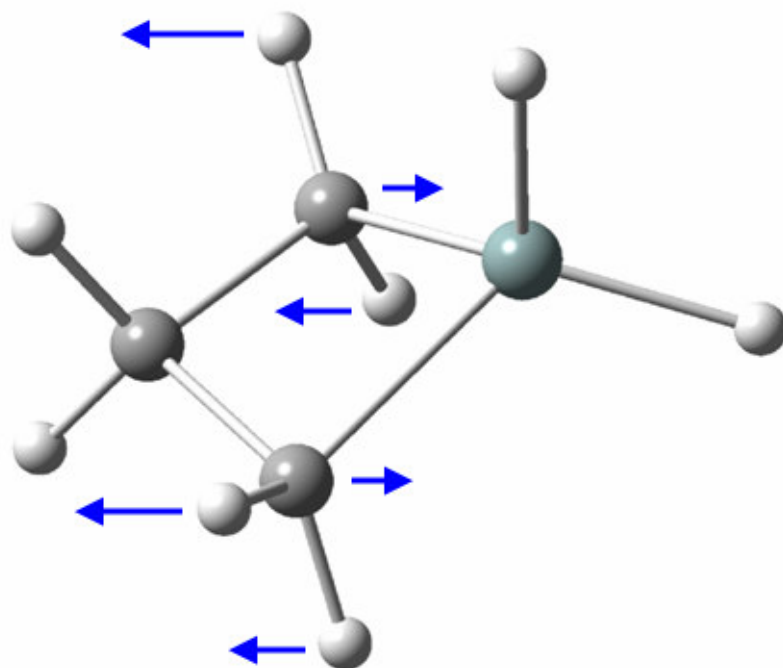


Fig. 50. Vector displacement representations of the in-phase α -CH₂ wagging vibration (ν_6) in silacyclobutane.

satisfactory results, even though it has implemented here to study the vibrational frequencies of highly strained four-membered ring molecules containing second-row elements. This has given us motivation to extend this study in the next chapter to some five-membered-ring silanes, namely silacyclopent-2-ene and silacyclopent-2-ene and a number of their derivatives.

CHAPTER X

**REINVESTIGATION OF THE STRUCTURE AND RING-
PUCKERING POTENTIAL ENERGY FUNCTIONS FOR
SILACYCLOPENT-2-ENE AND RELATED MOLECULES**

INTRODUCTION

Laane and Lord showed in 1967 that five-membered ring molecules containing a double bond can be thought of as pseudo-four-membered ring molecules [10,11]. As a result, the ring-puckering vibration could be described with the potential function of the form $V(\text{cm}^{-1}) = ax^4 + bx^2$. The quartic term in this function primarily affects the angle strain within the ring, while the quadratic term has contributions from both angle strain and torsional energy. For rings containing one or two silicon atoms, and under normal circumstances, the torsional interaction between the CH_2 and SiH_2 groups is considerably lower, and the ring has less inclination to be distorted from the planar form.

A series of ring molecules previously studied by infrared techniques include silacyclopent-2-ene, silacyclopent-2-ene-1,1- d_2 , 1,1-difluorosilacyclopent-2-ene, and 1,1-dichlorosilacyclopent-2-ene [40,129,130]. The far-infrared studies of silacyclopent-2-ene concluded that it is planar and unusually rigid [40], as is its 1,1- d_2 isotopomer [130]. The planar structure of the molecule was rationalized on the basis of an unusual

interaction between the d orbitals of the silicon atom and the π -electrons of the C=C double bond. The fact that the C=C stretching vibration in silacyclopent-2-ene shifts to a lower frequency was used to support that conclusion [40]. Standard MM2 calculations, however, predicted a double-minimum potential function characteristic of a nonplanar molecule [130].

The availability of high-level quantum mechanical calculation methods that have given reliable results for silicon-containing ring molecules has motivated us to restudy the conformation and vibrational spectra of silacyclopent-2-ene and its 1,1- d_2 isotopomer. The structures of 1,1-difluorosilacyclopent-2-ene and 1,1-dichlorosilacyclopent-2-ene have been also investigated. The results of this work are presented in this chapter.

COMPUTATIONS

Ab initio second-order Møller-Plesset (MP2) and coupled cluster theory with single and double excitation (CCSD) calculations using the Gaussian 03 program [67] were employed to study the structure of silacyclopent-2-ene in its planar and nonplanar forms. The structures of the difluoro and dichloro derivatives were optimized at the MP2 level, and their frequencies were calculated. The vibrational frequencies of the four molecules were computed using density functional theory (DFT) with the B3LYP hybrid functional using different basis sets. Because changing the basis sets used for the DFT treatments produced different results for the stable configurations of silacyclopent-2-ene, the 6-311++G(d,p) basis set, which predicted a slightly puckered structure for

silacyclopent-2-ene, was used to calculate the vibrational frequencies for the difluoro and dichloro derivatives.

New kinetic energy expressions for the 2-ene and its 1,1- d_2 isotopomer were calculated based on the optimized structure of the planar conformation determined from the CCSD/6-311++G(d,p) calculation. A program previously described [53] was used to generate the kinetic energy terms. These were then used to obtain the revised potential energy functions in terms of the ring-puckering coordinates for the two molecules.

RESULTS AND DISCUSSION

Previously, the observed far-infrared ring-puckering spectra of silacyclopent-2-ene were analyzed in terms of a rigid potential energy function characteristic of a planar molecule [40]. In the work presented here the MP2 theory using different basis sets was utilized to locate the stable conformation of silacyclopent-2-ene and the results are shown in Table 37. Smaller basis sets, which lack the diffuse and polarization functions, predicted the molecule to be totally planar. A barrier of about 50 cm^{-1} , however, was predicted when larger basis sets were used. On the other hand, the triple-zeta basis set when employed with the DFT calculations predicted a planar structure for silacyclopent-2-ene (Table 37). Thus, a higher level of quantum mechanical computation was needed to verify the nonplanar configuration of the molecule that was determined by the MP2 calculations.

The CCSD/6-311++G(d,p) calculations, which should in principle give more reliable results, confirmed that silacyclopent-2-ene is nonplanar with a puckering angle

Table 37

Calculated energies, barriers, and puckering frequencies for silacyclopent-2-ene and its 1,1- d_2 isotopomer^a using different levels of theories

Theory	Total energies (Hartree)		Puckering angle (deg.)	Puckering frequency ^b (cm ⁻¹)	Barrier (cm ⁻¹)
	Puckered	Planar			
MP2/3-21G			0°	9	----
MP2/6-31G			0°	27	----
MP2/6-31+G(d)	-445.6285629	-445.6282456	19°	99	70
MP2/6-311++G(d,p)	-445.7689100	-445.7685439	20°	102	80
MP2/cc-pVTZ	-445.8977514	-445.8975197	18°	91	51
CCSD/6-311++G(d,p)	-445.8251234	-445.8249104	17°	----	47
DFT-B3LYP/3-21G			0°	47	----
DFT-B3LYP/6-31G			0°	53	----
DFT-B3LYP/6-31+G(d)	-446.7245222	-446.7245127	8.8°	45 (46)	2.1
DFT-B3LYP/6-311++G(d,p)	-446.7880437	-446.7880384	7.6°	38 (36)	1.2
DFT-B3LYP/cc-pVTZ			0°	19 (17)	----
DFT-B3LYP/6-311++G(3d2f,2pd)			0°	13	----
Experimental ^c			13° ± 1°	59 (52)	26 (31)

^aValues in parentheses are for the 1,1- d_2 isotopomer.

^bScaling factors of 0.985 and 0.920 used to scale the frequencies obtained from DFT-B3LYP and MP2 calculations, respectively.

^cAs determined from this work.

of 17° and an inversion barrier of 47 cm^{-1} . Fig. 51 shows the optimized structure of silacyclopent-2-ene from the coupled cluster theory. Table 37 also shows the calculated isotope shift for the 1,1- d_2 molecule from the DFT calculations.

REASSIGNMENTS OF THE FAR-INFARED SPECTRA

The *ab initio* results showed the need to reassign the far-infrared spectra of silacyclopent-2-ene and its 1,1- d_2 isotopomer. In addition, the kinetic energy terms have also been calculated from coupled cluster calculations. The ring-puckering coordinate-dependent kinetic energy calculated for silacyclopent-2-ene with the rocking parameter $R=0$ is

$$g_{44}^{\text{H}_2}(x) = 0.0069801 - 0.0168419 x^2 - 0.0646870 x^4 + 0.2331390 x^6 \quad (38)$$

and for silacyclopent-2-ene-1,1- d_2 with $R=0$ is

$$g_{44}^{\text{D}_2}(x) = 0.0061189 - 0.0118251 x^2 - 0.0582123 x^4 + 0.1487240 x^6, \quad (39)$$

where x is the ring-puckering coordinate. Reassignments of the ring-puckering far-infrared spectra for silacyclopent-2-ene and its isotopomer were made and are listed in Table 38. Two possible calculations for the ring-puckering potential energy functions have been proposed. With these calculations, some of the far-infrared lines that were not fully interpreted in the previous work could be explained [40,130]. These calculations also accounted for the puckered structure of the two molecules. In Calculation I, a line of a moderate intensity at 107 cm^{-1} , which was not reported in the previous far-infrared experiment [40], was assigned to the 1-2 transition. The next lines were then assigned to higher transitions. Table 38 also shows another set of assignments based on Calculation

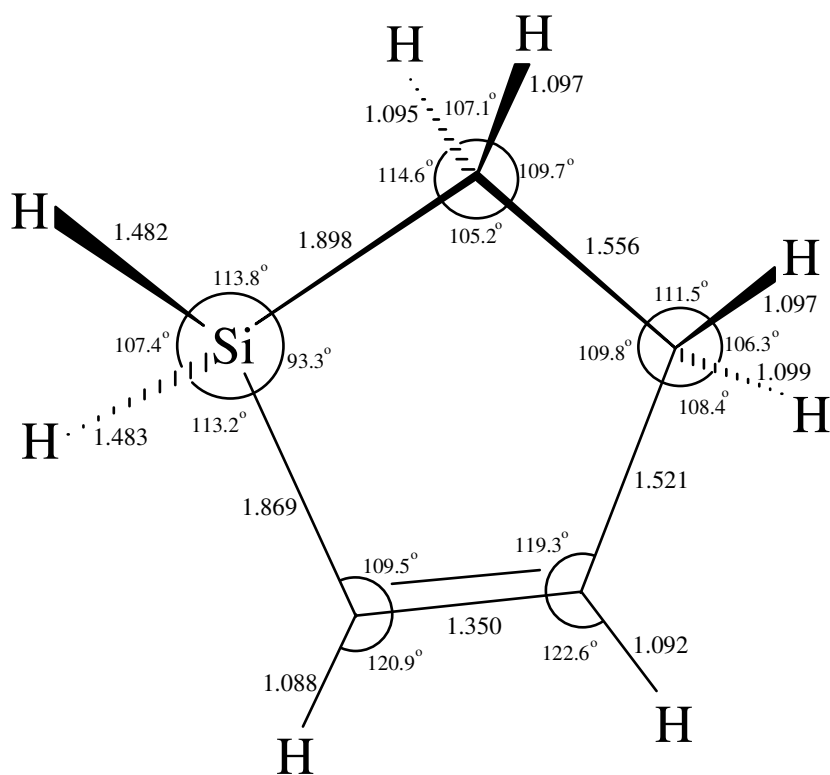


Fig. 51. Structure of silacyclopent-2-ene optimized from the coupled cluster theory with single and double excitation calculations (CCSD) using the 6-311++G(d,p) basis set.

Table 38
 Reassignments of the ring-puckering frequencies (cm^{-1}) for silacyclopent-2-ene and silacyclopent-2-ene-1,1- d_2

Transition	Silacyclopent-2-ene					Silacyclopent-2-ene-1,1- d_2				
	Frequency			Relative intensity		Frequency			Relative intensity	
	Obs.	Calc.	Δ^a	Obs.	Calc.	Obs.	Calc.	Δ^a	Obs.	Calc.
Calculation I										
0-1		59.4	---		0.4		52.3	---		0.4
1-2	107.0 ^b	107.1	-0.1		1.0		100.4	---		0.9
2-3	123.7	124.4	-0.7	1.0	1.0	116.7	116.2	0.5	0.9	1.0
3-4	139.3	140.9	-1.6	0.9	0.8	131.2	132.3	-1.1	1.0	0.8
4-5	155.6	154.2	1.4	0.8	0.5	145.9	145.2	0.7	1.0	0.6
5-6	167.6	165.7	1.9	0.7	0.3	156.8	156.2	0.6	0.8	0.4
6-7	177.4	175.8	1.4	0.5	0.2	165.0	166.0	-1.0	0.7	0.2
7-8	184.9	184.9	0.0	0.4	0.1	172.9	174.8	-1.9	0.6	0.1
8-9	192.1	193.1	-1.0	0.2	0.04	184.9	182.8	2.1		0.1
9-10	199.2	200.8	-1.6	0.1	0.02		190.2			0.02
Barrier (cm^{-1})		26					31			
Calculation II										
0-1		60.0	---		0.4		57.1	---		0.4
1-2	123.7	122.4	1.3	1.0	1.0	116.7	115.2	1.5	0.9	1.0
2-3	139.3	140.6	-1.3	0.9	0.9	131.2	132.6	-1.4	1.0	1.0
3-4	155.6	160.9	-5.3	0.8	0.7	145.9	151.6	-5.7	1.0	0.7
4-5	167.6	176.7	-9.1	0.7	0.4	156.8	166.6	-9.8	0.8	0.5
5-6	177.4	190.4	-13.0	0.5	0.3	165.0	179.5	-14.5	0.7	0.3
0-2	183.0 ^c	182.4	0.6	0.3	0.2	172.9	172.3	0.6		0.2
Barrier (cm^{-1})		46					36			

^a $\Delta = \text{obs.} - \text{calc.}$

^b Not reported in Ref. [40].

^c Not assigned in Ref. [40].

II. In the latter calculation the 123.7 cm^{-1} line of the d_0 and the 116.2 cm^{-1} line of the d_2 molecules were reassigned to the 1-2 transition. Both sets of new assignments are based on the assumption that a weak lower frequency band was previously not observed. That would not be surprising since the sample studies contained some of the silacyclopent-3-ene isomer which has a series of bands at lower frequencies.

The reassigned puckering-vibration transitions based on calculation I for the d_0 molecule can be fitted with a double-minimum potential function given by

$$V_{\text{H}_2} (\text{cm}^{-1}) = 27.74 \times 10^5 x^4 - 16.91 \times 10^3 x^2 \quad (40)$$

where x is in \AA . Similarly, for the d_2 isotopomer, the new potential function in terms of puckering coordinate becomes

$$V_{\text{D}_2} (\text{cm}^{-1}) = 28.82 \times 10^5 x^4 - 18.91 \times 10^3 x^2 \quad (41)$$

The fits of the ring-puckering vibrational levels are shown in Figs. 52 and 53. As can be seen from Table 32, the agreement between the experimental and calculated puckering transitions is fairly satisfactory for Calculation I, considering the asymmetric structure of the molecule. The barriers to planarity for the d_0 and d_2 molecules were determined from Eqs. (40) and (41) to be 26 cm^{-1} for the former and 31 cm^{-1} for the latter. The slightly higher barrier in the case of the d_2 molecule could be a result of a different amount of coupling between the low-lying vibrational modes.

Calculation II was also used to fit the lowest few transitions of the puckering vibration in the two molecules with the potential energy functions

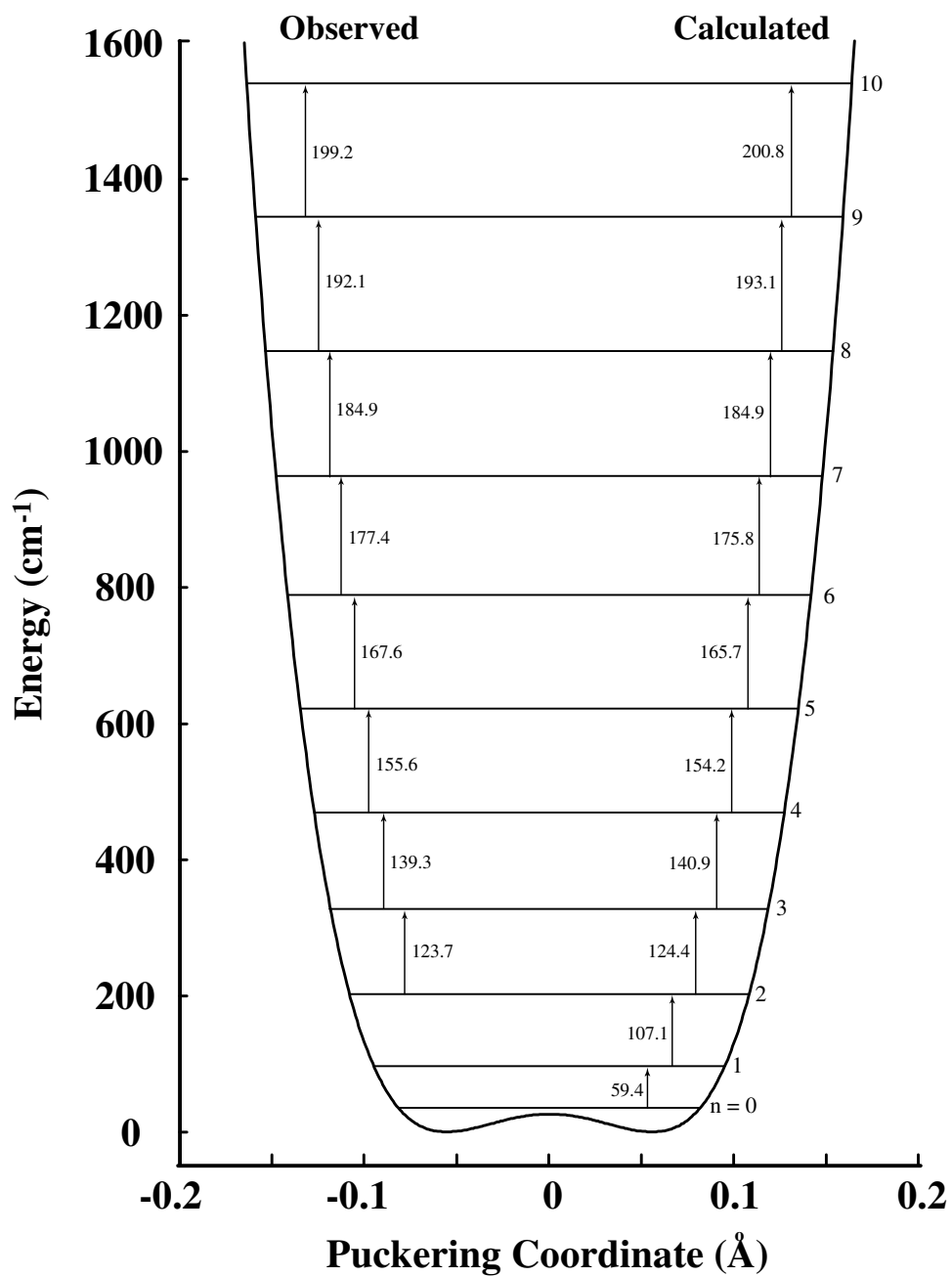


Fig. 52. Ring-puckering potential energy function of silacyclopent-2-ene from Calculation I.

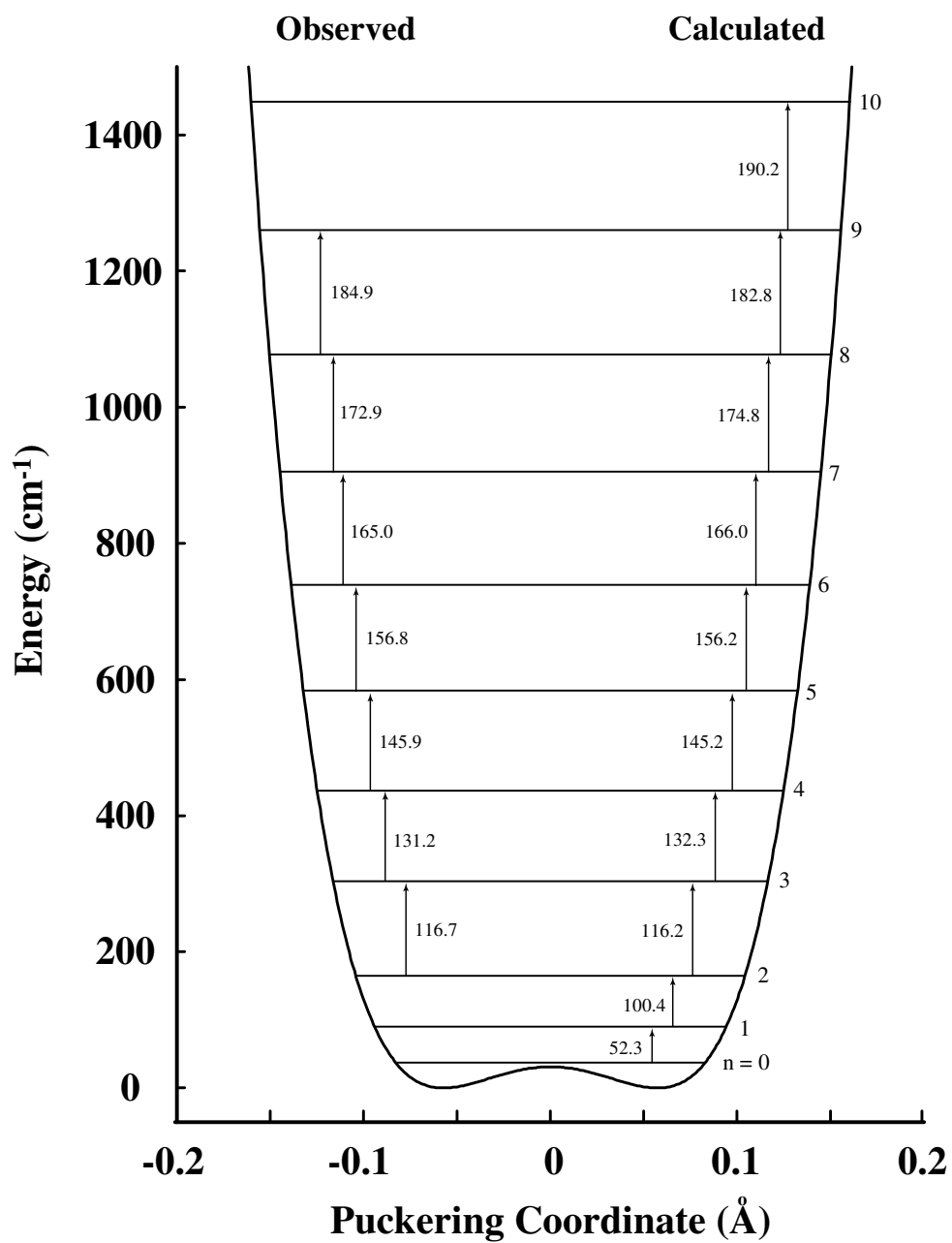


Fig. 53. Ring-puckering potential energy function of silacyclopent-2-ene-1,1-d₂ from Calculation I.

$$V_{\text{H}_2} (\text{cm}^{-1}) = 48.76 \times 10^5 x^4 - 29.97 \times 10^3 x^2 \quad (42)$$

for the hydride molecule and

$$V_{\text{D}_2} (\text{cm}^{-1}) = 49.47 \times 10^5 x^4 - 26.56 \times 10^3 x^2 \quad (43)$$

for the deuteride molecule. From these assignments the barriers were determined to be 46 cm^{-1} for the d_0 and 36 cm^{-1} for the d_2 molecules, while the puckering frequency was calculated to be 60 cm^{-1} for the former and 57 cm^{-1} for the latter.

The CCSD/6-311++G(d,p) calculations predicted a barrier of 47 cm^{-1} for silacyclopent-2-ene. Generally, for molecules with very low barriers, such as silacyclopent-2-ene, the barriers to planarity predicted by *ab initio* calculations, even with high-level ones, tend to deviate more from the experimental values. The puckering frequencies determined from the new fits are in reasonably good agreement with the values from DFT calculations (45 cm^{-1} for the d_0 and 46 cm^{-1} for the d_2 molecules) with the 6-31+G(d) basis set.

Table 39 shows that DFT calculations using different basis sets predict planar structures for 1,1-difluoro- and 1,1-dichlorosilacyclopent-2-ene. The MP2 theory with the triple- ζ basis set, however, predicts the dichloro derivative to be slightly puckered with a low barrier (16 cm^{-1}) and predicts the difluoro to be planar. The calculated ground state structures of the dihalo derivatives were confirmed by calculating their vibrational frequencies.

VIBRATIONAL FREQUENCIES

Table 40 lists the selected vibrational frequencies from the B3LYP/6-311++(d,p)

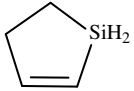
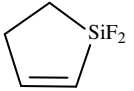
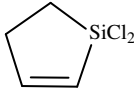
Table 39
 Calculated barriers and puckering frequencies^a (cm⁻¹) of 1,1-difluoro- and 1,1-dichlorosilacyclopent-2-ene

	1,1-Difluoro-silacyclopent-2-ene			1,1-Dichloro-silacyclopent-2-ene		
	Puckering angle	Puckering frequency	Barrier	Puckering angle	Puckering frequency	Barrier
MP2/cc-pVTZ	0°	13	0°	16°		13
DFT-B3LYP/6-31+G(d)	0°	57	0°	0°	20	0
DFT-B3LYP/6-311++G(d,p)	0°	56	0°	0°	20	0
DFT-B3LYP/cc-pVTZ	0°	57	0°	0°	31	0

^aScaled frequencies.

Table 40

Assignments of some characteristic frequencies^{a,b} in the mid-infrared spectra of silacyclopent-2-ene and its 1,1-difluoro and 1,1-dichloro derivatives

						Assignments
Exp.	calc.	exp.	calc.	exp.	calc.	
2990	2993 (16)	3020	3005 (16)	3020	3006 (15)	CH str.
2900	2892 (22)	2940	2905 (17)	2930	2905 (19)	CH ₂ sym. str.
1560	1595 (17)	1570	1590 (30)	1560	1592 (26)	C=C str.
1440	1461 (6)	1440	1457 (15)	1440	1456 (11)	CH ₂ def.
1320	1324 (4)	1320	1331 (19)	1320	1324 (8)	CH wag (o.p.)
1140	1162 (8)	1160	1169 (25)	1150	1169 (15)	CH ₂ wag
1100	1108 (2)	1100	1111 (8)	1100	1108 (1)	CH wag (i.p.)
990	971 (65)					SiH ₂ rock
		990	983 (16)	990	983 (10)	Ring mode
870	868 (47)	840	858 (100)	830	821 (29)	Ring mode
700	715 (34)	710	687 (10)	760	732 (40)	Ring mode

^aExperimental frequencies are within $\pm 5 \text{ cm}^{-1}$ uncertainty taken from Refs. [129,131]. Calculated frequencies were computed at the B3LYP/6-311++G(d,p) level of theory and were scaled.

^bNumbers in parentheses are calculated infrared intensities relative to the intensities of the strongest infrared band for each molecule.

calculations and compares them with corresponding experimental ones for silacyclopent-2-ene and its difluoro and dichloro derivatives. Approximate vibrational assignments were made for these frequencies. The observed shifts in the frequency of the C=C stretching vibration were reproduced by DFT calculations with fair agreement.

SILACYCLOPENT-3-ENES

The structures and vibrational spectra of silacyclopent-3-ene, as well as its deuterated, difluoro, and dichloro derivatives, were previously investigated. The one-dimensional potential energy function [132] which was refined a few years later with a two-dimensional analysis [133] and vibrational infrared and Raman spectra [134] were reported. These studies showed that silacyclopent-3-ene, silacyclopent-3-ene-1,1- d_2 , 1,1-difluorosilacyclopent-3-ene, and 1,1-dichlorosilacyclopent-3-ene are planar with the four carbon atoms and the silicon atom lying in the plane of the ring. Such a structure is unusual for a five-membered ring because the $\text{CH}_2\text{-SiH}_2$ torsional interactions can be expected to distort the ring structure from planarity. Silacyclopent-3-ene in its lowest energy structure was confirmed from far-infrared analyses [132,133] to possess the planar C_{2v} symmetry. In the present study, preliminary *ab initio* results for this molecule as well as the silacyclopent-3-ene-1,1- d_2 , 1,1-difluorosilacyclopent-3-ene, and 1,1-dichloro-silacyclopent-3-ene molecules will be presented.

The Gaussian 03 program [67] was used to carry out different levels of calculations on silacyclopent-3-ene and its derivatives. Density functional calculations (DFT-B3LYP) with the use of different basis sets predicted silacyclopent-3-ene to be

planar, as shown in Table 41. When second-order Møller-Plesset calculations were used with 6-311++G(d,p) and cc-pVTZ basis sets, the molecule came out to be slightly nonplanar with a very low barrier of 3 to 5 cm^{-1} (Table 41). When employing a more accurate quantum treatment, which is in this case the coupled cluster theory, the molecule was optimized at minima to be planar, in agreement with the experimental results. This demonstrates that for molecules where more than one type of intramolecular forces is affecting the structures, a higher level calculation is strongly recommended in order to attain more reliable results. For more details, the calculated structures from CCSD/6-311++G(d,p) and MP2/cc-pVTZ calculations are shown in Fig. 54.

Triple-zeta calculations of the DFT were used to compute the vibrational frequencies for the four molecules in their planar structures. The detailed vibrational reassignments of the infrared and Raman spectra based on the calculated DFT frequencies, intensities and depolarization ratios, are to be carried out in the future. For the time being, however, the calculated vibrational frequencies of CH_2 bending modes for different silicon-containing cyclic rings, and for cyclobutane and cyclopentene as well, are presented in Table 42. The table shows that a decrease in the frequencies for these bending vibrations is proportional to the number of silicon atoms in the ring. In the case of silacyclopent-2-ene, the frequencies of the bending vibrations of the CH_2 group next to the SiH_2 group are expected from DFT calculations to differ more as compared to those of the bending vibrations of the other CH_2 group. The results shown above correlate between the presence of silicon atoms in the ring and the shifts in these

Table 41

Calculated energies, barriers, and puckering frequencies for silacyclopent-3-ene from different levels of theories

	Puckering angle	Puckering frequency ^a (cm ⁻¹)	Barrier (cm ⁻¹)
MP2/3-21G	0.0°	73	0.0
MP2/6-31G	0.0°	78	0.0
MP2/6-31+G(d)	9.8°	38	2.9
MP2/6-311++G(d,p)	11.1°	45	3.0
MP2/cc-pVTZ	11.7°	41	5.0
CCSD/6-311++G(d,p)	0.0°		0.0
DFT-B3LYP/3-21G	0.0°	86	0.0
DFT-B3LYP/6-31G	0.0°	95	0.0
DFT-B3LYP/6-31+G(d)	0.0°	67	0.0
DFT-B3LYP/6-311++G(d,p)	0.0°	60	0.0
DFT-B3LYP/cc-pVTZ	0.0°	61	0.0
DFT-B3LYP/6-311++G(3d2f,2pd)	0.0°	52	0.0

^aScaled with scaling factors of 0.985 and 0.920 for the DFT-B3LYP and MP2 puckering frequencies, respectively.

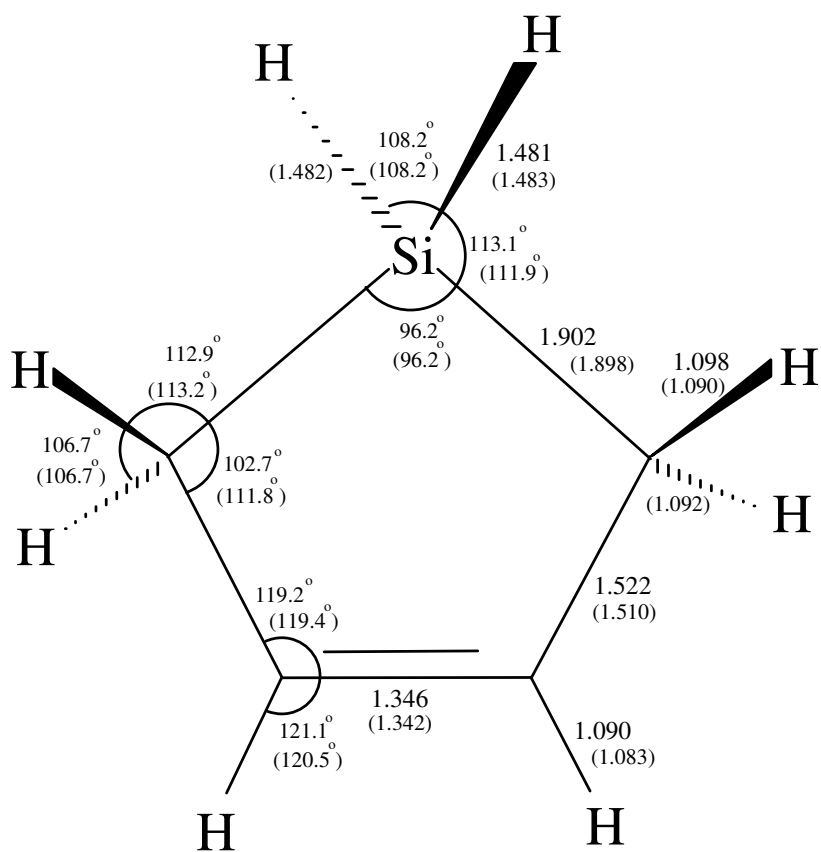
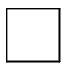
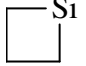

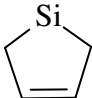
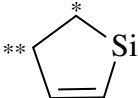
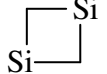
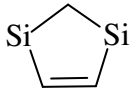


Fig. 54. Structure of silacyclopent-3-ene calculated at CCSD/6-311++G(d,p) and MP2/cc-pVTZ (in parentheses) levels of theory.

Table 42

Vibrational frequencies (cm^{-1}) for the CH_2 ring bending motions as determined from the DFT-B3LYP/cc-pVTZ level of theory in different cyclic silanes and in cyclobutane and cyclopentene

Vibrational Mode							
CH_2 deformation (i.p.)	1501, 1472	1443	1459	1430	1463	1393	
CH_2 deformation (o.p.)	1463 (<i>E</i>)	1426	1463	1431	1437	1379	1394
CH_2 wag (i.p.)	1270 (<i>E</i>)	1141	1303	1224	1313 ^{**}	964	
CH_2 wag (o.p.)	1245, 1152	1074	1296	1187	1160 [*]	924	1013
CH_2 twist (i.p.)	1230 (<i>E</i>)	1202	1209	1123	1235	978	
CH_2 twist (o.p.)	1240, 950	969	1287	1122	1132	967	978
CH_2 rock (i.p.)	1161, 630	908	1052	845	909 ^{**}	788	
CH_2 rock (o.p.)	744 (<i>E</i>)	737	875	833	779 [*]	464	752

frequencies. This supports the conclusion that electrostatic interactions play a major role for these shifts. Quantitatively, Fig. 55 compares the calculated atomic charges for these molecules to the molecules that do not contain silicon atoms. The difference in the magnitudes of charges on the hydrogen atoms of the CH₂ groups involved in these bending vibrations can be seen.

CONCLUSION

By utilizing high-level *ab initio* computations and reinvestigating the far-infrared spectra of silacyclopent-2-ene, the molecule was shown to be slightly puckered (17° from *ab initio* results) with a small barrier (26 cm⁻¹ from Calculation I and 46 cm⁻¹ from calculation II compared to 47 cm⁻¹ from *ab initio* results). Reassignments were also made on the far-infrared spectra of the 1,1-*d*₂ isotopomer. Recalculated kinetic energy expressions were utilized in this work. For silacyclopent-3-ene, CCSD calculations confirmed the planar conformation of the molecule in agreement with the experiment. The vibrational frequencies of the 2-ene and 3-ene and their derivatives as well were calculated and some of them were presented. A consistent trend in the frequency shift for the CH₂ bending vibrations was predicted from the calculated harmonic frequencies using the DFT-B3LYP theory. It was shown that the inclusion of silicon atoms in the cyclobutane and cyclopentene rings greatly affects the frequencies of these vibrations.

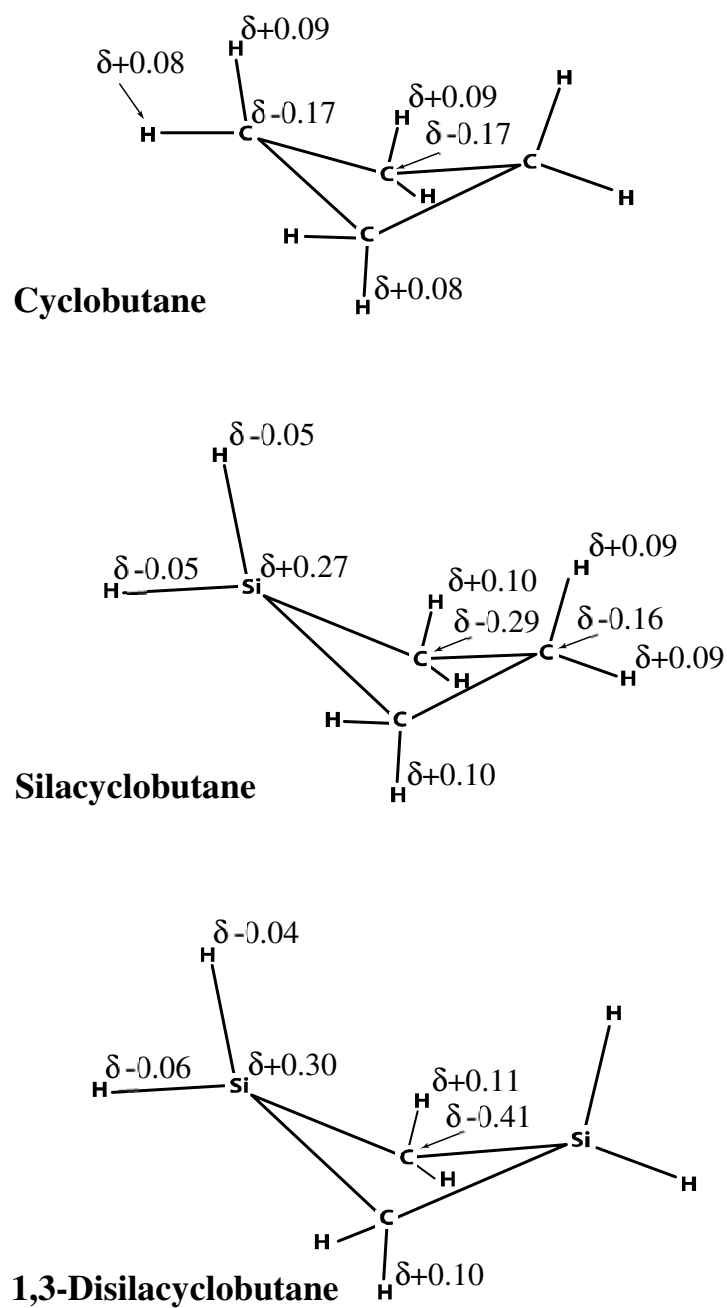
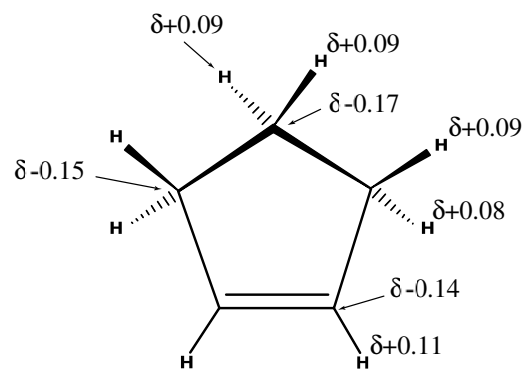
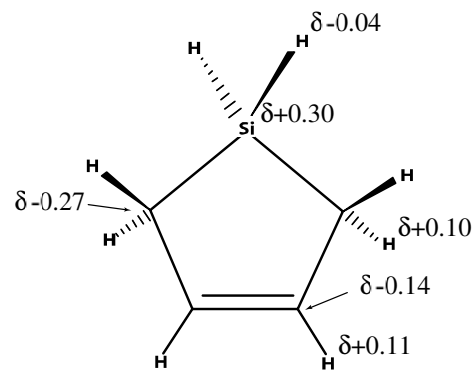


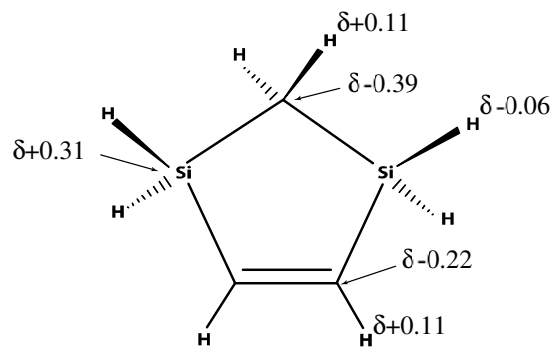
Fig. 55. Calculated atomic charges (MP2/cc-pVTZ) for some cyclic molecules.



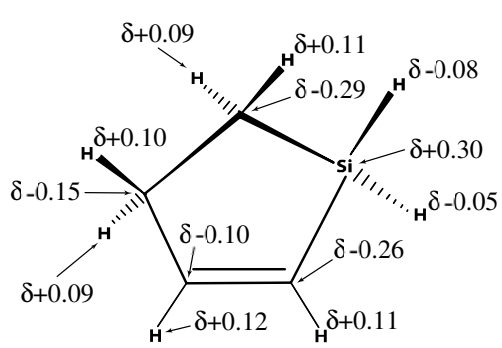
Cyclopentene



Silacyclopent-3-ene



1,3-Disilacyclopentene



Silacyclopent-2-ene

Fig. 55. Continued.

CHAPTER XI

CONCLUSION

In this dissertation, several spectroscopic techniques and *ab initio* calculations were used to investigate the conformational properties and vibrational spectra of several cyclic and bicyclic molecules. 2-Indanol in its most stable form is stabilized by internal hydrogen bonding which exists between the alcoholic hydrogen atom and the electron π -cloud of the benzene ring. A comprehensive *ab initio* calculation using the MP2/cc-pVTZ level of theory showed that 2-indanol can exist in four possible conformations, which can interchange through the ring-puckering vibration and the internal rotation of the OH group on the five-membered ring. A potential energy surface in terms of these two vibrational coordinates was calculated from the MP2 results. Density functional theory calculations were used to predict the vibrational frequencies and to help in normal mode assignments.

Fluorescence excitation spectra of 2-indanol confirmed the presence of the four conformers in the electronic ground and excited states. Several assignments of the low-frequency ring vibrations in the electronic ground (S_0) and excited (S_1) states were presented. For the conformer with the intramolecular hydrogen bonding, the 0_0^0 origin was detected at 37008 cm^{-1} and the puckering frequencies at 92 cm^{-1} for the S_0 state and

79.7 cm^{-1} for the S_1 state. For the next stable conformer with no hydrogen bonding, the 0_0^0 band was observed at 36937 cm^{-1} and the puckering frequencies at 86 cm^{-1} for the S_0 state and 77.0 cm^{-1} for the S_1 state. In general the puckering frequencies for the four isomers were shown from experiment and *ab initio* calculations to be within 7 cm^{-1} from each other in each electronic state. The spectral intensities indicate that 82% of the molecules exist in the most stable form with the intramolecular hydrogen bonding. The other isomers are present at approximately 11, 5, and 3%. The MP2/6-311++G(d,p) calculation predicts a distribution of 70, 13, 9, and 8% at 90°C which is the experimental sample temperature.

3-Cyclopenten-1-ol also undergoes intramolecular hydrogen bonding and exists in four possible conformations. *Ab initio* calculations showed that the conformation with the intramolecular molecular hydrogen bonding with the C=C double bonds is 693 cm^{-1} below the planar conformation. A two-dimensional potential energy surface in terms of the ring-puckering angle and the hydroxyl group internal rotation angle was constructed by utilizing the MP2/6-31+G(d,p) level of theory. DFT calculated frequencies were obtained for the four conformers and predicted two bands in the OH spectral region that are approximately 25 cm^{-1} apart, in very good agreement with the previously reported experimental infrared spectra. In addition, DFT calculations predicted that the puckering frequencies of the four conformers of 3-cyclopenten-1-ol are spread over a broad far-infrared region (70 cm^{-1} – 120 cm^{-1}), in contrast with the experimental values determined for 2-indanol. These theoretical calculations should provide a good basis for future experimental investigations on this molecule.

Infrared and Raman spectra were also collected for γ -crotonolactone. *Ab initio* calculations and vibrational assignments of the vapor-phase Raman spectra concluded that the molecule is rigidly planar in the electronic ground state. This conclusion agrees with the previously reported microwave studies and is attributed to the conjugation between the C=C and C=O double bonds of the ring. The potential energy function in terms of the puckering coordinate (x) was predicted from *ab initio* calculations to be nearly harmonic and is given by

$$V(\text{cm}^{-1}) = 10.08 \times 10^4 x^2 + 45.90 \times 10^4 x^4. \quad (44)$$

The vibrational levels associated with this potential function were computed using the kinetic energy expression

$$g_{44}(x) = 0.00473872 - 0.0394847 x^2 + 0.114150 x^4 - 0.198735 x^6 \quad (45)$$

and they are in very good agreement with the experimental value of 208 cm^{-1} . The harmonic frequency from DFT calculations is 203 cm^{-1} .

The vapor-phase Raman spectra were recorded for 2,3-cyclopentenopyridine (known as pyrindan). Even though the sample gave very weak Raman spectra, detailed vibrational analysis was carried out based on the infrared, and Raman (including polarization), with the help of DFT-B3LYP calculated frequencies for the C_1 puckered and C_s planar conformations. The calculated structure of pyrindan in the electronic ground state shows little difference from that of indan. The theoretically determined ring-puckering potential energy function from the MP2/cc-pVTZ calculation predicted a barrier of 587 cm^{-1} and a puckering angle of 32° as compared to a 488 cm^{-1} barrier and a 30° puckering angle for indan. The puckering frequency for pyrindan was calculated

using the B3LYP hybrid functional to be 139 cm^{-1} , and this is very close to the experimental value for indan (143 cm^{-1}).

In addition, detailed *ab initio* and DFT calculations were carried out for several molecules whose structures and vibrational spectra were previously characterized. Thus several cyclopentenes, silacyclobutanes, and silacyclopent-2-enes were reinvestigated. The results indicated a need for several revisions of the vibrational assignments for these molecules. In almost all the cases considered in this work, DFT calculations, when the B3LYP hybrid functional is utilized with either the cc-pVTZ or 6-311++G(d,p) basis sets, very reliably reproduced the observed vibrational infrared and Raman spectra. Also, the MP2 calculations, and the CCSD calculations for the more complicated cases, resulted in conformational and structural conclusions that agree very well with the previously reported experimental conclusions.

Ab initio calculations using the MP2/cc-pVTZ basis set do an excellent job of predicting the inversion barrier (247 vs. 232 cm^{-1}) and dihedral angle (26°) of cyclopentene. DFT calculations also do an excellent job of predicting the vibrational frequencies of the d_0 , d_1 , d_4 , and d_8 isotopomers. These computations have also allowed the reassignments of several of the vibrational frequencies. The calculations showed that the vibrational assignments for the d_4 and d_8 isotopomers are not straightforward, and strong interactions in their vibrational spectra have to be taken into account. The ring puckering frequencies of d_0 , d_1 , d_4 , and d_8 isotopomers were predicted from the B3LYP/cc-pVTZ calculations to be 133 , 131 , 122 , and 105 cm^{-1} , respectively. The corresponding experimental values are 127 , 126 , 120 , and 108 cm^{-1} .

The presence of the silicon and chlorine atoms in small, highly strained rings, such as silacyclobutane and its derivatives, did not prevent the DFT calculations from providing excellent agreement with experiments. Changing the basis sets utilized to run the MP2 calculations of the ring-puckering potential energy function for silacyclobutane resulted in a noticeable difference in the inversion barriers and puckering angles (from a 489 cm^{-1} barrier and 30° puckering angle for the 6-31G basis set to a 762 cm^{-1} barrier and 34° puckering angle for the 6-311++G(d,p) basis set). The calculated frequencies from DFT showed that frequency adjustments of about 300 cm^{-1} in magnitude were needed for some previous CH_2 bending vibrations. Similar reassignments were also noted from the DFT frequencies for other silicon-containing four- and five-membered rings as compared to cyclobutane and cyclopentene. The electrostatic charges on the hydrogen atoms of these CH_2 groups and those of the SiH_2 groups account for that considerable decrease in the calculated vibrational frequencies.

High-level *ab initio* calculations showed that silacyclopente-2-ene is slightly puckered with a small barrier to interconversion. The molecule was thought from previous far-infrared studies to be rigid and planar. These results have shown the need for reinvestigating the far-infrared spectra of silacyclopent-2-ene and its -1,1- d_2 isotopomer. Using existing data, two possible ring-puckering potential energy functions with small barriers were proposed. The revised potential functions for the two molecules (Calculation I) are

$$V_{\text{H}_2}(\text{cm}^{-1}) = 48.76 \times 10^5 x^4 - 29.97 \times 10^3 x^2 \quad (46)$$

and

$$V_{D_2} (\text{cm}^{-1}) = 49.47 \times 10^5 x^4 - 26.56 \times 10^3 x^2 \quad (47)$$

where x is the ring-puckering coordinate. The transition frequencies of the ring-puckering vibration for the two molecules fit very well with the two potential functions shown above. The barrier and puckering angle of silacyclopent-2-ene from Eq. (46) are 26 cm^{-1} and 13° . The *ab initio* barrier and puckering angle for silacyclopent-2-ene as determined from coupled cluster calculations were 47 cm^{-1} and 17° , respectively.

REFERENCES

- [1] L. A. Carreira, R. C. Lord, T. B. Malloy Jr., *Topics in Current Chemistry* 82 (1979) 1.
- [2] R. P. Bell, *Proc. Roy. Soc. London* 183A (1945) 328.
- [3] A. Danti, W. J. Lafferty, R. C. Lord, *J. Chem. Phys.* 33 (1960) 294.
- [4] S. I. Chan, J. Zinn, J. Fernandez, W. D. Gwinn, *J. Chem. Phys.* 33 (1960) 1643.
- [5] J. Laane, *J. Pure Appl. Chem.* 59 (1987) 1307.
- [6] J. Laane, in: J. Lanne, M. Dakkouri, B. van der Vaken, H. Oberhammer (Eds.), *Structures and Conformations of Non-Rigid Molecules*, Kluwer, Dordrecht, 1993.
- [7] J. Laane, *Annu. Rev. Phys. Chem.* 45 (1994) 179.
- [8] J. Laane, *Int. Rev. Phys. Chem.* 18 (1999) 301.
- [9] J. Laane, *J. Phys. Chem.* 104 (2000) 7715.
- [10] J. Laane, R. C. Lord, *J. Chem. Phys.* 47 (1967) 4941.
- [11] J. Laane, R. C. Lord, *J. Mol. Spectrosc.* 39 (1971) 340.
- [12] T. R. Borgers, H. L. Strauss, *J. Chem. Phys.* 45 (1966) 947.
- [13] J. Laane, R. C. Lord, *J. Chem. Phys.* 48 (1968) 1508.
- [14] F. A. Miller, R. J. Capwell, *Spectrochim. Acta* 27A (1971) 947.
- [15] A. Das, K. K. Mahato, S. S. Panja, T. Chakraborty, *J. Chem. Phys.* 119 (2003) 2523.

- [16] Y. He, W. Kong, *J. Chem. Phys.* 124 (2006) 204306.
- [17] P. Ottaviani, B. Velino, W. Caminati, *J. Mol. Struct.* 795 (2006) 194.
- [18] J. M. Bakke, L. H. Bjerkeseth, *J. Mol. Struct.* 470 (1998) 247.
- [19] J. M. Bakke, A. M. Schie, T. Skjente, *Acta Chem. Scand.* B40 (1986) 703.
- [20] E. F. Healy, J. D. Lewis, A. B. Minniear, *Tetrahedron Lett.* 35 (1994) 6647.
- [21] A. C. Legon, *Chem. Commun.* (1970) 838.
- [22] J. L. Alonso, A. C. Legon, *J. Chem. Soc., Faraday Trans.* 77 (1981) 2191.
- [23] R. N. Jones, C. L. Angell, T. Ito, R. J. D. Smith, *Can. J. Chem.* 37 (1959) 2007.
- [24] R. P. M. Bond, T. Chairns, J. D. Connolly, G. Eglinton, K. H. Overton, *J. Chem. Soc.* (1965) 3958.
- [25] R. A. Nyquist, H. A. Fouchea, G. A. Hoffman, D. L. Hasha, *Appl. Spectrosc.* 45 (1991) 860.
- [26] A. C. Fantoni, W. Caminati, *J. Mol. Spectrosc.* 186 (1997) 105.
- [27] R. P. Thummel, D. K. Kohli, *J. Org. Chem.* 42 (1977) 2742.
- [28] R. P. Thummel, D. K. Kohli, *J. Org. Chem.* 43 (1978) 2882.
- [29] L. E. Bauman, P. M. Killough, J. M. Cooke, J. R. Villarreal, J. Laane, *J. Phys. Chem.* 86 (1982) 2000.
- [30] T. H. Chao, J. Laane, *Chem. Phys. Lett.* 14 (1972) 595.
- [31] G. W. Rathjens, Jr., *J. Chem. Phys.* 36 (1962) 2401.
- [32] S. S. Butcher, C. C. Costain, *J. Mol. Spectrosc.* 15 (1965) 40.
- [33] T. Ueda, T. Shimanouchi, *J. Chem. Phys.* 47 (1967) 5018.
- [34] M. I. Davis, T. W. Muecke, *J. Phys. Chem.* 74 (1970) 529.

- [35] J. R. Villarreal, L. E. Bauman, J. Laane, W. C. Harris, S. F. Bush, *J. Chem. Phys.* 63 (1975) 3727.
- [36] J. R. Villarreal, L. E. Bauman, J. Laane, *J. Phys. Chem.* 80 (1976) 1172.
- [37] J. R. Villarreal, J. Laane, S. F. Bush, W. C. Harris, *Spectrochim. Acta* 35A (1979) 331.
- [38] J. Laane, *J. Am. Chem. Soc.* 89 (1967) 1144.
- [39] J. Laane, *Spectrochim. Acta* 26A (1970) 517.
- [40] J. Laane, *J. Chem. Phys.* 52 (1970) 358.
- [41] T. H. Chao, J. Laane, *Spectrochim. Acta* 28A (1972) 2443.
- [42] J. B. Foresman, A. Frisch, *Exploring Chemistry with Electronic Structure Methods*, Second ed., Gaussian, Inc., Pittsburg PA, 1996.
- [43] F. Jensen, *Introduction to Computational Chemistry*, Second ed., Wiley, Inc., New York, 2001.
- [44] D. Young, *Computational Chemistry*, First ed., Wiley, Inc., New York, 2001.
- [45] C. J. Cramer, *Essentials of Computational Chemistry*, First ed., Wiley, Inc., New York, 2002.
- [46] D. R. Hartree, *Proc. Cambridge Phil. Soc.* 24 (1928) 111.
- [47] D. A. McQuarrie, *Quantum Chemistry*, First ed., University Science Books, Sausalito CA, 1983.
- [48] C. J. Roothaan, *Rev. Mod. Phys.* 23 (1951) 69.
- [49] C. Møller, M. S. Plesset, *Phys. Rev.* 46 (1934) 618.
- [50] (a) P. Hohenberg, W. Kohn, *Phys. Rev.* 136 (1964) 864.

- (b) A. D. Becke, *J. Chem. Phys.* 98 (1993) 5648.
 - (c) C. Lee, W. Yang, R. G. Parr, *Phys. Rev. B* 37 (1988) 785.
 - (d) B. Miehlich, A. Savin, H. Stoll, H. Preuss, *Chem. Phys. Lett.* 157 (1989) 200.
 - (e) J. P. Perdew, J. A. Chevary, S. H. Vosko, K. A. Jackson, M. R. Pederson, D. J. Singh, C. Fiolhais, *Phys. Rev. B* 46 (1992) 523.
 - (f) J. P. Perdew, K. Burke, Y. Wang, *Phys. Rev. B* 54 (1996) 16533.
- [51] E. B. Wilson, Jr., J. C. Decius, P. C. Cross, *Molecular Vibrations*, Dover Publications, Inc., New York, 1980.
- [52] J. Laane, M. A. Harthcock, P. M. Killough, L. E. Bauman, J. M. Cooke, *J. Mol. Spectrosc.* 91 (1982) 286.
- [53] R. W. Schmude, Jr., M. A. Harthcock, M. B. Kelly, J. Laane, *J. Mol. Spectrosc.* 124 (1987) 369.
- [54] M. M. Tecklenburg, J. Laane, *J. Mol. Spectrosc.* 137 (1989) 65.
- [55] D. M. Dennison, G. E. Uhlenbeck, *Phys. Rev.* 41 (1932) 313.
- [56] C. C. Costain, G. B. Sutherland, *J. Phys. Chem.* 56 (1952) 321.
- [57] D. C. Harris, M. D. Bertolucci, *Symmetry and Spectroscopy*, Dover Publications, Inc., New York, 1989.
- [58] Z. Arp, N. Meinander, J. Choo, J. Laane, *J. Chem. Phys.* 116 (2002) 6648.
- [59] T. Klots, S. Sakurai, J. Laane, *J. Chem. Phys.* 108 (1998) 3531.
- [60] S. Sakurai, N. Meinander, J. Laane, *J. Chem. Phys.* 108 (1998) 3537.
- [61] E. Bondoc, S. Sakurai, K. Morris, W.-Y. Chiang, J. Laane, *J. Chem. Phys.* 112 (2000) 6700.

- [62] E. Bondoc, T. Klots, J. Laane, *J. Phys. Chem.* 104 (2000) 275.
- [63] J. Yang, K. Okuyama, K. Morris, Z. Arp, J. Laane, *J. Phys. Chem.* 109 (2005) 8290.
- [64] S. Sakurai, N. Meinander, K. Morris, J. Laane, *J. Am. Chem. Soc.* 121 (1999) 5056.
- [65] J. Laane, E. Bondoc, S. Sakurai, K. Morris, N. Meinander, J. Choo, *J. Am. Chem. Soc.* 122 (2000) 2628.
- [66] J. Laane, Z. Arp, S. Sakurai, K. Morris, , N. Meinander, T. Klots, E. Bondoc, K. Haller, J. Choo, *ACS Symposium Series* 828 (2002) 380.
- [67] M. J. Frisch, G. W. Trucks, H. B. Schlegel, G. E. Scuseria, M. A. Robb, J. R. Cheeseman, J. A. Montgomery, Jr., T. Vreven, K. N. Kudin, J. C. Burant, J. M. Millam, S. S. Iyengar, J. Tomasi, V. Barone, B. Mennucci, M. Cossi, G. Scalmani, N. Rega, G. A. Petersson, H. Nakatsuji, M. Hada, M. Ehara, K. Toyota, R. Fukuda, J. Hasegawa, M. Ishida, T. Nakajima, Y. Honda, O. Kitao, H. Nakai, M. Klene, X. Li, J. E. Knox, H. P. Hratchian, J. B. Cross, V. Bakken, C. Adamo, J. Jaramillo, R. Gomperts, R. E. Stratmann, O. Yazyev, A. J. Austin, R. Cammi, C. Pomelli, J. W. Ochterski, P. Y. Ayala, K. Morokuma, G. A. Voth, P. Salvador, J. J. Dannenberg, V. G. Zakrzewski, S. Dapprich, A. D. Daniels, M. C. Strain, O. Farkas, D. K. Malick, A. D. Rabuck, K. Raghavachari, J. B. Foresman, J. V. Ortiz, Q. Cui, A. G. Baboul, S. Clifford, J. Cioslowski, B. B. Stefanov, G. Liu, A. Liashenko, P. Piskorz, I. Komaromi, R. L. Martin, D. J. Fox, T. Keith, M. A. Al-Laham, C. Y. Peng, A. Nanayakkara, M. Challacombe, P. M. W. Gill, B. Johnson, W. Chen, M.

- W. Wong, C. Gonzalez, J. A. Pople, Gaussian 03, revision C.2, Gaussian, Inc., Wallingford CT, 2004.
- [68] P. R. Schleyer, D. S. Trifan, R. Bacskai, *J. Am. Chem. Soc.* 80 (1958) 6691.
- [69] M. Oki, H. Iwamura, *Bull. Chem. Soc.* 32 (1959) 567.
- [70] J. F. Bacon, J. H. van der Maas, *Spectrochim. Acta* 44A (1988) 1215.
- [71] A. A. Al-Saadi, M. Wagner, J. Laane, *J. Phys. Chem.* (2006) accepted.
- [72] T. H. Chao, J. Laane, *J. Mol. Spectrosc.* 48 (1973) 266.
- [73] D. Chadwick, A. C. Legon, D. J. Millen, *J. Chem. Soc., Faraday Trans.* 75 (1979) 302.
- [74] R. Cataliotti, G. Paliani, S. Santini, *J. Mol. Spectrosc.* 103 (1984) 56.
- [75] C. M. Cheatham, J. Laane, *J. Chem. Phys.* 94 (1991) 5394.
- [76] J. Choo, S. Kim, S. Drucker, J. Laane, *J. Phys. Chem.* 107 (2003) 10655.
- [77] C. M. Cheatham, J. Laane, *J. Chem. Phys.* 94 (1991) 7734.
- [78] N. R. Pillsbury, J. Choo, J. Laane, S. Drucker, *J. Phys. Chem.* 107 (2003) 10648.
- [79] E. Garcia-Exposito, M. J. Bearpark, R. M. Ortuno, V. Branchadell, M. A. Robb, S. Wilsey, *J. Org. Chem.* 66 (2001) 8811.
- [80] R. B. Sunoj, P. Lakshminarasimhan, V. Ramamurthy, J. Chandrasekhar, *J. Comput. Chem.* 22 (2001) 1598.
- [81] A. B. Wood, B. Buckingham, *Spectrochim. Acta* 26A (1970) 465.
- [82] V. J. Brunn, F. Peters, M. Dethloff, *J. Prakt. Chemie.* 318 (1976) 745.
- [83] K. Haller, W.-Y. Chiang, A. del Rosario, J. Laane, *J. Mol. Struct.* 379 (1996) 19.

- [84] J. Laane, K. Haller, S. Sakurai, K. Morris, D. Autrey, Z. Arp, W.-Y. Chiang, A. Combs, *J. Mol. Struct.* 650 (2003) 57.
- [85] J. R. Ferraro, K. Nakamoto, C. W. Brown, *Introductory Raman Spectroscopy*, Second ed., Academic Press, San Diego CA, 2003.
- [86] J. M. Hollas, *High Resolution Spectroscopy*, Second ed., Wiley, Inc., New York, 1998.
- [87] Z. Arp, W. A. Herrebout, J. Laane, B. J. Van der Veken, *J. Phys. Chem.* 104 (2000) 5222.
- [88] D. Autrey, J. Laane, *J. Phys. Chem.* 105 (2001) 6894.
- [89] D. Autrey, J. Yang, J. Laane, *J. Mol. Struct.* 661 (2003) 23.
- [90] D. Autrey, K. Haller, J. Laane, C. Mlynek, H. Henning, *J. Phys. Chem.* 108 (2004) 403.
- [91] C. Mlynek, H. Henning, J. Yang, J. Laane, *J. Mol. Struct.* 742 (2005) 161.
- [92] W. D. Allen, A. G. Csaszar, D. A. Horner, *J. Am. Chem. Soc.* 114 (1992) 6834.
- [93] G. De Alti, P. Decleva, *J. Mol. Struct.* 41 (1977) 299.
- [94] S. Saebo, F. R. Cordell, J. Boggs, *J. Mol. Struct. (Theochem)*, 104 (1983) 221.
- [95] C. Lapouge, D. Cavagnat, D. Gorse, M. Pesquer, *J. Phys. Chem.* 99 (1995) 2996.
- [96] M. K. Leong, V. S. Mastryukov, J. E. Boggs, *J. Mol. Struct.* 445 (1998) 149.
- [97] R. L. Rosas, C. Cooper, J. Laane, *J. Phys. Chem.* 94 (1990) 1830.
- [98] J. R. Villarreal, Ph.D. Thesis, Department of Chemistry, Texas A&M University, 1976.

- [99] L. V. Vilkov, V. S. Mastryukov, Y. V. Baurova, V. M. Vodvin, Dokl. Akad. Nauk SSSR 117 (1967) 1084.
- [100] V. T. Aleksanyan, G. M. Kuz'yants, V. M. Vdobin, P. L. Grinberg, O. V. Kuz'min, Zh. Strukt. Khim. 10 (1969) 397.
- [101] W. C. Pringle, J. Chem. Phys. 54 (1971) 4979.
- [102] V. S. Mastryukov, O. V. Dorofeeva, L. V. Vilkov, B. N. Cyvin, S. J. Cyvin, Zh. Strukt. Khim. 16 (1975) 438.
- [103] B. N. Cyvin, S. J. Cyvin, S. A. Strelkov, V. S. Mastryukov, L. V. Vilkov, A. V. Golubinskii, J. Mol. Struct. 144 (1986) 385.
- [104] B. Rempfer, G. Pfafferott, H. Oberhammer, N. Auner, J. E. Boggs, Acta Chem. Scand. A42 (1988) 352.
- [105] V. P. Novikov, S. A. Tarasenko, S. Samdal, L. V. Vilkov, J. Mol. Struct. 445 (1998) 207.
- [106] V. P. Novikov, M. Dakkouri, L. V. Vilkov, J. Mol. Struct. (2006) In press.
- [107] J. A. Boatz, M. S. Gordon, R. L. Hilderbrandt, J. Am. Chem. Soc. 110 (1988) 352.
- [108] E. T. Seidl, R. S. Grev, H. F. Schaefer III, J. Am. Chem. Soc. 114 (1992) 3643.
- [109] P. N. Skancke, J. Phys. Chem. 98 (1994) 3154.
- [110] V. S. Mastryukov, J. E. Boggs, J. Mol. Struct. (Theochem) 338 (1995) 235.
- [111] T. Fangstrom, S. Lunell, B. Engels, L. A. Eriksson, M. Shiotani, K. Komaguchi, J. Chem. Phys. 107 (1997) 297.
- [112] M. S. Gordon, T. J. Barton, H. Nakano, J. Am. Chem. Soc. 119 (1997) 11966.

- [113] V. N. Khabashesku, K. N. Kudin, J. L. Margrave, *Russ. Chem. Bull., Int. Ed.* 50 (2001) 20.
- [114] R. Damrauer, A. J. Crowell, C. F. Craig, *J. Am. Chem. Soc.* 125 (2003) 10759.
- [115] F. Freeman, C. Fang, B. A. Shainyan, *Int. J. Quantum Chem.* 100 (2004) 720.
- [116] M. R. Frierson, M. R. Imam, V. B. Zalkow, N. L. Allinger, *J. Org. Chem.* 53 (1988) 5248.
- [117] K. Chen, N. L. Allinger, *J. Phys. Org. Chem.* 10 (1997) 697.
- [118] R. M. Irwin, J. Laane, *J. Phys. Chem.* 82 (1978) 2845.
- [119] M. Z. Rishard, R. M. Irwin, J. Laane, *J. Phys. Chem.* (2006) Submitted.
- [120] A. A. Al-Saadi, J. Laane, *J. Mol. Struct.* (2006) doi:10.1016/j.molstruc.2006.06.030.
- [121] J. Laane, Ph.D. Thesis, Department of Chemistry, Massachusetts Institute of Technology, 1967.
- [122] N. B. Colthup, *Introduction to infrared and Raman spectroscopy*, Second ed., Academic Press, New York, 1975.
- [123] T. A. Mohamed, G. A. Guirgis, Y. E. Nashed, J. R. Durig, *Struct. Chem.* 9 (1998) 255.
- [124] D. C. McKean, *Spectrochim. Acta* 55A (1999) 1485.
- [125] D. C. McKean, I. Torto, *J. Mol. Spectrosc.* 216 (2002) 363.
- [126] D. C. McKean, *J. Phys. Chem.* 107 (2003) 6538.
- [127] D. F. Ball, P. L. Goggin, D. C. McKean, L. A. Woodward, *Spectrochim. Acta* 16 (1960) 1358.

- [128] D. C. McKean, G. Davidson, L. A. Woodward, *Spectrochim. Acta* 26A (1970) 1815.
- [129] T. H. Chao, S. L. Moore, J. Laane, *J. Organometal. Chem.* 33 (1971) 157.
- [130] M. B. Kelly, J. Laane, *J. Phys. Chem.* 92 (1988) 4056.
- [131] R. A. Benkeser, Y. Nagai, J. L. Noe, R. F. Cunico, P. H. Gund, *J. Am. Chem. Soc.* 86 (1964) 2446.
- [132] J. Laane, *J. Chem. Phys.* 50 (1969) 776.
- [133] T. H. Chao, J. Laane, *Spectrochim. Acta* 28A (1972) 2443.
- [134] P. M. Killough, J. Laane, *J. Chem. Phys.* 80 (1984) 5475.

VITA

Name: Abdulaziz A. H. Al-Saadi

Country of Citizenship: Saudi Arabia

Permanent Address: Chemistry Department
King Fahd University for Petroleum and Minerals
Dhahran 31261
Saudi Arabia

Email Address: aahsaadi@gmail.com

Marital status: Married with three children

Education: B.A., Chemistry, King Fahd University for Petroleum and Minerals, Dhahran, Saudi Arabia, 1996

M.S., Chemistry, King Fahd University for Petroleum and Minerals, Dhahran, Saudi Arabia, 2000

Ph.D., Chemistry, Texas A&M University, College Station, Texas, USA, 2006